Contribution to the evaluation of the compaction characteristics of asphalt mixtures

Doctoral Thesis

Panos Georgiou

Supervisor: Professor Andreas Loizos

Athens, November 2016

ΕΘΝΙΚΟ ΜΕΤΣΟΒΙΟ ΠΟΛΥΤΕΧΝΕΙΟ
ΣΧΟΛΗ ΠΟΛΙΤΙΚΩΝ ΜΗΧΑΝΙΚΩΝ
ΤΟΜΕΑΣ ΜΣΥ
ΕΡΓΑΣΤΗΡΙΟ ΟΔΟΠΟΙΙΑΣ

Συμβολή στην αξιολόγηση των χαρακτηριστικών συμπύκνωσης ασφαλτομιγμάτων

Διδακτορική Διατριβή

Πάνος Β. Γεωργίου

Επιβλέπων: Καθηγητής Ανδρέας Λοΐζος

Αθήνα, Νοέμβριος 2016

Η Επταμελής Εξεταστική Επιτροπή για την κρίση της παρούσας Διατριβής αποτελείται από τα ακόλουθα μέλη:

Συμβουλευτική Επιτροπή:	Α. Λοΐζος, Καθηγητής Ε.Μ.Π. (Επιβλέπων)
	Γ. Κανελλαΐδης, Ομότιμος Καθηγητή Ε.Μ.Π.
	Χ. Πλατή, Επ. Καθηγήτρια Ε.Μ.Π.
Μέλη Εξεταστικής Επιτροπής:	Σ. Κουρκουλής, Καθηγητής Ε.Μ.Π.
	Β. Ψαριανός, Καθηγητής Ε.Μ.Π.
	Γ. Αποστολόπουλος, Αν. Καθηγητής Ε.Μ.Π.
	Ε. Μπαδογιάννης, Επ. Καθηγητής Ε.Μ.Π.

ΕΥΧΑΡΙΣΤΙΕΣ

Θα ήθελα να εκφράσω την ειλικρινή ευγνωμοσύνη μου στον Επιβλέπων Καθηγητή κ. Ανδρέα Λοΐζο για την καθοδήγησή του, τις πολύτιμες συζητήσεις, συμβουλές και ενθαρρύνσεις κατά τη διάρκεια αυτής της διαδικασίας.

Θα ήθελα να ευχαριστήσω ιδιαίτερα και τα άλλα δύο μέλη της Συμβουλευτικής επιτροπής, τον Ομότιμο Καθηγητή κ. Γεώργιο Κανελλαΐδη και την Επίκουρη Καθηγήτρια κα. Χριστίνα Πλατή για τις εποικοδομητικές παρατηρήσεις τους για τη διαμόρφωση του κειμένου της διατριβής.

Επίσης, θα ήθελα να εκφράσω τις θερμές ευχαριστίες μου στα μέλη της ερευνητικής ομάδας του Εργαστηρίου Οδοποιίας του ΕΜΠ για την υποστήριξη και ουσιαστική συμβολή τους στην υλοποίηση της έρευνας.

Τέλος, θα ήθελα να ευχαριστήσω τους γονείς μου για τις θυσίες τους και τα εφόδια που μου προσέφεραν, καθώς και την οικογένειά μου για την αμέριστη συμπαράσταση, υπομονή και υποστήριξη τους στην επιτυχή ολοκλήρωση της διαδικασίας.

Στη Δήμητρα

Στην Ελίνα

Στο Βασίλη

ABSTRACT

Asphalt mixture compaction has been well recognized as one of the most critical factors affecting the pavement behavior, providing all desirable mixture design characteristics are met. This poses a challenge the laboratory compaction to simulate the field compaction, so that a reliable assessment of the on-site asphalt mixture's characteristics, both mechanical and surface, is enabled to ensure proper asphalt pavement behavior.

Comparative evaluation between the commonly available laboratory compaction methods has reached inconclusive results as to which method is the best in terms of simulating the field compaction conditions. However, it is widely acknowledged that compaction method has direct impact on the aggregate structure within the compacted mixture, and hence studying this can lead to understanding of the mechanism of the aggregate inter-particle arrangement. It is believed that linking this to the changes in asphalt mixture performance-based characteristics can thus lead to better understanding of the dominant compaction parameters and the resulting mechanical response. Furthermore, the pavement surface shall provide adequate skid resistance, which is vital for the safety of the driving public. This implies that pavement engineers shall be able to precisely evaluate and quantify before construction the field compaction-based surface texture characteristics of asphalt mixtures, which so far has been investigated to a limited extent. Hence, a practical methodology shall be developed to allow the prediction of the on-site asphalt surface characteristics of the mixture with respect to the compaction process from laboratory produced specimens.

The aim of this Thesis was to contribute to a better simulation of in-situ conditions through laboratory compaction methods, so that reliable results can be obtained to assess, as accurately as possible, the on-site characteristics of field-compacted asphalt mixtures.

To reach this aim, extensive laboratory (based on impact, gyratory and roller compaction methods) and field experiments were designed and performed, including the implementation of modern Non Destructive Testing (NDT) technologies for rigorous evaluation purposes. A holistic approach, including investigations for both the compaction dependent surface and mechanical characteristics of asphalt mixtures, was adopted.

In this methodology, at first the compaction factors affecting significantly the compactability, stiffness and rut resistance characteristics of asphalt mixtures are identified, characteristics which have been found to be strongly influenced from compaction methods. Secondly, evaluating the internal structure of asphalt mixtures by means of 2-D image analyses understanding of the compaction factors controlling the formation of aggregate skeleton, in terms of aggregate 'contact points', orientation and segregation, is obtained. This is important to understand the interplay between the internal structure and mechanical performance of asphalt mixtures and relate this to the compaction methodology. Based on the experimental findings, a clear understanding of the key compaction parameters for each compaction method has been reached. For instance, the compaction temperature, (initial) diameter and angle of gyration, compaction temperature and effort were found to be the dominant parameters for the impact, gyratory and roller compaction, respectively. These factors eventually form the basis for laboratory compaction regimes to contribute to bridge the gap with the field compaction-based mechanical characteristics, which will have a significant influence when using mechanistic-empirical pavement analyses methods to improve the pavement analysis outcome towards better representing the actual pavement behavior.

This research' findings also indicated that the laboratory compaction testing during mixture design process cannot reliably reflect the compactability of asphalt mixtures in the field and hence provide essential input to be used for the construction process. In practice, achieving on-site the target compaction degree is still a heuristic process, mainly, on the basis of installation of a trial section. Within this procedure, contractors seek to establish the rolling pattern to achieve the target density by determining the

compaction density curve with number of roller passes without however taking into consideration dominant parameters controlling the compaction process, such as mixture temperature properties. In this Thesis, attempting to maximize the benefits from the installation of a trial section, an improved and practical NDT-based methodology to establish effectively the rolling pattern has been developed making due allowance for the mixture temperature properties and the variability in construction conditions. Furthermore, an integrated GPR-based methodology to assess reliably the in-place density was introduced, which enables within production rolling to verify the effectiveness of the established rolling pattern to fulfill the compaction requirements. Both these methodologies can benefit contractors and agencies to improve not only the on-site compaction methodology to ensure a proper pavement initial condition, but also the compaction quality control procedures offering the benefit, compared to more traditional destructive test methods, of full coverage nondestructive evaluation of the pavement mat. Particularly, through enhanced field compaction a proper pavement initial condition, according to design criteria, will be ensured and the positive influences will therefore be not only a substantial decrease in needs for maintenance works and thereby in the total life cycle cost, but also less disruption to road users.

Moreover, in this Thesis a simple, yet, and practical methodology has been developed, which allows to estimate the field compaction-based surface texture characteristics of asphalt mixtures. With this methodology, which includes the roller compaction method for producing laboratory specimens to be subjected to typical laboratory tests (namely the sand patch and British pendulum), it was demonstrated that the performance of different mixtures in terms of skid resistance and the efficacy of the various compaction modes may be effectively evaluated. Also, the preliminary experimental results indicated a good correlation between the skid resistance characteristics of laboratory- and field compaction-based asphalt surface. Hence, this methodology can benefit pavement engineers offering them the possibility to quantify and optimize the skid resistance-related properties of asphalt mixtures during the laboratory design process, as well as helpful information that may be potentially used to assess the safety of road users at the early stage of asphalt pavement in service. Further, this methodology offers essential

information for contractors to establish an effective field compaction mode to achieve conformity with construction requirements.

ΠΕΡΙΛΗΨΗ

Η συμπύκνωση των ασφαλτικών μιγμάτων έχει αναγνωρισθεί διεθνώς ότι αποτελεί ίσως την πιο κρίσιμη παράμετρο της συμπεριφοράς του οδοστρώματος, εφόσον κατά τον σχεδιασμό εξασφαλισθούν τα επιθυμητά χαρακτηριστικά του ασφαλτομίγματος. Αυτό θέτει ως πρόκληση η εργαστηριακή συμπύκνωση να προσομοιάζει τη συμπύκνωση στο πεδίο, ώστε να μπορεί να επιτευχθεί αξιόπιστη εκτίμηση των επιτόπου μηχανικών και επιφανειακών χαρακτηριστικών του ασφαλτομίγματος για τη διασφάλιση της κατάλληλης συμπεριφοράς του οδοστρώματος.

Από τη συγκριτική αξιολόγηση μεταξύ των διεθνώς εφαρμοζόμενων μεθόδων εργαστηριακής συμπύκνωσης δεν έχει υπάρξει μέχρι στιγμής ομοφωνία ως προς τη μέθοδο η οποία προσομοιάζει καλύτερα τη συμπύκνωση στο πεδίο. Ωστόσο, έχει ευρέως αναγνωρισθεί ότι η μέθοδος συμπύκνωσης έχει άμεση επίπτωση στην εσωτερική δομή του ασφαλτομίγματος, και ως εκ τούτου η μελέτη της εσωτερικής δομής μπορεί να οδηγήσει στην κατανόηση του μηχανισμού διάταξης των αδρανών στη μάζα του συμπυκνωμένου ασφαλτομίγματος. Η σύνδεση της εσωτερικής δομής με τις μεταβολές στα χαρακτηριστικά συμπεριφοράς του ασφαλτομίγματος πιστεύεται ότι μπορεί να οδηγήσει σε καλύτερη κατανόηση των κύριων παραμέτρων συμπύκνωσης που διαφοροποιούν τη μηχανική συμπεριφορά των ασφαλτομιγμάτων. Επισημαίνεται επίσης ότι η επαρκής αντιολισθητική ικανότητα της επιφάνειας του οδοστρώματος είναι ζωτικής σημασίας για την ασφάλεια των οδηγών. Αυτό σημαίνει ότι οι μηχανικοί οδοστρωμάτων θα πρέπει να είναι σε θέση να αξιολογήσουν με ακρίβεια και να ποσοτικοποιήσουν πριν την κατασκευή τα επιφανειακά χαρακτηριστικά υφής λόγω της συμπύκνωσης στο έργο, αντικείμενο που μέχρι στιγμής έχει διερευνηθεί μόνο σε περιορισμένη έκταση. Ως εκ τούτου, αναδεικνύεται η ανάγκη να αναπτυχθεί μια μέθοδος, η οποία θα επιτρέπει την πρόβλεψη των επιτόπου επιφανειακών χαρακτηριστικών υφής του ασφαλτομίγματος σε σχέση με τη διαδικασία συμπύκνωσης μέσω εργαστηριακών δοκιμίων.

Στόχο της Διδακτορικής Διατριβής αποτέλεσε η συμβολή στην καλύτερη προσέγγιση των επιτόπου συνθηκών μέσω των εργαστηριακών μεθόδων συμπύκνωσης για την, κατά το δυνατόν, ακριβέστερη εκτίμηση των χαρακτηριστικών συμπεριφοράς των ασφαλτικών μιγμάτων με συμπύκνωση στο πεδίο.

Για την επίτευξη του υπόψη στόχου, πραγματοποιήθηκε σχεδιασμός και υλοποίηση πειραμάτων μεγάλης κλίμακας στο εργαστήριο (με εφαρμογή των μεθόδων συμπύκνωσης: κρουστικής, γυροσκοπικής και με κύλινδρο) και στο πεδίο, συμπεριλαμβανομένης της εφαρμογής σύγχρονων τεχνολογιών μη καταστρεπτικών δοκιμών για λόγους κριτικής αξιολόγησης. Στο πλαίσιο αυτό υιοθετήθηκε μια ολιστική προσέγγιση, η οποία περιλαμβάνει διερευνήσεις των επιφανειακών και των μηχανικών χαρακτηριστικών των ασφαλτομιγμάτων.

Μέσω της υπόψη μεθοδολογίας, αρχικά, αναγνωρίσθηκαν οι κρίσιμες παράμετροι συμπύκνωσης που επηρεάζουν σημαντικά τη συμπυκνωσιμότητα, τη δυσκαμψία και την ανθεκτικότητα σε παραμένουσες παραμορφώσεις των ασφαλτομιγμάτων, χαρακτηριστικά τα οποία έχει βρεθεί ότι επηρεάζονται σημαντικά από τη μέθοδο συμπύκνωσης. Επίσης, από την αξιολόγηση της εσωτερικής δομής των ασφαλτομιγμάτων μέσω αναλύσεων εικόνας δισδιάστατης μορφής επιτεύχθηκε κατανόηση των κρίσιμων παραμέτρων συμπύκνωσης που διαμορφώνουν τον σκελετό, υπό την έννοια του αριθμού των «σημείων επαφής», προσανατολισμού και διαχωρισμού των αδρανών στο μίγμα. Αυτό είναι σημαντικό ώστε να υπάρξει κατανόηση της αλληλεπίδρασης μεταξύ της εσωτερικής δομής και της μηχανικής συμπεριφοράς των ασφαλτομιγμάτων και συσχέτιση με τη μεθοδολογία συμπύκνωσης. Με βάση τα πειραματικά ευρήματα, επιτεύχθηκε σαφής κατανόηση, για κάθε εργαστηριακή μέθοδο, των βασικών παραμέτρων που επηρεάζουν σημαντικά τη διαδικασία συμπύκνωσης και κατ' επέκταση τη συμπεριφορά του ασφαλτομίγματος. Για παράδειγμα, βρέθηκε ότι η θερμοκρασία συμπύκνωσης, η (αρχική) διάμετρος και η γωνία περιστροφής, η θερμοκρασία και η ενέργεια συμπύκνωσης αποτελούν τις κυριότερες παραμέτρους της κρουστικής, γυροσκοπικής και της συμπύκνωσης με κύλινδρο, αντίστοιχα. Οι υπόψη παράμετροι αποτέλεσαν τελικά τη βάση πρότασης οδηγιών εργαστηριακής

συμπύκνωσης, η οποία συμβάλλει στην καλύτερη εκτίμηση των μηχανικών χαρακτηριστικών των ασφαλτομιγμάτων με συμπύκνωση στο έργο. Σημειώνεται ότι η συμβολή αυτή θα έχει σημαντική επιρροή στο πλαίσιο της εφαρμογής μηχανιστικών-εμπειρικών μεθόδων ανάλυσης του οδοστρώματος κατά τρόπο που θα βελτιώνει τα αποτελέσματα των αναλύσεων ώστε να αποδίδουν καλύτερα την πραγματική συμπεριφορά του οδοστρώματος.

Τα ευρήματα της έρευνας έδειξαν επίσης ότι οι δοκιμές συμπύκνωσης στο εργαστήριο κατά τη διαδικασία σχεδιασμού των μιγμάτων δεν αποδίδουν αξιόπιστα τα χαρακτηριστικά συμπυκνωσιμότητας των ασφαλτομιγμάτων στο πεδίο, ώστε να παρέχουν ουσιαστική βοήθεια που θα μπορεί να χρησιμοποιηθεί στη διαδικασία της κατασκευής. Στην πράξη, εξακολουθεί να γίνεται αναζήτηση της μεθοδολογίας συμπύκνωσης για την οποία επιτυγχάνεται επιτόπου ο βαθμός συμπύκνωσης που έχει τεθεί ως στόχος, διαδικασία η οποία υλοποιείται, κυρίως, μέσω της κατασκευής ενός δοκιμαστικού τμήματος. Στο πλαίσιο της διαδικασίας αυτής, οι κατασκευαστές επιδιώκουν να διαμορφώσουν την κατάλληλη- με στόχευση την επίτευξη της πυκνότητας αναφοράς- μεθοδολογία συμπύκνωσης μέσω προσδιορισμού της καμπύλης πυκνότητας συμπύκνωσης σε σχέση με τον αριθμό των διελεύσεων του οδοστρωτήρα, χωρίς ωστόσο να λαμβάνουν υπόψη σημαντικές παραμέτρους που επηρεάζουν τη διαδικασία συμπύκνωσης, όπως οι θερμικές ιδιότητες του ασφαλτομίγματος. Στο πλαίσιο της διατριβής, στην προσπάθεια να μεγιστοποιηθούν τα οφέλη από την κατασκευή ενός δοκιμαστικού τμήματος, αναπτύχθηκε μια βελτιωμένη και πρακτική μεθοδολογία η οποία βασίζεται σε επιτόπου μη καταστρεπτικές δοκιμές για τη διαμόρφωση της μεθοδολογίας συμπύκνωσης, μέσω της οποίας λαμβάνονται υπόψη οι θερμικές ιδιότητες του ασφαλτομίγματος και η μεταβλητότητα των συνθηκών κατασκευής. Επιπλέον, διαμορφώθηκε μια ολοκληρωμένη μεθοδολογία -με βάση την γεωφυσική μέθοδο GPR- για την αξιόπιστη εκτίμηση της επιτόπου πυκνότητας, μέσω της οποίας δίνεται η δυνατότητα αξιολόγησης, κατά τη διάρκεια των κύριων εργασιών συμπύκνωσης, της αποτελεσματικότητας της προσδιορισμένης μεθοδολογίας συμπύκνωσης ως προς την εξασφάλιση των απαιτήσεων συμπύκνωσης. Οι υπόψη μεθοδολογίες μπορεί να ωφελήσουν τους κατασκευαστές και τις Υπηρεσίες

οδοστρωμάτων στη βελτίωση της μεθοδολογίας επιτόπου συμπύκνωσης, καθώς και των διαδικασιών ποιοτικού ελέγχου. Συγκεκριμένα, μέσω της βελτίωσης της μεθοδολογίας συμπύκνωσης στο έργο μπορεί να εξασφαλισθεί η κατάλληλη, σύμφωνα με τα κριτήρια σχεδιασμού, αρχική κατάσταση του οδοστρώματος, η οποία θα μειώσει την ανάγκη εργασιών συντήρησης και κατ' επέκταση το κόστος συντήρησης, καθώς επίσης θα περιορίσει την όχληση των χρηστών της οδού. Επίσης, η χρήση των μη καταστρεπτικών δοκιμών, σε σχέση με τις παραδοσιακές καταστρεπτικές μεθόδους, προσφέρει το πλεονέκτημα της αξιολόγησης σε πλήρη κλίμακα της ποιότητας συμπύκνωσης του ασφαλτοτάπητα βελτιώνοντας τις διαδικασίες του ποιοτικού ελέγχου της κατασκευής.

Επιπλέον, στην υπόψη έρευνα αναπτύχθηκε μια απλή, αλλά και πρακτική μέθοδος, η οποία επιτρέπει την πρόβλεψη των επιφανειακών χαρακτηριστικών υφής των ασφαλτομιγμάτων με συμπύκνωση στο πεδίο. Με τη μέθοδο αυτή, η οποία περιλαμβάνει τη συμπύκνωση με κύλινδρο για τη δημιουργία εργαστηριακών δοκιμίων τα οποία υποβάλλονται στη συνέχεια σε τυπικές εργαστηριακές δοκιμές (δηλαδή της κηλίδας άμμου και του Βρετανικού εκκρεμούς), αποδείχθηκε ότι μπορεί να αξιολογηθούν αποτελεσματικά η συμπεριφορά διαφορετικών μιγμάτων ως προς την αντιολισθητική ικανότητα, καθώς και η αποδοτικότητα της μεθοδολογίας συμπύκνωσης. Επίσης, τα προκαταρκτικά πειραματικά αποτελέσματα έδειξαν καλή συσχέτιση μεταξύ των επιφανειακών χαρακτηριστικών με εργαστηριακή συμπύκνωση και των αντίστοιχων που επιτυγχάνονται με συμπύκνωση στο πεδίο. Ως εκ τούτου, η μέθοδος αυτή μπορεί να ωφελήσει δίνοντας αφενός τη δυνατότητα στους μηχανικούς οδοστρωμάτων να ποσοτικοποιήσουν και να βελτιώσουν τις ιδιότητες που σχετίζονται με την αντιολισθητική ικανότητα των ασφαλτομιγμάτων κατά το στάδιο της μελέτης σύνθεσης και αφετέρου δίνοντας κατάλληλες πληροφορίες που μπορεί δυνητικά να χρησιμοποιηθούν για την αξιολόγηση της ασφάλειας των χρηστών του οδικού δικτύου κατά το αρχικό στάδιο λειτουργίας του ασφαλτικού οδοστρώματος. Η υπόψη μεθοδολογία προσφέρει επίσης ωφέλιμες πληροφορίες στους κατασκευαστές ώστε να διαμορφώσουν μια αποτελεσματική μέθοδο συμπύκνωσης στο πεδίο, μέσω της οποίας θα επιτυγχάνεται συμμόρφωση με τις κατασκευαστικές απαιτήσεις.

ΕΚΤΕΤΑΜΕΝΗ ΠΕΡΙΛΗΨΗ

1. ΕΙΣΑΓΩΓΗ – ΑΝΤΙΚΕΙΜΕΝΟ ΔΙΔΑΚΤΟΡΙΚΗΣ ΔΙΑΤΡΙΒΗΣ

Η συμπύκνωση του ασφαλτομίγματος αφορά στη διαδικασία μέσω της οποίας μειώνεται ο όγκος των κενών αέρα που εμπεριέχονται στη μάζα του και κατ' επέκταση αυξάνεται η πυκνότητα του μίγματος. Κατά τη διαδικασία συμπύκνωσης τα αδρανή, μέσω των ασκούμενων δυνάμεων, έρχονται σε επαφή μεταξύ τους, το οποίο οδηγεί στην αύξηση της αλληλοεμπλοκής και κατ' επέκταση της εσωτερικής τριβής, αναδιατάσσονται και κατανέμονται στη μάζα του ασφαλτομίγματος διαμορφώνοντας την εσωτερική δομή του, η οποία αναφέρεται στα σημεία επαφής, τον προσανατολισμό και την χωρική κατανομή των αδρανών. Μέσω του υπόψη μηχανισμού το ασφαλτόμιγμα αναπτύσσει τα χαρακτηριστικά συμπεριφοράς του, τα οποία δεν μπορούν να βελτιωθούν μετά την ολοκλήρωση της διαδικασίας συμπύκνωσης. Σημειώνεται ότι, η ανεπαρκής συμπύκνωση συνδέεται με την εμφάνιση πρόωρων φθορών στο οδόστρωμα, ενώ αντίθετα η 'καλή' συμπύκνωση οδηγεί στην αύξηση της ανθεκτικότητας έναντι κόπωσης και παραμενουσών παραμορφώσεων, στη μείωση του φαινομένου οξείδωσης ή γήρανσης της ασφάλτου που σχετίζεται με ρηγματώσεις και της φθοράς λόγω υγρασίας, καθώς και στην αύξηση της ευστάθειας και αντοχής του ασφαλτομίγματος και της βελτιστοποίησης των επιφανειακών χαρακτηριστικών υφής των ασφαλτικών στρώσεων. Γίνεται αντιληπτό ότι κατά την κατασκευή θα πρέπει να εξασφαλιστεί μέσω της διαδικασίας συμπύκνωσης η κατάλληλη, σύμφωνα με τα κριτήρια σχεδιασμού, αρχική κατάσταση των ασφαλτικών στρώσεων και κατ' επέκταση του οδοστρώματος, η οποία με τη σειρά της θα μειώσει την ανάγκη εργασιών συντήρησης και θα περιορίσει την όχληση των χρηστών της οδού.

Με βάση τα παραπάνω, έχει προ πολλού αναγνωρισθεί ότι η συμπύκνωση των ασφαλτικών μιγμάτων αποτελεί ίσως την πιο κρίσιμη παράμετρο της συμπεριφοράς του οδοστρώματος, εφόσον κατά το σχεδιασμό εξασφαλισθούν τα επιθυμητά

χαρακτηριστικά του ασφαλτομίγματος. Αυτό θέτει ως πρόκληση η εργαστηριακή συμπύκνωση να προσομοιάζει τη συμπύκνωση στο πεδίο, ώστε να μπορεί να επιτευχθεί αξιόπιστη εκτίμηση των επιτόπου μηχανικών και επιφανειακών χαρακτηριστικών του ασφαλτομίγματος για τη διασφάλιση της κατάλληλης συμπεριφοράς του οδοστρώματος.

Στόχο της Διδακτορικής Διατριβής αποτέλεσε η συμβολή στην καλύτερη προσέγγιση των επιτόπου συνθηκών μέσω των εργαστηριακών μεθόδων συμπύκνωσης, για την, κατά το δυνατόν, ακριβέστερη εκτίμηση των μηχανικών και επιφανειακών χαρακτηριστικών συμπεριφοράς των ασφαλτικών μιγμάτων με συμπύκνωση στο πεδίο.

2. ΜΕΘΟΔΟΛΟΓΙΑ

Για την επίτευξη του στόχου της Διατριβής τέθηκε σε εφαρμογή ένα μεθοδολογικό πλαίσιο, το οποίο αποτελείται από τα ακόλουθα βασικά στάδια:

α) Εκτενής βιβλιογραφική ανασκόπηση

β) Σχεδιασμός και υλοποίηση πειραματικών ερευνών

γ) Ανάλυση πειραματικών δεδομένων

2.1 Βιβλιογραφική ανασκόπηση

Αρχικά, πραγματοποιήθηκε εκτενής βιβλιογραφική ανασκόπηση με σκοπό να συλλεχθούν χρήσιμες πληροφορίες σχετικά με: α) την επιρροή των μεθόδων συμπύκνωσης στις ιδιότητες και τη συμπεριφορά του ασφαλτομίγματος και β) τους παράγοντες που επηρεάζουν τη συμπύκνωση τόσο στο πεδίο όσο και στο εργαστήριο. Από τη βιβλιογραφική ανασκόπηση προέκυψε ότι η συμπυκνωσιμότητα, η δυσκαμψία και η ανθεκτικότητα σε παραμένουσες παραμορφώσεις, τα χαρακτηριστικά της εσωτερικής δομής καθώς και της υφής των ασφαλτομιγμάτων επηρεάζονται σημαντικά από τη διαδικασία συμπύκνωσης. Επιπλέον, από τα ευρήματα της διαδικασίας αυτής προέκυψε ότι, μεταξύ άλλων, η θερμοκρασία, η ενέργεια και η μεθοδολογία

συμπύκνωσης είναι οι βασικές παράμετροι που επηρεάζουν τα χαρακτηριστικά συμπεριφοράς των ασφαλτομιγμάτων.

Επίσης, αξιολογήθηκαν συγκριτικά οι εφαρμοζόμενες διεθνώς μέθοδοι εργαστηριακής συμπύκνωσης και προέκυψε ότι δεν υπάρχει μέχρι στιγμής ομοφωνία ως προς τη μέθοδο η οποία προσομοιάζει καλύτερα τη συμπύκνωση στο έργο. Αναγνωρίσθηκε ότι η μέθοδος συμπύκνωσης έχει άμεση επίπτωση στην εσωτερική δομή του ασφαλτομίγματος και κατ' επέκταση στη συμπεριφορά του ασφαλτομίγματος. Ταυτόχρονα, αναδείχθηκε ότι η σύνδεση της εσωτερικής δομής με τις μεταβολές στα χαρακτηριστικά συμπεριφοράς του ασφαλτομίγματος, μέσω της οποίας μπορεί να προκύψει καλύτερη κατανόηση των κύριων παραμέτρων συμπύκνωσης που διαφοροποιούν τη μηχανική συμπεριφορά των ασφαλτομιγμάτων ώστε να διαμορφωθούν κατάλληλες οδηγίες συμπύκνωσης που προσομοιάζουν, κατά το δυνατόν, τις επιτόπου συνθήκες, είναι αντικείμενο το οποίο μέχρι στιγμής έχει διερευνηθεί μόνο σε περιορισμένη έκταση.

Επιπλέον, αναδείχθηκε η ανάγκη ανάπτυξης μεθόδου, η οποία θα επιτρέπει την πρόβλεψη μέσω εργαστηριακών δοκιμίων των επιτόπου επιφανειακών χαρακτηριστικών υφής του ασφαλτομίγματος σε σχέση με τη διαδικασία συμπύκνωσης. Οι σχετικές έρευνες που έχουν πραγματοποιηθεί μέχρι στιγμής επικεντρώνονται στη γυροσκοπική μέθοδο συμπύκνωσης και τα αποτελέσματα συσχέτισης έχουν δείξει ότι η γυροσκοπική μέθοδος συμπύκνωσης δεν είναι αντιπροσωπευτική της συμπύκνωσης στο πεδίο.

2.2 Σχεδιασμός και υλοποίηση πειραματικών ερευνών

Με βάση τα ευρήματα της βιβλιογραφικής ανασκόπησης, πραγματοποιήθηκε σχεδιασμός και υλοποίηση πειραματικών ερευνών τόσο στο πεδίο όσο και στο εργαστήριο. Σκοπός των συνδυασμένων συστηματικών διερευνήσεων στο εργαστήριο και στο πεδίο ήταν η αξιολόγηση της συμπεριφοράς ασφαλτομιγμάτων διαφόρων τύπων υπό την έννοια της κοκκομετρικής διαβάθμισης, του ονομαστικού μέγιστου κόκκου του μίγματος των αδρανών, του ποσοστού και τύπου ασφάλτου, καθώς και της στρώσης, δηλαδή διερευνήθηκαν μίγματα επιφανειακής, συνδετικής και ασφαλτικής βάσης, ενώ

για την αξιολόγηση της συμπεριφοράς τους χρησιμοποιήθηκαν παραδοσιακές μέθοδοι αλλά και σύγχρονες μη καταστρεπτικές μέθοδοι.

Στο πλαίσιο αυτό υλοποιήθηκε κατασκευή πειραματικών τμημάτων ασφαλτικών οδοστρωμάτων (trial sections) για τις ανάγκες της έρευνας, η οποία περιέλαβε τη διάστρωση και τη συμπύκνωση με συμβατικές εφαρμοζόμενες μεθόδους διαφόρων τύπων ασφαλτομιγμάτων, των οποίων η σύνθεση πραγματοποιήθηκε μέσω της μεθόδου Marshall. Κατά τη διάρκεια της κατασκευής έγινε συλλογή στοιχείων από επιτόπου καταγραφές με μη καταστρεπτικές μεθόδους (Non Destructive Testing: NDT) για τη διερεύνηση της συμπεριφοράς των ασφαλτομιγμάτων στο έργο, καθώς και δειγματοληψίες ασφαλτικών πυρήνων οι οποίοι χρησιμοποιήθηκαν ως αναφορά για τη συγκριτική αξιολόγηση των εργαστηριακών μεθόδων και της επιτόπου συμπύκνωσης. Επίσης, πραγματοποιήθηκαν δειγματοληψίες χαλαρού ασφαλτομίγματος, το οποίο χρησιμοποιήθηκε για την υλοποίηση των πειραματικών ερευνών μέσω των εργαστηριακών μεθόδων συμπύκνωσης, δηλαδή της κρουστικής, της γυροσκοπικής και της συμπύκνωσης με κύλινδρο. Ειδικότερα, όσον αφορά στα εργαστηριακά πειράματα θα πρέπει να αναφερθεί ότι έγιναν διερευνήσεις και ως προς τις λειτουργικές παραμέτρους κάθε μεθόδου. Στο πλαίσιο αυτό επιλέχθηκαν βασικές παράμετροι, όπως η θερμοκρασία, η γωνία περιστροφής, η διάμετρος των δοκιμίων, ο αριθμός των διελεύσεων και η λειτουργία συμπύκνωσης (εφαρμογή στατικής φόρτισης ή σε συνδυασμό με δόνηση), για τη διαμόρφωση ποικίλλων μεθοδολογιών συμπύκνωσης για κάθε εργαστηριακή μέθοδο και τα συμπυκνωμένα δοκίμια υποβλήθηκαν σε ελέγχους ως προς τα βασικά χαρακτηριστικά συμπεριφοράς τους. Ειδικότερα, στόχο των παραμετρικών διερευνήσεων αποτέλεσε η αξιολόγηση της επίδρασης τους ως προς τη συμπυκνωσιμότητα, τη δυσκαμψία, την ανθεκτικότητα σε παραμένουσες παραμορφώσεις, την εσωτερική δομή, καθώς και την αντιολισθητική ικανότητα των ασφαλτομιγμάτων.

2.3 Ανάλυση πειραματικών δεδομένων

Η μεθοδολογική προσέγγιση που ακολουθήθηκε περιέλαβε επίσης την ανάλυση των πειραματικών δεδομένων των συνδυασμένων διερευνήσεων στο εργαστήριο και στο

πεδίο για κάθε επιμέρους ενότητα. Για το σκοπό αυτό χρησιμοποιήθηκαν μέθοδοι περιγραφικής στατιστικής, παλινδρόμησης, καθώς και ανάλυσης διακύμανσης (ANOVA) για επίπεδο εμπιστοσύνης 95%, ενώ με βάση τη σύνθεση των ευρημάτων δόθηκαν απαντήσεις σχετικά με τον κύριο στόχο της Διατριβής.

3. ΕΥΡΗΜΑΤΑ ΠΕΙΡΑΜΑΤΙΚΩΝ ΔΙΕΡΕΥΝΗΣΕΩΝ

3.1 Συμπυκνωσιμότητα

Για την αξιολόγηση της συμπυκνωσιμότητας χρησιμοποιήθηκαν δύο δείκτες: α) η κλίση της καμπύλης ημι-λογαριθμικής μορφής (σύμφωνα με τα ευρωπαϊκά πρότυπα) του ποσοστού κενών αέρα σε σχέση με την ενέργεια συμπύκνωσης (δηλαδή τον αριθμό περιστροφών ή διελεύσεων) και β) ο αριθμός περιστροφών/ διελεύσεων που αντιστοιχεί σε συγκεκριμένο ποσοστό κενών αέρα. Από τις σχετικές αναλύσεις των πειραματικών δεδομένων στο εργαστήριο, όσον αφορά στη γυροσκοπική μέθοδο προέκυψε ότι η επιρροή της γωνίας περιστροφής και της γεωμετρίας των δοκιμίων στο επίπεδο συμπύκνωσης είναι στατιστικά σημαντική, ενώ για την περίπτωση της μεθόδου με κύλινδρο στατιστικά σημαντική προέκυψε η επιρροή της θερμοκρασίας και του αριθμού διελεύσεων. Αντίστοιχα, προσδιορίσθηκαν οι δείκτες συμπυκνωσιμότητας με βάση τα πειραματικά δεδομένα συμπύκνωσης των μιγμάτων στο πεδίο. Από τη συγκριτική αξιολόγηση μεταξύ εργαστηρίου και πεδίου προέκυψαν διαφορετικά χαρακτηριστικά συμπυκνωσιμότητας και ως εκ τούτου δε μπορεί να γίνει αξιόπιστη εκτίμηση των επιτόπου χαρακτηριστικών μέσω των εργαστηριακών δοκιμών συμπύκνωσης.

Συνέπεια των προαναφερθέντων ευρημάτων αποτέλεσε η ανάγκη διερεύνησης της δυνατότητας αξιολόγησης της επιτόπου συμπυκνωσιμότητας μέσω μη καταστρεπτικών δοκιμών, σύμφωνα και με τη σύγχρονη αντίληψη για την αξιολόγηση των οδοστρωμάτων. Στο πλαίσιο της υπόψη έρευνας διερευνήθηκαν οι μέθοδοι της Υπέρυθρης θερμογραφίας και της γεωφυσικής μεθόδου GPR (Ground Penetrating Radar).

Αρχικά, μέσω της μεθόδου της Υπέρυθρης θερμογραφίας διερευνήθηκε η επιρροή της θερμοκρασίας και ενέργειας συμπύκνωσης στο βαθμό συμπύκνωσης. Από την ανάλυση των πειραματικών δεδομένων προέκυψε ότι η θερμοκρασία συμπύκνωσης έχει σημαντική επίδραση στην αύξηση του βαθμού συμπύκνωσης, συνεπώς θα μπορούσε να αναπτυχθεί σχέση που να περιγράφει την πυκνότητα ως συνάρτηση της θερμοκρασίας και της ενέργειας συμπύκνωσης λαμβάνοντας υπόψη τη μέθοδο της Υπέρυθρης θερμογραφίας.

Επίσης, μέσω της μεθόδου GPR και της διηλεκτρικής σταθεράς ε_{HMA} του ασφαλτομίγματος, η οποία προσδιορίζεται μέσω της ανάλυσης των γεωφυσικών δεδομένων συλλογής με κεραία συγκεκριμένης συχνότητας, διερευνήθηκε η επιρροή της μεθοδολογίας συμπύκνωσης στο βαθμό συμπύκνωσης. Από την ανάλυση των πειραματικών δεδομένων που συλλέχθηκαν στο πλαίσιο των εργασιών διάστρωσης-συμπύκνωσης ασφαλτομιγμάτων με διάφορες, συνήθεις στην πράξη, μεθοδολογίες συμπύκνωσης προέκυψε διαφοροποίηση ως προς τη μεταβολή της διηλεκτρικής σταθεράς του ασφαλτομίγματος σε σχέση με τον αριθμό των διελεύσεων των οδοστρωτήρων. Το εύρημα αυτό αποκτά ιδιαίτερη αξία στην περίπτωση κατά την οποία θα μπορούσε, μέσω της διηλεκτρικής σταθεράς του ασφαλτομίγματος, να προσδιορισθεί η επιτόπου πυκνότητα, η οποία αποτελεί μέτρο συμπυκνωσιμότητας και απαίτηση της κατασκευής. Για το σκοπό αυτό, αρχικά, ενεργοποιήθηκαν μοντέλα πρόβλεψης που βασίζονται στην ηλεκτρομαγνητική θεωρία (δηλαδή CRIM, Rayleigh and ALL) σε συνδυασμό με τη χρήση περιορισμένου αριθμού πυρήνων για λόγους βαθμονόμησης, τα οποία εκτιμούν την πυκνότητα των ασφαλτομιγμάτων ως συνάρτηση των διηλεκτρικών ιδιοτήτων του ασφαλτομίγματος και των συστατικών του. Από τις σχετικές αναλύσεις προέκυψε ότι μέσω του μοντέλου πρόβλεψης ALL μπορεί να γίνει πρόβλεψη της επιτόπου πυκνότητας με ικανοποιητική ακρίβεια.

Με βάση τα ενθαρρυντικά αποτελέσματα των προκαταρκτικών διερευνήσεων έγινε περαιτέρω έρευνα για την αξιολόγηση της επιτόπου πυκνότητας μέσω της μεθόδου GPR αλλά και της μεθόδου PQI (που χρησιμοποιείται διεθνώς) ως προς το σφάλμα εκτίμησης τους σε σχέση με την πυκνότητα αναφοράς των πυρήνων. Ειδικότερα, ως προς τη

μέθοδο GPR διερευνήθηκαν συγκριτικά διάφορα μοντέλα πρόβλεψης της επιτόπου πυκνότητας, καθώς και η επιρροή του αριθμού των πυρήνων βαθμονόμησης και της συχνότητας της κεραίας στην ακρίβεια πρόβλεψης. Από τις αναλύσεις προέκυψε ότι αριθμός 3 πυρήνων είναι επαρκής για λόγους βαθμονόμησης των μοντέλων πρόβλεψης, το μικρότερο σφάλμα εκτίμησης επιτυγχάνεται με χρήση κεραίας συχνότητας 2 Ghz, ενώ ικανοποιητική ακρίβεια στην εκτίμηση της επιτόπου πυκνότητας ασφαλτομιγμάτων επιτυγχάνεται μέσω των αλγορίθμων PANK και ALL, σύμφωνα με το Σχήμα 1.

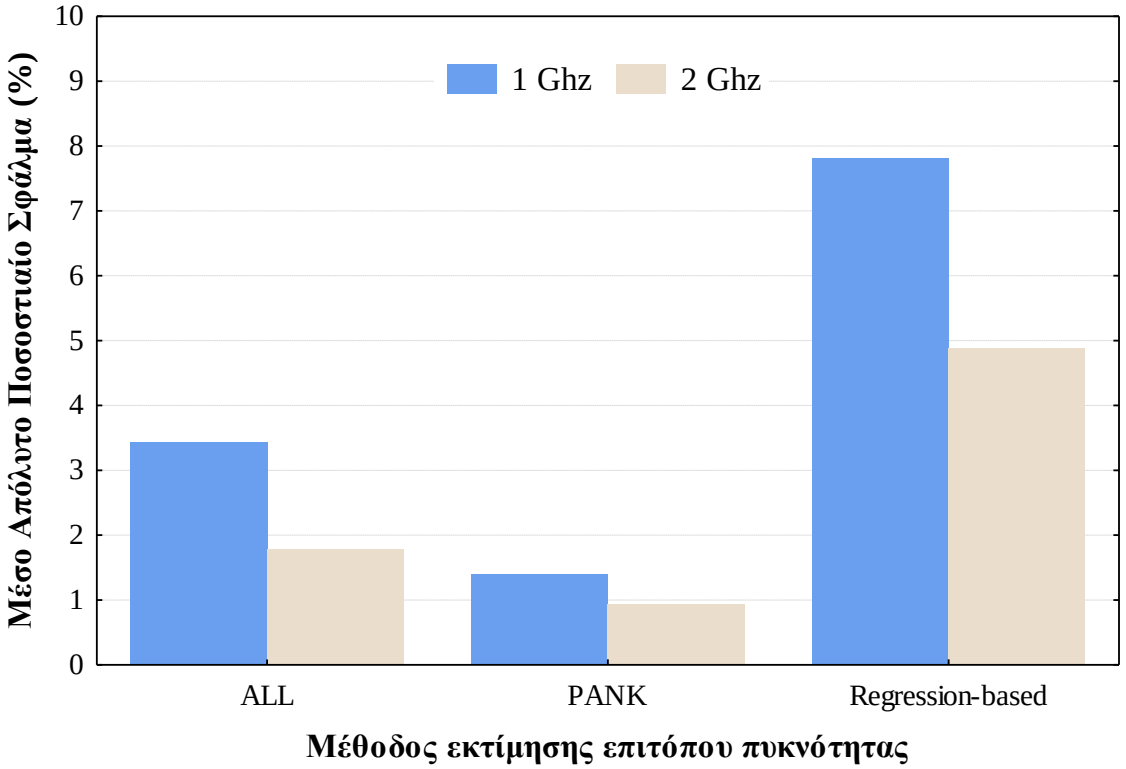

Σχήμα 1. Σφάλμα εκτίμησης σε σχέση με τα μοντέλα πρόβλεψης και τη συχνότητα της κεραίας του συστήματος GPR.

Επιπλέον, λαμβάνοντας υπόψη ευρήματα της έρευνας αυτής που έδειξαν ότι η θερμοκρασία έχει σημαντική επιρροή στην αύξηση της πυκνότητας, διερευνήθηκε αν μπορεί να επιτευχθεί ικανοποιητική εκτίμηση της επιτόπου πυκνότητας μέσω εξίσωσης που υπάρχει στη βιβλιογραφία, η οποία περιγράφει την πυκνότητα ως συνάρτηση της μεταβολής της θερμοκρασίας του ασφαλτομίγματος και του αριθμού των διελεύσεων των οδοστρωτήρων. Στο πλαίσιο αυτό έγινε προσπάθεια προσαρμογής, στη σχέση αυτή,

πειραματικών δεδομένων συμπύκνωσης ασφαλτομίγματος στο πεδίο, όπως φαίνεται στο Σχήμα 2.

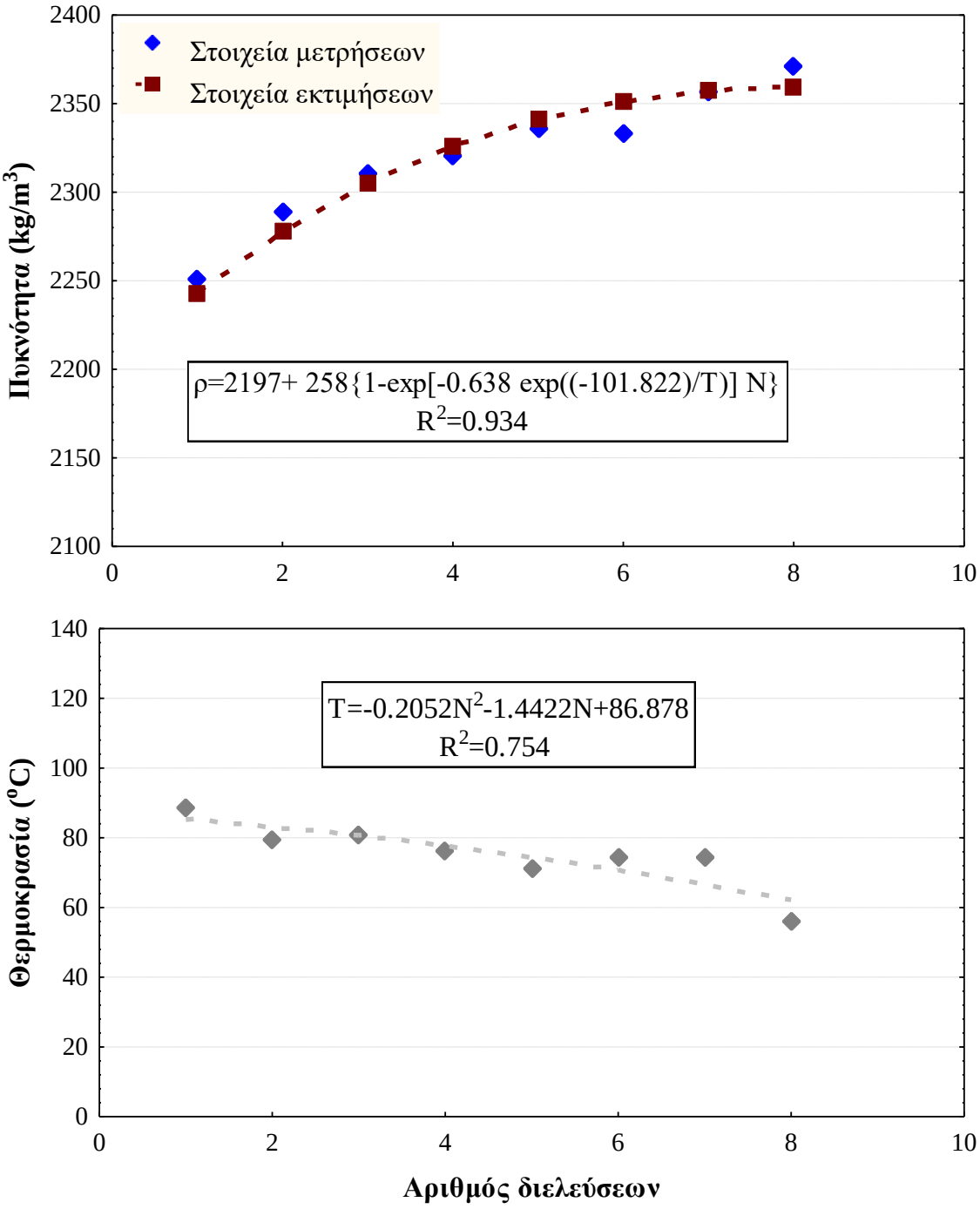

Σχήμα 2. Επιρροή θερμοκρασίας ασφαλτομίγματος και αριθμού διελεύσεων οδοστρωτήρων στη μεταβολή της επιτόπου πυκνότητας.

Μέσω της προσέγγισης αυτής βρέθηκε ότι το σφάλμα εκτίμησης είναι εξαιρετικά χαμηλό (της τάξης του 0.03%). Κατά συνέπεια θα μπορούσε να γίνει εκτίμηση της επιτόπου πυκνότητας μέσω της ανάπτυξης σχέσεων της πυκνότητας συναρτήσει της θερμοκρασίας και του αριθμού των διελεύσεων.

3.2 Δυσκαμψία

Πεδίο διερεύνησης αποτέλεσε επίσης ο έλεγχος των μηχανικών ιδιοτήτων των ασφαλτομιγμάτων, μεταξύ άλλων και της δυσκαμψίας τους μέσω της μεθόδου έμμεσου εφελκυσμού ITSM (Indirect Tensile Stiffness Modulus) σύμφωνα με τις ευρωπαϊκές νόρμες. Μέσω των ελέγχων που πραγματοποιήθηκαν αρχικά διερευνήθηκε η επιρροή των παραμέτρων εργαστηριακής συμπύκνωσης στη δυσκαμψία των ασφαλτομιγμάτων. Από τα ευρήματα προέκυψε ότι όσον αφορά στην κρουστική συμπύκνωση, η αύξηση της θερμοκρασίας συμπύκνωσης οδηγεί στην αύξηση της δυσκαμψία των ασφαλτομιγμάτων και η μεταβολή αυτή είναι στατιστικά σημαντική για επίπεδο εμπιστοσύνης 95%. Όσον αφορά στη γυροσκοπική συμπύκνωση, παρατηρείται μείωση της δυσκαμψίας με την αύξηση της θερμοκρασίας συμπύκνωσης στα συμβατικά ασφαλτομίγματα, ενώ η μικρότερη δυσκαμψία αντιστοιχεί στη γωνία 1.45^{o} και η μεγαλύτερη στη γωνία 1.16^{o} η οποία προδιαγράφεται στα αμερικάνικα πρότυπα. Επίσης, η επιρροή της διαμέτρου στη δυσκαμψία των ασφαλτομιγμάτων είναι στατιστικά σημαντική με τα δοκίμια διαμέτρου 100 mm να εμφανίζουν μεγαλύτερη δυσκαμψία σε σχέση με τα αρχικής διαμέτρου 150 mm. Όσον αφορά στη μέθοδο με κύλινδρο, η δυσκαμψία επηρεάζεται σημαντικά από τη θερμοκρασία και τον αριθμό των διελεύσεων, ενώ αντίθετα η μεθοδολογία συμπύκνωσης δε φαίνεται να έχει σαφή επίδραση.

Πραγματοποιήθηκε επίσης συγκριτική αξιολόγηση μεταξύ των μεθόδων εργαστηριακής και επιτόπου συμπύκνωσης λαμβάνοντας υπόψη και το επίπεδο συμπύκνωσης που επιτεύχθηκε για κάθε μέθοδο. Με βάση τα πειραματικά δεδομένα προέκυψε ότι για παρόμοιο επίπεδο συμπύκνωσης τα δοκίμια γυροσκοπικής συμπύκνωσης εμφανίζουν γενικά υπερ-διπλάσιες τιμές δυσκαμψίας σε σχέση με τους πυρήνες, όπως φαίνεται στο Σχήμα 3. Επίσης, τα δοκίμια κρουστικής συμπύκνωσης παρά το γεγονός ότι έχουν

υψηλότερο ποσοστό κενών αέρα σε σχέση με τους πυρήνες εμφανίζουν ωστόσο μεγαλύτερες τιμές δυσκαμψίας. Αντίθετα, τα δοκίμια συμπύκνωσης με κύλινδρο και οι πυρήνες εμφανίζουν συγκρίσιμες τιμές δυσκαμψίας αν ληφθούν υπόψη οι διαφορές τους ως προς το επίπεδο συμπύκνωσης.

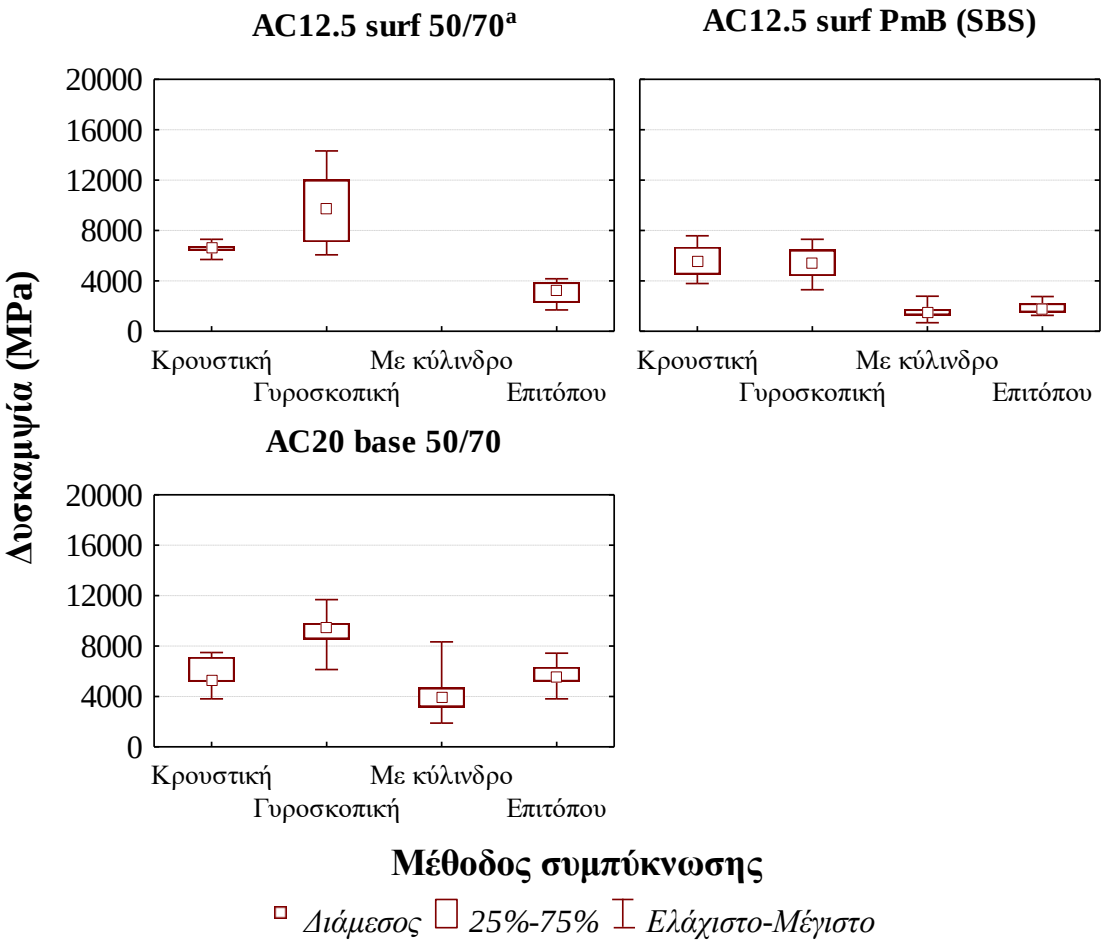

Σχήμα 3. Δυσκαμψία σε σχέση με τη μέθοδο συμπύκνωσης.

Επιπλέον, έγινε προκαταρκτική διερεύνηση της επίδρασης των μέτρων δυσκαμψίας με τις διάφορες μεθόδους συμπύκνωσης στην ανάλυση οδοστρωμάτων. Στο πλαίσιο αυτό έγινε ανάλυση τυπικής διατομής, η οποία περιλαμβάνει τα ασφαλτομίγματα που ελέγχθηκαν και υπολογίστηκαν τα παραμορφωσιακά μεγέθη στις κρίσιμες θέσεις του οδοστρώματος, δηλαδή στον πυθμένα των ασφαλτικών στρώσεων και στην επιφάνεια της στρώσης έδρασης. Από τα αποτελέσματα της ανάλυσης προέκυψε ότι οι μέθοδοι

κρουστικής και γυροσκοπικής συμπύκνωσης υποεκτιμούν τα κρίσιμα παραμορφωσιακά μεγέθη της κατασκευασθείσας διατομής, Αντίθετα, μέσω της συμπύκνωσης με κύλινδρο υπερεκτιμώνται τα κρίσιμα μεγέθη και ως εκ τούτου η προσέγγιση αυτή θα μπορούσε να θεωρηθεί συντηρητική (υπέρ της ασφαλείας) στο πλαίσιο της πρόβλεψης της διάρκειας ζωής έναντι κόπωσης των ασφαλτικών στρώσεων σε σχέση με τη συμπεριφορά της κατασκευασθείσας διατομής. Τα ευρήματα αυτά οδηγούν στην ανάγκη προσδιορισμού συντελεστών μετατροπής με βάση το λόγο των τιμών δυσκαμψίας των εργαστηριακών μεθόδων ως προς τις τιμές δυσκαμψίας της επιτόπου συμπύκνωσης, σύμφωνα με το Σχήμα 4.

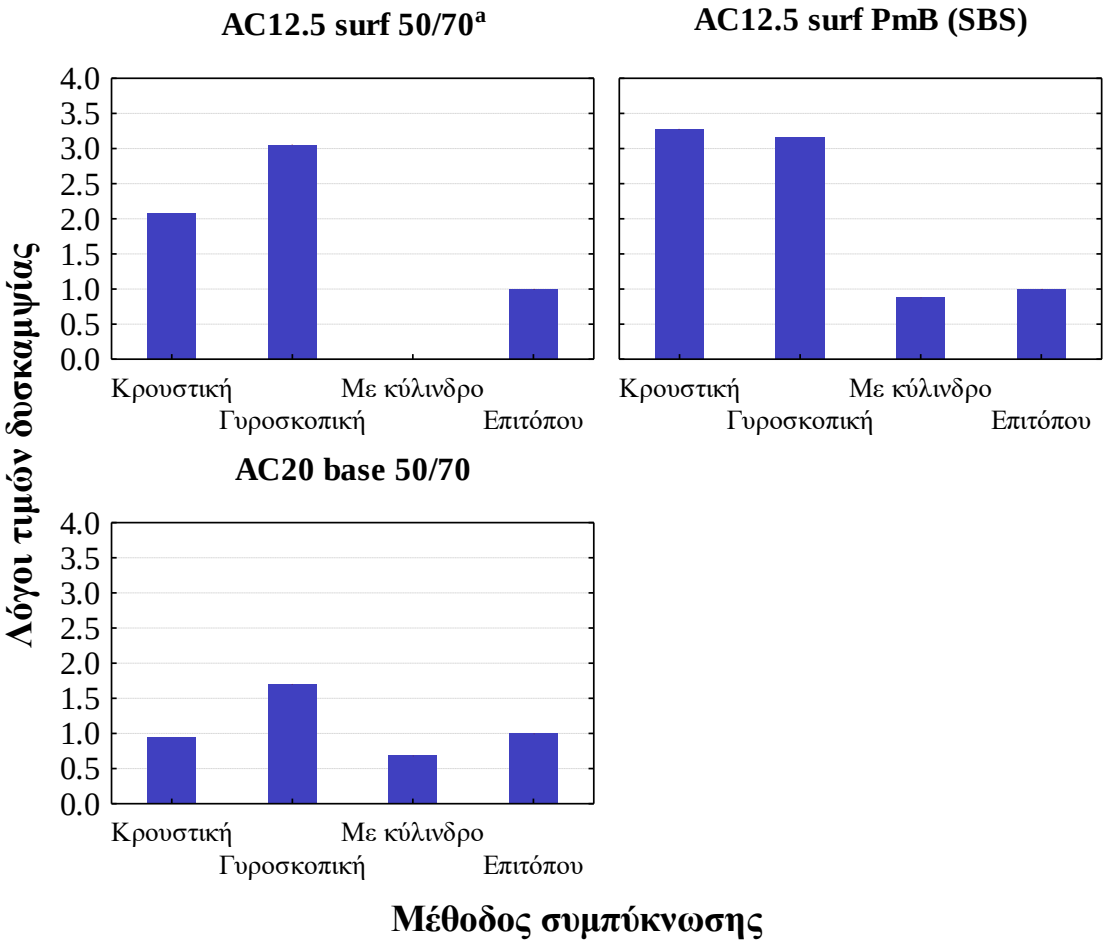

Σχήμα 4. Λόγοι τιμών δυσκαμψίας εργαστηριακής και επιτόπου συμπύκνωσης.

3.3 Ανθεκτικότητα σε παραμένουσες παραμορφώσεις

Τα δοκίμια εργαστηριακής και επιτόπου συμπύκνωσης ελέγχθηκαν επίσης ως προς την ανθεκτικότητα τους σε παραμένουσες παραμορφώσεις μέσω της δοκιμής έμμεσης εφελκυστικής αντοχής ITS (Indirect Tensile Strength) σε υψηλή θερμοκρασία ελέγχου 50^{o}C. Σκοπός των ελέγχων ήταν αφενός η διερεύνηση της επιρροής των παραμέτρων εργαστηριακής συμπύκνωσης στη συμπεριφορά των ασφαλτομιγμάτων, από τις οποίες προέκυψαν σε γενικές γραμμές παρόμοια ευρήματα με τη δυσκαμψία, καθώς και η συγκριτική αξιολόγηση μεταξύ εργαστηριακών μεθόδων και επιτόπου συμπύκνωσης.

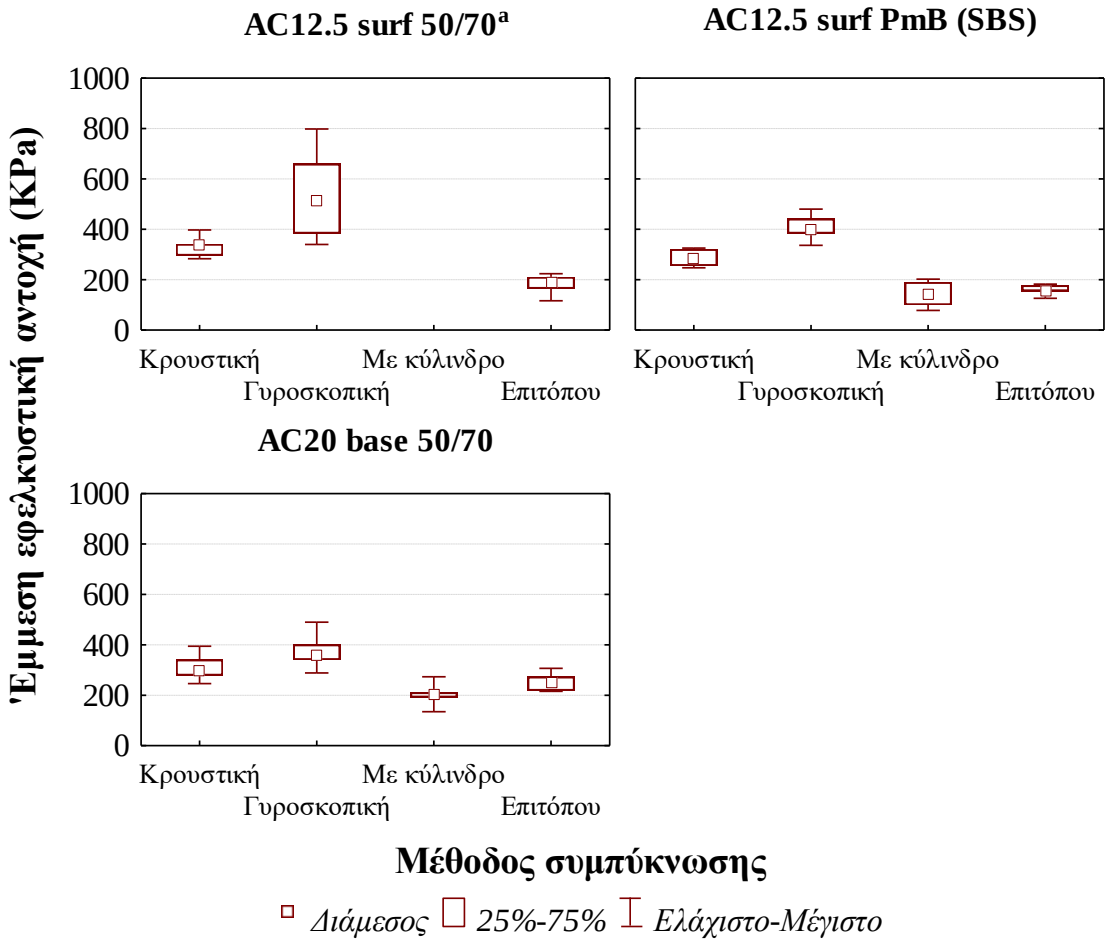

Σχήμα 5. Ανθεκτικότητα σε παραμένουσες παραμορφώσεις σε σχέση με τη μέθοδο συμπύκνωσης.

Αξίζει να σημειωθεί ότι, από την υπόψη διερεύνηση προέκυψε ότι η κρουστική και γυροσκοπική μέθοδος συμπύκνωσης παράγουν δοκίμια μεγαλύτερης ανθεκτικότητας σε παραμένουσες παραμορφώσεις (με συντελεστή της τάξης του 1.6 και 2.2, αντίστοιχα) συγκριτικά με την επιτόπου συμπύκνωση. Αντίθετα, τα δοκίμια συμπύκνωσης με κύλινδρο και οι πυρήνες εμφανίζουν παρόμοια συμπεριφορά, όπως φαίνεται στο Σχήμα 5.

3.4 Εσωτερική δομή

Αναγνωρίζοντας ότι μέσω των παραδοσιακών μεθόδων δε μπορεί να εξηγηθούν οι διαφορές στα χαρακτηριστικά συμπεριφοράς των ασφαλτομιγμάτων λόγω των μεθόδων συμπύκνωσης, διερευνήθηκε επίσης η εσωτερική δομή (internal structure) των ασφαλτομιγμάτων μέσω σύγχρονων τεχνικών ανάλυσης ψηφιακής εικόνας (image analysis). Ειδικότερα, μέσω της σάρωσης οριζόντιων τομών των δοκιμίων ασφαλτομιγμάτων και της εφαρμογής κατάλληλων φίλτρων επεξεργασίας έγινε ποσοτικοποίηση των χαρακτηριστικών της εσωτερικής δομής.

Αρχικά, διερευνήθηκε η επιρροή των παραμέτρων των εργαστηριακών μεθόδων συμπύκνωσης σε δείκτες χαρακτηρισμού της εσωτερικής δομής των μιγμάτων, οι οποίοι σχετίζονται με τα σημεία επαφής (δηλαδή αριθμός επαφών (CP), μήκος επαφής (CL), μήκος επαφής αδρανών σε διακλάδωση (CLB)), τον προσανατολισμό (επικρατούσα γωνία δ και τάση Α προσανατολισμού υπό συγκεκριμένη γωνία) και τον διαχωρισμό (χωρική κατανομή (S_L)) των αδρανών. Από την αξιολόγηση της επιρροής των παραμέτρων συμπύκνωσης, όσον αφορά στην κρουστική συμπύκνωση προέκυψε ότι η θερμοκρασία συμπύκνωσης δεν επιδρά σημαντικά στους δείκτες εσωτερικής δομής. Όσον αφορά στη γυροσκοπική συμπύκνωση, η διάμετρος και η γωνία περιστροφής επηρεάζουν τις επαφές και τον προσανατολισμό των αδρανών, ενώ η επιρροή της θερμοκρασίας συμπύκνωσης περιορίζεται στις επαφές των αδρανών. Όσον αφορά στη μέθοδο με κύλινδρο, η θερμοκρασία και η ενέργεια συμπύκνωσης επηρεάζουν τα χαρακτηριστικά εσωτερικής δομής, αντίθετα η μεθοδολογία συμπύκνωσης δε φαίνεται να έχει κάποια επιρροή.

Από τη συγκριτική αξιολόγηση μεταξύ των δοκιμίων εργαστηριακής και επιτόπου συμπύκνωσης προκύπτει ότι οι επαφές μεταξύ των αδρανών όπως διαμορφώνονται στο πεδίο μέσω της επιτόπου συμπύκνωσης προσεγγίζονται καλύτερα στο εργαστήριο με τη γυροσκοπική μέθοδο και σε μικρότερο βαθμό με τη συμπύκνωση με κύλινδρο, όπως φαίνεται στο Σχήμα 6. Αντίστοιχα ευρήματα προέκυψαν και όσον αφορά στην επικρατούσα γωνία προσανατολισμού, σύμφωνα με το Σχήμα 7. Ως προς το διαχωρισμό των αδρανών προέκυψε, με βάση το Σχήμα 8, ότι η χωρική κατανομή των αδρανών στους πυρήνες προσομοιάζεται καλύτερα μέσω της συμπύκνωσης με κύλινδρο.

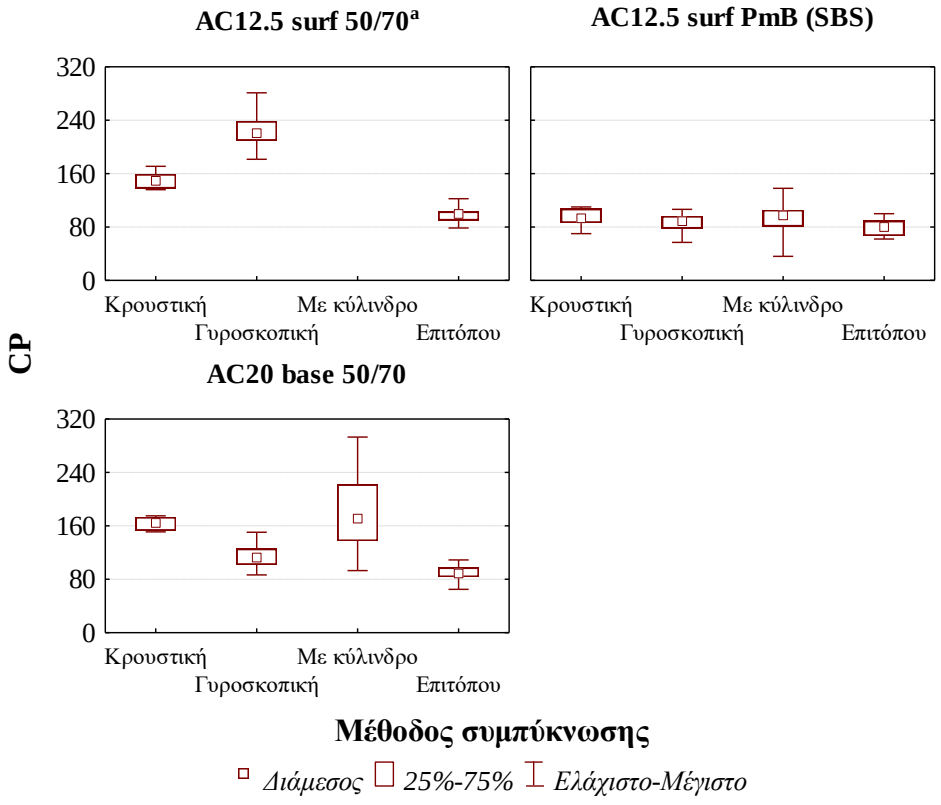

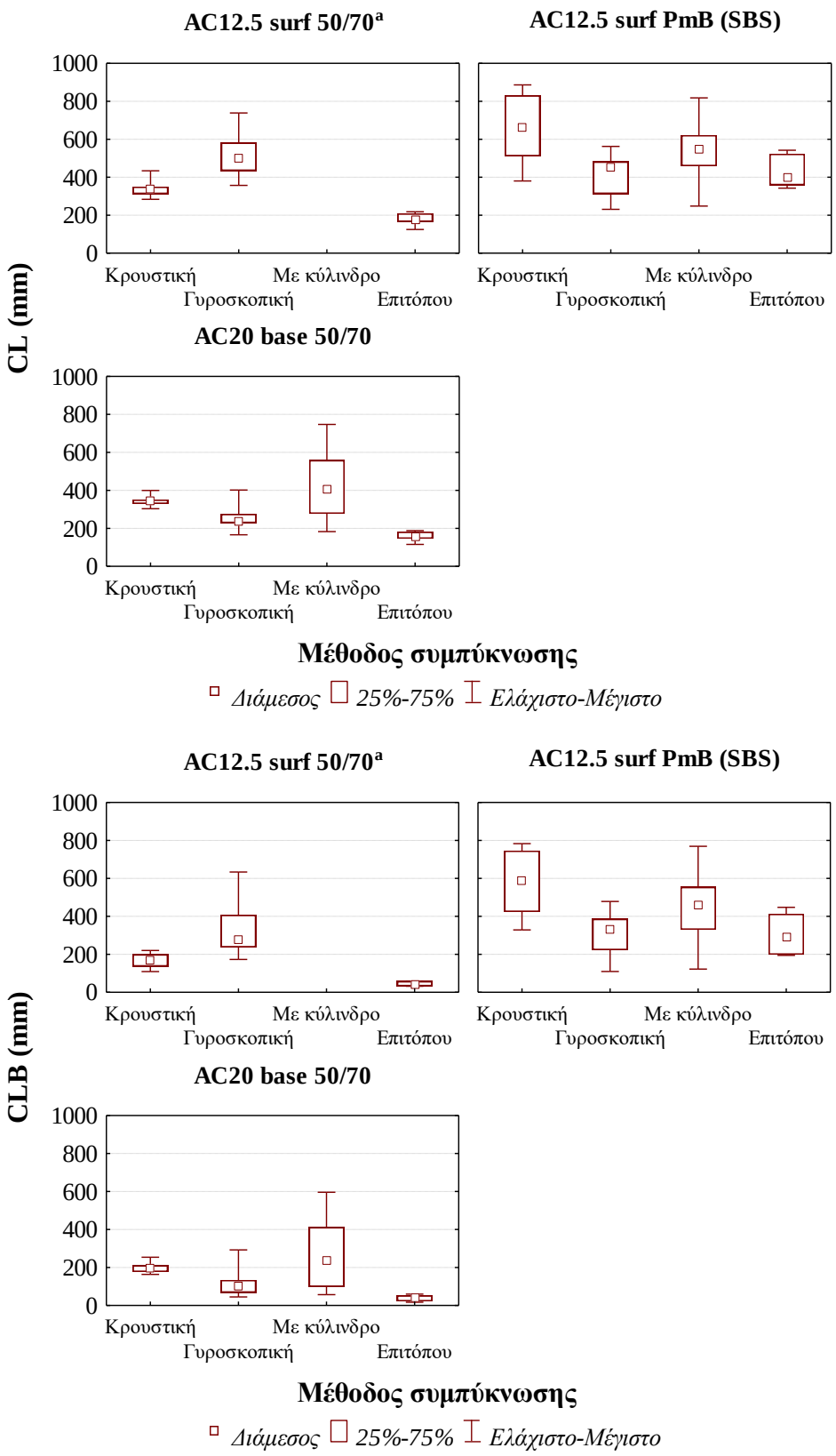

Σχήμα 6. Δείκτες επαφών αδρανών σε σχέση με τη μέθοδο συμπύκνωσης.

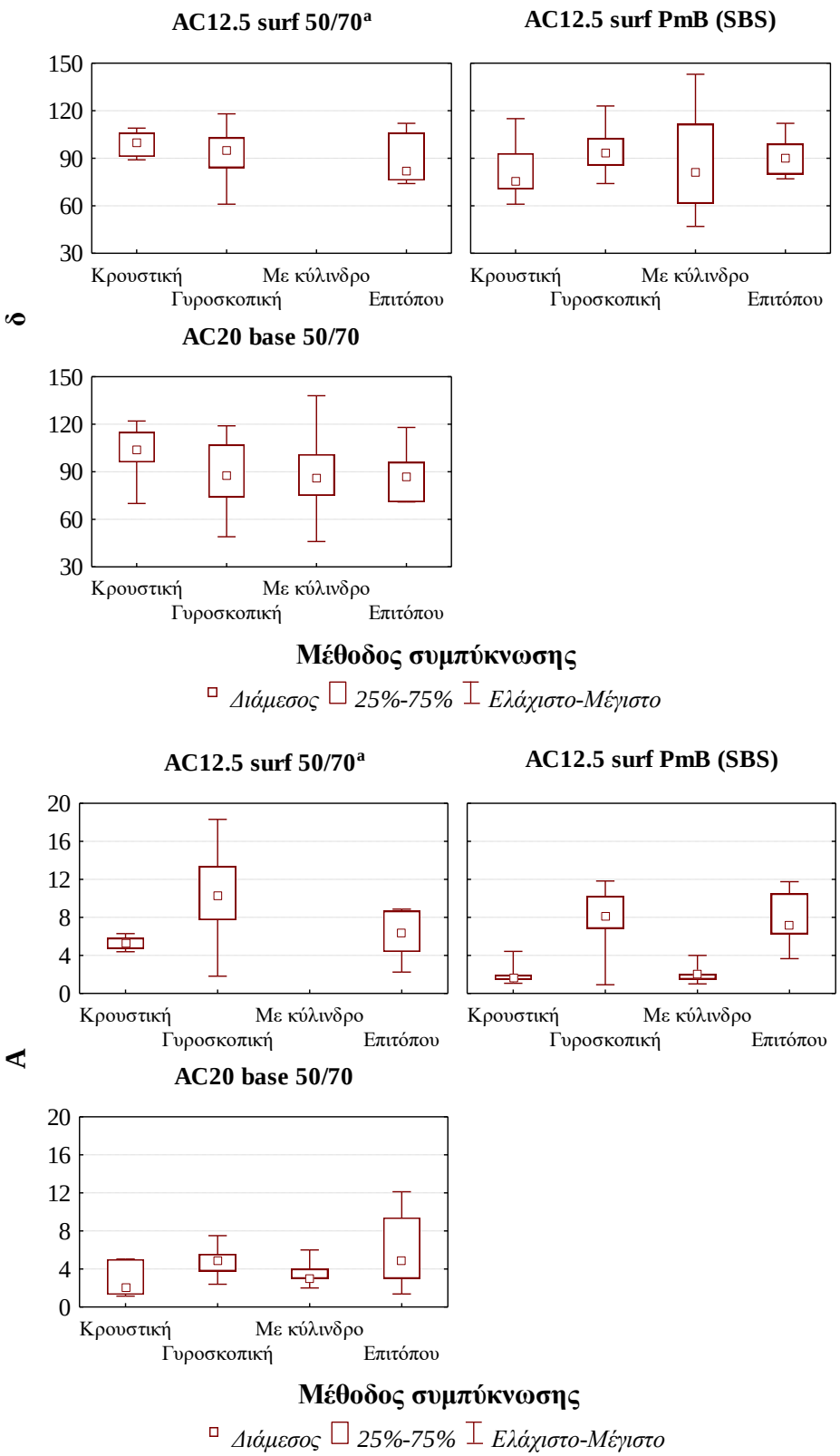

Σχήμα 7. Δείκτες προσανατολισμού αδρανών σε σχέση με τη μέθοδο συμπύκνωσης.

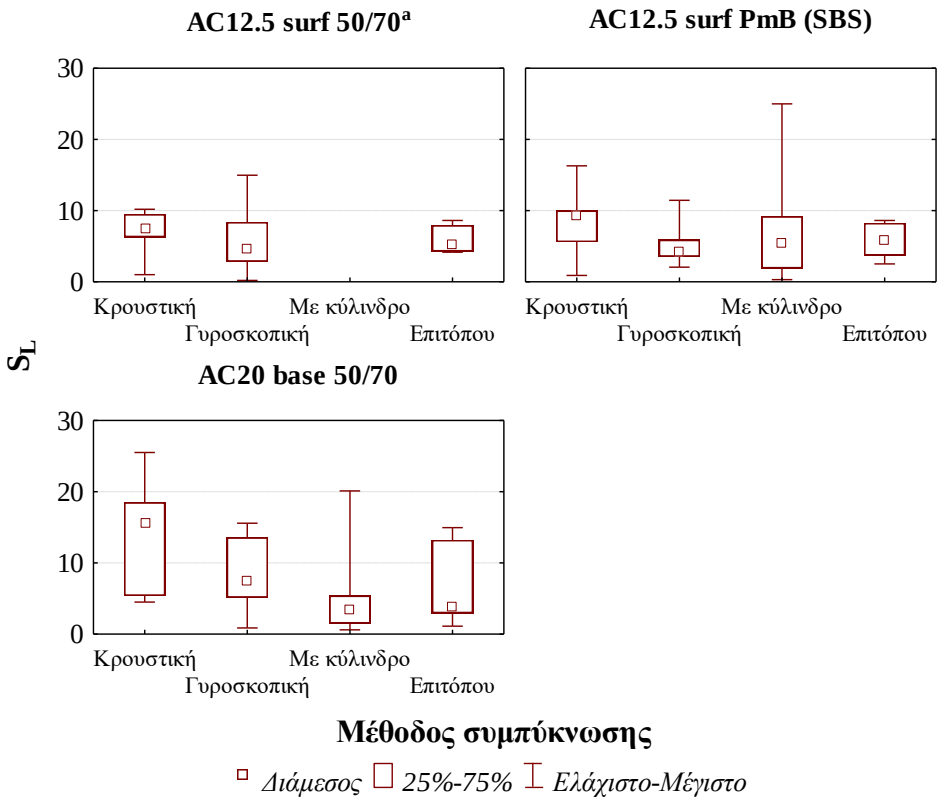

Σχήμα 8. Δείκτης διαχωρισμού αδρανών σε σχέση με τη μέθοδο συμπύκνωσης.

Επιπλέον, έγινε προσπάθεια αναζήτησης διαδικασιών συμπύκνωσης, για κάθε επιμέρους εργαστηριακή μέθοδο, για τις οποίες επιτυγχάνεται καλύτερη προσέγγιση των επιτόπου συνθηκών ως προς την εσωτερική δομή. Στο πλαίσιο αυτό θα πρέπει να αναφερθεί ότι για την περίπτωση της κρουστικής συμπύκνωσης προσέγγιση της επιτόπου συμπύκνωσης προκύπτει για θερμοκρασία συμπύκνωσης 135^{o}C για τα συμβατικά ασφαλτομίγματα, ενώ ελαφρώς υψηλότερη για τα τροποποιημένα με ελαστομερή άσφαλτο. Όσον αφορά στη γυροσκοπική συμπύκνωσης προσομοίωση των επιτόπου συνθηκών επιτυγχάνεται για συνδυασμό υψηλής γωνίας περιστροφής 1.45^{o} και αρχικής διαμέτρου δοκιμίου 150 mm, ενώ όσον αφορά στη μέθοδο με κύλινδρο διάφοροι συνδυασμοί θερμοκρασίας και αριθμού διελεύσεων προσεγγίζουν ικανοποιητικά τις επιτόπου συνθήκες.

3.5 Σχέση εσωτερικής δομής και μηχανικών ιδιοτήτων ασφαλτομιγμάτων

Τα αποτελέσματα των συνδυασμένων διερευνήσεων των χαρακτηριστικών εσωτερικής δομής και των μηχανικών χαρακτηριστικών αξιοποιήθηκαν περαιτέρω για την αξιολόγηση της επιρροής των δεικτών εσωτερικής δομής στη δυσκαμψία και την ανθεκτικότητα σε παραμένουσες παραμορφώσεις. Από τις σχετικές αναλύσεις προέκυψε ότι οι δείκτες που σχετίζονται με την αλληλοεμπλοκή των αδρανών επιδρούν σημαντικά στη δυσκαμψία των δοκιμίων γυροσκοπικής μεθόδου και συμπύκνωσης με κύλινδρο, σύμφωνα με τα στοιχεία του Πίνακα 1. Θα πρέπει επίσης να επισημανθεί ότι μικρή αύξηση στις επαφές μεταξύ των αδρανών οδηγεί σε σημαντική αύξηση της δυσκαμψίας των δοκιμίων γυροσκοπικής συμπύκνωσης.

Πίνακας 1. Ανάλυση διακύμανσης (p-values) δυσκαμψίας και δεικτών εσωτερικής δομής για όλες τις μεθόδους συμπύκνωσης.

Μέθοδος συμπύκνωσης	CP	CL	CLB	δ	A	S_L
Κρουστική	.631	.958	.876	.270	.221	.657
Γυροσκοπική	.000	.030	.047	.129	.104	.478
Με κύλινδρο	.000	.374	.535	.296	.568	.902
Επιτόπου	.264	.384	.696	.857	.496	.879

Πίνακας 2. Ανάλυση διακύμανσης (p-values) ανθεκτικότητας σε παραμένουσες παραμορφώσεις και δεικτών εσωτερικής δομής για όλες τις μεθόδους συμπύκνωσης.

Μέθοδος συμπύκνωσης	CP	CL	CLB	δ	A	S_L
Κρουστική	.522	.693	.659	.332	.478	.803
Γυροσκοπική	.010	.343	.093	.208	.888	.613
Με κύλινδρο	.003	.678	.950	.003	.312	.164
Επιτόπου	.129	.441	.649	.835	.966	.678

Αντίστοιχη διαδικασία ακολουθήθηκε και ως προς την ανθεκτικότητα σε παραμένουσες παραμορφώσεις και προέκυψαν αντίστοιχα ευρήματα. Συγκεκριμένα, οι επαφές μεταξύ των αδρανών έχουν σημαντική επιρροή, ενώ για την περίπτωση των δοκιμίων συμπύκνωσης με κύλινδρο σημαντική είναι επίσης και η επίδραση του προσανατολισμού των αδρανών, σύμφωνα με τα στοιχεία του Πίνακα 2.

3.6 Αντιολισθητική ικανότητα

Οι Υπηρεσίες οδοστρωμάτων, διεθνώς, προδιαγράφουν ποιοτικούς ελέγχους μετά την κατασκευή, οι οποίοι μεταξύ άλλων περιλαμβάνουν την αξιολόγηση της μακροϋφής σε σχέση με τις απαιτήσεις συμμόρφωσης. Παρά το γεγονός ότι η μακροϋφή έχει αναγνωρισθεί ότι συνεισφέρει σημαντικά στην αντιολισθητική ικανότητα των ασφαλτικών οδοστρωμάτων στη φάση λειτουργίας τους, μέχρι στιγμής δεν είναι διαθέσιμη οποιαδήποτε τυποποιημένη μέθοδος που να επιτρέπει την αξιόπιστη εκτίμηση των επιτόπου χαρακτηριστικών υφής της επιφάνειας μέσω εργαστηριακών δοκιμών. Ως εκ τούτου, πρέπει να αναπτυχθεί μια μεθοδολογία στο εργαστήριο μέσω της οποίας θα επιτυγχάνεται αξιόπιστη εκτίμηση των επιτόπου χαρακτηριστικών υφής στο εργαστήριο πριν την κατασκευή. Στο πλαίσιο αυτό, η εργαστηριακή μέθοδος συμπύκνωσης φαίνεται να αποτελεί καθοριστικό παράγοντα για να εξασφαλισθεί ότι τα μορφολογικά χαρακτηριστικά της επιφάνειας των δοκιμίων είναι αντιπροσωπευτικά αυτών που προκύπτουν με συμπύκνωση του ασφαλτομίγματος στο πεδίο.

Λαμβάνοντας υπόψη τα προγενέστερα ευρήματα της έρευνας αυτής, η υπόψη διερεύνηση επικεντρώθηκε στη μέθοδο συμπύκνωσης με κύλινδρο. Θα πρέπει να σημειωθεί ότι η κρουστική μέθοδος δεν επιλέχθηκε να συμπεριληφθεί στις πειραματικές διερευνήσεις συνέπεια αφενός της αδυναμίας της υπόψη μεθόδου να προσομοιάσει τη διαδικασία της συμπύκνωσης των οδοστρωτήρων στο έργο και αφετέρου του θρυμματισμού των αδρανών που δημιουργείται λόγω του μηχανισμού συμπύκνωσης. Ειδικότερα, θα πρέπει να αναφερθεί ότι ο θρυμματισμός των αδρανών που προκαλείται μέσω της κρουστικής συμπύκνωσης αντανακλάται στον αυξημένο αριθμό επαφών μεταξύ των αδρανών, συγκριτικά με τα δοκίμια επιτόπου συμπύκνωσης, γεγονός το οποίο πιστεύεται ότι έχει επιρροή στα χαρακτηριστικά μικροϋφής. Επίσης, παρατηρήθηκε ότι η μέθοδος αυτή προκαλεί χωρική ανισοκατανομή των αδρανών σε σχέση με την επιτόπου συμπύκνωση, η οποία πιστεύεται ότι επηρεάζει τα χαρακτηριστικά μακροϋφής. Με βάση τα παραπάνω κρίνεται ότι η κρουστική συμπύκνωση δε μπορεί να προσομοιάσει τα μορφολογικά χαρακτηριστικά της επιφάνειας των ασφαλτομιγμάτων με συμπύκνωση στο πεδίο. Αντίστοιχα, τα ευρήματα

των διερευνήσεων για τη γυροσκοπική συμπύκνωση κατέδειξαν ότι μέσω της μεθόδου αυτής η κατανομή των αδρανών διαφοροποιείται σε σχέση με την επιτόπου συμπύκνωση, αν και σε μικρότερο βαθμό συγκριτικά με την κρουστική συμπύκνωση. Ωστόσο, θα πρέπει να επισημανθεί ότι τα δοκίμια γυροσκοπικής συμπύκνωσης έχουν περιορισμένη διαθέσιμη επιφάνεια για τον προσδιορισμό των χαρακτηριστικών υφής. Τα παραπάνω φαίνεται να εξηγούν τα ευρήματα προγενέστερων ερευνών που αναφέρονται στη βιβλιογραφία, σύμφωνα με τα οποία η γυροσκοπική μέθοδος συμπύκνωσης δεν είναι αντιπροσωπευτική, από την άποψη των χαρακτηριστικών που σχετίζονται με την αντιολισθητική ικανότητα, της συμπύκνωσης στο πεδίο. Ως εκ τούτου, κρίθηκε ότι η γυροσκοπική μέθοδος συμπύκνωσης δεν πρέπει να μελετηθεί έτι περαιτέρω. Υπό το πρίσμα αυτό, μέσω της διαδικασίας συμπύκνωσης στο εργαστήριο με κύλινδρο διερευνήθηκε η δυνατότητα προσομοίωσης της επιφάνειας των μιγμάτων και κατ' επέκταση των ιδιοτήτων της αντιολισθητικής τους ικανότητας με συμπύκνωση στο πεδίο.

Αρχικά, διερευνήθηκε η δυνατότητα αξιολόγησης της αντιολισθητικότητας μιγμάτων με διαφορετικά χαρακτηριστικά (ως προς την κοκκομετρική διαβάθμιση, το μέγιστο κόκκο του μίγματος των αδρανών και το ποσοστό ασφάλτου) και τα αποτελέσματα έδειξαν ότι μέσω της συμπύκνωσης με κύλινδρο στο εργαστήριο μπορεί να γίνει αποτελεσματικά αξιολόγηση των χαρακτηριστικών ιδιοτήτων των μιγμάτων.

Επίσης, πραγματοποιήθηκε πειραματική διερεύνηση συνδυαστικά στο εργαστήριο και στο πεδίο για την αξιολόγηση της επίδρασης της μεθοδολογίας συμπύκνωσης στην αντιολισθητική ικανότητα των ασφαλτομιγμάτων. Με βάση τα αποτελέσματα των αναλύσεων προέκυψε ότι η μεθοδολογία συμπύκνωσης επηρεάζει τη συμπεριφορά του μίγματος και επιπλέον υπάρχει συσχέτιση μεταξύ του δείκτη αντιολισθητικότητας IFI (International Friction Index) όπως προσδιορίζεται στο εργαστήριο και στο πεδίο από μετρήσεις παράλληλα και κάθετα στη διεύθυνση συμπύκνωσης, σύμφωνα με το Σχήμα 9.

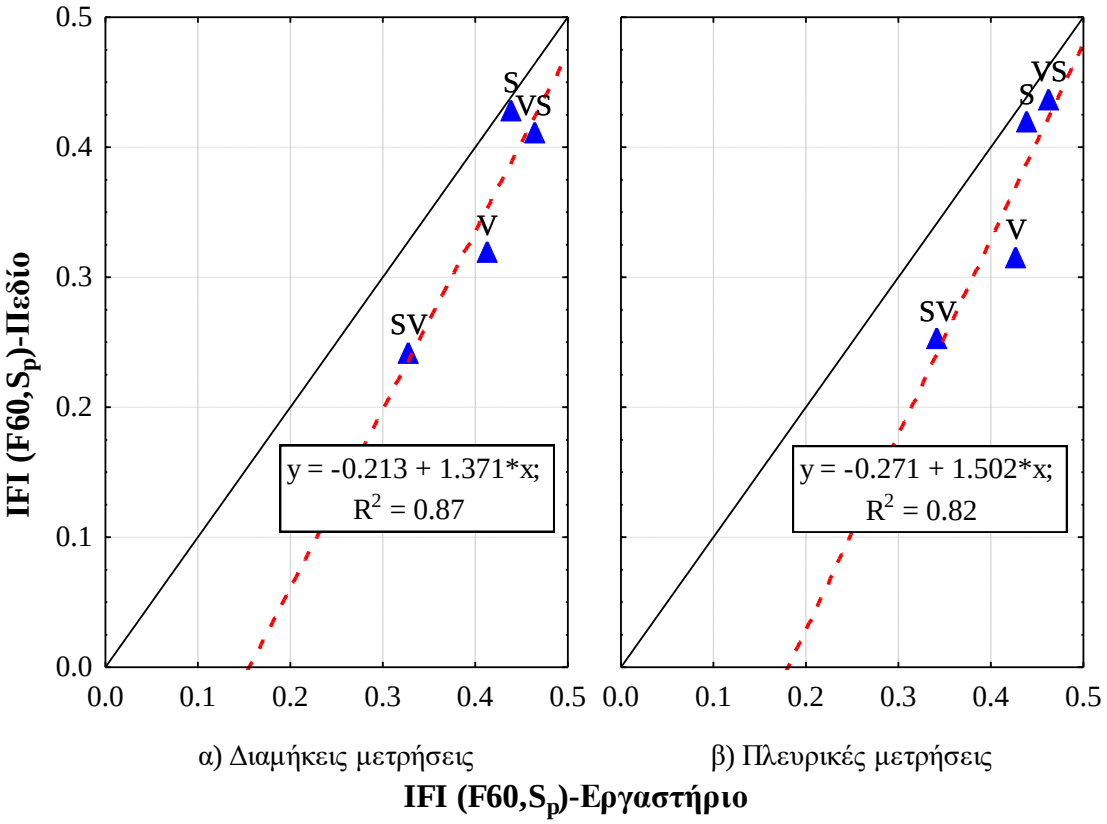

α) Διαμήκεις μετρήσεις β) Πλευρικές μετρήσεις

Σχήμα 9. Συσχέτιση μεθόδων εργαστηριακής και επιτόπου συμπύκνωσης ως προς το δείκτη αντιολισθητικής ικανότητας IFI.

4. ΣΥΜΠΕΡΑΣΜΑΤΑ

Με βάση τη σύνθεση των κύριων ευρημάτων της έρευνας, αναπτύχθηκαν και προτείνονται **τέσσερις μεθοδολογικές προσεγγίσεις**, οι οποίες αποτελούν τα κύρια σημεία της επιστημονικής συνεισφοράς αυτής της Διατριβής, για την, κατά το δυνατόν, ακριβέστερη εκτίμηση των μηχανικών και επιφανειακών χαρακτηριστικών συμπεριφοράς των ασφαλτικών μιγμάτων με συμπύκνωση στο πεδίο.

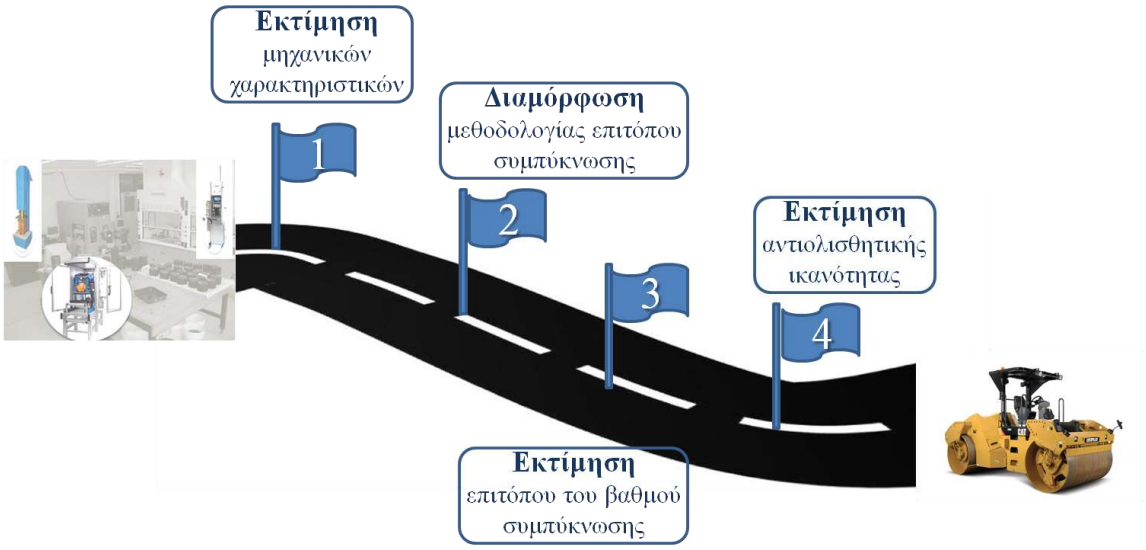

Σχήμα 10. Σημεία επιστημονικής συνεισφοράς έρευνας.

Η **πρώτη μεθοδολογική προσέγγιση** σχετίζεται με την εκτίμηση, μέσω των εργαστηριακών μεθόδων συμπύκνωσης, των μηχανικών χαρακτηριστικών των ασφαλτομιγμάτων με συμπύκνωση στο πεδίο. Με βάση τη διαθέσιμη μέχρι στιγμής γνώση λίγη ερευνητική προσπάθεια έχει αφιερωθεί στο παρελθόν να προτείνει κατευθυντήριες οδηγίες συμπύκνωσης σε σχέση με τις, κατά κύριο λόγο, εφαρμοζόμενες διεθνώς εργαστηριακές μεθόδους συμπύκνωσης, δηλαδή την κρουστική, τη γυροσκοπική ή τη συμπύκνωση με κύλινδρο, για την καλύτερη προσέγγιση των επιτόπου συνθηκών. Η Διατριβή αυτή πιστεύεται ότι προσφέρει σημαντική συμβολή προς αυτή την προοπτική.

Συγκεκριμένα, με βάση τα πειραματικά ευρήματα επιτεύχθηκε σαφής κατανόηση για κάθε εργαστηριακή μέθοδο των βασικών παραμέτρων που επηρεάζουν σημαντικά τη διαδικασία συμπύκνωσης και κατ' επέκταση τη συμπεριφορά του ασφαλτομίγματος. Για παράδειγμα, βρέθηκε ότι η θερμοκρασία συμπύκνωσης, η (αρχική) διάμετρος και η γωνία περιστροφής, και η θερμοκρασία και η ενέργεια συμπύκνωσης αποτελούν τις κυριότερες παραμέτρους της κρουστικής, γυροσκοπικής και της συμπύκνωσης με κύλινδρο, αντίστοιχα. Οι υπόψη παράμετροι αποτελούν τη βάση πρότασης οδηγιών εργαστηριακής συμπύκνωσης (compaction regimes), η οποία συμβάλει στην καλύτερη

προσέγγιση των μηχανικών χαρακτηριστικών των ασφαλτομιγμάτων με συμπύκνωση στο πεδίο με αναφορά τον ίδιο βαθμό συμπύκνωσης. Ειδικότερα:

- Όσον αφορά στην κρουστική συμπύκνωση, προτείνεται η συμπύκνωση των εργαστηριακών δοκιμίων που πρόκειται να υποβληθούν σε δοκιμές προσδιορισμού των μηχανικών χαρακτηριστικών να πραγματοποιείται εντός του εύρους θερμοκρασιών 125-135^{o}C για τα συμβατικά κλειστού τύπου ασφαλτομίγματα. Για την περίπτωση μιγμάτων με τροποποιημένη ελαστομερή άσφαλτο προτείνεται να καθιερωθούν ελαφρώς υψηλότερες θερμοκρασίες (της τάξης των 5-10^{o}C).
- Όσον αφορά στη γυροσκοπική συμπύκνωση, από τις διάφορες μεθοδολογίες συμπύκνωσης που αξιολογήθηκαν, συμπεριλαμβανομένων των πρωτοκόλλων της ευρωπαϊκής (CEN) και αμερικάνικης προδιαγραφής (AASHTO), η καλύτερη προσέγγιση των συνθηκών του πεδίου επιτυγχάνεται μέσω της συμπύκνωσης με γωνία περιστροφής 1.45^{o}, σε συνδυασμό με τη διαδικασία πυρηνοληψίας από δοκίμιο διαμέτρου 150 mm ώστε να προκύψει δοκίμιο διαμέτρου 100 mm.
- Όσον αφορά στη συμπύκνωση με κύλινδρο, διάφορες μεθοδολογίες συμπύκνωσης (υπό την έννοια συνδυασμών θερμοκρασίας και ενέργειας συμπύκνωσης) βρέθηκαν να αντικατοπτρίζουν τα μηχανικά χαρακτηριστικά λόγω της συμπύκνωσης στο πεδίο. Κατ' ουσία, μέσω της εφαρμογής ενός σταθερού φορτίου και καθορίζοντας τη θερμοκρασία συμπύκνωσης (συστήνεται αυξημένη θερμοκρασία) ή, εναλλακτικά την ενέργεια συμπύκνωσης (δηλαδή αριθμό διελεύσεων) μπορεί να προσδιοριστεί η εναπομένουσα μεταβλητή για να επιτευχθεί ο βαθμός συμπύκνωσης που έχει τεθεί ως στόχος.

Περαιτέρω, αναγνωρίζοντας τη σύγχρονη τάση εφαρμογής μηχανιστικών-εμπειρικών μεθόδων ανάλυσης οδοστρωμάτων που περιλαμβάνουν ως μεταβλητές σχεδιασμού τα μηχανικά χαρακτηριστικά του ασφαλτομίγματος, όπως η δυσκαμψία, θα πρέπει να τονιστεί ότι οι ιδιότητες των υλικών που προσδιορίζονται μέσω εργαστηριακών δοκιμών κατεδείχθη ότι επηρεάζουν σημαντικά την πρόβλεψη της συμπεριφοράς της διατομής

του οδοστρώματος. Ως εκ τούτου, στην προσπάθεια να βελτιωθεί το αποτέλεσμα της ανάλυσης ώστε να αντιπροσωπεύει την πραγματική συμπεριφορά του οδοστρώματος προτείνεται να υιοθετηθεί μια ιεραρχική προσέγγιση δύο επιπέδων για την εκτίμηση της δυσκαμψίας των ασφαλτομιγμάτων. Μέσω των δύο επιπέδων γίνεται διάκριση σε σχέση με τη σημασία της δυσκαμψίας όταν χρησιμοποιείται ως μεταβλητή σε αναλυτικούς υπολογισμούς, με το Επίπεδο Ι να αντιπροσωπεύει την περίπτωση απαίτησης για αυξημένη αξιοπιστία των εξαγόμενων αποτελεσμάτων. Τα δύο επίπεδα απεικονίζονται στο ακόλουθο σχήμα και περιγράφονται κατωτέρω:

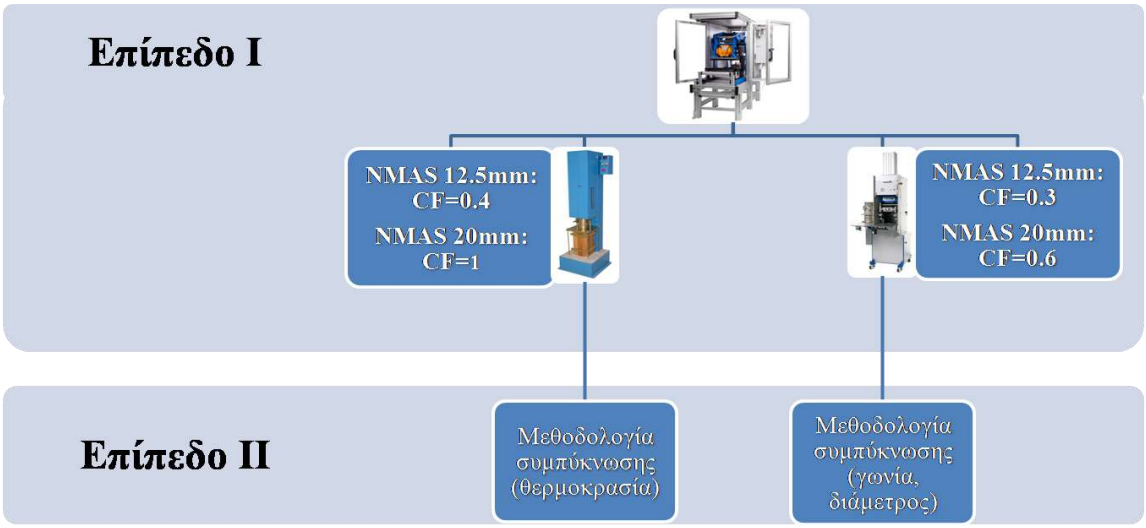

Σχήμα 11. Μεθοδολογική προσέγγιση για την εκτίμηση, μέσω των εργαστηριακών μεθόδων συμπύκνωσης, της δυσκαμψίας με συμπύκνωση στο πεδίο.

Επίπεδο Ι: αφορά στη δυσκαμψία που προσδιορίζεται μέσω δοκιμών α) σε δοκίμια συμπυκνωμένων μέσω κυλίνδρου ή β) σε δοκίμια κρουστικής ή γυροσκοπικής συμπύκνωσης εφαρμόζοντας ταυτόχρονα κατάλληλους συντελεστές μετατροπής (CF) σε συνάρτηση με το ονομαστικό μέγεθος αδρανών του μίγματος (NMAS).

Επίπεδο ΙΙ: αφορά στη δυσκαμψία που προσδιορίζεται μέσω δοκιμών σε δοκίμια κρουστικής ή γυροσκοπικής συμπύκνωσης εφαρμόζοντας τις προτεινόμενες, ανωτέρω, μεθοδολογίες συμπύκνωσης (compaction regimes).

Η **δεύτερη μεθοδολογική προσέγγιση** σχετίζεται με τη διαμόρφωση της μεθοδολογίας συμπύκνωσης στο πεδίο, ώστε να επιτευχθεί ο επιθυμητός βαθμός συμπύκνωσης. Με βάση τα ευρήματα της παρούσας έρευνας προέκυψε ότι μέσω των εργαστηριακών δοκιμών συμπύκνωσης δεν προκύπτουν αξιόπιστα στοιχεία για να χρησιμοποιηθούν στη διαμόρφωση των διαδικασιών κατασκευής. Σημειώνεται επίσης ότι η μεθοδολογία συμπύκνωσης για την οποία εξασφαλίζονται οι απαιτήσεις συμπύκνωσης διαμορφώνεται από τους κατασκευαστές, συνήθως και εφόσον το απαιτούν οι προδιαγραφές, στο πλαίσιο της κατασκευής ενός δοκιμαστικού τμήματος, χωρίς ωστόσο να λαμβάνονται υπόψη σημαντικές παράμετροι που επηρεάζουν τη συμπυκνωσιμότητα, όπως οι θερμικές ιδιότητες του ασφαλτομίγματος και η μεταβλητότητα των συνθηκών κατασκευής. Από αυτή την άποψη, για την περίπτωση κατά την οποία η θερμοκρασία του μίγματος διαφοροποιείται από τις αντίστοιχες τιμές κατά την κατασκευή του δοκιμαστικού τμήματος είναι πιθανό ότι για να επιτευχθεί ο επιθυμητός βαθμός συμπύκνωσης θα χρειαστεί ένας διαφορετικός αριθμός διελεύσεων, χωρίς ωστόσο να μπορεί να εκτιμηθεί. Υπό το πρίσμα αυτό, η επιστημονική συμβολή της Διατριβής αφορά στην ανάπτυξη μιας βελτιωμένης και πρακτικής μεθοδολογίας για τη διαμόρφωση μια αποτελεσματικής μεθοδολογίας συμπύκνωσης, μέσω της οποίας λαμβάνονται υπόψη οι θερμικές ιδιότητες του ασφαλτομίγματος και η μεταβλητότητα των συνθηκών κατασκευής αποσκοπώντας στη μεγιστοποίηση των οφελών από την κατασκευή ενός δοκιμαστικού τμήματος.

Η μεθοδολογία αυτή, η οποία απεικονίζεται σχηματικά ακόλουθα, περιλαμβάνει στο πλαίσιο της κατασκευής ενός δοκιμαστικού τμήματος την εφαρμογή σύγχρονων μη καταστρεπτικών μεθόδων, δηλαδή της Υπέρυθρης θερμογραφίας και της τεχνικής PQI, για τη μέτρηση της θερμοκρασίας και της επιτόπου πυκνότητας ανά διέλευση του οδοστρωτήρα για κάθε υπό αξιολόγηση μεθοδολογία συμπύκνωσης.

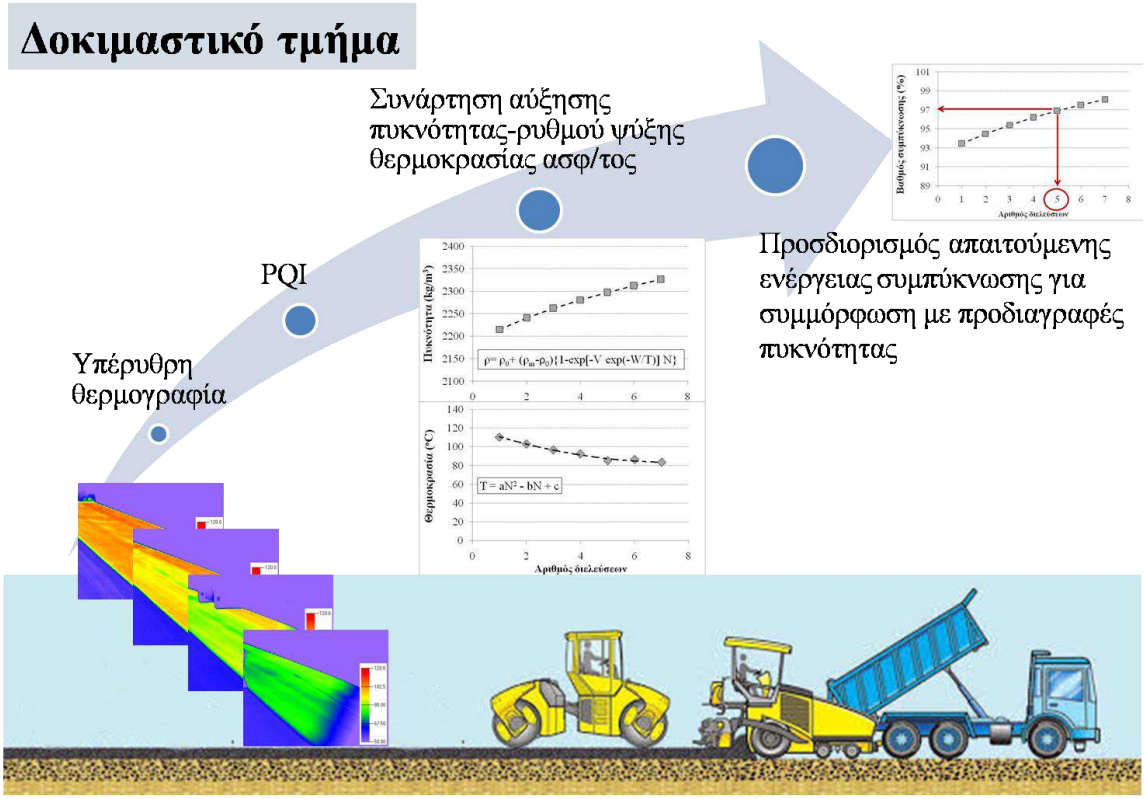

Σχήμα 12. Μεθοδολογική προσέγγιση για τη διαμόρφωση της επιτόπου μεθοδολογίας συμπύκνωσης.

Αξίζει να αναφερθεί ότι η εφαρμογή των υπόψη μεθόδων συμβάλλει σε σαφή κατανόηση της επίδρασης της θερμοκρασίας ασφαλτομίγματος στην εξέλιξη της πυκνότητας. Η κατανόηση αυτή μπορεί να βελτιωθεί περαιτέρω μέσω της συμπύκνωσης υποτμημάτων σε α) τυπικές και β) την χαμηλότερη επιτρεπτή, κατά την παράδοση στο έργο, θερμοκρασία του ασφαλτομίγματος ώστε να επιτραπεί να προσδιοριστούν ενδεχόμενες τροποποιήσεις στον απαιτούμενο αριθμό διελεύσεων λόγω της μεταβλητότητας των θερμοκρασιών του ασφαλτομίγματος στο έργο. Ως εκ τούτου, η προτεινόμενη μεθοδολογία πλεονεκτεί έναντι της διαδικασίας που ακολουθείται συνήθως στην πράξη προσφέροντας τη δυνατότητα να προσδιοριστεί η αύξηση της πυκνότητας σε σχέση με την πτώση της θερμοκρασίας του ασφαλτομίγματος, πληροφορία η οποία είναι καθοριστική για τη διαμόρφωση μιας αποτελεσματικής μεθοδολογίας συμπύκνωσης.

Επίσης, επισημαίνεται ότι τα στοιχεία επιτόπου μετρήσεων μπορεί να αξιοποιηθούν περαιτέρω για να περιγράψουν μαθηματικά τη διαδικασία συμπύκνωσης. Στο πλαίσιο αυτό μπορεί να χρησιμοποιηθεί μια εξίσωση, η οποία έχει επιβεβαιωθεί μέσω των πειραματικών δεδομένων της έρευνας ότι είναι πολύ αποτελεσματική για την υπόψη ανάλυση. Η εξίσωση αυτή, μέσω της προσαρμογής των πειραματικών δεδομένων, περιγράφει την εξέλιξη της πυκνότητας σε σχέση με τον αριθμό των διελεύσεων του οδοστρωτήρα και το ρυθμό ψύξης του ασφαλτομίγματος. Κατά συνέπεια, ελέγχοντας αυτές τις δύο παραμέτρους, αναμένεται να καταστεί ευκολότερο να επιτευχθεί η επιθυμητή πυκνότητα συμπύκνωσης. Αυτή η ολοκληρωμένη προσέγγιση, η οποία προσφέρει τη δυνατότητα να λαμβάνεται δεόντως υπόψη η μεταβλητότητα των συνθηκών κατασκευής, δίνει τη δυνατότητα να καθοριστεί όχι μόνο η πιο αποτελεσματική στρατηγική συμπύκνωσης, αλλά και η απαιτούμενη ενέργεια συμπύκνωσης ώστε να εξασφαλιστεί συμμόρφωση με τις απαιτήσεις των προδιαγραφών.

Ωστόσο, η αποτελεσματικότητα της διαμορφωμένης μεθοδολογίας συμπύκνωσης σε σχέση με την επίτευξη του επιθυμητού βαθμού συμπύκνωσης θα πρέπει να επαληθευθεί κατά τη διαδικασία των κύριων εργασιών κατασκευής. Από την άποψη αυτή, η ποιότητα συμπύκνωσης πρέπει να αξιολογηθεί με αναφορά στις προδιαγραφές πυκνότητας (κατά κύριο λόγο το βαθμό συμπύκνωσης). Στην πράξη, σύμφωνα με τις υπάρχουσες προδιαγραφές η αξιολόγηση της επιτευχθείσας πυκνότητας πραγματοποιείται μέσω πυρήνων ή επιτόπου δοκιμών με (μη) πυρηνικές συσκευές. Τυπικά, οι προδιαγραφές ορίζουν την υλοποίηση δειγματοληπτικών δοκιμών, τοπικά, σε τυχαίες θέσεις της κατασκευασθείσας στρώσης και με βάση τα αποτελέσματα των υπόψη δοκιμών αξιολογείται η ποιότητα συμπύκνωσης στο σύνολο της ασφαλτικής στρώσης. Επομένως, υπάρχει ο κίνδυνος η πυκνότητα που προσδιορίζεται μέσω σημειακών ελέγχων να μην είναι αντιπροσωπευτική της συνολικής κατάστασης και ως εκ τούτου αναδεικνύεται η ανάγκη αξιολόγησης της ποιότητας συμπύκνωσης στο σύνολο της ασφαλτικής στρώσης.

Στο πλαίσιο αυτό εισάγεται η **τρίτη μεθοδολογική προσέγγιση**, η οποία αφορά σε μια μεθοδολογία, η οποία βασίζεται στη γεωφυσική μέθοδο GPR σε συνδυασμό με κατάλληλους αλγορίθμους, για την αξιόπιστη εκτίμηση της επιτόπου πυκνότητας. Μέσω της υπόψη προσέγγισης δίνεται η δυνατότητα αξιολόγησης, κατά τη διάρκεια των κύριων εργασιών συμπύκνωσης, της αποτελεσματικότητας της προσδιορισμένης μεθοδολογίας συμπύκνωσης ως προς την εξασφάλιση των απαιτήσεων συμπύκνωσης. Συγκεκριμένα, με αναφορά την υπάρχουσα γνώση και διευρύνοντας την μέσω πειραματικών παραμετρικών διερευνήσεων που πραγματοποιήθηκαν ως προς την επίδραση των διαφόρων διαθέσιμων αλγορίθμων, της συχνότητας της κεραίας και του αριθμού των πυρήνων βαθμονόμησης στην εκτίμηση της επιτόπου πυκνότητας, στο πλαίσιο της Διατριβής διαμορφώθηκε η ολοκληρωμένη μεθοδολογία που απεικονίζεται στο ακόλουθο σχήμα.

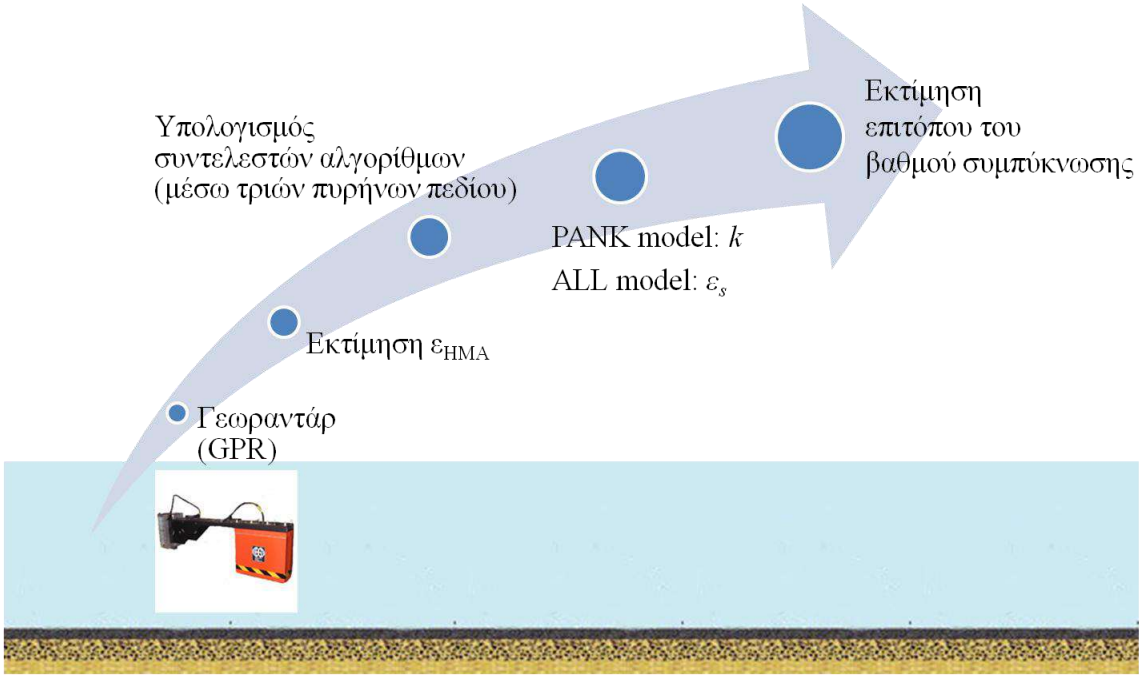

Σχήμα 13. Μεθοδολογική προσέγγιση για την επιτόπου εκτίμηση του βαθμού συμπύκνωσης.

Η μεθοδολογία αυτή αποτελείται από α) εκτεταμένες μετρήσεις GPR με κεραία συχνότητας 2 GHz για την πλήρη σάρωση των υπό αξιολόγηση ασφαλτικών στρώσεων, β) εκτίμηση της διηλεκτρικής σταθεράς του ασφαλτομίγματος ε_{HMA}, γ) προσδιορισμό

της φαινόμενης πυκνότητας τριών πυρήνων πεδίου, δ) ανάστροφο υπολογισμό των συντελεστών προσαρμογής των αλγορίθμων με βάση τα στοιχεία πυκνότητας των πυρήνων και ε) ενεργοποίηση των αλγορίθμων (δηλαδή PANK ή/και ALL) για την επιτόπου εκτίμηση του βαθμού συμπύκνωσης.

Οι υπόψη μεθοδολογικές προσεγγίσεις πιστεύεται ότι θα συνεισφέρουν σημαντικά στην ουσιαστική βελτίωση της μεθοδολογίας επιτόπου συμπύκνωσης, καθώς και των διαδικασιών ποιοτικού ελέγχου. Συγκεκριμένα, μέσω της βελτίωσης της μεθοδολογίας συμπύκνωσης στο έργο μπορεί να εξασφαλισθεί η κατάλληλη, σύμφωνα με τα κριτήρια σχεδιασμού, αρχική κατάσταση του οδοστρώματος, η οποία με τη σειρά της θα μειώσει την ανάγκη εργασιών συντήρησης και κατ' επέκταση θα περιορίσει την όχληση των χρηστών της οδού. Επίσης, η χρήση των μη καταστρεπτικών δοκιμών, σε σχέση με τις παραδοσιακές καταστρεπτικές μεθόδους, προσφέρει το πλεονέκτημα της αξιολόγησης σε πλήρη κλίμακα της ποιότητας συμπύκνωσης του ασφαλτοτάπητα βελτιώνοντας τις διαδικασίες του ποιοτικού ελέγχου της κατασκευής.

Η **τέταρτη μεθοδολογική προσέγγιση** αφορά στην εκτίμηση μέσω εργαστηριακών δοκιμών, στο πλαίσιο του σχεδιασμού των ασφαλτομιγμάτων, των χαρακτηριστικών αντιολισθητικής ικανότητας με συμπύκνωση στο πεδίο.

Στην πράξη, οι Υπηρεσίες οδών διεθνώς προδιαγράφουν ποιοτικούς ελέγχους μετά την κατασκευή, οι οποίοι μεταξύ άλλων περιλαμβάνουν την αξιολόγηση της μακροϋφής σε σχέση με τις απαιτήσεις συμμόρφωσης. Παρά το γεγονός ότι η μακρουφή, η οποία συνεισφέρει σημαντικά στην αντιολισθητική ικανότητα που αναπτύσσεται στη διεπιφάνεια μεταξύ τροχού-οδοστρώματος, έχει αναγνωρισθεί ως ένα βασικό χαρακτηριστικό συμπεριφοράς των ασφαλτομιγμάτων, μέχρι στιγμής δεν είναι διαθέσιμη οποιαδήποτε τυποποιημένη μεθοδολογία που να επιτρέπει την αξιόπιστη εκτίμηση των χαρακτηριστικών της επιφάνειας του οδοστρώματος μέσω εργαστηριακών δοκιμών. Για παράδειγμα, το ευρωπαϊκό πρότυπο (EN 13108) ως προς το σκέλος αυτό περιορίζεται στην παροχή καθοδήγησης για την κάλυψη απαιτήσεων που σχετίζονται μόνο με την κοκκομετρική διαβάθμιση, το ποσοστό ασφάλτου (ελάχιστη τιμή) και το ποσοστό κενών αέρα (ελάχιστη- μέγιστη τιμή) των ασφαλτομιγμάτων. Από αυτή την

άποψη, μέσω της συμμόρφωσης με τις υπόψη κατευθυντήριες οδηγίες ή της προγενέστερης εμπειρίας οι μηχανικοί που ασχολούνται με το σχεδιασμό ασφαλτομιγμάτων υποθέτουν ότι τελικά μετά τη συμπύκνωση στο πεδίο θα καλυφθούν οι απαιτήσεις σε σχέση με το αρχικό βάθος υφής, χωρίς να μπορούν *a priori* στο στάδιο του σχεδιασμού του μίγματος στο εργαστήριο να εκτιμήσουν τα απαιτούμενα χαρακτηριστικά υφής.

Στην παρούσα έρευνα αναπτύχθηκε μια απλή, αλλά και πρακτική μεθοδολογία, η οποία επιτρέπει την πρόβλεψη των επιφανειακών χαρακτηριστικών των ασφαλτομιγμάτων με συμπύκνωση στο πεδίο και απεικονίζεται στο Σχήμα 14.

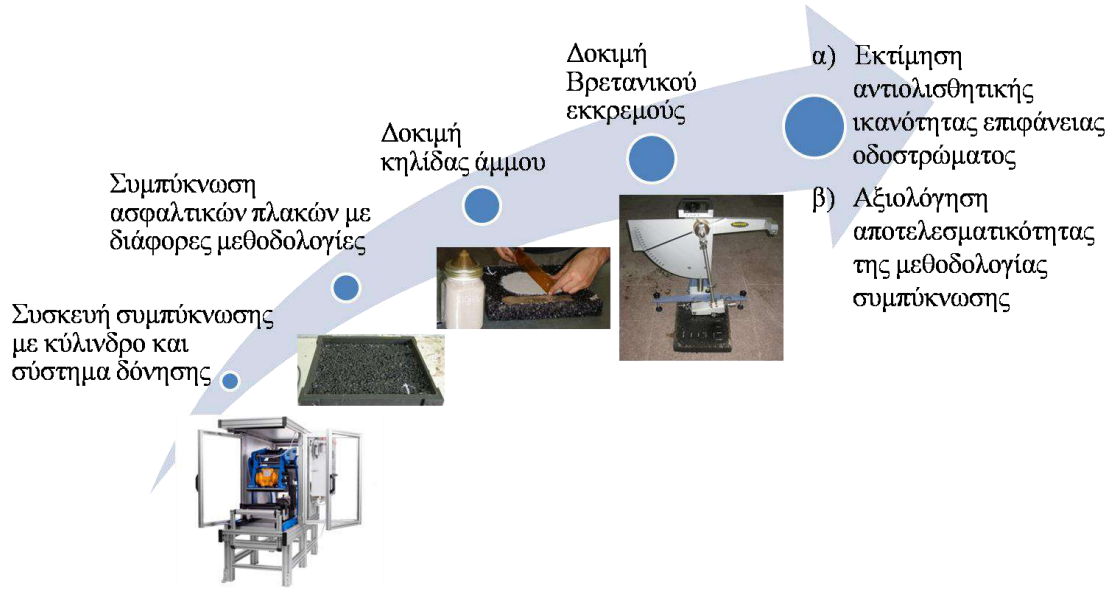

Σχήμα 14. Μεθοδολογική προσέγγιση για την εκτίμηση της αντιολισθητικής ικανότητας των ασφαλτομιγμάτων.

Η μεθοδολογία αυτή, η οποία περιλαμβάνει τη μέθοδο συμπύκνωσης με κύλινδρο για τη δημιουργία εργαστηριακών δοκιμίων, αντίστοιχου πάχους με την προβλεπόμενη ασφαλτική στρώση, τα οποία υποβάλλονται στη συνέχεια σε τυπικές εργαστηριακές δοκιμές (δηλαδή της κηλίδας άμμου και του Βρετανικού εκκρεμούς), αποδείχτηκε ότι μπορεί να αξιολογήσει αποτελεσματικά τη συμπεριφορά διαφορετικών μιγμάτων ως προς την αντιολισθητική ικανότητα, καθώς και την αποδοτικότητα της μεθοδολογίας συμπύκνωσης. Επίσης, τα προκαταρκτικά πειραματικά αποτελέσματα έδειξαν καλή

συσχέτιση μεταξύ των επιφανειακών χαρακτηριστικών λόγω της εργαστηριακής συμπύκνωσης και των αντίστοιχων που επιτυγχάνονται στο πεδίο. Ως εκ τούτου, η μεθοδολογία αυτή μπορεί να ωφελήσει δίνοντας αφενός τη δυνατότητα στους μηχανικούς οδοστρωμάτων να ποσοτικοποιήσουν και να βελτιώσουν τις ιδιότητες που σχετίζονται με την αντιολισθητική ικανότητα των ασφαλτομιγμάτων κατά το στάδιο της μελέτης σύνθεσης και αφετέρου πολύτιμες πληροφορίες στους κατασκευαστές ώστε να διαμορφώσουν μια αποτελεσματική μεθοδολογία συμπύκνωσης στο πεδίο.

Συμπερασματικά, αναφέρεται ότι οι μεθοδολογικές προσεγγίσεις που περιγράφτηκαν ανωτέρω έχουν πρακτική σημασία για τους κατασκευαστές, τις Υπηρεσίες και τους μηχανικούς οδοστρωμάτων. Πιστεύεται επίσης ότι θα συμβάλλουν σημαντικά στη βελτίωση από τη μια μεριά των διαδικασιών σχεδιασμού ασφαλτομιγμάτων και οδοστρωμάτων και από την άλλη μεριά των διαδικασιών επιτόπου συμπύκνωσης και ποιοτικού ελέγχου, ενθαρρύνοντας την εφαρμογή σύγχρονων μη καταστρεπτικών δοκιμών.

CONTENTS

1. Introduction

1.1 General

Compaction is the process by which the volume of an asphalt mixture is reduced. Compaction increases the unit weight and reduces the air voids in the asphalt mixture by applying external forces (Corps of Engineers 2000). During the compaction process the internal structure of the asphalt mixture, which refers to the content and the spatial and directional distribution of air voids and asphalt-coated aggregates, evolves. The asphalt-coated aggregates in the mixture are forced closer together, which increases aggregate interlock and interparticle friction and leads to the formation of the aggregate skeleton. Through this process the asphalt mixture gains its characteristics and strength which cannot be improved after completing the compaction.

Asphalt mixture compaction has been well recognized as one of the most critical factors affecting the pavement behavior, providing all desirable mixture design characteristics are met. Inadequate compaction has been associated with poor asphalt pavement performance. On the contrary, the good or proper compaction of asphalt mixture increases fatigue life, decreases permanent deformation or rutting, reduces the amount of oxidation or aging, decreases moisture damage or stripping, increases strength and internal stability and optimizes the surface texture (Crispino et al. 2007; Brown 1990; Linden et al. 1989; Bell et al. 1989).

Achieving consistency in both laboratory and site compaction is key to proper asphalt pavement behavior. Over times numerous laboratory compaction methods have been developed which vary in terms of specimen preparation, compaction type etc. Hence, the challenge is to adopt a compaction procedure in the laboratory that accurately simulates field production and construction conditions.

Although numerous studies have been carried out to assess the relationship between laboratory and field compaction methods and the resulting mechanical performance of the mixture, limited research has been devoted to evaluate the prediction of asphalt pavement surface characteristics from laboratory testing (Boscaino et al. 2009; Goodman et al. 2006). By studying the relationship between laboratory and field compaction

methods pavement engineers have long recognized that different laboratory compaction methods create volumetrically identical but mechanically different specimens; hence density alone cannot characterize the asphalt mixture mechanical performance. While yet no consensus has been reached as to which laboratory method is the best in terms of simulating the field compaction conditions (Airey et al. 2006; Peterson et al. 2004; Hartman et al. 2001; Khan et al. 1998; Sousa et al. 1991; Von Quintus et al. 1991), there is agreement among researchers that the compaction method has a direct impact on the aggregate structure within the compacted mixture and hence characterization of the internal structure of the asphalt mixture is needed.

Previous research has demonstrated that asphalt mixture internal structure, which refers to the distribution of aggregates and their associated voids, can be characterized using imaging techniques (Hunter et al. 2004; Saadeh et al. 2002; Masad et al. 1999a, Masad et al. 1999b; Yue et al. 1995). Due to technological advances, the competence of these techniques in terms of image capturing, processing and analysis has been improved significantly over time, hence providing the users with methods to characterize efficiently the asphalt mixture internal structure (Coenen et al. 2012).

The focus on the asphalt mixtures' internal structure generated by the use of various laboratory compaction methods can lead to thorough assessment of the impact of specimen fabrication on the mixture performance along with the differences between asphalt mixture compaction in laboratory and in-field (Sefidmazgi and Bahia 2014). In this framework, the internal structure-based approach is believed to assist in establishing compaction regimes for specimen fabrication in the laboratory towards better resembling the field conditions (Georgiou et al. 2016).

1.2 Problem statement and objectives

Numerous methods - which vary in terms of specimen preparation, compaction type and procedure, including impact compaction (Marshall hammer), gyratory (kneading) compaction, and roller compaction - are used to compact hot mix asphalt (HMA) specimens in the laboratory. Extensive research has been carried out to assess the influence of various compaction methods, both in the laboratory and in the field, on asphalt mixture performance. Particular emphasis has been given to evaluate the

fundamental mechanical properties of asphalt mixtures, whereas few studies focused on the assessment of predicting the surface characteristics by using gyratory compaction. From this limited research it has been shown that the gyratory specimens cannot be considered representative of the real mixture in-situ in terms of assessing the texture characteristics, which in turn highlights the need for systematic research in this area. Moreover, the remaining studies while emphasize the significant influence of the compaction methods on the formation of asphalt specimen structure and subsequently on its performance-based properties such as stiffness, permanent deformation etc., they limit to provide a comparative assessment between the various laboratory methods and the field compaction based on conventional laboratory testing. Although the results obtained in this area are contradictory and the laboratory compaction method which is the best in terms of simulating the field compaction conditions is still hotly debated, it can be argued that it is of more vital importance to attempt improving the efficacy of each available compaction method by defining test procedures, based on its dominant operational factors, which result in emulating, as closely as possible, the conditions generated during the field rolling operations. This challenge becomes more essential considering that, for instance, the European specifications not only offer the potential of selection among several compaction methods (CEN 2007a; CEN 2007b; CEN 2007c; CEN 2007d) for fabricating asphalt specimens prior to their performance-based testing (CEN 2006), but also within each compaction method let the pavement engineers the initiative to specify several compaction related parameters which is likely to influence the outcome of asphalt performance testing. To the best of the author's knowledge, little effort has been devoted in the past to develop a framework for an improved procedure for each laboratory compaction method to simulate the field compaction with reference its compaction level (namely compaction degree or void content), based on the comprehensive evaluation of varying compaction regimes.

In light of the above, this Thesis aims to contribute to a better simulation of in-situ conditions through laboratory compaction methods, so that reliable results can be obtained to assess, as accurately as possible, the on-site characteristics of field-compacted asphalt mixtures, as illustrated schematically in Fig. 1.1. A holistic approach,

accounting for both the compaction dependent surface and mechanical characteristics of asphalt mixtures, was adopted.

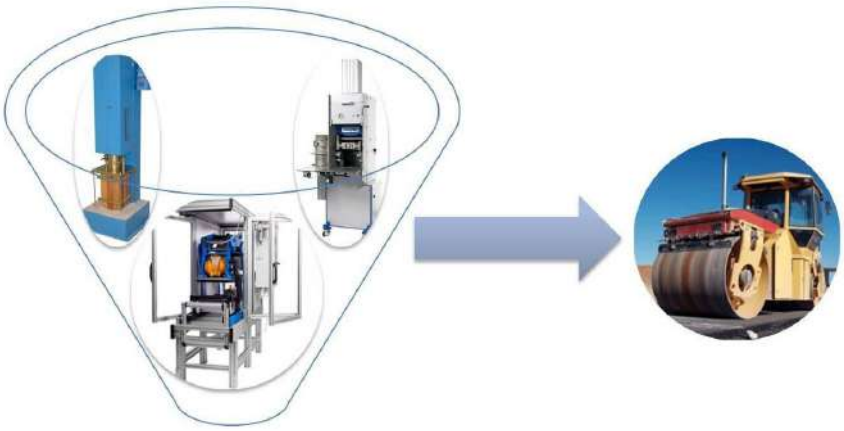

Fig. 1.1 Main aim of thesis

On this purpose, extensive laboratory experiments (based on impact, gyratory and roller compaction methods) and field investigations were designed and performed. Also, not only conventional testing -similarly to previous studies- was conducted, but also emerging Non Destructive Testing (NDT) techniques were employed both in the laboratory and field in order to maximize the benefits of gaining a deep insight of compaction.

1.3 Research methodology

For this research, a methodological framework was implemented which consists of several essential steps:

- The first step concerns an extensive literature review covering several fields of the overall research area.
- In the second step, extensive field and laboratory experiments were designed and performed, including the implementation of modern Non Destructive Testing (NDT) technologies for rigorous evaluation purposes.
- In the third step, the large dataset that was collected from the experimental investigations both in the field and laboratory were statistically analyzed.

More specifically, in the first step a comprehensive literature search was conducted in order to collect pertinent information on: a) influence of compaction methods on

mixture properties and performance, b) factors that influence compaction in both the field and the laboratory and c) influence of compaction methods on the internal structure of asphalt mixtures. The findings of the literature review form the basis for the selection of the mixture compaction dependent **key performance characteristics**, as depicted in Fig. 1.2. Based on this, extended literature review is also carried out regarding the **key compaction parameters** that influence the mixture performance both in the laboratory and in the field, which will form the basis for subsequent experimental investigations.

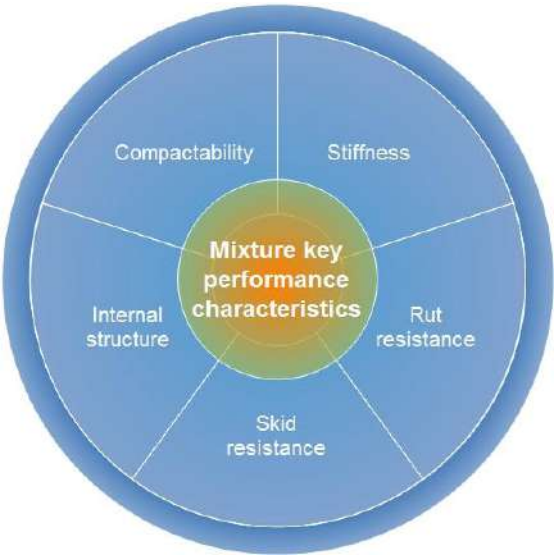

Fig. 1.2 Mixture key performance characteristics

The second step, which constitutes the core of the methodological framework, concerns the design and implementation of experimental investigations both in field and in the laboratory, regarding the influence of the compaction on mixture key performance characteristics. Within this framework, multiple tasks were executed, as listed hereinafter and presented thoroughly in the following chapters, in order to meet the thesis objectives.

a) Evaluation of field and laboratory compactability
b) Evaluation of field and laboratory stiffness
c) Evaluation of field and laboratory rut resistance
d) Evaluation of mixture internal structure due to the compaction in the field and in the laboratory

e) Evaluation of the relationship between the mixture internal structure and mechanical properties
f) Evaluation of mixture skid resistance due to the compaction in the field and in the laboratory

The third step concerns the analysis of the comprehensive experimental dataset of each subtask mentioned above. Moreover, based on the pertinent findings of each subtask, a statistical analysis of the interrelation between key parameters of laboratory compaction methods and asphalt mixture performance with respect to the in-situ compaction is performed. On this basis, the complete results are discussed and based on this synthesis answers on the research objectives are given.

1.4 Thesis outline

This document is divided into ten chapters.

The **first chapter** provides an introduction about the research and its objectives. The **second chapter** presents the current state of knowledge regarding a) the influence of the compaction on mixture performance characteristics, b) the factors that influence the compaction in both the field and the laboratory and c) the influence of compaction methods on the internal structure of asphalt mixtures.

The **third chapter** provides a brief description of the asphalt mixtures and the pavement trial sections (test sites) under investigation.

The **fourth chapter** addresses the issue of the asphalt mixture compactability. Key compaction parameters are being highlighted and the relationship between the asphalt mixture compactability in the field and the laboratory is being discussed.

The **fifth chapter** documents the differences in terms of stiffness properties of asphalt mixtures as a function of laboratory and field compaction methods. Moreover, the effect of various compaction factors on the stiffness of laboratory-compacted specimens were also investigated to gain more insight to the key parameters affecting the asphalt mix mechanical properties.

The **sixth chapter,** similarly to previous chapter, documents the differences in terms of rut resistance characteristics of asphalt mixtures as a function of laboratory and field compaction methods.

The **seventh chapter** presents the results of the image analysis techniques that were used to analyze the internal structure of asphalt mixture specimens by means of cross sectional (i.e. 2D) images. These procedures and techniques were used to quantify the aggregate skeleton of asphalt specimens in terms of contact points, orientation and segregation.

The **eighth chapter** gives particular emphasis in evaluating the relationship between the internal structure and the stiffness-rut resistance characteristics of asphalt specimens. The findings offer useful insight to identify and quantify the controlling parameters influencing the internal structure and in turn the mechanical properties of asphalt specimens.

The **ninth chapter** documents the effort to evaluate the feasibility of characterizing efficiently in the laboratory the frictional performance of asphalt mixtures. Moreover, the relationship between laboratory and field compaction methods from a frictional point of view is investigated.

Lastly, the **tenth chapter** discusses the main findings, and concluding suggestions of this study, and presents recommendations for further research.

2. Literature review

2.1 Introduction

Following the methodological framework discussed in the previous chapter, a literature survey on earlier attempts to evaluate the asphalt mixture compaction is presented in this chapter.

The first part of the chapter focuses on the evaluation methods regarding the asphalt mixture compactability, underlining the key parameters affecting the asphalt mixture compaction characteristics both in the field and in the laboratory.

In the second part of the chapter the impact of the compaction methods on mixture performance is discussed, highlighting the mixture properties that are mostly influenced by the compaction methods and reviewing which laboratory compaction method better reflects the field-compacted asphalt mixture characteristics.

The third part of the chapter reports the state of the art regarding the influence of compaction methods on the internal structure of asphalt mixtures, as characterized and quantified by means of image analysis methods. It also reviews the relationship between internal structure indicators and mixture mechanical properties.

Finally, on the basis of the literature review the past research findings are discussed and reviewed in order to set the key parameters which will form the basis for the experimental investigations of the present research.

2.2 Compactability

In-situ field density (or air voids) is often regarded as one of the most important controls used to ensure that a pavement being placed is of high quality because it is a good indicator of future performance (Brown 1990). Hence, it is vital to relate field compaction to laboratory compaction in order to predict asphalt mixture compactability based on laboratory measurements.

Leiva and West (2008a, b) evaluated the compactability of asphalt mixtures in the laboratory by means of gyratory compaction and attempted to relate compaction parameters measured in the laboratory to compactability in the field in terms of ACP

(Accumulated Compaction Pressure) indicator. These researchers did not find a simple relationship between field and laboratory compaction for different asphalt mixtures. However, a multiple regression analysis was used to relate field compaction to various mixture characteristics such as laboratory compaction slope, number of gyrations to achieve 92 percent of maximum specific gravity (N92), number of gyrations required to reach locking of the mixture, and mixture characteristics (binder content, aggregate shape, gradation, and volumetric properties).

Schmitt et al. (2009) evaluated the effect of temperature, roller passes, roller type and binder grade on density growth. Moreover, a laboratory experiment was carried out to understand the effects of temperature, pressure, and related variables on laboratory compaction using the Superpave Gyratory Compactor (SGC). The statistical results from the laboratory data analysis revealed that temperature and pressure significantly affect the densification of asphalt mixtures. Moreover, the field data analysis showed that the factors affecting density gain in rank order were mat temperature, number of passes, roller type, and binder grade. Delgadillo and Bahia (2008) reached similar conclusions with regard to the effect of pressure on HMA compaction and further suggested that a lower limit for the compaction temperature can be set without affecting the compaction effort required to achieve density.

Kassem et al. (2008) found that the efficiency of the compactive effort across the steel rollers was found to be non-uniform and proposed the Compaction Index (CI), which quantifies the compaction effort at any point in the pavement, with the aim to achieve uniformity of the desired percent air voids across the pavement section. A relationship between slope of laboratory compaction curve obtained from the SGC and CI calculated from field compaction was found. Further research on CI, which is determined on project basis with respect to the roller equipment used, demonstrated that the compaction temperature and mode had a great effect on compaction (Kassem et al. 2012). The same study presented a field experimental-based method to determine the compaction pattern required to achieve the desired density of asphalt pavements. This method may be integrated in an automated system that can be used by roller operators to estimate density during construction, similarly to the Intelligent Compaction (IC) technology.

Asphalt technologists have also demonstrated that the density that can be obtained under normal rolling conditions is clearly related to the lift thickness (t) and in particular to its ratio with the nominal maximum aggregate size (NMAS). The study results indicate that care must be exercised when the thickness gets too large to ensure that adequate density is obtained and they also indicate that one of the reasons for low density at thinner sections (lower t/NMAS) is the more rapid cooling of the mixture (Williams et al. 2015; Brown et al. 2005).

Although these studies highlight the key parameters affecting asphalt mix compactability in terms of density (or air voids), it is vital that the desired in-situ compaction degree is achieved during construction and the quality control/quality assurance (QC/QA) specifications are met. Hence, monitoring and assessment of the real time HMA compaction should be performed to fully support the compaction procedures. Over time conventional methods for assessment of in-situ density, such as through coring of asphalt samples which is both an intrusive and a time-consuming method requiring that the mat temperature has sufficiently cooled, tend to be less implemented and replaced mainly from non-destructive testing (NDT) methods. As such, contractors and agencies have implemented for many years both non-destructive nuclear and non-nuclear density gauges for quality control and in some cases acceptance (Smith and Diefenderfer 2008; Choubane et al. 1999). Non-destructive gauges allow for a more rapid assessment of the in-situ density during construction, however nuclear density gauges use radioactive material and require special licensing to transport and operate, a fact that results in increased operational costs. An alternative method for estimating pavement density is by using more recently developed non-nuclear gauges (Megali et al. 2010; Hurley et al. 2004). However, both nuclear and non-nuclear gauges provide density readings at randomly selected discrete locations of the mat; judgment about the density level of the entire roadway is made based on the results of this spot testing. Unfortunately, density measurement from a small number of spots may not be representative of the density of the pavement mat; hence, full coverage evaluation of compaction quality of the pavement mat is needed. To overcome the aforementioned limitations, multiple recent studies have investigated emerging technologies, such as

intelligent compaction, infrared thermography (IRT) and Ground Penetrating Radar (GPR) for the assessment of in-situ density during construction.

The intelligent compaction (IC) technology has recently been implemented in the USA and Japan to improve compaction quality and process. IC produces massive amounts of geospatial data with 100% coverage of the compacted area in real time, which needs to be effectively analyzed and managed for quality control and acceptance (QC/QA) applications for HMA pavement (Xu et al. 2012; Commuri et al. 2011; Furuya et al. 2010).

The infrared thermography technique has been implemented for the evaluation of pavement construction operations by means of temperature profiling of the pavement mat surface (Stroup-Gardiner et al. 2004). IRT allows continuous real time data collection during both the laydown and compaction process, which provide useful insight for the compaction quality (ter Huerne et al. 2009; Elsafey et al. 2009). It has been demonstrated that temperature differentials in the mat during HMA paving can result in substantial density differentials (Rahman et al. 2013; Henault and Larsen 2006; Willoughby et al. 2002; Mahoney et al. 2000; Stroup-Gardiner et al. 2000). Research in this area has emphasized the identification of cooler areas in the mat and its relationship with final HMA density. Evaluation of the final density has indicated that areas experiencing overall large mat temperature differentials exhibited higher air void contents when compared to areas with more normal temperature differentials. Considering the above, asphalt mix density-growth curves, with respect to the IRT-based mat temperature evolution, need to be established for the enhancement of pavement compaction quality.

The Ground Penetrating Radar (GPR) is a non-invasive sensing technique, whose principles emerged from the electromagnetic theory. Although GPR has been effectively used in multiple pavement surveys, such as determining layer thickness, detecting subsurface distresses, estimating moisture content, detecting voids and others (Plati and Loizos 2013; Benedetto 2010; Diamanti et al. 2010; Loizos and Plati 2007; Benedetto and Pensa 2007; Al-Qadi and Lahouar 2005, 2004; Loulizi et al. 2003), limited research has been devoted to the evaluation of pavement compaction. Saarenketo (1997) used the dielectric constants of the pavement to predict the asphalt pavement density based on the

concept that the dielectric constant of asphalt mixture is a function of the dielectric constants of its components. More recent studies have shown promising results with respect to its capability, coupled with the use of novel algorithms based on the dielectric properties of HMA, to predict the in-situ field density. This can be achieved by utilizing density prediction models that are based on Electromagnetic Mixing (EM) theory (Shangguan et al. 2013; Leng et al. 2012; Leng et al. 2011; Al-qadi et al. 2010). The practice of using GPR to predict in-situ field density of compacted asphalt mixture material is still under development and research (Shangguan et al. 2014); however the related research findings seem to be promising and further research in terms of monitoring compaction during construction is needed.

2.3 Mechanical and surface mixture properties

It is of utmost importance that the laboratory-compacted specimens have similar properties to field cores. Over the years, significant research effort has been devoted to assess the relationship between laboratory and field compaction methods and the resulting mechanical performance of the mixture. However, research in this area has reached conflicting conclusions as to the laboratory compaction method that best resembles field conditions. In this section, some of the most significant previous studies on this topic are reviewed and their findings are presented.

Consuegra et al. (1989) evaluated the ability of different compaction devices to simulate the compaction in the field in terms of similarity between engineering properties. The field cores and the laboratory specimens of similar air void contents were evaluated for indirect tensile strength, indirect tensile creep, and diametral resilient modulus. Five different laboratory compaction methods were used in this study, namely the (a) the mobile steel wheel simulator, (b) the Texas gyratory compactor, (c) the California kneading compactor, (d) the Marshall impact hammer, and (e) the Arizona vibratory-kneading compactor. The field compaction procedure used at the sites was the standard procedure used by the state highway departments responsible for the highways involved. The results analysis showed that the engineering mechanical properties of asphalt mixtures were dependent on the compaction method. Overall, the Texas gyratory compactor demonstrated the ability to produce mixtures with engineering properties

nearest to those determined from field cores. The study ranked the compaction methods in terms of simulation of mechanical properties of field cores as follows: (1) Texas gyratory compactor, (2) California kneading compactor, (3) mobile steel wheel simulator, (4) Arizona vibratory-kneading compactor, and (5) Marshall mechanical hammer.

Von Quintus et al. (1991) investigated the differences between five laboratory compaction methods, namely Texas gyratory compactor, ASTM kneading compactor, Arizona vibratory/kneading compactor, Marshall hammer and a steel roller, as a part of the Asphalt-Aggregate Mixture Analysis System (AAMAS) study in the NCHRP project. The aim was to identify promising laboratory compaction techniques which may simulate actual site condition. From the analysis of the results, it was found that the specimens compacted by the Texas gyratory compactor showed similar behaviour to actual site cores in terms of mechanical properties.

Sousa et al. (1991) investigated the permanent deformation characteristics of laboratory-compacted specimens in the SHRP project. In this study, three compaction methods namely Texas gyratory, kneading and rolling-wheel compactor were compared to analyze the differences of compaction methods. In addition to this, three types of mechanical test were performed in order to examine fundamental mixture properties among three types of compacted specimen. From their research, it was found that the rolling-wheel compaction most closely represents the aggregate structure characteristics of field cores. Also, their research indicated that the kneading compactor produces specimen with the strongest aggregate structure, while gyratory compaction produces the weakest specimens. This research also concluded that fatigue performance of asphalt mixes is not greatly affected from the compaction method. These findings were confirmed by a similar study (Harvey et al. 1994).

Button et al. (1994) examined the correlation between field cores and laboratory-compacted specimens. In their study, field cores were obtained from five different highway pavements, whereas specimens were manufactured using four laboratory compaction methods (i.e. Exxon rolling wheel, Texas gyratory, rotating base Marshall hammer, and the Elf linear kneading compactor) and using materials and mixture designs identical to those used in the pavement cores. Various physical properties of

pavement cores as well as the laboratory specimens were measured. Based on the results analysis their study concluded that the Texas gyratory compactor is the most suitable compaction method to simulate site compaction. The Exxon rolling compactor and Elf linear kneading compactor often simulated the behaviour of actual site cores, whereas the Marshall hammer did not show any similarities to site cores. However, specimens compacted by Exxon rolling-wheel compactor did not have similar air void contents to other laboratory-compacted specimens and therefore the specimens were not comparable to field cores.

Khan et al. (1998) evaluated the relationship between three laboratory compaction methods, namely Marshall (both manual and automatic), California kneading, and gyratory shear compaction (angles 1.25^{o} and 6^{o}) and field compaction. Laboratory-compacted specimens and field cores were evaluated in terms of resilient modulus, air voids, bulk density, and static creep behavior. Overall, the gyratory shear compactor (1.25^{o} angle of gyration) appeared to most closely represent the engineering properties of the field cores. The gyratory shear compactor (6^{o} angle of gyration) ranked second on the basis of its elastic and viscoelastic behavior as compared to that of the field samples, while the Marshall automatic impact compactor exhibited the poorest comparison to the field cores.

Renken (2000) studied the effect of various laboratory compaction methods relative to the field compaction. The mechanical characteristics - namely deformation, low-temperature and fatigue - of asphalt specimens, which were compacted in the laboratory using the Marshall, gyratory, slab compactor with sliding plates and slab segmented roller compactor, were determined and compared to cores compacted by rollers in the field. The results indicated that contrary to the Marshall and gyratory compactor which produce specimens with mechanical characteristics considerably better from the roller-compacted specimens, the segmented roller-compacted specimens show nearly the same mechanical behavior like the field cores.

Hartman et al. (2001) investigated the effect of different laboratory compaction procedures (roller, Marshall, vibrating hammer, and gyratory) on the indirect tensile stiffness and fatigue properties of two standard Irish bituminous mixtures (hot-rolled asphalt and dense base coarse macadam). The results indicated that the roller-compacted

specimens had lower stiffness properties that were similar to site compacted specimens; higher stiffnesses were measured for Marshall- and gyratory-compacted specimens. The findings of this study also suggest that using either the Marshall or the roller compaction methods similar indirect tensile fatigue strengths would be concluded when measuring in practice for HRA mixtures. Nevertheless, for continuously graded mixtures the Marshall compaction technique would probably produce specimens with significantly inferior indirect tensile fatigue strengths.

Peterson et al. (2004) evaluated field and Superpave gyratory compaction. Particularly, this study focused on the effect of various SGC control parameters, namely angle of gyration, height of specimen, compaction pressure, and compaction temperature on the mechanical properties of a conventional HMA measured with the Superpave shear tester. Results of this comparative study indicated that current gyratory protocol produces specimens with significantly different mechanical properties than field cores produced with the same material and compacted to the same air voids. However, the study results demonstrated that the 1.5° angle of gyration along with a specimen height of 50 or 75 mm would better simulate mechanical properties of roadway cores. Similar results may be also achieved by using the current 1.25° angle along with a 400 kPa pressure.

More recent studies compared field cores with specimens compacted in the laboratory by means of gyratory, vibratory and roller compactor (Airey and Collop 2016; Hunter et al. 2009; Airey et al. 2006). These studies considered the influence of laboratory compaction methods on the mechanical properties (stiffness modulus, permanent deformation and fatigue) of several continuously- and gap-graded asphalt mixtures relative to what is found in standard field compaction. The results demonstrated that in general mold-based compaction methods, namely gyratory and vibratory, tend to produce asphalt mixture specimens of greater stiffness and permanent deformation resistance than roller-compacted specimens. In terms of fatigue cracking resistance, the results indicated that mode of compaction does not significantly affect this mechanical property. Overall, the site compacted specimens tend to have mechanical properties that are more aligned with roller-compacted specimens than gyratory- or vibratory-compacted specimens particularly with regard to their stiffness modulus. On a similar

study, researchers found that the impact (Marshall) and gyratory compaction produces specimens with superior resistance to permanent deformation compared to field cores. On the contrary, laboratory roller-compacted specimens better represent field compaction-based deformation characteristics (Mollenhauer and Wistuba 2016).

Other researchers acknowledged the need to describe the magnitude of difference in stiffness modulus behaviour of asphalt mixes compacted in the laboratory (using the Marshall and Superpave Gyratory Compactor) and field (Thenoux and Sandoval 2011; Katicha et al. 2011). The results indicated that the modulus values of laboratory-compacted specimens (both Marshall and gyratory) are higher than the respective modulus values of field-compacted specimens by a factor of the order of 1.5. This finding seems to be confirmed from the results of a similar recent study, which found a stiffness ratio of the order of 1.8 between gyratory and field compaction (Airey and Collop 2016).

Engineers involved with asphalt mix design attempt to account for several key mixture parameters, including stiffness, fatigue resistance and permanent deformation. The above mentioned parameters characterize the asphalt mix and control the asphalt pavement structural performance. However, the asphalt pavement should provide road safety, as well. Pavement surface frictional characteristics play an important role in road safety and thus the incorporation of the skid resistance evaluation in the asphalt mix design practices is of extreme importance.

In particular, it is important for the safety of the driving public that roads provide adequate friction at the tire-pavement interface. Various factors affect the frictional characteristics of a tire- pavement surface system. These factors can be grouped into four categories; pavement surface characteristics, vehicle operational parameters, tire properties, and environmental factors. Among these categories the microtexture and macrotexture of asphalt mixture surface are key components of the tire- pavement surface interaction (Ergun et al. 2005; Dahir 1979). The microtexture and macrotexture of the surface and its friction are integrally related.

The texture of a new pavement is a consequence of HMA composition (mix-design) and of construction techniques, especially considering the compaction process. Currently, the design of asphalt mix accounting for skid resistance is rather empirical,

based on previous experience gained from typical textures achieved in the field from dense, gap or open-graded aggregate gradation and selection of high polish resistant aggregates.

As such, research has been launched to evaluate various aggregates blends to optimize the combination of micro- and macro-texture and achieve a satisfactory level of friction (Friel et al. 2013; Kowalski et al. 2008). Moreover, a laboratory polishing device and testing procedure was developed to accelerate polishing and evaluate the surface friction characteristics of HMA laboratory samples. However, this approach needs to be verified with field polishing results. Results from another study showed that the simulated road friction evolution curve, based on Wehner/ Schulze polishing test method, is similar to laboratory aggregate friction after 2 years (Do et al. 2007). However, the assessment of road polishing cannot be done only from the results of aggregate tests and should be complemented with the initial road surface friction information.

Other laboratory studies investigated the relationship between mix components properties and friction. A statistical model was developed to predict mix friction based on gradation and aggregates resistance to polishing (Rezaei et al. 2009). The British Pendulum Number (BPN) value of aggregates was recognized to affect the mix skid resistance and thus the proposed model may help in selecting the appropriate aggregate type for the desired mixture friction. A relationship between the initial field friction and mix properties (asphalt content, fineness modulus, bulk density and percent of aggregate passing the 4.75 mm sieve) was also proposed. A good correlation between macrotexture in terms of the mean texture depth (MTD) (measured using the sand patch method) of field- and gyratory-compacted specimens was further concluded (Goodman et al. 2006). However, poor correlation was observed between the British Pendulum Numbers recorded on unpolished field specimens versus gyratory specimens. The results suggested that the gyratory compactor orients the aggregate particles in a different manner compared to field compaction equipment. A more recent study evaluated the gyratory compactor ability to represent the surface properties of an asphalt mixture when laid on site (Boscaino et al. 2009). Based on the experimental results the authors concluded that, when predicting the surface characteristics (in terms of BPN and MTD)

of asphalt mixture, the gyratory compaction is not representative of the compaction in-situ.

2.4 Internal structure

Studying the relationship between laboratory and field compaction methods pavement engineers have recognized that the compaction method has a direct impact on the aggregate structure within the compacted mixture and hence characterization of internal structure of asphalt mixture is needed (Thyagarajan et al. 2010; Iwama et al. 2007; Hunter et al. 2004; Tashman et al. 2002). Previous researches have demonstrated that asphalt mixture internal structure, which refers to the distribution of aggregates and their associated voids, can be characterized using imaging techniques (Hunter et al. 2004; Saadeh et al. 2002; Masad et al. 1999a, b; Yue et al. 1995).

Among the several well-known laboratory compaction methods gyratory compaction, which has developed and improved over the past 50 years, has been the subject of significant research effort over time. Especially, after the implementation of the Superpave mixture design method where the use of Superpave Gyratory Compactor is integral part of mixture design, many research studies focused on evaluating and analyzing the asphalt mixtures behavior including the internal structure with respect to this method.

For example, Yue et al. (1995) published one of the first comprehensive studies on defining internal aggregate parameters in asphalt concrete (AC) mixtures derived from imaging, namely major and minor axes of aggregate particles, area, Feret diameter, major axis orientation, shape factor, and compactness. The quantitative results of AC microstructure study indicated the following findings: a) major and minor axes of aggregate particles are essential for quantifying both aggregate shape and orientation, b) the area gradation of aggregate cross sections by the Feret diameter gives an excellent prediction of the sieve gradation of coarse aggregates (greater than or equal to 2 mm) used in the design of AC mixtures and c) shape factor and compactness are measures of the aggregate particle shape and circularity. Moreover, the digital image-processing technique applied was found to be effective to evaluate the effect of two laboratory and two field compaction techniques in terms of preferred aggregate distribution within the

mixtures. Particularly, the study results indicated that asphalt mixture samples prepared by the gyratory compactor in the laboratory and the AMIR compactor in the field had more uniform distribution of coarse aggregate compared to the Marshall compactor and the conventional field roller compactor.

Masad et al. (1999a, b) proposed computer-automated image analysis procedures to quantify the internal structure of AC in terms of aggregate orientation, aggregate contacts, and air void distribution. The new procedures were used to study the difference in internal structure of AC specimens compacted with the SGC and the linear kneading compactor (LKC). Digital images of specimen sections were analyzed for aggregate contact and orientation and computed tomography (CT) images were used for quantifying the air void. Specimens compacted with the SGC were found to have aggregates with more preferred orientation (towards horizontal) and fewer contacts than specimens compacted with the LKC. Both compaction method samples (SGC and LKC) have non-uniform air void distributions. SGC specimens were found to have higher air void percentage at the top and bottom than in the middle, whereas air voids in LKC specimens were found to increase from the top to the bottom. In a follow-up study, the internal structure of asphalt samples prepared using the SGC varying the compaction level in terms of gyrations, namely 8, 50, 100, 109, 150, and 174 gyrations, was compared to that of samples from field cores. The internal structure parameters quantified in this study were air void distribution, aggregate orientation, and gradation. A similar finding with respect to air void distribution was found with more internal voids concentrated at the top and the bottom portions of the gyratory-compacted specimen. Moreover, it appeared that preferred orientation of the aggregates became more pronounced with compaction until an optimum value was reached (i.e. 100 gyrations); thereafter aggregates tended to have random orientation. Comparison of the internal structure of the gyratory-compacted specimens with field cores showed that the gyratory specimens reached the initial aggregate orientation of the field cores at a higher number of gyrations whereas they reached the percentage of air voids in cores at a lower number of gyrations. Moreover, coarse aggregate gradation of gyratory-compacted specimens was well captured using the image analysis techniques, while no change in gradation was observed with compaction.

Tashman et al. (2001) studied the factors affecting the internal structure of asphalt mixtures using the specimens compacted by SGC and field cores taken from three different sites. The asphalt mixtures were compacted changing four factors: gyratory angle; pressure; height and temperature, while the field pavements were constructed with different compaction methods. The results of the air void distributions for the gyratory-compacted samples were similar to previous studies, while the different patterns for field compaction did not influence the air void distribution. The aggregate contacts had random distribution in both gyratory specimens and field cores. The analysis showed that aggregate orientation was not affected by field compaction patterns. However, for the gyratory-compacted samples, both gyration angle and the height of the sample affected the aggregate orientation. Also, there was statistically no significant difference between gyratory specimens and field cores in terms of the separation between coarse and fine aggregates, although it was noticed that coarse aggregates had a slight tendency to move towards the circumference of a gyratory specimen. Overall, the findings suggested the use of an angle of 1.5^{o} and a specimen height of 50 mm to 75 mm in the gyratory compactor to better simulate the internal structure of field cores; pressure of 600 kPa gave the closest results to field cores although it was not a significant factor in influencing the internal structure. A similar study demonstrated that laboratory specimens compacted to a height close to that of field cores and using an angle of gyration of 1.25^{o} were better in simulating the aggregate distribution in the field (Saadeh et al. 2002).

Further research studies evaluated the air void distribution in gyratory specimens by means of X-ray computed tomography (Thyagarajan et al. 2010; Partl et al. 2003; Tashman et al. 2002). Air voids were found to be non-uniformly distributed along the horizontal and vertical directions in Superpave gyratory-compacted specimens. Tashman et al. (2002) found that more air voids were present in the outer region, while Partl et al. (2003) showed that the difference between the average air-void content of the core and exterior zone of the specimen is as large as 8.7% after initial compaction and decreases rapidly to less than 1% for the higher compaction levels. Moreover, both studies found that more air voids are concentrated in the top and bottom regions of a specimen. This suggests that the kneading process just below the center of the top and bottom loading

plate of the gyratory is not very effective and the compaction energy distribution follows a cone-shape pattern related to the geometry of the specimen (Thyagarajan et al. 2010). The compaction homogeneity within the gyratory-compacted specimens has been further investigated and cutting/coring process has been proposed to reduce the heterogeneity in the vertical direction, although this process did not seem to be sufficient in improving homogeneity in the lateral direction (Airey and Collop 2016; Thyagarajan et al. 2010; Muraya 2007).

Given the previously acknowledged capabilities of imaging techniques, research effort was also devoted to evaluate the influence of various compaction methods on internal structure of asphalt mixtures. Hunter et al. (2004) undertook research on the aggregate orientation and segregation of asphalt mixture laboratory specimens compacted using gyratory, vibratory and roller compaction. By means of image analysis techniques on cut surfaces of asphalt specimens using Image ProPlus software, it was concluded that significantly more aggregate orientation was obtained in mould-based specimens, namely gyratory and vibratory compacted specimens. This behavior is more pronounced in larger aggregate particles and in those with an aspect ratio (maximum length/ maximum width) greater than two. This performance may be attributed to the combined effects of compaction dynamics and the confining effect of the mould. Roller-compacted specimens showed random particle orientation. Moreover, whilst overall levels of aggregate particle density are similar across all the compaction methods considered, greater segregation occurs in vibratory and to a lesser extent in gyratory-compacted specimens. On the contrary, the slab compacted specimens showed a near uniform particle size distribution across the regions considered. Airey et al. (2006) also studied the aggregate orientation and segregation of laboratory-compacted specimens (i.e. gyratory, vibratory, roller compactor) compared to field specimens. The results indicated overall that slab compacted specimens tend to show closer correlation with field cores than gyratory and vibratory compacted specimens. Building on previous gained knowledge, the internal aggregate structure of laboratory-compacted specimens as a function of compaction method, specimen size and specimen orientation was also investigated (Iwama et al. 2007). Particularly, with regards to specimen size, it was demonstrated that specimens cored from larger specimens were less affected by mould

confining effects. Therefore, a more random particle orientation for both the gyratory and vibratory compacted specimens is observed. Similar conclusions were also drawn by means of X-ray CT image analyses (Hassan et al. 2012).

With advancements in technology, the capabilities of both 2-D and 3-D imaging techniques in terms of image capturing, processing and analysis have been improved significantly over time (Papagiannakis et al. 2014; Coenen et al. 2012; Zelelew and Papagiannakis 2011a, b). In this framework, new software for processing and analysis of two-dimensional images of asphalt mixtures has been developed to quantify the internal aggregate structure in terms of meaningful indices (Sefidmazgi et al. 2012). This software was used to analyze mixtures and quantify the effect of compaction methods and conditions on aggregate structure, as discussed hereinafter.

Coenen et al. (2012) studied the effect of varying compaction temperatures and pressures used in the SGC on aggregate structure indices. Lower temperature and pressure led to less contact points, no clear trend was identified with respect to the orientation results, while the results showed no evidence of segregation. Within the same study, various compaction methods, including Hveem, Marshall, German steel sector and Superpave Gyratory were compared. The results indicated compaction method influences significantly the aggregate orientation. Although the Superpave Gyratory showed the highest influence on the aggregate orientation in a radial fashion, this method seems to best resemble the predominant aggregate orientation seen in the field. However, it is worth mentioning that the level of influence (severity) observed in the field was similar to alternate laboratory methods such as the Marshall or the Hveem; hence additional investigation was suggested to determine which laboratory compaction method better reproduces internal structure parameters of field-compacted mixtures. In a follow-up study, newly developed image analysis indices, namely number of aggregate-to-aggregate proximity zones; total proximity zone length; and proximity zone plane orientation, were proposed to characterize the aggregate structure (Sefidmazgi and Bahia 2014). The study results showed that these indices can capture the effect of compaction conditions on the mixture internal structure; overall, samples compacted using different methods in the laboratory can lead to highly different microstructure.

Bessa et al. (2012), evaluating the effect of the Superpave gyratory compactor and LCPC compactor on the internal structure of various mixtures, found that the specimens extracted from the roller-compacted slabs have a higher level of contact points compared with the SGC ones. Regarding aggregates orientation after compaction, the aggregates distribution and orientation in terms of the vector magnitude were very similar for both compaction methods; however LCPC compactor mixtures presented lower segregation compared to SGC ones.

2.5 Lessons learned from the literature review

Regarding the asphalt mixture **compactability**, the literature review clearly indicates that among multiple factors affecting asphalt densification, the key compaction parameters are temperature; compaction energy (effort) and methodology; and lift thickness. Several studies attempted to examine the relationship between laboratory and field compactability, by means of gyratory method and field compaction methods, however results showed that a single correlation could not describe this relationship. It seems that evaluating in-situ the compaction characteristics of asphalt mixtures more essential information can be obtained in real-time, hence contributing to the improvement of compaction process and its effectiveness. Within this framework, the emerging technologies of infrared thermography and GPR have shown promising results. However, further research should be conducted in an effort towards standardization and inclusion of these technologies in compaction quality assurance practices.

Extensive research has been carried out to assess the influence of various compaction methods both in the laboratory and in the field on asphalt mixture mechanical properties. The results demonstrated that **permanent deformation (or rutting)** characteristics of asphalt mixtures are significantly affected from compaction methods. Also, the results indicated that between the asphalt mixture performance-based properties which interrelate with analytical pavement analyses, fatigue characteristics appear to be less influenced from the compaction method. On the contrary, **stiffness** properties of an asphalt mixture vary significantly with respect to the compaction method and also the stiffness modulus in laboratory does not necessarily correspond to

stiffness modulus in the field. This implies that for pavement analyses purposes either conversion factors should be established between laboratory and field compaction-based stiffness or research should be conducted to develop laboratory compaction regimes which tend to produce specimens with similar properties to field cores. This challenge becomes more essential considering that the European specifications offer the potential of selection among several compaction methods for the fabrication of asphalt specimens prior to its performance-based testing and hence comparability between the test results is vital. On this basis, within any compaction method, operational factors such as angle of gyration, number of roller passes etc. need to be evaluated.

Moreover, from research regarding the asphalt mixture **internal structure**, it has been manifested that gyratory specimens are heterogeneous in terms of air void distribution in vertical and lateral directions. Given the gyratory compactor wide spread and use, a limited number of studies focused to evaluate the ability of the Superpave gyratory compactor to simulate the internal structure of asphalt pavements. The results indicated that gyration angle and specimen thickness influence asphalt microstructure. Better simulation of field compaction is obtained using an angle of 1.25^{o} or 1.5^{o} and height close to that of field cores. Comparative studies also showed mixed results concerning compaction method best simulating field compaction in terms of aggregate orientation and segregation. Although new image analysis indices can be obtained due to technological advancements, for these indices to be meaningful it is essential that they are related with asphalt mixture engineering properties. This will provide insight to the impact of compaction factors on asphalt mixture microstructure and subsequently its performance; then image analysis can be an effective tool to improve the compaction process towards reproducing the field conditions.

Also, the importance to incorporate the **skid resistance** evaluation in the asphalt mixture design practices implies that the asphalt surface characteristics of specimens produced in the laboratory may be considered representative of the real mixture in-situ. Study results based on gyratory compaction demonstrated that this method is not representative, from a frictional point of view, of the field compaction. Hence, the effect of compaction on surface frictional characteristics still calls for further research to

identify the most adequate method for producing specimens that allow predicting the frictional properties of the as-constructed pavement surfaces.

3. Test sites and materials

3.1 Introduction

To accomplish the thesis objectives the research plan included three main tasks. Initially, the field sites, from which test samples would be collected, were selected; these were sections where paving and compaction was commenced. Secondly, loose mixtures from these sites were compacted using laboratory methods. Lastly, laboratory tests were conducted on the laboratory-compacted specimens and their performance, in terms of the key characteristics described in Fig.1.2, was compared to the performance of the field cores obtained from the selected sites. For the research purposes, laboratory batched and compacted specimens would alternatively be used to be compared with the field-compacted specimens. However, it is worth mentioning that differences generally exist between laboratory produced and plant produced mixtures. This variation would possibly affect the experimental results, thus adding complexity in evaluating differences in behavior of asphalt mixtures related to the compaction methods. In that respect, the approach that all specimens (laboratory- and field-compacted) are from mixtures produced in the plant was followed in terms of better understanding the differences induced from the laboratory- and field compaction methods. This chapter describes the test sites and HMA mixtures used for this research study.

3.2 Test sites

Three pavement construction projects were selected for the purposes of the present study. In each project, field test sections were constructed using various asphalt mixtures and compaction methods and monitored to record compaction-related parameters.

The first pavement construction project involved the paving and compaction of a 40mm surface course and 150mm asphalt base course over a 250mm granular base-subbase layer and subgrade. The asphalt base course was placed in three 5cm lifts; particular focus of this study was the top lift. Compaction was undertaken through common techniques. The rollers used was 10-ton steel double drum rollers, able to

operate in vibratory or static mode and a 9-ton rubber wheeled roller consisting of 8 tires.

The second pavement construction project involved the paving of a 50mm asphalt overlay surface course, using different dense-graded mixtures and compaction methods over the existing flexible pavement structure. Three new full-scale HMA pavement test sections were selected and evaluated, from which one section was divided into four subsections, which were compacted using different compaction modes. A 10-ton steel double drum roller, able to operate in vibratory or static mode was utilized to construct the test subsections.

The third pavement construction project involved the paving of a 30mm asphalt surface course, a 50mm binder course and 140mm base course over compacted unbound granular materials. This study concentrated only into the binder and base course mixtures. Field compaction was undertaken through common techniques and similar rolling patterns were followed for both mixtures.

3.3 Materials

As mentioned earlier, three construction projects were selected to provide the materials for this research study. Particularly, during paving plant-produced mix samples were collected, when feasible, to be used for the laboratory compaction studies. Moreover, after the asphalt layers construction and prior to trafficking, an adequate number of field cores (100mm in diameter) were retrieved from characteristic pavement locations to be used as ground truth data for comparative analysis, as shown in Fig. 3.1.

Fig. 3.1 Mix sampling (left) and field coring (right)

The experimental testing program included a range of asphalt mixtures designed by the standard Marshall Mix design method. Table 3.1 provides a description of mixtures used in this research study. Mixtures designation indicates the aggregate size on the mix, the course and the bitumen type (CEN 2006). Also, Fig. 3.2-3.3 show the gradation curves for the surface courses and binder-base course mixture types.

Table 3.1 Study mixtures information

Construction Layer	Designation	Bitumen type	Bitumen content (%)	Aggregate	Design air void (%)
SURFACE COURSE	AC12.5 surf PmB (SBS)	80/100+ 4%SBS	4.5	Steel slag-limestone	11.5
	AC12.5 surf 50/70[a]	50/70	4.3	Limestone	5.3
	AC12.5 surf 50/70[b]	50/70	4.3	Limestone	5.2
	AC12.5 surf 50/70[c]	50/70	4.3, 4.8, 5.2, 5.7	Limestone	6.3, 4.8, 4.0, 3.2
	AC 20 surf 50/70	50/70	3.8, 4.3, 4.8	Limestone	5.1, 4.0, 3.2
BINDER COURSE	AC12.5 binder 50/70+8%SLN	50/70+ 8%SLN	4.3	Limestone	3.3
BASE COURSE	AC20 base 50/70	50/70	4.3	Limestone	4.5
	AC20 base 50/70+8%SLN	50/70+ 8%SLN	4.2	Limestone	3.6
	AC20 base 50/70+10%SLN	50/70+ 10%SLN	4.3	Limestone	3.1

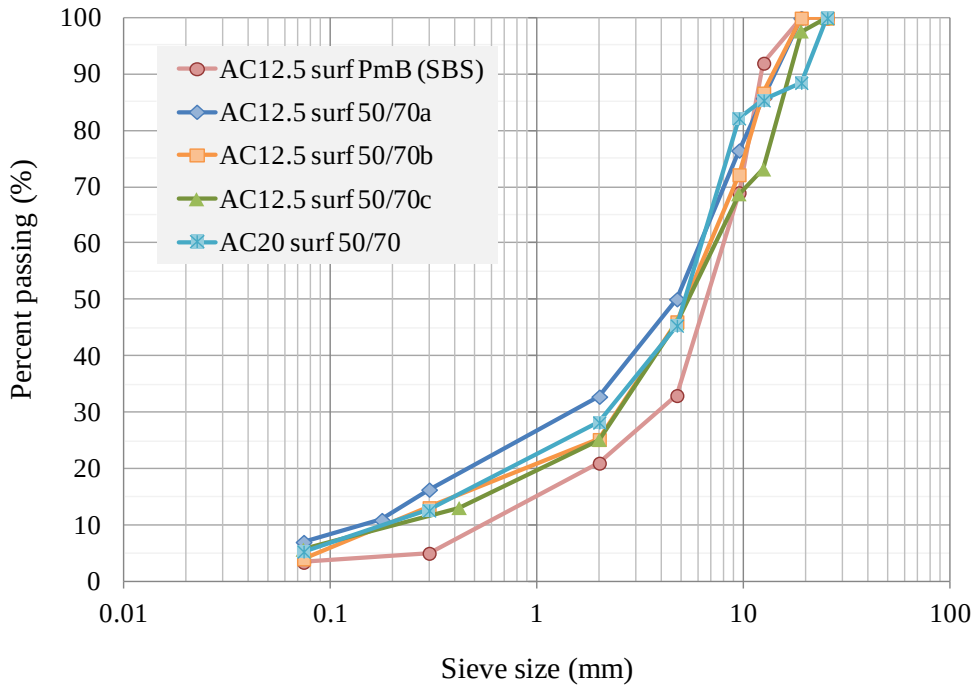

Fig. 3.2 Gradations of surface course mixes

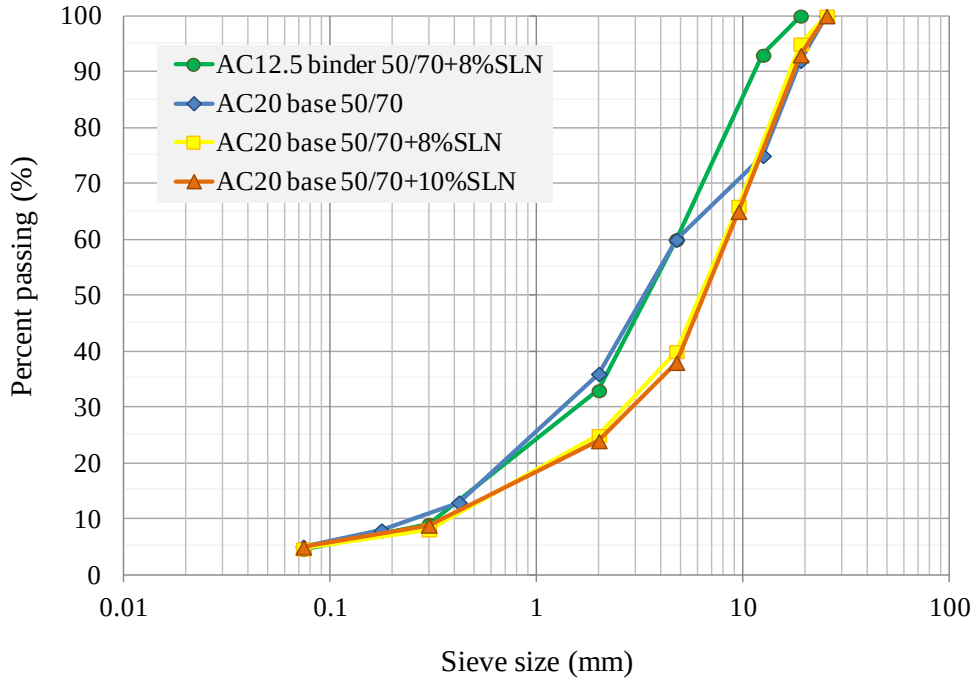

Fig. 3.3 Gradations of binder and base course mixes

It is worthwhile to mention that the mixtures were carefully chosen to represent varying aggregate gradations, sizes and bituminous binders and was expected to exhibit different performance. Also, the mixtures selected include basic mix designs used in the construction practice in Greece. Particularly, different types of surface course mixes - designed with crushed limestone and steel slag aggregates of various sizes (e.g. 12.5mm etc), pure (namely 50/70) and polymer modified bitumen (PmB) with SBS - were used in this Thesis. All surface course mixtures were dense-graded, except for the PmB mixture which consists of a semi-open gradation. Binder and base course mixtures, designed with crushed limestone aggregate and Selenizza (SLN) asphaltite modified bitumen along with a base mix with 50/70 bitumen, were also studied.

4. Compactability

4.1 Introduction

In the literature review presented in Chapter 2, the profound influence of compaction temperature, energy (effort) and methodology on the asphalt mix compactability was underlined. For this reason, a multi-factorial evaluation of the compactability of various asphalt mixes is commenced, by means of modern test methods, on the basis of extensive laboratory and field experiments.

Starting with an introductory overview of the test methods, focusing on the Non Destructive Testing (NDT) technologies and its principles used for the research, in the second part of this Chapter the laboratory experiments conducted by means of gyratory and roller compaction methods for the assessment of compactability of various HMA types are presented.

In the third part of this Chapter, the field experimental surveys for the assessment of the in-situ HMA compactability are also presented. Moreover, the performance of various models to predict the in-situ density along with the relationship between laboratory and field compactability indicators is evaluated.

4.2 Test methods

4.2.1 Gyratory compaction

Among the several well-known laboratory compaction methods gyratory (kneading) compaction, developed and improved over the past 50 years, now enjoys popularity throughout the worldwide asphalt pavement industry (Harman et al. 2002). This compaction method is widely used in USA, France, Australia and other countries, while many countries are involved in a transition process from Marshall to Gyratory compaction.

Compaction by means of gyratory compactor is achieved by the simultaneous action of a low static compression, and of the shearing action. This results from the motion of the axis of the mould which generates a conical surface of revolution, while the ends of the test piece should ideally remain perpendicular to the axis of the conical surface, as

shown in Fig. 4.1. Using a gyratory compactor, compaction is governed by vertical pressure, angle of gyration and gyratory speed. According to European norm vertical pressure, gyratory speed and angle of gyration are specified as 0.6 MPa; 30 revolutions per minute; and 0.82° respectively (CEN 2007), while the AASHTO specifies 1.16° for the angle of gyration (AASHTO 2012).

Fig. 4.1 Gyratory compactor

Different approaches can be followed when using a gyratory compactor: a) compaction with a set number of gyrations, b) compaction to a target density or air voids content and c) compaction to a target specimen height. During compaction the height of the sample (i.e. $h(n_{(g)})$) is automatically measured and displayed to the nearest 0.1 mm. Using the height data taken throughout the compaction cycle, the density of the mix at various numbers of gyrations is determined, as mathematically expressed in Eq. 4.1. Then, the air voids content of the mix is calculated and may be plotted on a semi-logarithmic graph with the log of the number of gyrations on the x-axis.

$$\rho(n_g) = \frac{M}{\pi \frac{D^2}{4} h(n_g)} \quad (4.1)$$

where M is the mass of the mixture to be introduced in the mould, D is the internal diameter of the mould, $h(n_{(g)})$ is the height of the specimen after a number of gyrations n_g.

It is also worth mentioning that researchers, on the basis of the gyratory compaction curves, developed indicators to assess the HMA compactability. Many indices have been reported in the literature (Dessouky and Diaz 2015). In this research, meaningful indices - namely the slope of compaction curve and the gyrations to achieve 8 percent air voids- as described hereinafter, have been accounted for the evaluation of the mix compactability. The aim was to compare the results obtained for gyratory compaction, as well as roller compaction, of specimens with the results achieved by field compaction and hence to establish laboratory test conditions to obtain field-like compaction characteristics.

The slope of compaction curve (b) may be used as criterion to assess whether compaction is difficult or easy. For example, higher slope indicates that there is an elevated reduction of air voids as a function of gyrations.

The number of gyrations to achieve 8 percent air voids (N_8) reflects the uppermost compaction level to be achieved in the field for dense asphalt mixtures and can be used to assess the requisite number of field roller passes.

4.2.2 Roller compaction

The steel roller compactor provides a means of compacting parallelepipedal specimens (slabs) of bituminous mixtures in the laboratory under conditions which simulate in-situ compaction.

Fig. 4.2 Roller compactor

The roller compactor consists of a curved steel segment, pivoting on a hinge and applying downwards force, as illustrated in Fig. 4.2a. Different levels of vertical force can be selected up to approximately 30 kN. The width of the roller is 305 mm, thus the compactive effort of the largest site roller can be reproduced. Applied load can be constant throughout the compaction, or can be increased at a preset number of cycles. A vibration option is also available to simulate on-site vibratory rollers, as illustrated in Fig. 4.2b.

Three different approaches can be followed when using a smooth steel roller: a) compaction by a specified energy, b) compaction with controlled compaction energy and c) compaction to obtain compaction degree (CEN 2007).

4.2.3 Infrared thermography

Infrared thermography makes use of the infrared spectral band and Planck's law, which claims that all objects with temperatures above absolute zero (-273.15°C or -459.67°F) emit infrared radiation. The magnitude of the radiation emitted is heavily dependent on the objects' temperature. Based on this, it is possible to produce images of that radiation and consequently the objects' temperature, called thermographs (Arndt 2010).

The radiation emitted by an object is a percentage of the radiation emitted by a blackbody at the same temperature (Maldague 2001; Gaussorgues 1994). A blackbody is defined as an object capable of totally absorbing all incident radiation, whatever its wavelength. According to Kirchhoff's Law, the blackbody is also an emitter of radiation of all wavelengths, transferring energy to the surrounding until a state of thermodynamic equilibrium is achieved. Real objects, however, never comply with these laws over an extended wavelength region, although they may approach the blackbody behavior in certain spectral intervals.

There are three events that occur and prevent a real object from behaving as a blackbody: a portion of the energy received is absorbed (α), a portion is reflected (r) and if the body is not opaque a portion is transmitted through (t). The sum total of the three individual parts must always add up to the initial value of radiation which left the source, as (Eq. 4.2):

$$a + r + t = 1 \quad (4.2)$$

An object's ability to radiate infrared energy depends on several factors which include material type, surface condition and wavelength. The value of emissivity (ε) for an object is an expression of its ability to radiate infrared energy. Emissivity is really a comparison between the energy emitted by the target object and an ideal emitter or black body at the same temperature. Hence, emissivity may be expressed as follows:

$$\varepsilon = \frac{E_0}{E_b} \quad (4.3)$$

where E_0 is the radiation emitted by target object at temperature T, and E_b is the radiation emitted by ideal emitter or black body at the same temperature T.

Emissivity (ε) of an object is not constant, as it depends on temperature, wavelength and direction. However, it may be considered as a constant within a certain bandwidth, range of temperature and cone of direction. Theoretically, it ranges from 0 (completely non-emitting materials) to 1 (completely emitting materials). For example, a mirror would exhibit emissivity below 0.1, while the human skin has an emissivity of 0.98. For asphalt pavement surfaces, emissivity is also a measure of the ability of asphalt mixtures to radiate absorbed energy. It is worth mentioning that for an opaque object Eq 4.2. changes as:

$$a + r = 1 \quad (4.4)$$

This means that a target surface such as an asphaltic one, which is non-reflective, has a high emissivity. For instance, asphalt concrete's emissivity ranges from 0.93 (in-service pavements) to 0.98 (new pavement constructions) (Ibos et al. 2006).

The systems used to measure and image the emitted infrared radiation from an object are based on complex infrared or thermal cameras. When viewing an object, the camera receives radiation not only from the object itself, but it also collects radiation from the surroundings reflected via the object surface. Both of these radiations are affected to some extent by the atmosphere in the measurement path (Maldague 2001).

In summary, there are three major contributors to infrared radiation:

a) the emission from the object $\varepsilon\tau W_{obj}$, where ε is the emittance of the object, τ is the transmittance of the atmosphere and W_{obj} is the radiation power from a blackbody source of temperature T_{source}, while the temperature of the object is T_{obj},

b) the reflected emission from ambient sources $(1\text{-}\varepsilon)\tau W_{refl}$, where $(1\text{-}\varepsilon)$ is the reflectance of the object, while the ambient sources have the temperature T_{refl} and

c) the emission of the atmosphere $(1\text{-}\tau)W_{atm}$, where $(1\text{-}\tau)$ is the emmitance of the atmosphere, the atmosphere has the temperature T_{atm}.

The total received radiation power is expressed as following:

$$W_{tot} = \varepsilon\tau W_{obj} + (1-\varepsilon)\tau W_{refl} + (1-\tau)W_{atm} \quad (4.5)$$

By using Eq. 4.5, W_{obj} can be calculated and the object's temperature T_{obj} can be defined. Figure 4.3 shows a schematic representation of the thermographic measurement.

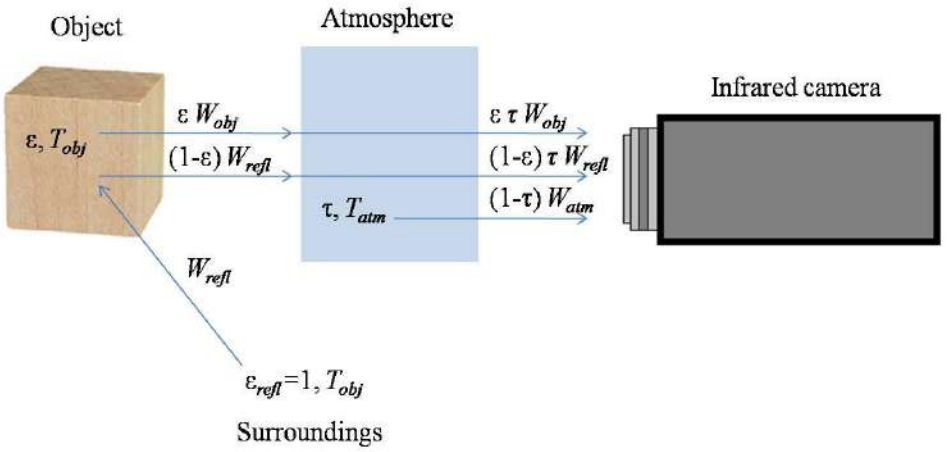

Fig. 4.3 Representation of a thermographic measurement

The thermographic system used in this thesis, consists of a ThermoVision A325G infrared camera developed by Flir Systems (Flir Systems 2007) and a conventional digital camera. The ThermoVision camera provides a 320 x 240 pixel image, temperature measurements ranging from –20 to 350°C with an accuracy of ± 2°C, operating in the far infrared spectrum (7.5-13μm). The system collects data as scans of temperature, is portable and is mounted on a properly modified vehicle, as shown in Fig. 4.4.

Fig. 4.4 The NTUA thermographic system

The NTUA thermographic system was used to record surface mat temperature during the laying and compaction of several pavement test sections. The collected data were preprocessed and analyzed with suitable software and the results are presented in the following sections.

4.2.4 Ground Penetrating Radar

The Ground Penetrating Radar technique is an example of a non-intrusive technique that is increasingly being employed in pavement surveying. The principle of GPR systems operation is based on sending an electromagnetic pulse through an antenna to the pavement surface and then recording the reflected pulses from the internal interfaces, where there is a contrast in the dielectric properties. Depending on the way the antennas are used, GPR systems are classified as either air-coupled or ground-coupled systems.

In air-coupled systems, the antennas (usually horn antennas) are typically deployed 150–500 mm above the surface. These systems give a clean radar signal and allow for highway speed surveys. For flexible pavements, the air-coupled system is usually preferred over the ground-coupled system, as data collected by the air-coupled system allows for the estimation of the dielectric properties of the layers, which are necessary for accurate GPR data interpretation (Saaranketo and Scullion 2000).

In general, air-coupled GPR systems operate in the range from 500 MHz to 2.5 GHz. Their penetration depth is typically 0.5-0.9 m and they are consistent with the impulse technique. The impulse radar technique is based on the principle that a short (0.5 to 1.5 ns) electromagnetic pulse is transmitted into the pavement through its surface. The pulse travels through the pavement layers and reflects off surfaces or objects, which cause discontinuities in electrical properties such as changes in the type of material or in either moisture content or density (Daniels 2004). The recorded reflections depend on the velocity of the waves' propagation, which is governed by the electromagnetic properties of the materials. The propagation velocity of electromagnetic waves in pavement materials is a function of the electric permittivity of the material mixture and is influenced by the water content.

The electric permittivity, which is the key property for GPR applications, describes the behavior of the material to polarize in response to the electric field (Al-Qadi et al. 2001). For a layered structure, such as a flexible pavement, the electric permittivity of the HMA layer ε_{HMA} can be estimated from the amplitudes of the reflected pulses as following, referred among others by Maser and Scullion (1991):

$$\varepsilon_{HMA} = \frac{1 + \frac{A_0}{A_p}}{1 - \frac{A_0}{A_p}} \quad (4.6)$$

where ε_{HMA} is the electric permittivity of the HMA layer, A_0 is the amplitude of the surface reflection (Fig. 4.5) and Ap is the amplitude of the incident GPR wave obtained by collecting data over a metallic plate placed on the surface of the pavement (Fig. 4.6).

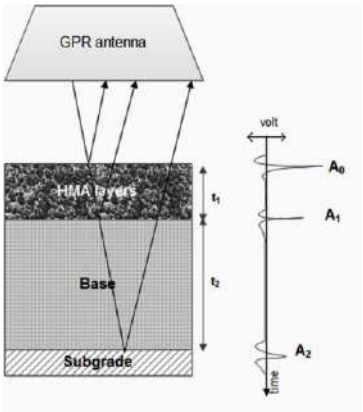

Fig. 4.5 GPR trace reflection amplitude in HMA pavements

Fig. 4.6 Calibration procedure using a metallic plate

It is worthwhile mentioning that by using Eq. 4.6 the attenuation of the GPR signal with increased propagation distance is not considered. This aspect is not binding towards the accuracy of the electric permittivity value referred to the initial air-surface reflection, as the attenuation of the GPR signal in air is limited. However, signal attenuation in the pavement subsurface layers is not negligible and may reduce the accuracy of the permittivity value arising from amplitude data recorded for deeper pavement layers (Saarenketo and Scullion 2000).

4.2.4.1 Density prediction models

Recent improvements in hardware, as well as the advancements in computer and software technologies have contributed to the rapidly expanding popularity and usability of GPR technique in pavement engineers' community. Further to popular GPR applications in pavements, such as determining layer thickness, detecting subsurface distresses, estimating moisture content, detecting voids and others, limited research studies concerning evaluation of pavement compaction have shown promising results. Particularly, researchers have demonstrated the potential of GPR coupled with the use of novel algorithms to predict the in-situ field density.

HMA is a composite material that contains asphalt binder, aggregates and air. Similar to HMA density, which depends on the specific gravities and volumetric fractions of its components, the electric permittivity of HMA is considered to be a function of the dielectric and volumetric properties of its components, as well. On this basis, researchers have recently developed various models, based on the Electromagnetic

Mixing (EM) theory, to assess the electric permittivity of HMA and predict its bulk specific gravity (density) in the field (Leng et al. 2012; Leng et al. 2011). These models, namely the Complex Refractive Index Model (CRIM), the Rayleigh model, and the Al-Qadi, Lahouar and Leng (ALL) model are expressed, respectively, as follows:

$$G_{mb} = \frac{\sqrt{\varepsilon_{HMA}} - 1}{\left(\frac{P_b}{G_b}\right)\sqrt{\varepsilon_b} + \left(\frac{1 - P_b}{G_{sb}}\right)\sqrt{\varepsilon_s} - \left(\frac{1}{G_{mm}}\right)} \quad (4.7)$$

$$G_{mb} = \frac{\frac{\varepsilon_{HMA} - \varepsilon_b}{\varepsilon_{HMA} + 2\varepsilon_b} - \frac{1 - \varepsilon_b}{1 + 2\varepsilon_b}}{\left(\frac{\varepsilon_s - \varepsilon_b}{\varepsilon_s + 2\varepsilon_b}\right)\left(\frac{1 - P_b}{G_{sb}}\right) - \left(\frac{1 - \varepsilon_b}{1 + 2\varepsilon_b}\right)\left(\frac{1}{G_{mm}}\right)} \quad (4.8)$$

$$G_{mb} = \frac{\frac{\varepsilon_{HMA} - \varepsilon_b}{3\varepsilon_{HMA} - 2.3\varepsilon_b} - \frac{1 - \varepsilon_b}{1 - 2.3\varepsilon_b + 2\varepsilon_{HMA}}}{\left(\frac{\varepsilon_s - \varepsilon_b}{\varepsilon_s - 2.3\varepsilon_b + 2\varepsilon_{HMA}}\right)\left(\frac{1 - P_b}{G_{se}}\right) - \left(\frac{1 - \varepsilon_b}{1 - 2.3\varepsilon_b + 2\varepsilon_{HMA}}\right)\left(\frac{1}{G_{mm}}\right)} \quad (4.9)$$

where G_{mb} and G_{mm} is the bulk and maximum specific gravity (density) of asphalt mixture respectively, G_{se} is the effective specific gravity of aggregate, G_{sb} is the bulk specific gravity of aggregate, P_b is the bitumen content, G_b is the specific gravity of binder, ε_{HMA} is the electric permittivity of the asphalt mixture, ε_b is the electric permittivity of the bitumen, and ε_s is the electric permittivity of the aggregate.

According to the above equations, G_{mb} is the model output, while ε_{HMA} is measured from GPR, ε_b is assumed as constant with a value of 3 and ε_s is the electric permittivity which depends on the aggregate type and source; thus it should be determined from a back calculation procedure. The remaining parameters G_{mm}, G_{se}, G_{sb}, P_b and G_b can be obtained from the mix design.

Moreover, Finnish researchers in previous studies (Saaranketo 2012; Roimela 1998) based on statistical analysis results developed an exponential model, described by Eq. 4.10 and known as PANK model, relating the asphalt pavement surface electric permittivity and air void content. Using the air void content values determined using laboratory methods from the drill cores, and their respective electric permittivity values, the calibration coefficient k is determined. Then, based on the established function, the

air voids in the asphalt pavement layers can be predicted by plugging the ε_{HMA} into Eq. 4.10.

$$\text{Air voids (\%)} = 272.93\text{e}^{-1.3012\text{k}\varepsilon_{HMA}} \quad (4.10)$$

where *k* is the calibration factor

Certainly, regression equations can be developed using the same exponential form and relating the electric permittivity ε_{HMA} and density ρ_b (or air voids content), as shown in Eq. 4.11. In this case, the calibration factors *a*, *b* should be determined on the basis of fitting the experimental data.

$$\rho_b = \text{ae}^{\text{b}\varepsilon_{HMA}} \quad (4.11)$$

where *a*, *b* are regression-based calibration factors.

4.2.5 Nuclear/ Non-nuclear density gauges

Conventionally, in-situ density is monitored using three basic methods: cores, nuclear- or non-nuclear density gauge measurements. Cores are generally considered to be the most accurate means of measuring in-situ density, this method however is both intrusive and time consuming. Cores can be taken only after the compacted bituminous mixture has cooled sufficiently and the cored samples need to be completely dry before bulk density measurements can be performed in the field or laboratory using the surface saturated dry (SSD) method and by dimensions method (CEN 2007). Because of the destructive nature of extracting cores, contractors and agencies have implemented for many years both non-destructive nuclear and non-nuclear density gauges for quality control, and in some cases for acceptance (Smith and Diefenderfer 2004; Choubane et al. 1999). Further, non-destructive gauges allow more rapid assessment of in-situ density during construction.

The application of the nuclear gauges is based on the transmission and reception of gamma rays (ASTM 2005). Nuclear gauges usually contain a small gamma source such as the Cesium-137 on the end of the retractable rod (Fig. 4.7). Gamma rays emitted from the source interact with electrons in the pavement; some rays are absorbed by the HMA and only those which are scattered back into the Geiger-Mueller detectors are counted. Although nuclear density gauges can work in a back-scatter or a direct transmission mode, most pavements are tested in back-scatter mode where both the source and

detectors are placed on the pavement surface. The number of photons reaching the detectors is inversely related to the density of HMA; namely, the fewer the photons, the higher the density. However, calibration of nuclear gauges is required to achieve better correlation between the nuclear gauge density values and core sample density values.

Fig. 4.7 Troxler gauge

Recently, non-nuclear electromagnetic density gauges have entered the market, which have the potential to replace nuclear density gauges and the coring process. These non-nuclear devices use electromagnetic signals to measure in-place density (ASTM 2010). The use of electromagnetic signals has the advantages of completely eliminating nuclear source licensing, training and certification of operators, specialized storage, and risks associated with devices that use a radioactive source, while also being non-destructive. The most popular of these devices is the Pavement Quality Indicator (PQI), commercially available by Trans-Tech Systems Inc. (Fig. 4.8).

Fig. 4.8 PQI gauge

The PQI operation is based on a novel toroidal electrical sensing field that is established in the material to be measured (e.g., HMA) via a flat sensing plate. Density, or compaction degree, is measured by the response of the PQI's electrical sensing field to changes in electrical impedance of the material matrix, which in turn is a function of the composite dielectric constant of the paving material and the air trapped in the voids of the material. Once calibrated, respectively to the nuclear method, direct density readings can be consistently obtained. PQI is also equipped with an infrared temperature probe and hence mat temperature can be measured and displayed during measurements.

4.3 Laboratory study

4.3.1 Gyratory compaction

Primarily, the objective of the gyratory compaction study was to investigate the influence of the compaction temperature, internal angle of gyration- which is believed to be related to the compactive effort, and specimen geometry on the compactability of asphalt mixtures. However, recalling the literature review a further investigation was carried out to gain more insight regarding the non-homogeneity of air void distribution induced by means of gyratory compaction.

The test matrix included gyratory compaction at various temperatures, a typical and higher one, while the vertical pressure was held constant at standard 600kPa, which is believed to approximate the contact pressures at which most of the compaction happens in the field (Delgadillo and Bahia 2008). Also, three different values of internal angle of gyration, which hereafter will be found as gyration angle or, simply, angle for sake of brevity, were selected which are specified in different international standards. Specifically, the gyration angles selected were: 0.82^{o} as suggested by the European Standard (CEN 2007), 1.16^{o} according to AASHTO specifications (AASHTO 2012) and a higher value of 1.45^{o} for which it was hypothesized to produce specimens with different compaction characteristics. Specimens of different geometries in terms of diameter (100 mm and 150 mm) and height (70 mm and 170 mm) were fabricated. After compaction, specimens dedicated for evaluation of air void distribution were trimmed, while the 150 mm diameter specimens were cored and 100 mm diameter specimens were obtained. Hence, two groups were obtained, namely cut and cut/cored gyratory

specimens to evaluate air voids in both the vertical and lateral directions in comparison with the as-compacted specimens. Also, additional specimens were fabricated at the same compaction energy (in terms of gyration number) for the compactability assessment. Overall, the gyratory compaction parameters studied are summarized in Table 4.1.

Table 4.1 Gyratory compaction study parameters

Parameters	Level
Temperature (^{o}C)	135, 150
Internal gyration angle (^{o})	0.82, 1.16, 1.45
Specimen geometry (diameter-height) (mm)	100-70, 100-170, 150-70, 150-170

Two hot-mix asphalt mixtures were used in the investigation. Both represent 'production' mixes, sampled during placement. The two mixes include: (1) a surface course mix with 50/70 binder and (2) a base course mix with 50/70 binder, denoted, respectively, as AC12.5 surf 50/70^{a} and AC20 base 50/70 as described in Chapter 3. Buckets of HMA were heated and the loosened mixtures were compacted. A total of 72 specimens for both mixtures were fabricated. After fabrication, the HMA laboratory-prepared specimens were tested for density and air voids content (CEN 2007).

4.3.1.1 Influence of gyratory compaction on air void homogeneity

This subsection discusses the influence of the gyratory compaction parameters on the air void distribution, both vertical and lateral, by means of mechanical process. Particularly, fabricated specimens were tested to evaluate the air voids after: a) compaction (denoted as-compacted), b) cutting of both top-bottom surfaces (denoted cut), and c) coring, only for 150mm diameter specimens (denoted cut/cored). Based on the bulk densities measured (using the SSD method) and the maximum density of each mixture, the air voids contents were calculated for all as-compacted and cut/cut-cored specimens (CEN 2007a; CEN 2007b; CEN 2007c).

Figures 4.9-4.12 show the air void test results with respect to the various specimens' geometries concerning the AC12.5 surf 50/70^{a}, while Fig. 4.13-4.16 show the counterparts related to the AC20 base 50/70 mix.

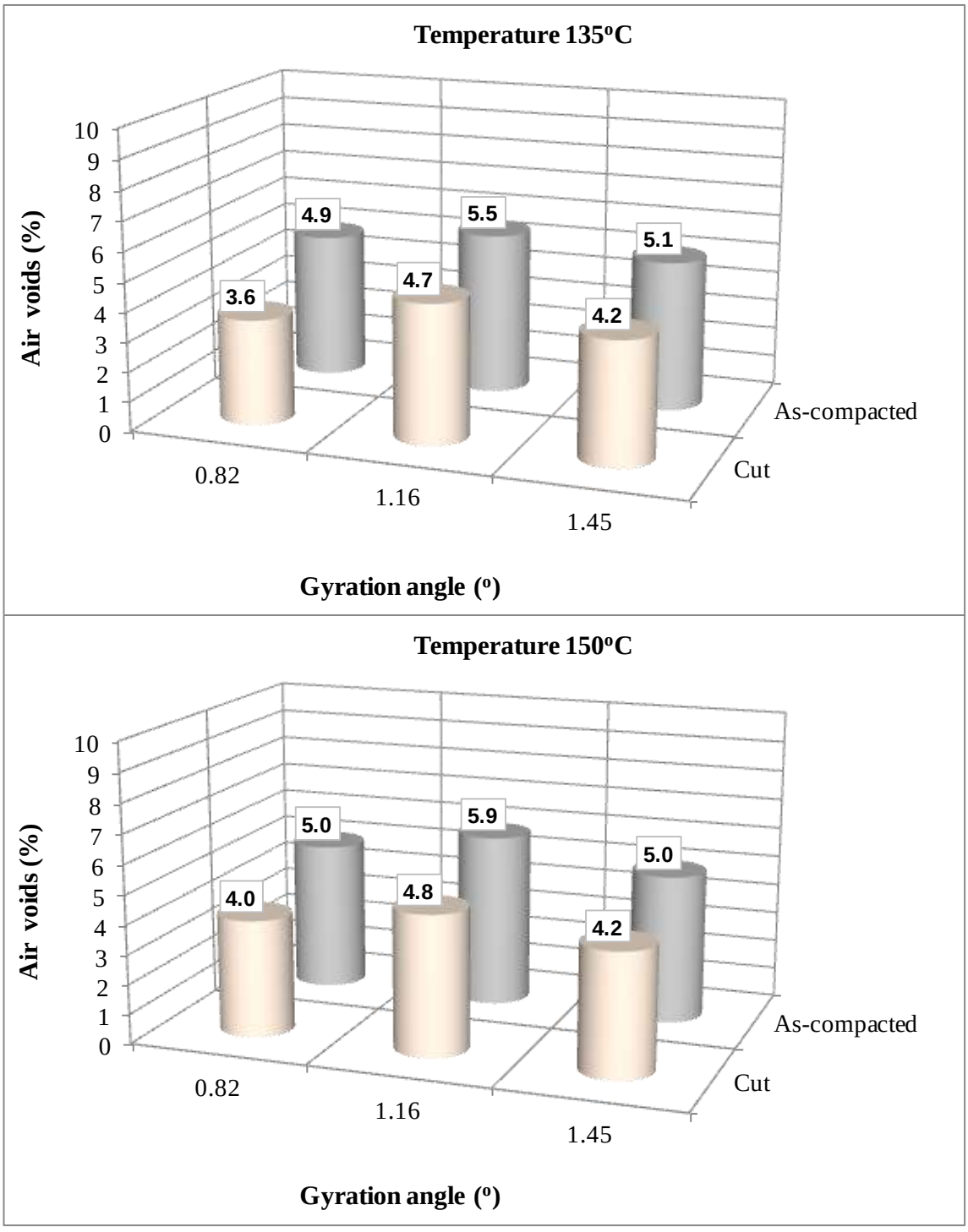

Fig. 4.9 Air void results concerning type 100-70 specimens (AC12.5 surf 50/70[a])

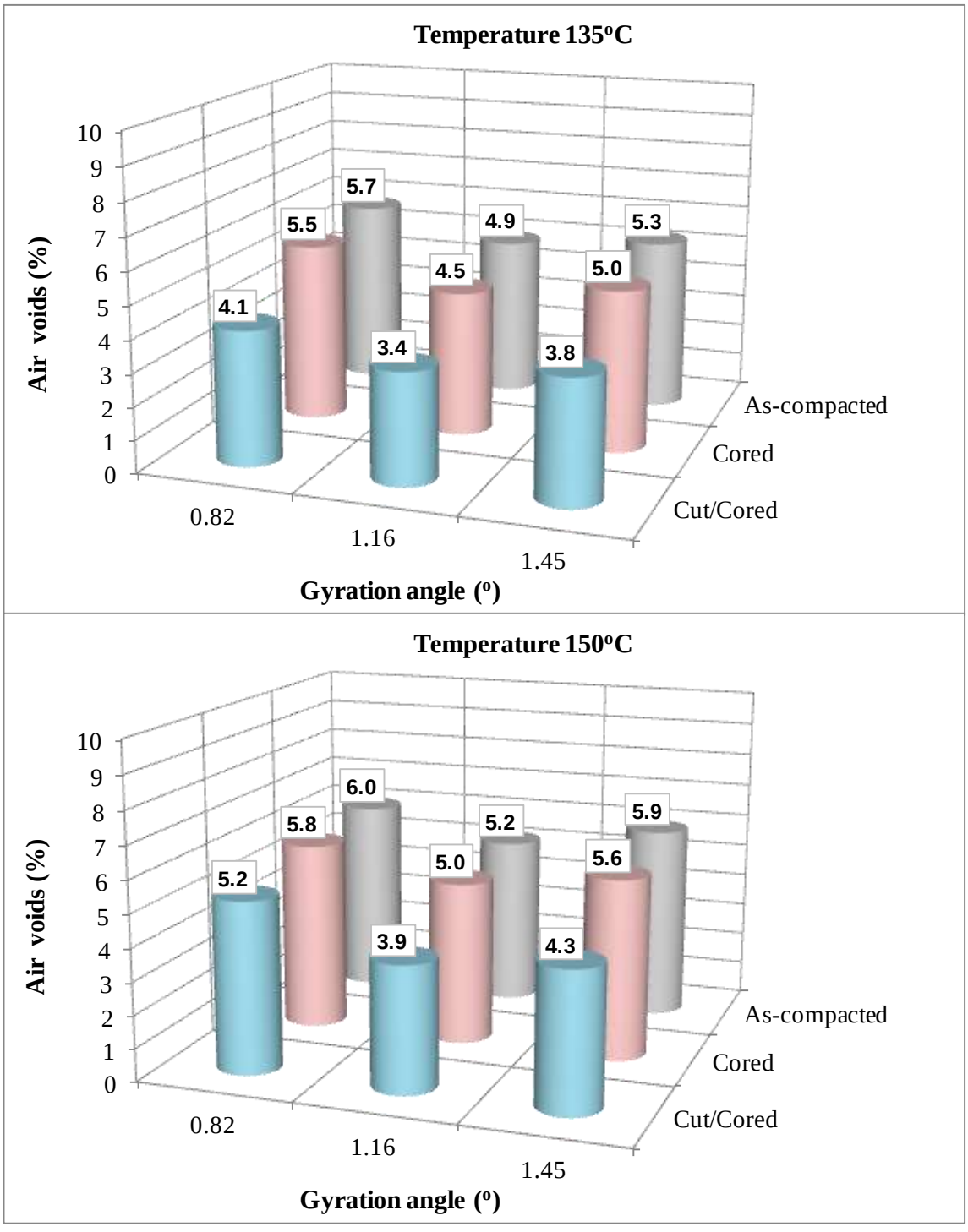

Fig. 4.10 Air void results concerning type 150-70 specimens (AC12.5 surf 50/70[a])

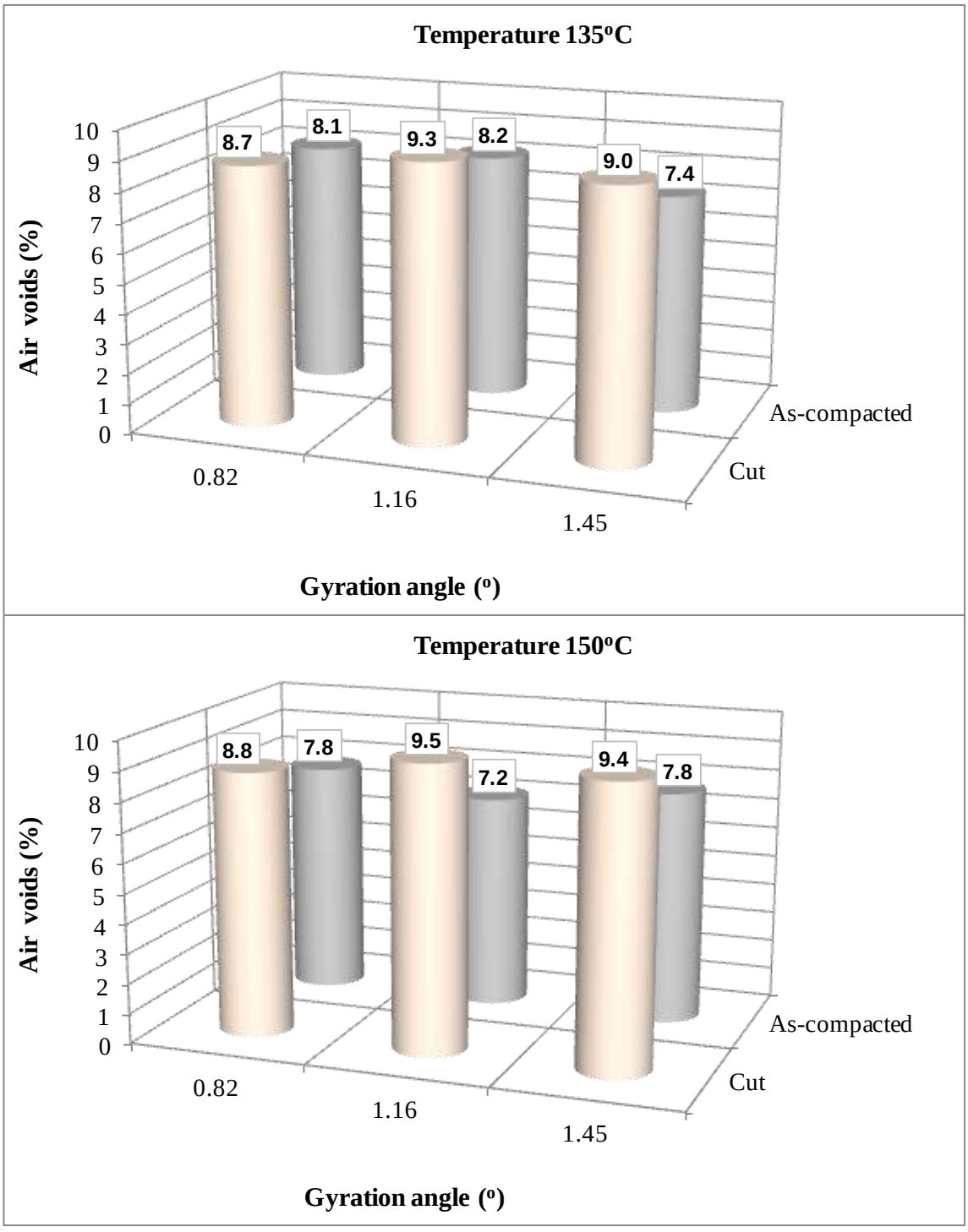

Fig. 4.11 Air void results concerning type 100-170 specimens (AC12.5 surf 50/70[a])

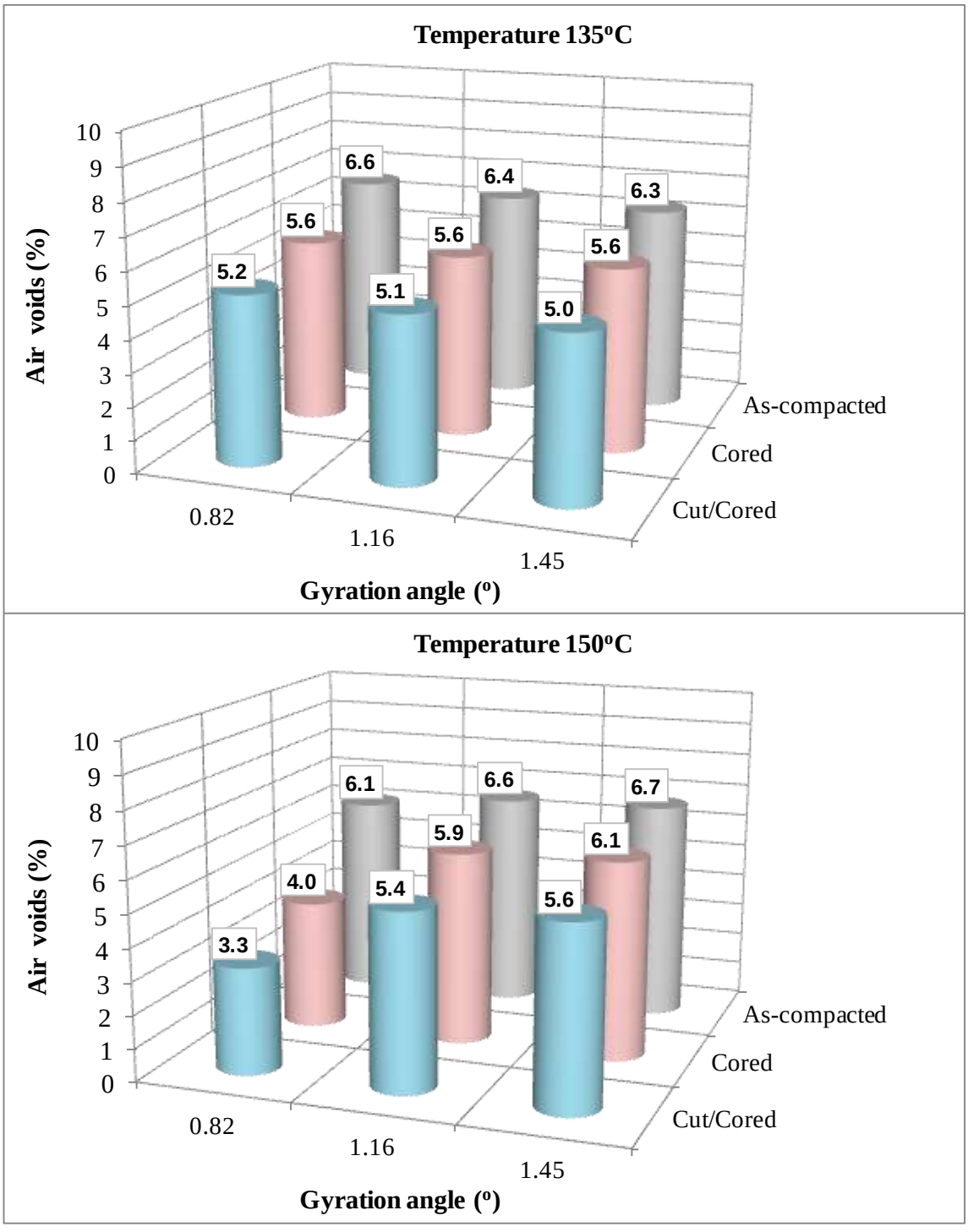

Fig. 4.12 Air void results concerning type 150-170 specimens (AC12.5 surf 50/70[a])

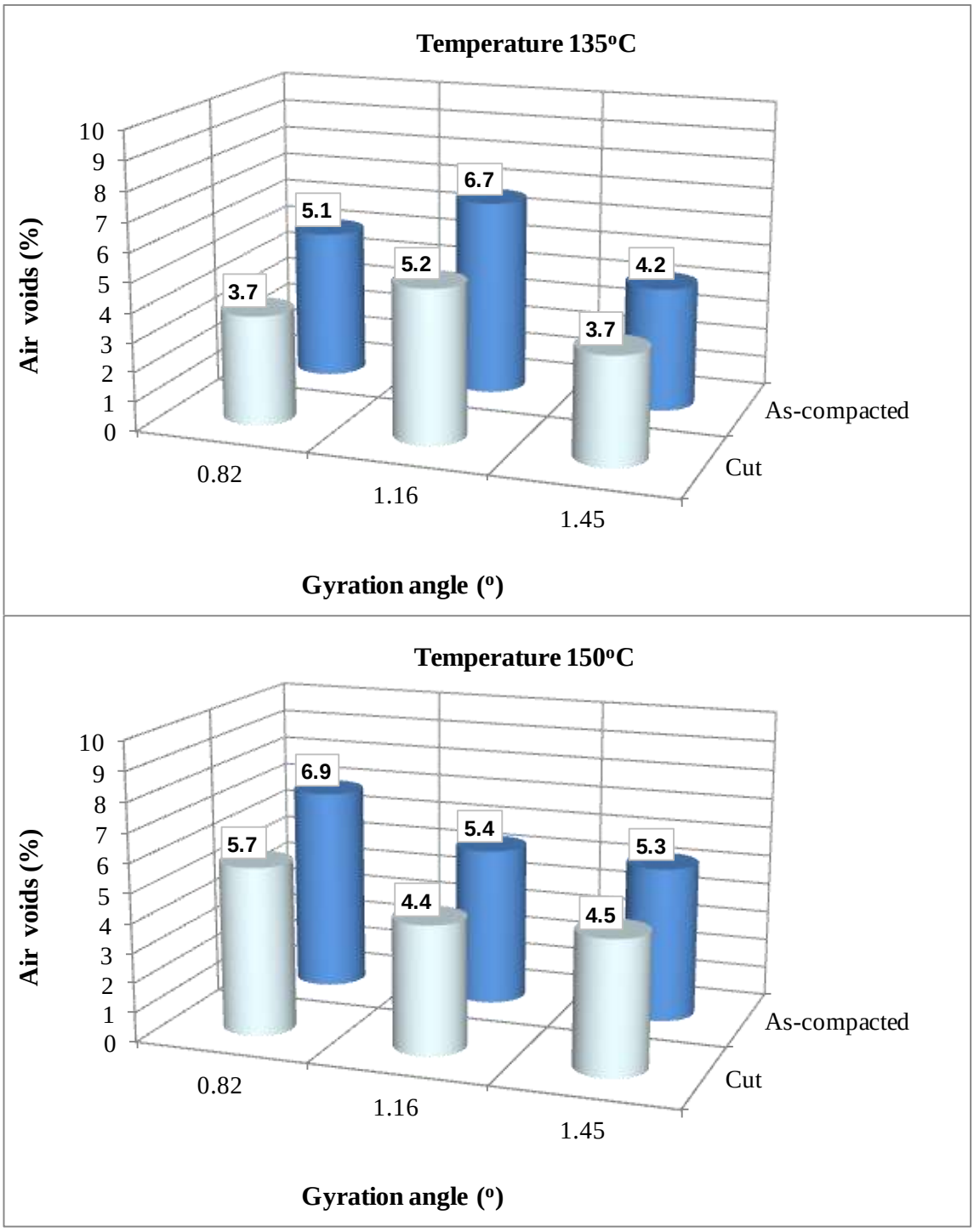

Fig. 4.13 Air void results concerning type 100-70 specimens (AC20 base 50/70)

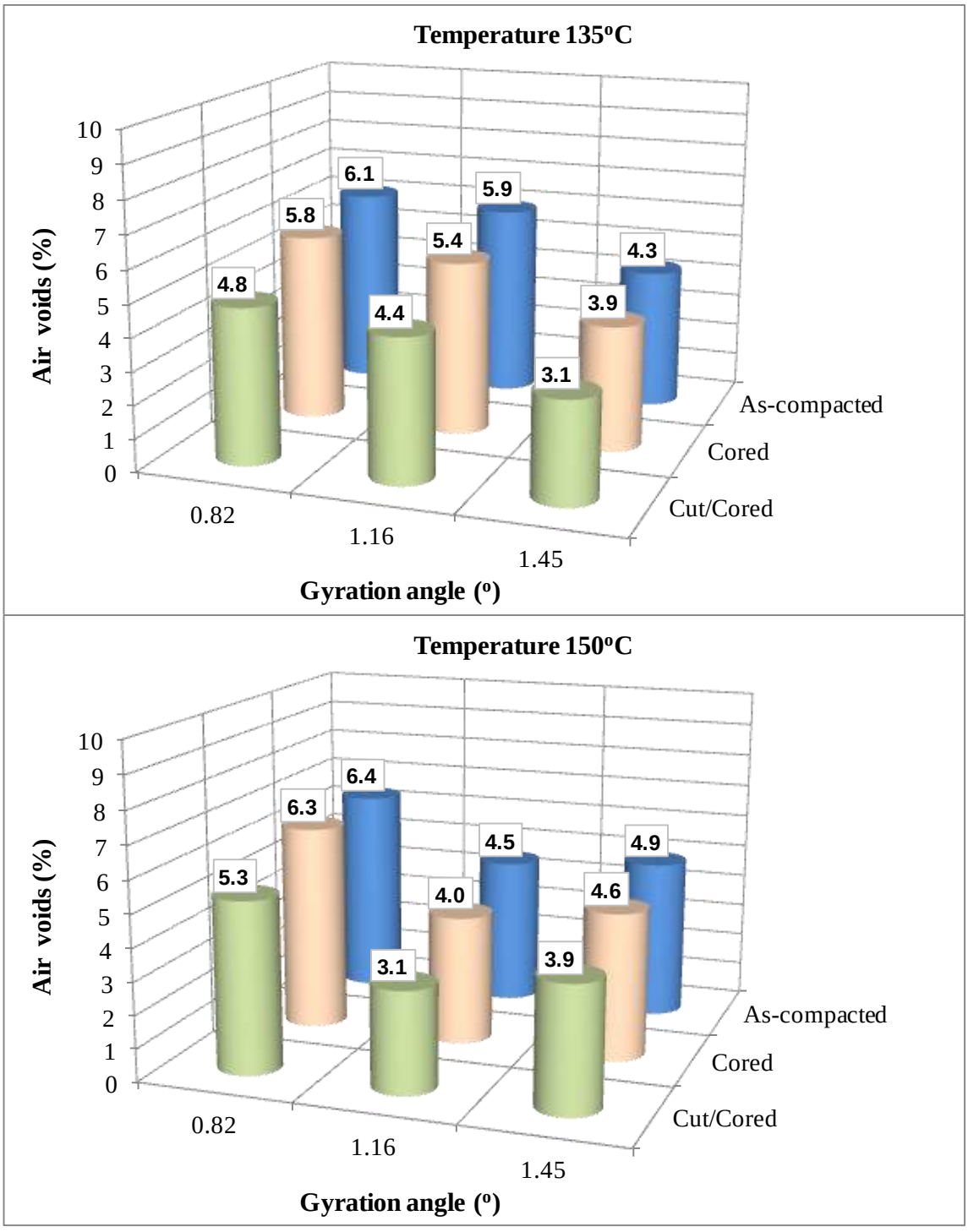

Fig. 4.14 Air void results concerning type 150-70 specimens (AC20 base 50/70)

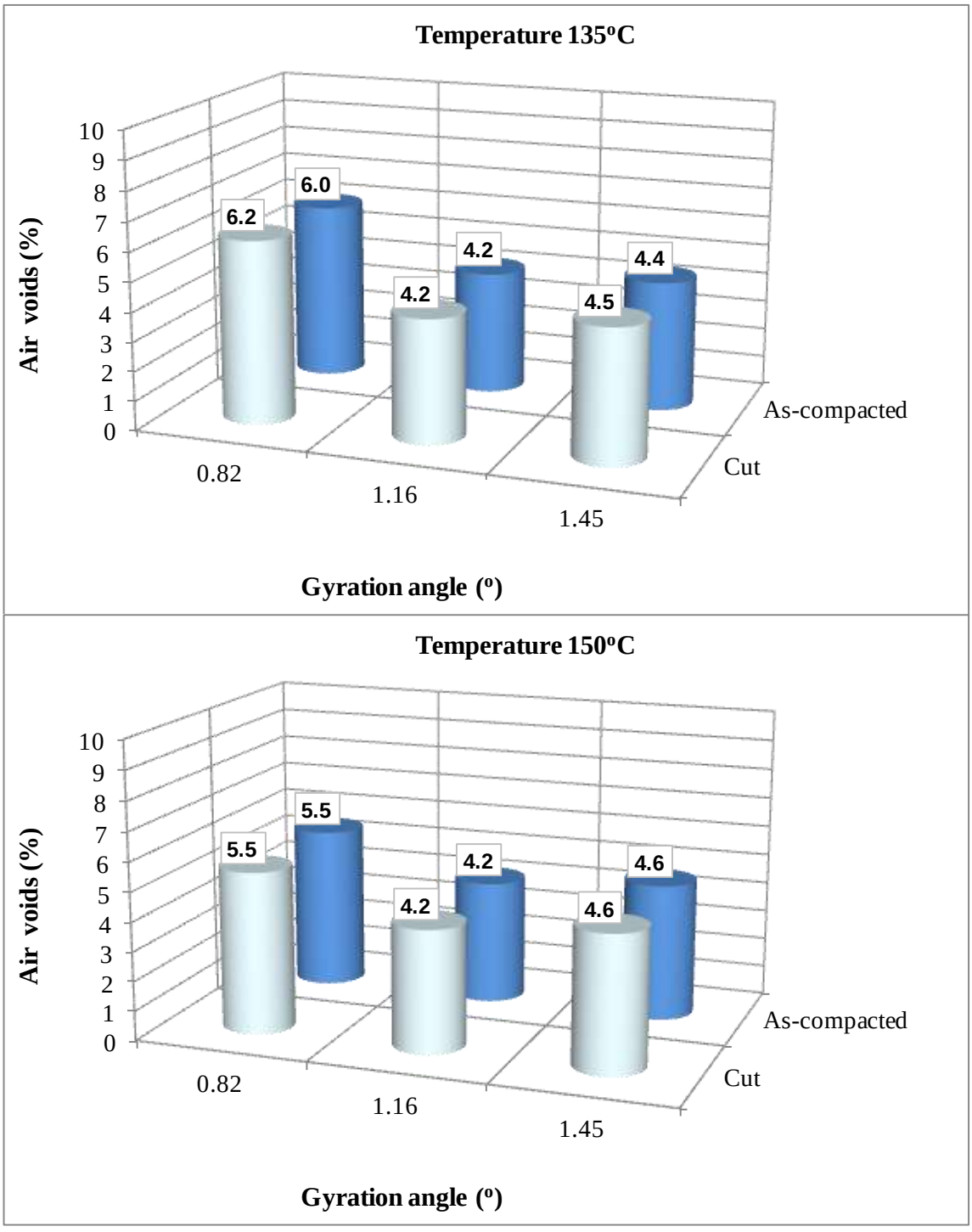

Fig. 4.15 Air void results concerning type 100-170 specimens (AC20 base 50/70)

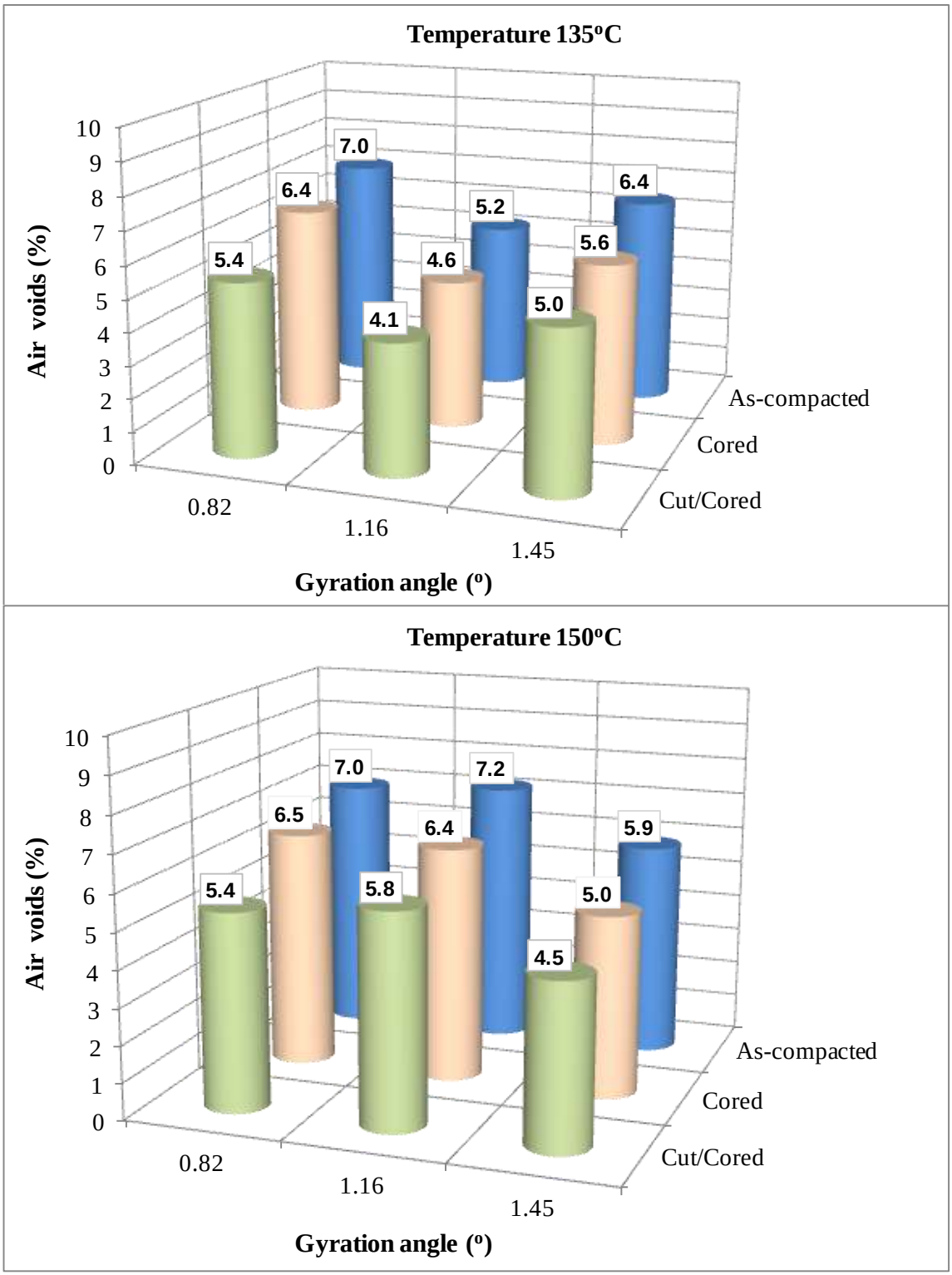

Fig. 4.16 Air void results concerning type 150-170 specimens (AC20 base 50/70)

Regarding the AC12.5 surf 50/70[a] mix, when comparing the air void content of the specimens before and after coring, there is a mean reduction of approximately 0.7%. The paired t-test analysis, as reported in Table 4.2, demonstrates significant difference at 95% confidence level between the air voids in as-compacted and cored specimens. This indicates non-uniformity in the lateral air void distribution, which can be attributed to the mould-induced restrictions in aggregates movement towards its circumference. Similar findings were obtained with respect to the AC20 base 50/70 mix. The analysis results are tabulated in Table 4.2.

Table 4.2 Paired t-test results

Mix type	Air voids (%)		P-value	Are differences significant (a=0.05)
	As-compacted	Cored		
AC12.5 surf 50/70[a]	6.0	5.3	0.0017	Yes
AC20 base 50/70	5.9	5.3	0.00001	Yes
Mix type	As-compacted	Cut/Cored	P-value	Are differences significant (a=0.05)
AC12.5 surf 50/70[a]	5.9	5.6	0.243	No
	(5.2)	(4.4)	(0.00000001)	(Yes)
AC20 base 50/70	5.6	4.6	0.0000002	Yes

Moreover, after cutting, the air voids of specimens further decreased. A mean air void decrease of approximately 0.3% was calculated for all specimens, although this value is masked due to the results concerning the 100-170 specimens, as illustrated in Fig. 4.11. For this type of specimens, after cutting 10mm of the top and bottom regions of the specimens, the air voids increase. Given the above, when the air voids variations regarding the 100-170 specimens are excluded from the t-test analysis, the statistical results showed in parentheses demonstrate a significant air void decrease between the as-compacted and cut/cored specimens. This could be due to the ‘cone effect’ as concluded from Thyagarajan et al. (2010). Particularly, tall specimens tend to receive less shearing action at the center, and hence less compaction compared to the top and bottom regions,

as illustrated in Fig. 4.17. On the contrary, if the specimen is thick, compaction pressure from both sides interferes, creating overlapping cones in the middle region and thus higher compaction. Similar results were generally obtained regarding the AC20 base 50/70 mix as shown in Table 4.2, although the 'cone effect' seems to be less pronounced for this mix.

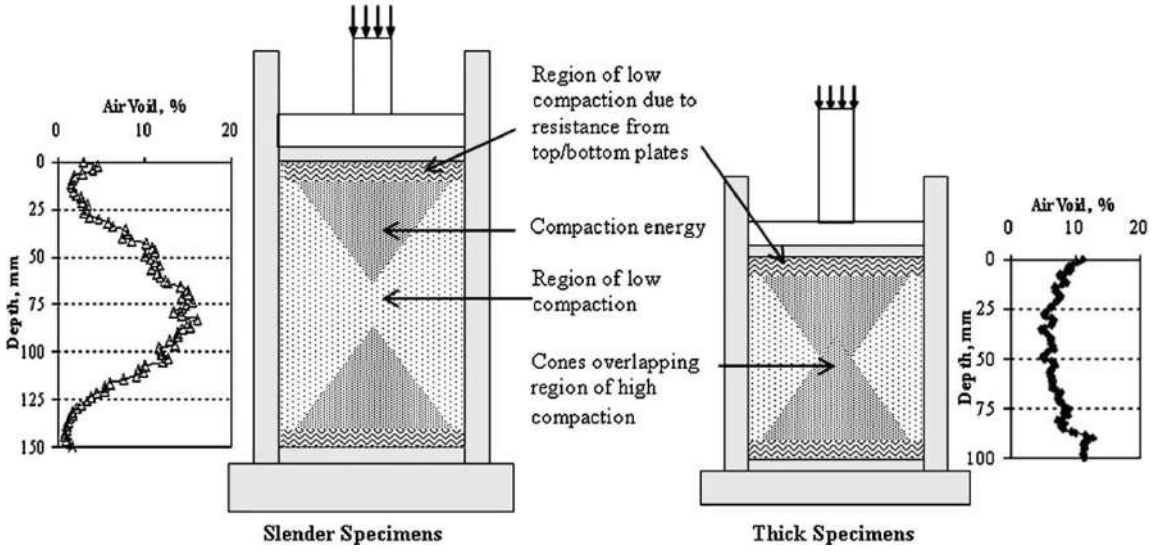

Fig. 4.17 Effect of specimen geometry on gyratory compaction (cone effect) (after Thyagarajan et al. 2010)

The above results support previous findings which indicated the non-uniform air void distribution that HMA gyratory specimens typically experience (Thyagarajan et al. 2010; Partl et al. 2003; Tashman et al. 2002). Cutting and coring process tent to reduce the heterogeneity. Also, it is clear that when aiming to fabricate specimens at a target air void content, the as-compacted specimens need to be prepared at much higher air void contents.

Moreover, it is worthwhile to mention that the general trend observed from the plots indicates that the variation in air voids is particularly attributed to the gyration angle and specimen geometry rather than the compaction temperature. The latter is confirmed by means of one-way analysis of variance (ANOVA) shown in Table 4.3.

Table 4.3 ANOVA test results for air voids differences between the compaction temperatures (α = 0.05)

Mix type	Compaction temperature	Sum of squares	df	Mean Square	F.	Sig.
AC12.5 surf 50/70[a]	Between groups	.024	1	.024	.020	.888
	Within groups	25.887	22	1.177		
	Total	25.911	23			
AC20 base 50/70	Between groups	.220	1	.220	.209	.652
	Within groups	23.239	22	1.056		
	Total	23.460	23			

The ANOVA analysis indicated that there was not a significant effect of compaction temperature on the air voids of as-compacted gyratory specimens at the 95% confidence level. This indicates that a similar compaction level can be achieved for compaction temperature range 135-150^{o}C. Hence, further analysis to evaluate the influence of gyratory compaction on asphalt mix densification will be restricted to more significant parameters, namely gyration angle and specimen geometry.

4.3.1.2 Influence of gyratory compaction parameters on HMA compactability

This subsection discusses the influence of the gyratory compaction parameters on asphalt mix compactability in terms of air voids content. On the basis of the previous results, the test matrix included compaction varying the gyration angle and specimen geometry as presented in Table 4.1. The standard conditions for compaction of all specimens were the pressure 600 KPa, number of gyrations N=205 and rotational speed 30rpm.

During compaction, the height of the specimen is recorded at various gyrations levels. By recording the sample height, an entire history of compaction may be developed using Eq. 4.12, in contrast to the traditional Marshall impact compaction process. After complete compaction, the bulk density ρ_b of the sample is measured. With this parameter and knowledge of the maximum theoretical density ρ_m of the mixture, the air voids are back-calculated at any given gyration of interest as follows (ASTM 2009):

$$\rho_b(n_g x) = \rho_b(n_g final)\frac{h_{final}}{h_x} \quad (4.12)$$

$$Air\ voids(\%) = \left(1 - \frac{\rho_b(n_g x)}{\rho_m}\right) * 100 \quad (4.13)$$

where $\rho_b(n_g x)$ is the bulk density of the extruded specimen at any gyration x; ρ_m is the maximum theoretical density of the mixture; h_{final} is the height of the specimen recorded at the final gyration (mm); h_x is the height of the specimen recorded at any gyration x during the compaction process (mm); $\rho_b(n_g final)$ is the bulk density of the extruded specimen at the final gyration.

Figures 4.18-4.20 shows the compaction curves with respect to the various gyration angles and specimens' geometries concerning the AC12.5 surf 50/70[a], while Fig. 4.21-4.23 show the counterparts related to the AC20 base 50/70 mix.

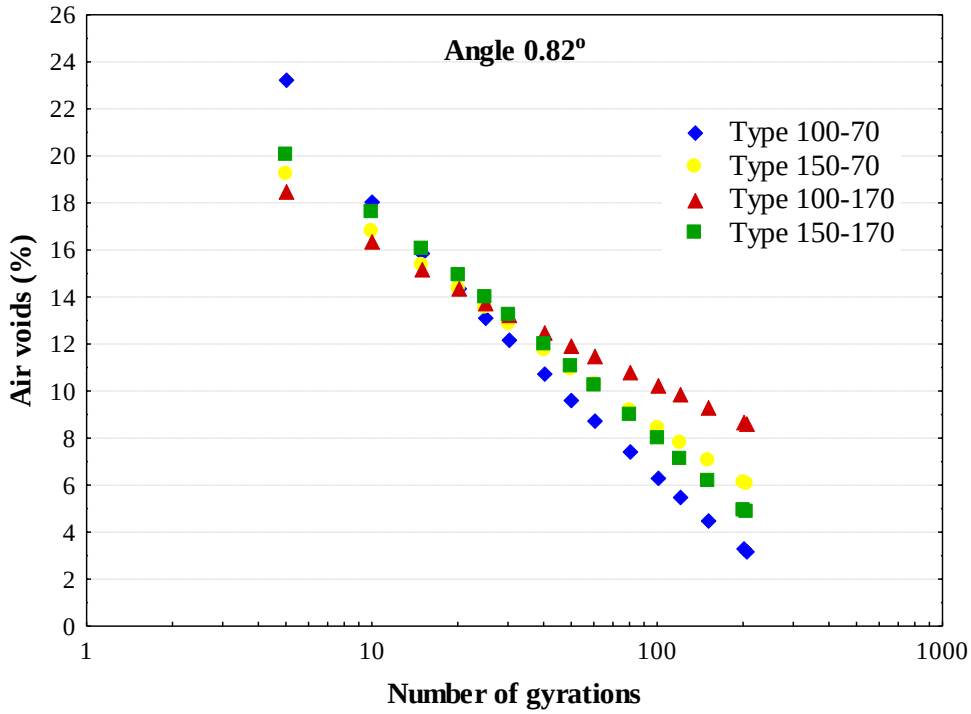

Fig. 4.18 Compaction curves for different specimens geometries using 0.82° angle (AC12.5 surf 50/70[a])

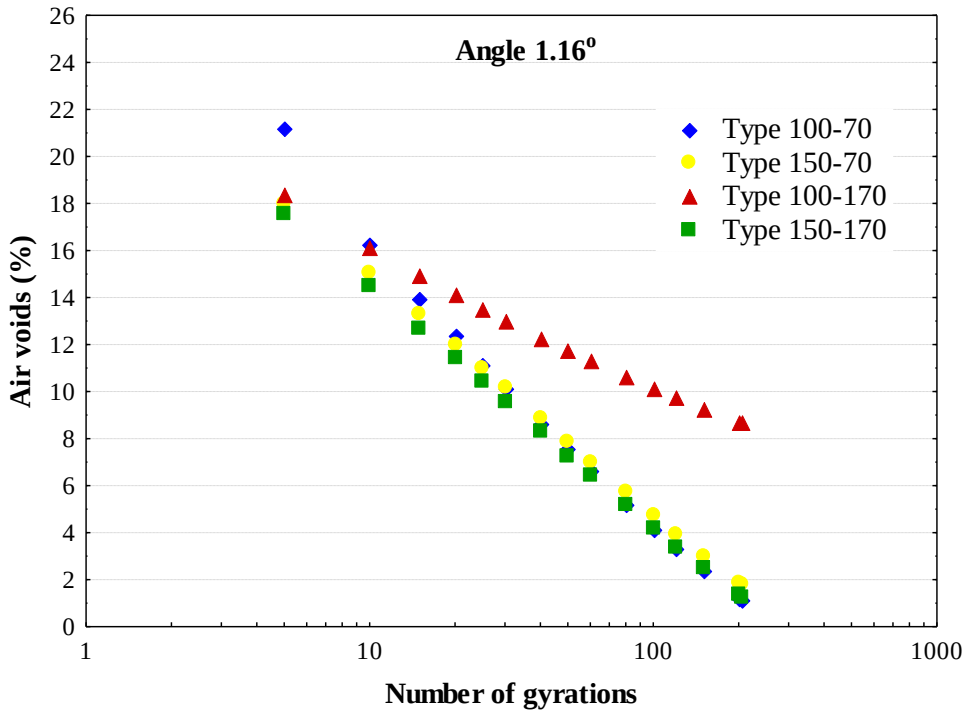

Fig. 4.19 Compaction curves for different specimens geometries using 1.16° angle (AC12.5 surf 50/70[a])

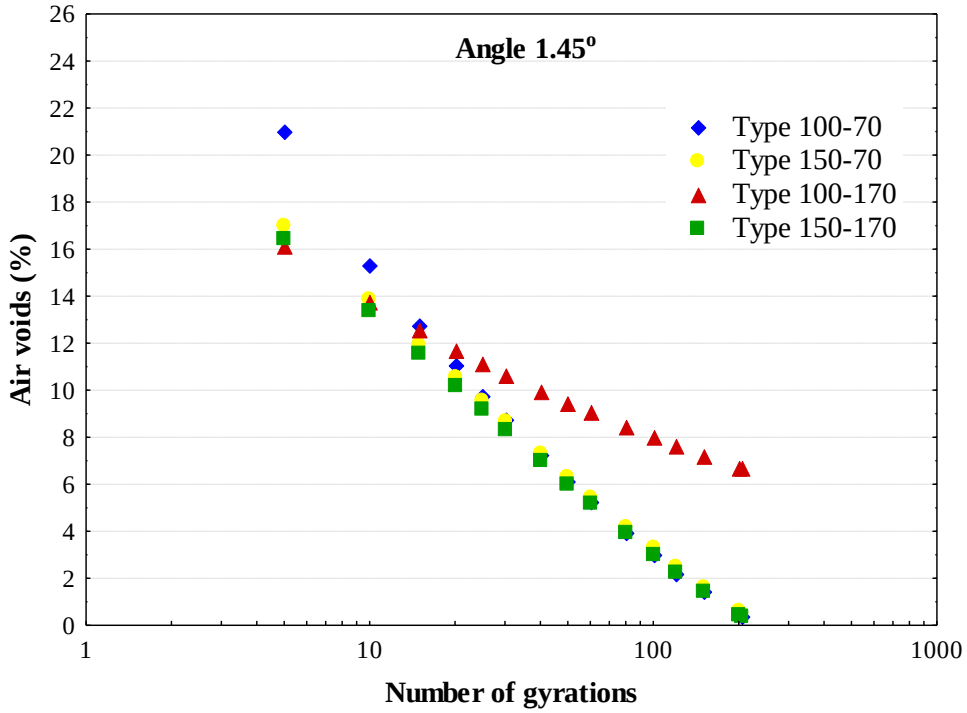

Fig. 4.20 Compaction curves for different specimens geometries using 1.45° angle (AC12.5 surf 50/70[a])

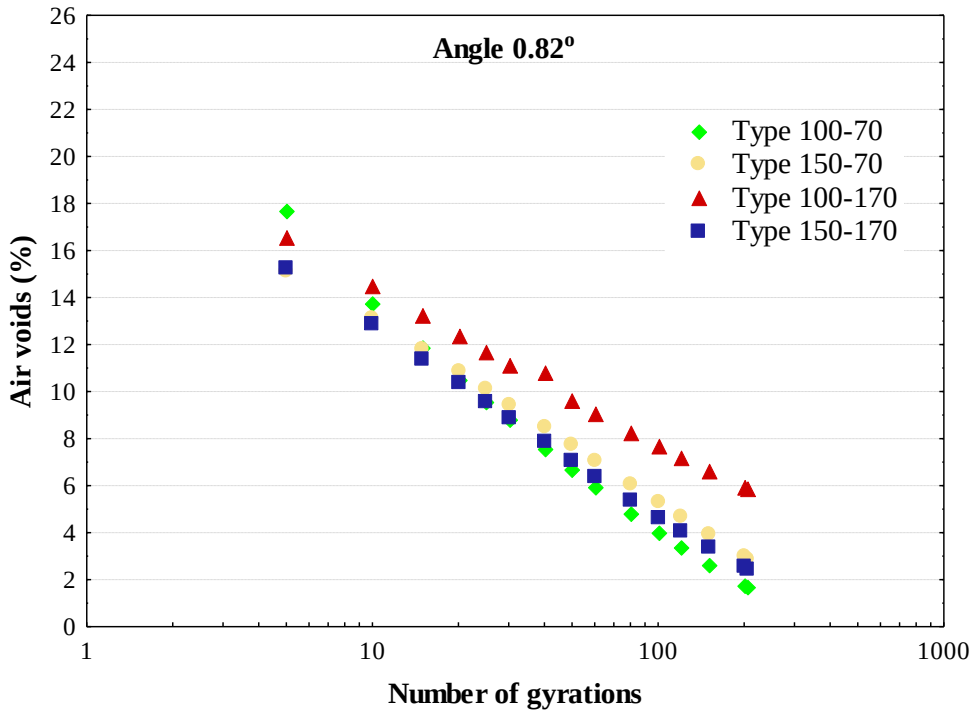

Fig. 4.21 Compaction curves for different specimens geometries using 0.82º angle (AC20 base 50/70)

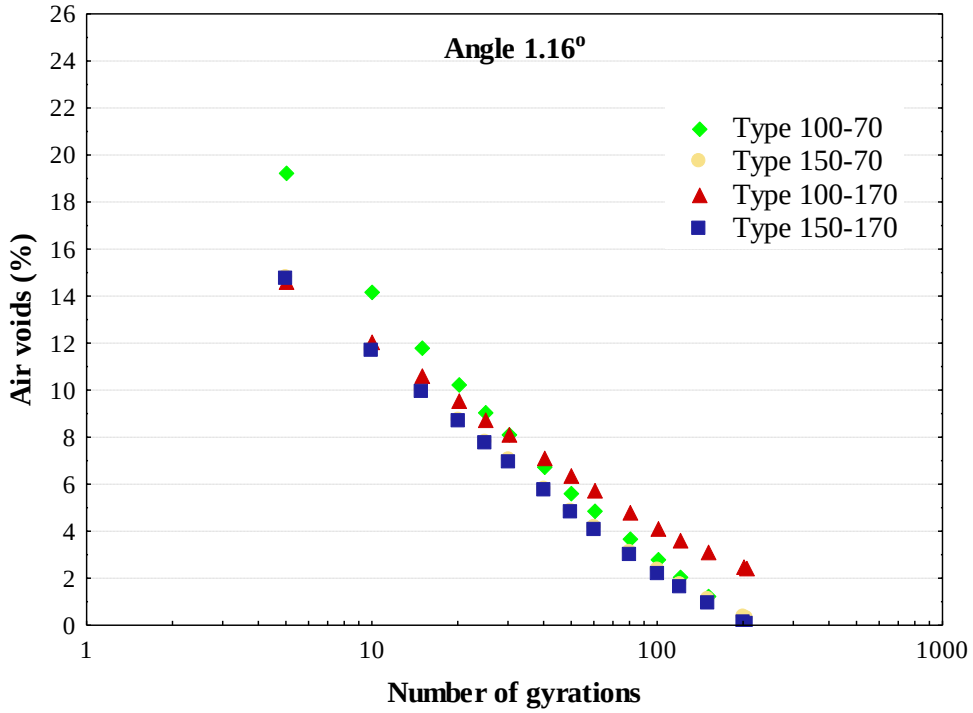

Fig. 4.22 Compaction curves for different specimens geometries using 1.16º angle (AC20 base 50/70)

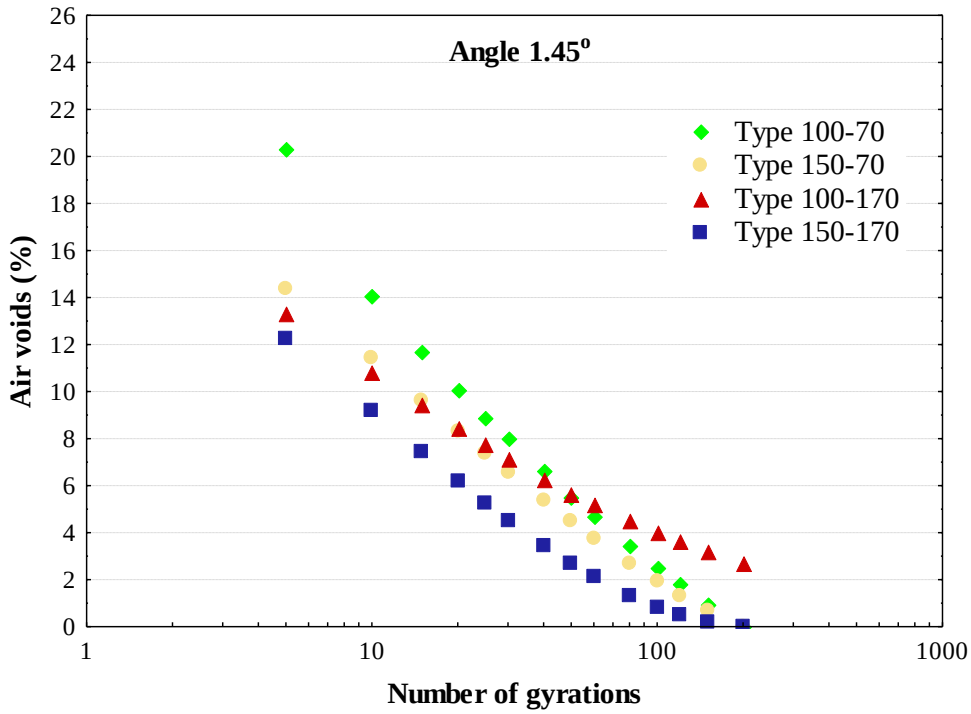

Fig. 4.23 Compaction curves for different specimens geometries using 1.45° angle (AC20 base 50/70)

From the above plots, it was observed that the lowest compaction level is achieved using the 100-170 type specimens for both mixtures under investigation. Also, with respect to the gyration angles the highest compaction level is achieved using the 1.45° and the lowest using the 0.82° suggested by the European Standard. Intermediate compaction level is achieved using the 1.16° as specified by AASHTO.

A detailed statistical analysis was performed to evaluate the significance of the effect of different variables on the air voids of gyratory specimens. Main compaction parameters were investigated at 95% confidence interval by means of Analysis of variance (ANOVA) test. Using a 95% confidence interval means that a p-value of 0.05 or less is statistically significant. From the statistical analysis results, as tabulated in Table 4.4, it was demonstrated that both the gyration angle and specimen geometry are important factors affecting the asphalt mix compactability.

Table 4.4 ANOVA test results of air voids (α = 0.05)

Mix type	Factor	Sum of squares	df	Mean Square	F.	Sig.
AC12.5 surf 50/70[a]	Model	266.872	6	44.749	41.792	.000
	Angle	28.422	2	14.211	13.410	.006
	Spec. geometry	79.309	3	26.436	24.947	.001
	Error	6.358	6	1.060		
	Total	273.230	12			
AC20 base 50/70	Model	65.045	6	10.841	68.110	.000
	Angle	18.870	3	6.290	39.518	.000
	Spec. geometry	17.345	2	8.673	54.487	.000
	Error	.955	6	.159		
	Total	66.000	12			

4.3.1.3 Evaluation of compactability indicators

To further evaluate the compaction characteristics of the mixtures, subjected to different test conditions, namely gyration angle and specimen geometry, a semi-logarithmic curve fit, in accordance with the European standard (CEN 2001), was performed between the air void percentage and the number of gyrations applied to the mix. The change in the air void content in the compacted samples in relation to the compaction energy was expressed as follows:

$$v(n_g) = a - bln(n_g) \quad (4.14)$$

where $v(n_g)$ is the air void content for a number of gyrations (%), a and b are regression-based constants, and n_g is the number of gyrations.

On the basis of the gyratory compaction curves, the slope of compaction curve and the gyrations to achieve 8 percent air voids were determined using regression analysis to evaluate the mix compactability.

Tables 4.5-4.6 show the results of the above study.

Table 4.5 Compactability indicators for AC12.5 surf 50/70[a] mix

Specimen geometry	Angle	Regression equation	R^2	b factor	N_8
100-70	0.82	y= 30.18- 5.17lnx	.993	5.17	73
150-70		y= 25.06- 3.59lnx	.999	3.59	116
100-170		y= 22.32- 2.61lnx	.997	2.61	241
150-170		y= 27.29- 4.19lnx	.998	4.19	100
100-70	1.16	y= 28.36- 5.24lnx	.993	5.24	49
150-70		y= 25.20- 4.42lnx	.999	4.42	49
100-170		y= 21.92- 2.55lnx	.993	2.55	235
150-170		y= 24.62- 4.42lnx	.999	4.42	43
100-70	1.45	y= 27.40- 5.27lnx	.981	5.27	40
150-70		y= 24.01- 4.48lnx	.999	4.48	36
100-170		y= 19.26- 2.44lnx	.986	2.44	101
150-170		y= 23.31- 4.38lnx	.999	4.38	33

Table 4.6 Compactability indicators for AC20 base 50/70 mix

Specimen geometry	Angle	Regression equation	R^2	b factor	N_8
100-70	0.82	y= 23.30- 4.16lnx	.992	4.16	39
150-70		y= 20.82- 3.36lnx	.999	3.36	45
100-170		y= 21.06- 2.89lnx	.998	2.89	92
150-170		y= 20.76- 3.47lnx	.999	3.47	39
100-70	1.16	y= 25.47- 4.92lnx	.986	4.92	35
150-70		y= 20.58- 3.91lnx	.994	3.91	25
100-170		y= 19.49- 3.29lnx	.995	3.29	33
150-170		y= 20.76- 3.47lnx	.999	3.47	39
100-70	1.45	y= 26.37- 5.20lnx	.976	5.20	34
150-70		y= 20.32- 3.97lnx	.995	3.97	22
100-170		y= 17.23- 2.87lnx	.986	2.87	25
150-170		y= 16.61- 3.40lnx	.969	3.40	13

Comparing specimens with different geometries, for example, those fabricated using gyration angle 0.82^o, it can be established in terms of the slope factor *b* that the specimens with diameter-height 100-70 are more easily compactable. On the contrary, the 100-170 type specimens densify with a slower rate. This finding is also supported from the compaction effort needed to achieve compaction level corresponding to 8% of air voids; the number of gyrations (N_8) needed is significantly higher compared to the other specimens.

Table 4.7 Statistical results

Mix type	Angle	b factor		N_8	
		Mean	StDev	Mean	StDev
AC12.5 surf 50/70[a]	0.82	4.3	.8	96	21.5
	1.16	4.7	.5	47	3.3
	1.45	4.7	.5	36	3.3
AC20 base 50/70	0.82	3.7	.4	41	3.5
	1.16	4.1	.7	33	7.4
	1.45	4.2	.9	23	10.8

It should be pointed out that excluding the 100-170 type specimens, the variance of results in terms of the compactability indicators is significantly reduced. This is clearly supported from the statistical results shown in Table 4.7. Also, clear trends may be revealed regarding the compactability and angle of gyration for both mixtures. For instance, it can be concluded that by using 1.45^o angle less compaction effort compared to both the 0.82^o and 1.16^o is needed to obtain the prescribed compaction level.

4.3.2 Roller compaction

Several factors that control HMA densification were varied in order to assess their impact on mixtures compactability by means of Roller compactor. For the current research study, the approach of compaction by specified energy was followed adjusting three compaction factors, namely the compaction mode, effort and temperature, which are summarized in Table 4.8.

Table 4.8 Roller compaction study parameters

Parameters	AC12.5 surf PmB (SBS)	AC20 base 50/70
Temperature (^{o}C)	130, 140, 150, 160	125, 135, 145
Effort (number of passes)	90, 110, 130	70, 90, 110
Mode	Static, Vibratory, Static-Vibratory, Vibratory-Static	

The laboratory experimental study was meant to mirror the four phases of field compaction; pre-compaction and the three main compaction phases. During the pre-compaction phase minimum compaction energy of 5 kN was applied in the asphalt mix in order to avoid bow effects and achieve a smooth surface in the compacted slab, while

the main compaction phases simulated roller compaction in the field. Four modes of roller compaction (i.e. static (S), vibratory (V), static-vibratory (SV) and vibratory-static (SV)) were established including the pattern followed during field compaction, while varying the compaction effort (i.e. number of passes) and temperature. The main compaction energy and vibration frequency (i.e. 10 kN and 40 Hz, respectively) reflected the operational characteristics of the steel wheel rollers used in the field compaction.

Two hot-mix asphalt mixtures were used in the investigation. Both represent 'production' mixes, sampled directly from paver during placement. The two mixes include: (1) a surface course mix with polymer modified bitumen (SBS) and (2) a base mix with 50/70 bitumen, as described in Chapter 3. Taking into consideration the above operational principles, multiple batches of the asphalt mixture were heated gently and placed in steel mould, moved beneath the roller and the compaction procedures were commenced. A total of 36 slabs were fabricated with regards to the base course mix and 48 slabs with regards to the surface course mix at heights representing the field layer thicknesses. After cooling of the slabs to room temperature, coring of four 100-mm diameter specimens was commenced from the top of each compacted slab. Then, the HMA laboratory-prepared specimens were tested for density and air voids content.

4.3.2.1 Influence of roller compaction on air void homogeneity

Similar to the gyratory compaction study, this subsection discusses the influence of the roller compaction on the compaction homogeneity achieved within the slabs. Compaction homogeneity was assessed by comparing the air voids of the four 100-mm specimens cored from each slab, as shown schematically in Fig. 4.24.

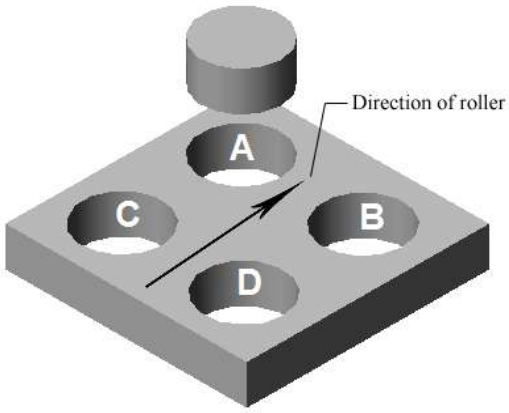

Fig. 4.24 Coring layout of roller-compacted slabs

Figures 4.25-4.26 show the air void test results for the slab cored specimens, denoted as A, B, C, D, concerning the AC12.5 surf PmB (SBS) and the AC20 base 50/70 mixtures. The box plot of air voids content data provides information about the center and spread of the compaction data. It is based on the median and interquartile range, which is believed to provide a realistic interpretation of the results. The ends of the vertical lines or whiskers indicate the minimum and maximum data values.

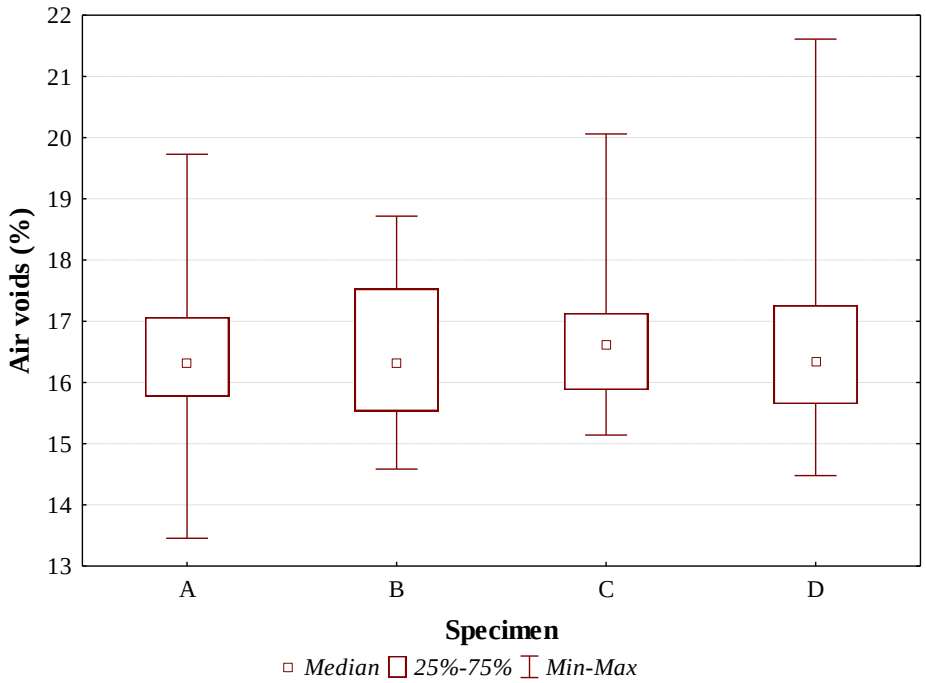

Fig. 4.25 Air void results of cored slab specimens (AC12.5 surf PmB (SBS))

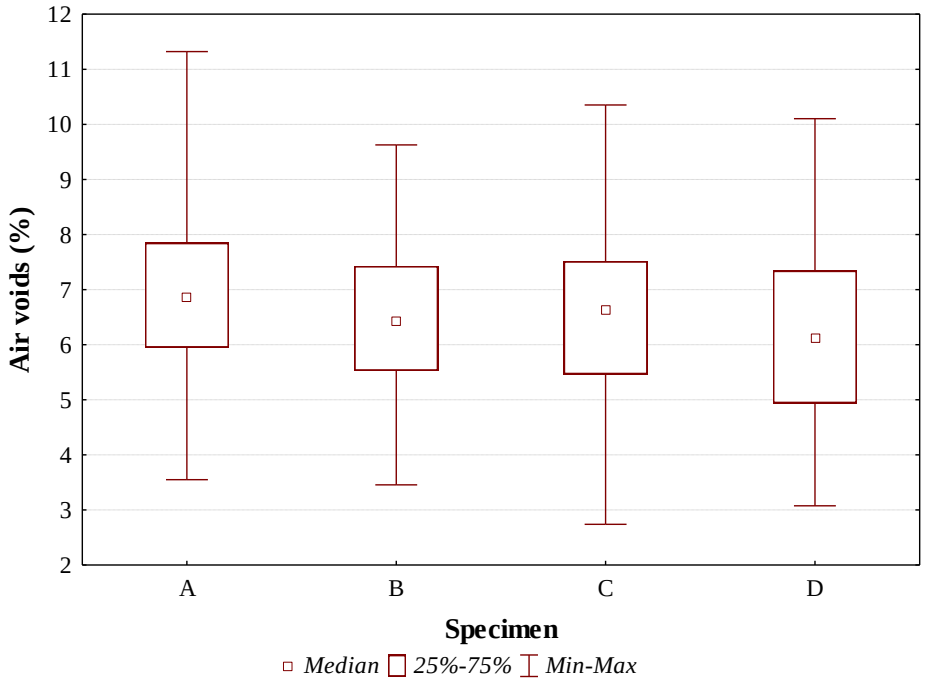

Fig. 4.26 Air void results of cored slab specimens (AC20 base 50/70)

Regarding the AC20 base 50/70 mix, the median values were calculated as 6.9%, 6.4%, 6.7% and 6.1% for the specimens denoted as A, B, C and D, hence indicating that the compaction level is rather homogeneous within the roller-compacted slab. Similar results are observed regarding the AC12.5 surf PmB (SBS) mix, where the median values ranging from 16.3-16.6% for the A-D specimens.

To validate the homogeneity of air voids in the compacted slabs a statistical analysis was undertaken to compare the results of each cored specimens (i.e. A, B, C & D) with the others. The laboratory compaction data was analyzed using the ANOVA test.

Table 4.9 ANOVA test results for air voids differences the slab cored specimens (α = 0.05)

Mix type	Air voids	Sum of squares	df	Mean Square	F.	Sig.
AC12.5 surf PmB (SBS)	Between groups	1.552	3	.517	.397	.755
	Within groups	244.963	188	1.303		
	Total	246.515	191			
AC20 base 50/70	Between groups	9.491	3	3.164	1.01	.388
	Within groups	436.599	140	3.119		
	Total	446.090	143			

The ANOVA results, as shown in Table 4.9, indicated that there was not a significant difference among the means of the four specimens cored from each slab. This indicates uniform air void distributions in the center of the slab and hence it can be stated that the roller compactor offers homogeneous samples.

4.3.2.2 Influence of roller compaction parameters on HMA compactability

This subsection discusses the influence of the roller compaction parameters on asphalt mix compactability in terms of air voids content (Plati et al. 2016). The test matrix included the compaction varying the compaction temperature, effort and mode as presented in Table 4.8. The air void contents of all laboratory fabricated specimens were calculated. Based on previous results which indicate air void homogeneity within the slab, the average of the four specimens cored from each slab was calculated as a representative value for the data analysis interpretation.

Figure 4.27 illustrates the compaction level achieved as a function of compaction temperature, covering the full spectrum of roller compaction effort and modes regarding the AC12.5 surf PmB (SBS) mix.

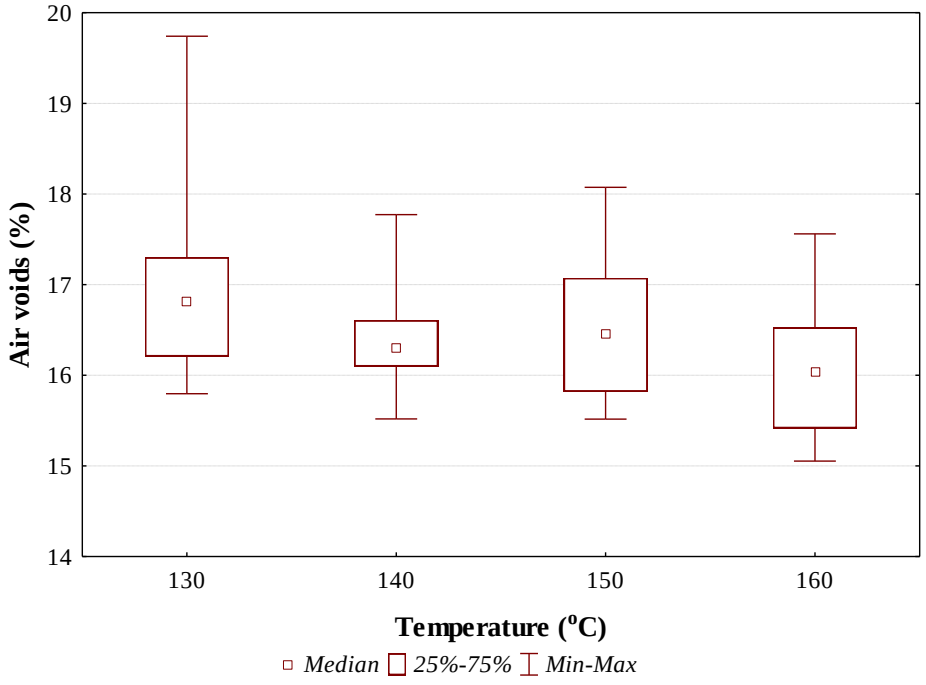

Fig. 4.27 Air voids as a function of compaction temperature (AC12.5 surf PmB (SBS))

Accordingly, Fig. 4.28-4.29 show the compaction level achieved as a function of compaction effort and mode.

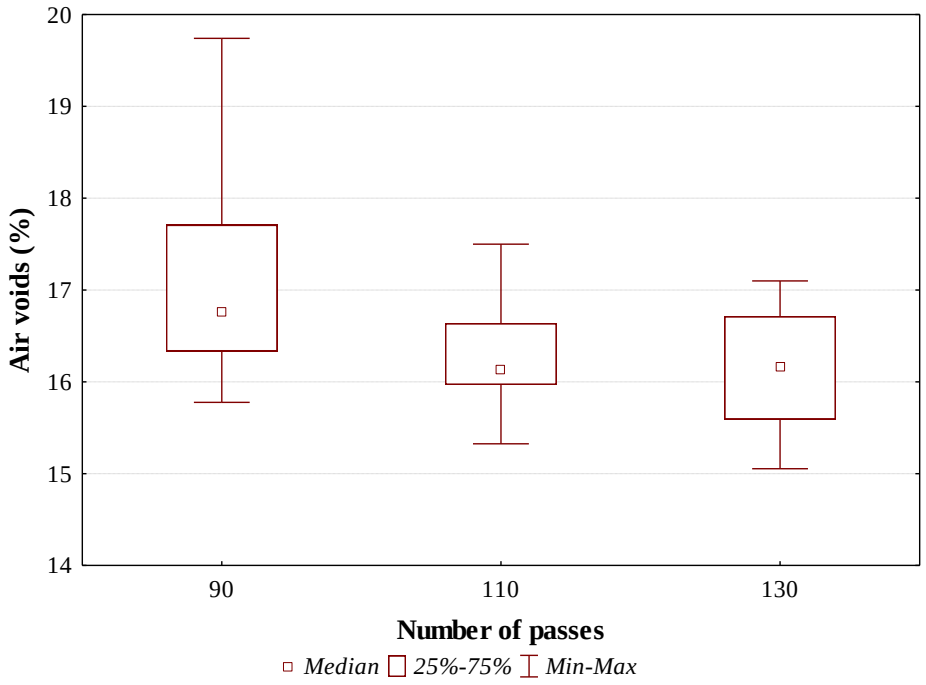

Fig. 4.28 Air voids as a function of compaction effort (AC12.5 surf PmB (SBS))

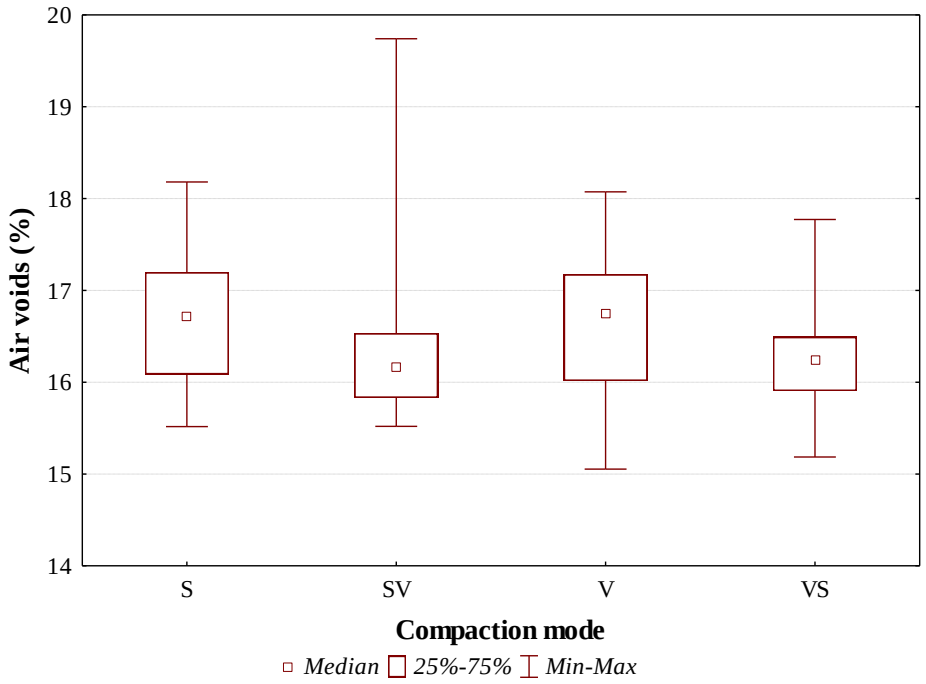

Fig. 4.29 Air voids as a function of compaction mode (AC12.5 surf PmB (SBS))

The counterpart results related to the AC20 base 50/70 mix are presented in Fig. 4.30-4.32.

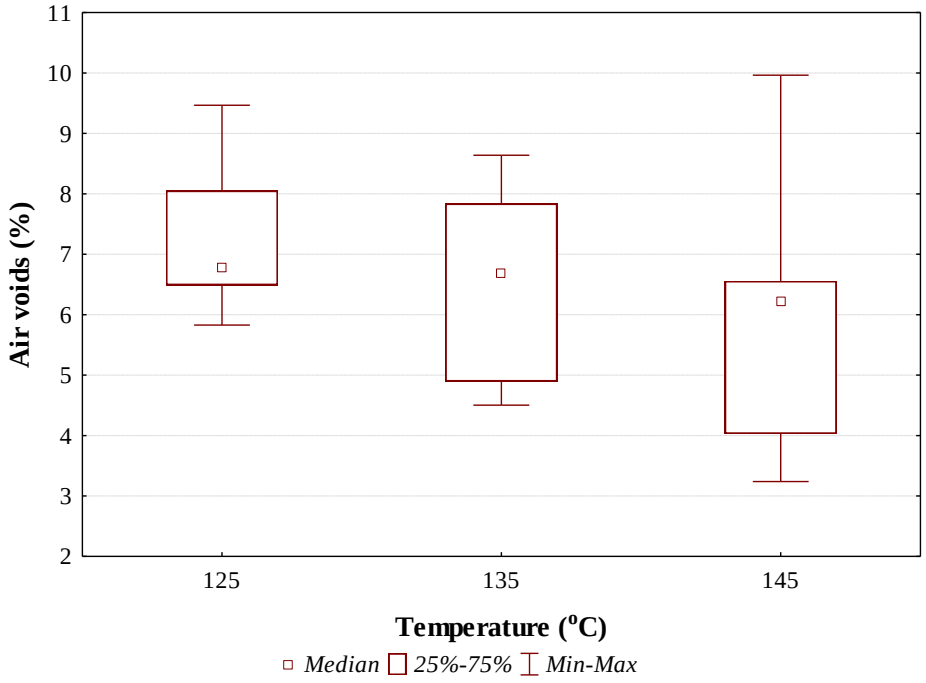

Fig. 4.30 Air voids as a function of compaction temperature (AC20 base 50/70)

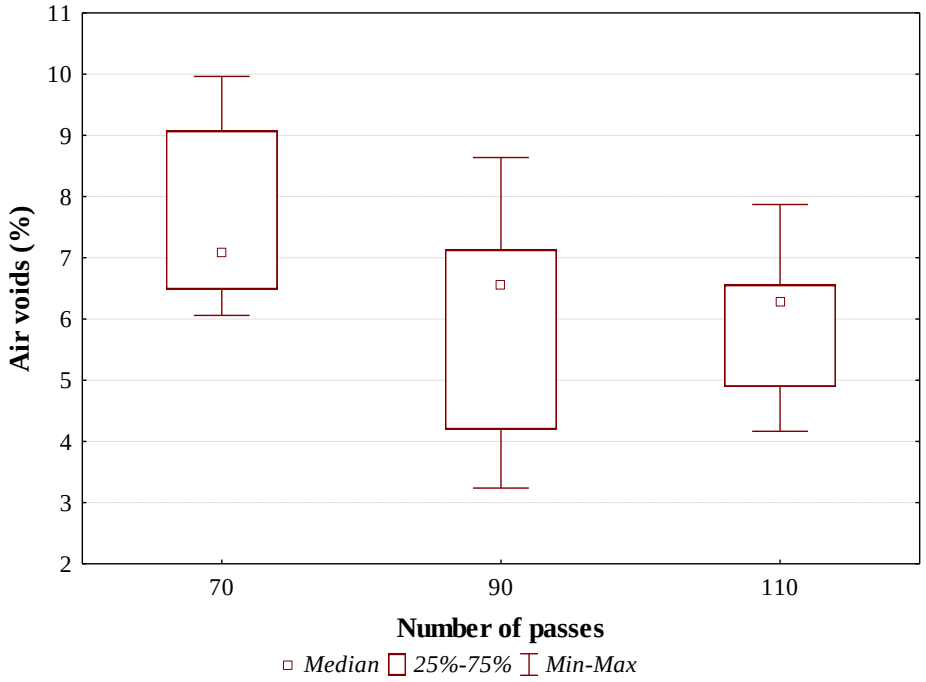

Fig. 4.31 Air voids as a function of compaction effort (AC20 base 50/70)

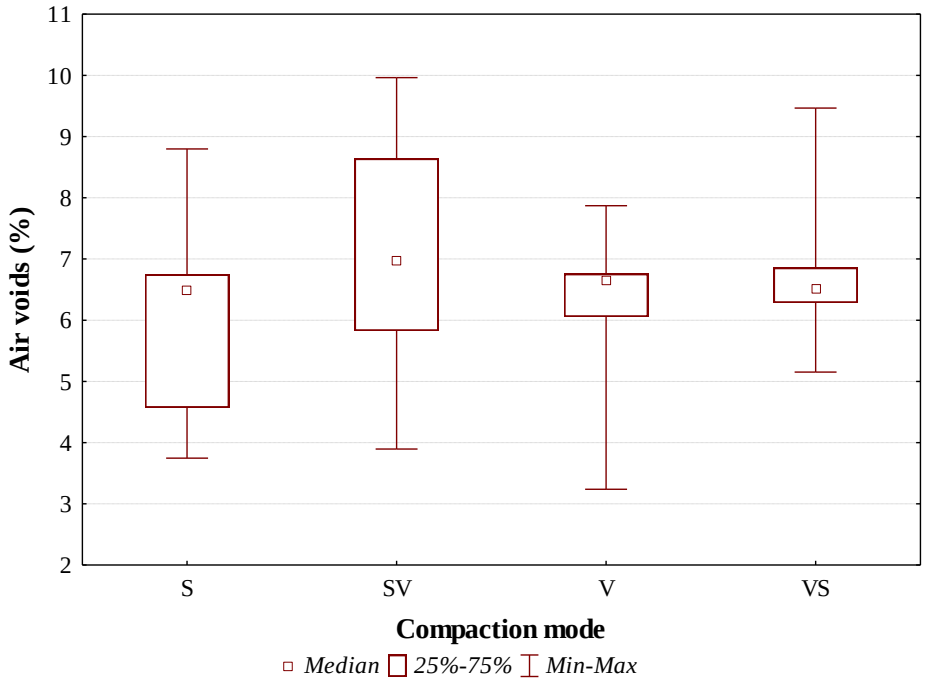

Fig. 4.32 Air voids as a function of compaction mode (AC20 base 50/70)

From Fig. 4.27, it is demonstrated that the air voids box plot of the AC12.5 surf PmB (SBS) mix is rather narrow, except for the 130^{o}C, and that if the compaction temperature is increased, the air voids generally decrease. Also, it is observed that as the number of roller passes increased from 90 to 110, the air voids decreased, as expected. However, an additional compaction effort (20 passes) applied did not enhance HMA densification, as observed in Fig. 4.28. Variability of air voids content is observed both between and within the various compaction modes, as illustrated in Fig. 4.29.

Regarding the AC20 base 50/70 mix, the general trend indicates that the air voids decrease when there is an increase in the compaction temperature, as illustrated in Fig. 4.30. However, the air voids box plot is wide, indicating variability of the achieved compaction level. Similar to the surface mix, the air voids decreased as the number of roller passes increased from 70 to 90, while additional roller passes marginally affected the compaction level, as shown in Fig. 4.31. From Fig. 4.32, increased variability of air voids is also observed among the various roller compaction modes.

Table 4.10 ANOVA test results of air voids (α = 0.05)

Mix type	Factor	Sum of squares	df	Mean Square	F.	Sig.
AC12.5 surf PmB (SBS)	Model	13107.613	9	1456.401	2834.756	.000
	Temperature	5.671	3	1.890	3.679	.020
	Effort	9.712	2	4.856	9.451	.000
	Mode	1.121	3	.374	.727	.542
	Error	20.037	39	.514		
	Total	13127.650	48			
AC20 base 50/70	Model	1582.270	8	197.784	106.233	.000
	Temperature	12.184	2	6.092	3.272	.053
	Effort	21.111	2	10.555	5.669	.009
	Mode	7.104	3	2.368	1.272	.303
	Error	52.130	28	1.862		
	Total	1634.400	36			

A detailed statistical analysis was performed to evaluate the significance of the effect of different variables on the air voids of roller specimens. Main compaction parameters were investigated at 95% confidence interval by means of Analysis of variance (ANOVA) test. From the statistical analysis results, as tabulated in Table 4.10, it was demonstrated that both the compaction temperature and effort (in terms of roller passes) are important factors affecting the asphalt mix compactability.

4.3.2.3 Evaluation of compactability indices

The compaction characteristics of the mixtures under investigation were also evaluated by means of indicators related to semi-logarithmic densification curves fitted to the experimental data. Similar to the gyratory compaction study, the slope *b* and the number of passes to achieve 8 percent air voids (N_8) were used, as described earlier. In addition, the number of passes to achieve 15 percent air voids (N_{15}) was also determined for the AC12.5 surf PmB (SBS) mix, which reflects the uppermost compaction level to be achieved in the field for open-graded surface mixtures. On the basis of the ANOVA results (see Table 4.10), the significant parameters were considered to determine the evolution of the air void content, covering the full spectrum of compaction modes, in relation to the number of passes for each temperature as follows:

$$v(n_p) = a - bln(n_p) \quad (4.15)$$

where $v(n_p)$ is the air void content for a number of passes (%), a and b are regression-based constants, and n_p is the number of passes.

It should be pointed out that for the AC12.5 surf PmB (SBS) mix the air void content with respect to compaction temperature and passes indicate little variation, as demonstrated from the statistical results of Table 4.11. Hence, the mean value of air void contents may be considered appropriate for the purpose of the analyses regarding the determination of compactability indicators. Although, for the AC20 base 50/70 mix the results indicate variance of air voids, for consistency reasons in analyses the mean values were selected for both mixtures.

Table 4.11 Statistical results

Mix type	Temp (°C)	Effort	Air voids (%)	
			Mean	StDev
AC12.5 surf PmB (SBS)	130	90	17.7	1.6
		110	16.6	.8
		130	16.7	.4
	140	90	17.1	.7
		110	16.1	.2
		130	16.1	.4
	150	90	17.0	1.0
		110	16.6	.5
		130	16.0	.6
	160	90	16.7	.6
		110	15.7	.4
		130	15.7	.8
AC20 base 50/70	125	70	8.7	1.0
		90	6.7	.2
		110	6.3	.4
	135	70	6.9	.6
		90	7.2	1.9
		110	5.6	1.6
	145	70	7.3	1.8
		90	4.3	1.4
		110	5.9	1.2

Figures 4.33-4.34 illustrate the experimental compaction data for both mixtures, while Tables 4.12-4.13 tabulate the analytical results of the above study.

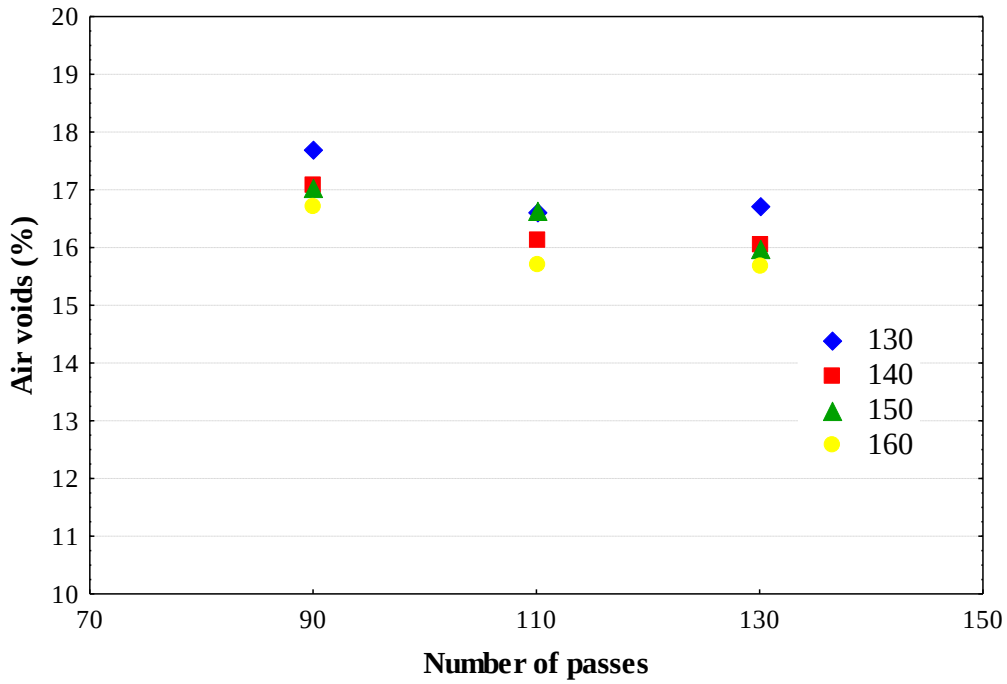

Fig. 4.33 Air voids variation as a function of compaction effort and temperature (AC12.5 surf PmB (SBS))

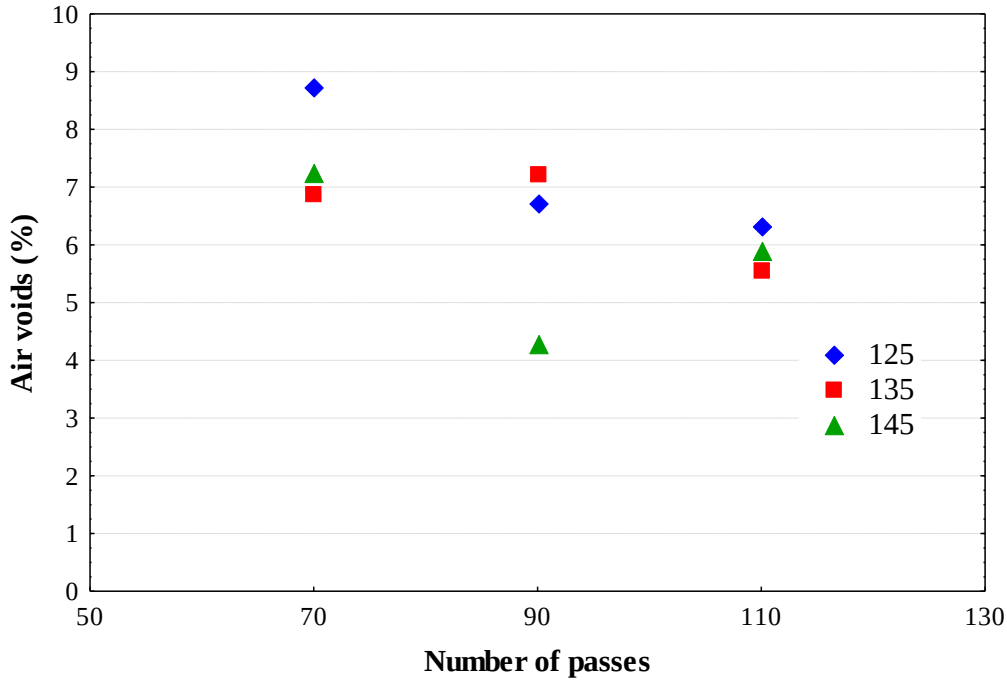

Fig. 4.34 Air voids variation as a function of compaction effort and temperature (AC20 base 50-70)

Table 4.12 Compactability indicators for AC12.5 surf PmB (SBS) mix

Temperature	Regression equation	R^2	b factor	N_{15}
130	y= 29.75- 2.72lnx	.709	2.72	228
140	y= 29.69- 2.83lnx	.842	2.83	180
150	y= 29.82- 2.83lnx	.964	2.83	188
160	y= 29.71- 2.91lnx	.825	2.91	156

Table 4.13 Compactability indicators for AC20 base 50/70 mix

Temperature	Regression equation	R^2	b factor	N_8
125	y= 31.62- 5.43lnx	.912	5.43	77
135	y= 18.86- 2.75lnx	.505	2.75	52
145	y= 20.83- 3.35lnx	.260	3.35	46

Regarding the AC12.5 surf PmB (SBS) mix, Fig. 4.33 shows that when increasing the compaction temperature, the specimens are more easily compactable; this finding is also supported from the gradual increase of slope factor b, as well as the decreasing number of roller passes (N_{15}) to achieve compaction level corresponding to 15% of air voids with the increase of compaction temperature, as shown in Table 4.12.

With regards to the AC20 base 50/70 mix, the data in general do not appear to follow a semi-logarithmic curve. For instance, with respect to 145^{o}C, the compaction data seems to follow a polynomial curve which shows that the ultimate compaction level is achieved for 90 passes and continued rolling beyond this point may lead to mix decompaction. This may be the reason to obtain low R^2 values for fitted regression equations and subsequently some ambiguous indicator *b* values. With this in mind, it could be however stated that the increase of compaction temperature enhances mix densification and hence the roller passes (N_8) needed to obtain the prescribed compaction level decreases.

4.4 Field study

Primarily, the first task involved the evaluation of the compaction temperature, effort and mode on HMA compactability, giving particular emphasis on the lab-studied mixtures. The second task consisted of the estimation of field density using various methodologies. The third task involved the evaluation of the relationship between laboratory compaction and field compaction in terms of various compactability indicators.

4.4.1 Assessment of mat temperature during construction operations

The initial stage of field surveys focused on the applicability of the IRT technique to obtain full coverage evaluations on new HMA layers (Plati et al. 2014). The aim was to identify factors or conditions that contribute to the occurrence of mat temperature differentials during paving and compaction process. Mat temperature differentials are defined as the maximum temperature differences in-between any two points within the specified test volume at a given instant. Commonly, temperature differentials are associated with poor compaction, segregation and premature distress of asphalt pavements (Elsafey et al. 2009; Herold et al. 2008; Mahoney et al. 2000; Stroup-Gardiner et al. 2000). Considering the mat surface temperature as representative measure, two HMA types were monitored during paving and compaction using the thermographic system in order to identify the existence of temperature homogeneity on the mat. Temperature homogeneity can be considered as evidence for the good compaction of the mixtures.

During the full coverage data collection of mat placement temperatures of the AC20 base 50/70 mixture, a section was identified in which there was a delay in delivery of the mixture that resulted in paver pause (cold area). In this section a temperature differential of 15^{o}C was detected while the paver was waiting for the next truck. Once the paver resumed progress a temperature differential of 22°C was revealed between the hot and cold area, as illustrated in Fig.4.35.

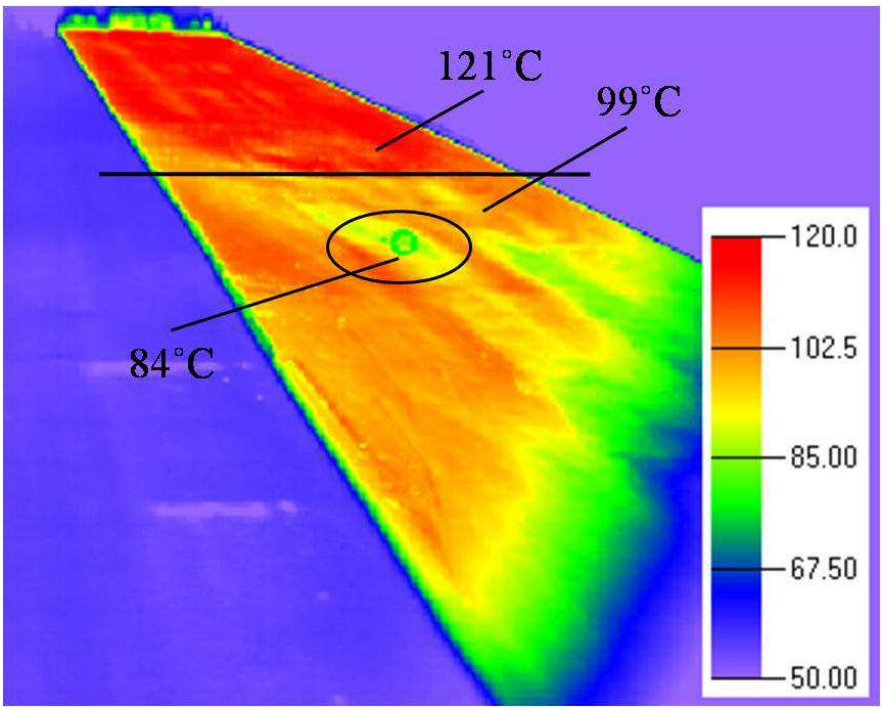

Fig. 4.35 Temperature differentials of base course mixture due to paver pause

It is also worthwhile to mention that based on the analysis of thermal images collected during rolling operations a thin longitudinal line was detected. This defect seemed to be expanded with time, as shown in Fig. 4.36a-b. In addition, the dynamic force imparted by the vibratory tandem roller increased the line width (Fig. 4.36c), while the compaction effect of the pneumatic rubber wheeled roller had the opposite effect (Fig. 4.36d), minimizing the line width till disappearance. It is of particular interest to highlight that the above mentioned defect was only captured from the infrared camera, as illustrated in the left side of Fig. 4.36a-d. Conventional digital camera did not manage to record the phenomenon, as illustrated in the right side of Fig. 4.36a-d.

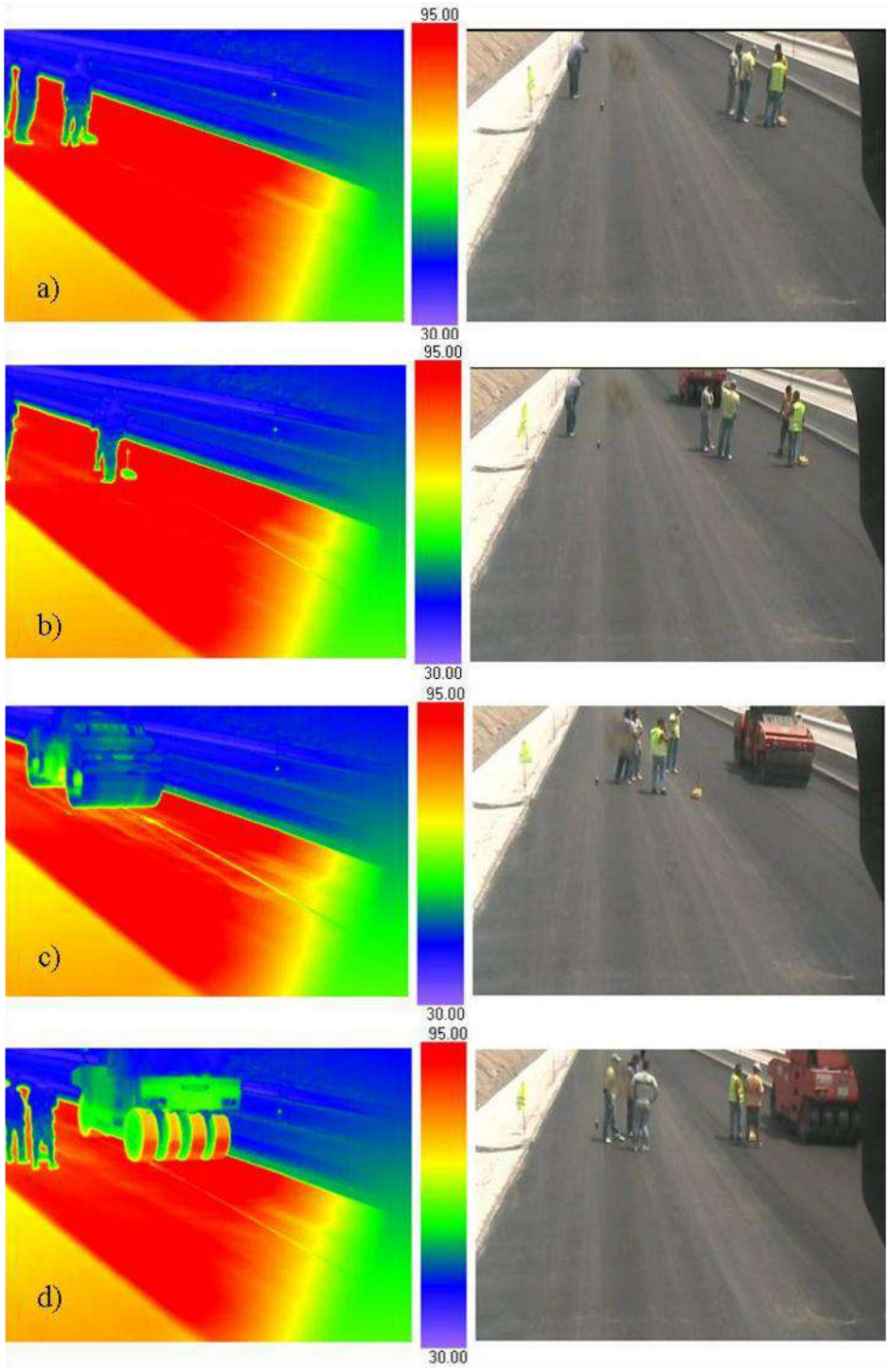

Fig. 4.36 Infrared and conventional images of defect at base course mixture

Trying to explain this defect, it could be stated that the line is perhaps a micro-crack indicating mix tenderness (Scherocman 2006). Tender mixes tend to move or shove excessively under the weight of the compaction equipment while being rolled, which

causes areas of localized tension in the mat surface. If this tension is enough to overcome hot mix asphalt cohesive forces, micro-cracks will develop on the surface. The subsequent passes of the pneumatic tire roller can lead to disappearance of these cracks due to their kneading compaction effect. The non-existence of the micro-crack, after the compaction had finished and the mat had cooled down, produces evidence in support of the mechanism described above. Given the above, it can be argued that the IRT offers the potential of quick diagnosis of defects, hence contributing essentially to the benefit of the compaction's results that are desirable for satisfactory pavement performance.

During monitoring of the AC12.5 surf PmB (SBS) mixture, the average mat surface temperature -after paving but before breakdown- was 111°C, while the maximum temperature differential was observed to be approximately 29°C. Figure 4.37 illustrates the thermal profile of the uncompacted mat for a section which exhibited minimal thermal fluctuations and a temperature differential of 9°C approximately.

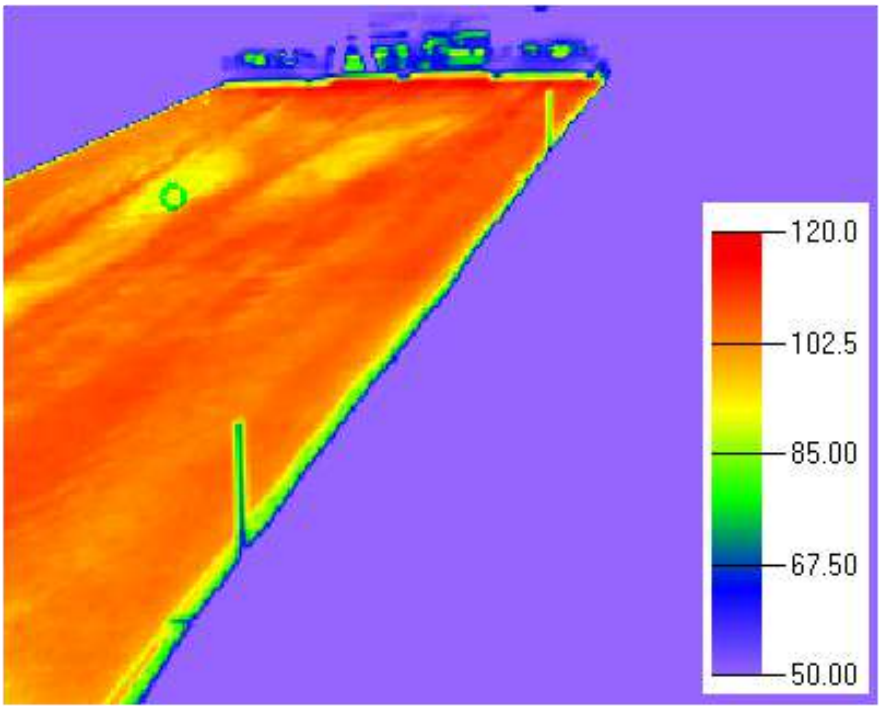

Fig. 4.37 Temperature differentials of surface course mixture

The examples above produce evidence in support of the statement that commonly, pavement temperature differentials result from the concentrated placement of a cooler

mass of hot mix into the mat. This cooler mass is generally associated with the crust that can develop on the hot mix during transport from the mixing plant to the paver.

It is always worth remembering that temperature differentials frequently occur during HMA pavement construction projects, causing lack of homogeneity of the mixture and consequently, failure to achieve the desirable performance of the HMA layer(s). However, temperature differentials may be minimized or even eliminated by HMA remixing, shorter hauling distances, warmer environmental conditions, and good rolling practices. The knowledge of specific cold areas on the mat is valuable for the engineer in order to decide either to apply further compaction or to test the compaction level and reinforce properly the affected area. It seems that this knowledge is readily available through the use of IRT systems, as they can measure the surface temperature and present the data visually, leading also in the identification of cold spots.

4.4.2 Influence of compaction temperature and energy on HMA compactability

Asphalt material is compacted to obtain the desired density for maximum strength and wear and of course to provide a smooth riding surface. It is well-known that the initial (as-constructed) density of HMA depends on the ease with which the mixture can be compacted, the type of compaction equipment, the rolling sequence and procedure, the mixture temperature during compaction and of course, the weather conditions during construction. Although, the above mentioned factors have a synergic effect on asphalt mix compaction, temperature is a key factor on mix compactability. Specifically, HMA temperature has a direct effect on the viscosity of the asphalt binder and thus on compaction. As the mix cools, the asphalt binder becomes more viscous, which results in smaller density gain for a given compactive effort. Furthermore, the effects of temperature on the density growth of HMA in the field, as defined in Eq. 4.16, combined with the applied compaction effort were evaluated in the present study (Plati et al. 2014).

$$\Delta C_d = (C_d)_{i+1} - (C_d)_i \quad (4.16)$$

where C_d: compaction degree (%); i: compaction phase

For this purpose, a pavement test section was established covering a 2x3 m^2 mat area and sixteen (16) stations were located defining a grid with fixed distances, as shown in Fig. 4.38. At these stations, thermographic measurements were conducted during

laydown and compaction until the end of rolling operations. This was carried out for each HMA layer (i.e. AC12.5 surf PmB (SBS) and AC20 base 50/70 mixtures). It is worthwhile to mention that the reason for sampling 16 stations was to provide a balance with statistical requirements, while minimizing interference with construction operations.

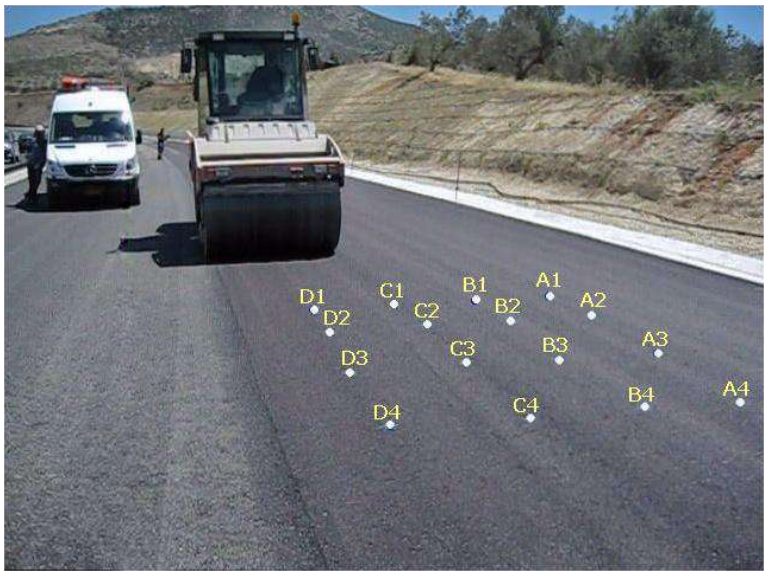

Fig. 4.38 Test section

In addition, a nuclear density gauge was used to measure the in-place HMA density (ASTM 2005). Although the nuclear density gauge offers portability and quick results, due to the short time between roller passes it was not feasible to obtain density readings after each pass for the whole test stations. Thus, it was decided to conduct density measurements at the end of each compaction phase, for each HMA layer.

Figure 4.39 illustrates the surface temperature readings on the base course mixture at the a) breakdown, b) intermediate and c) finish phase of compaction. In correspondence the density growth is calculated according to Eq. 4.16. Figure 4.40 summarizes the density growth values of the base course mixture due to the different compaction phases for each station. The roller compaction train of the HMA course layer used two rollers. The breakdown roller was a 10-ton steel double drum roller. First passes of this roller were in static mode. Then compaction was conducted with the steel drum roller in vibration mode and a pneumatic rubber wheeled roller with tire pressures of 73 psi. For final leveling, the steel drum roller in static mode was used.

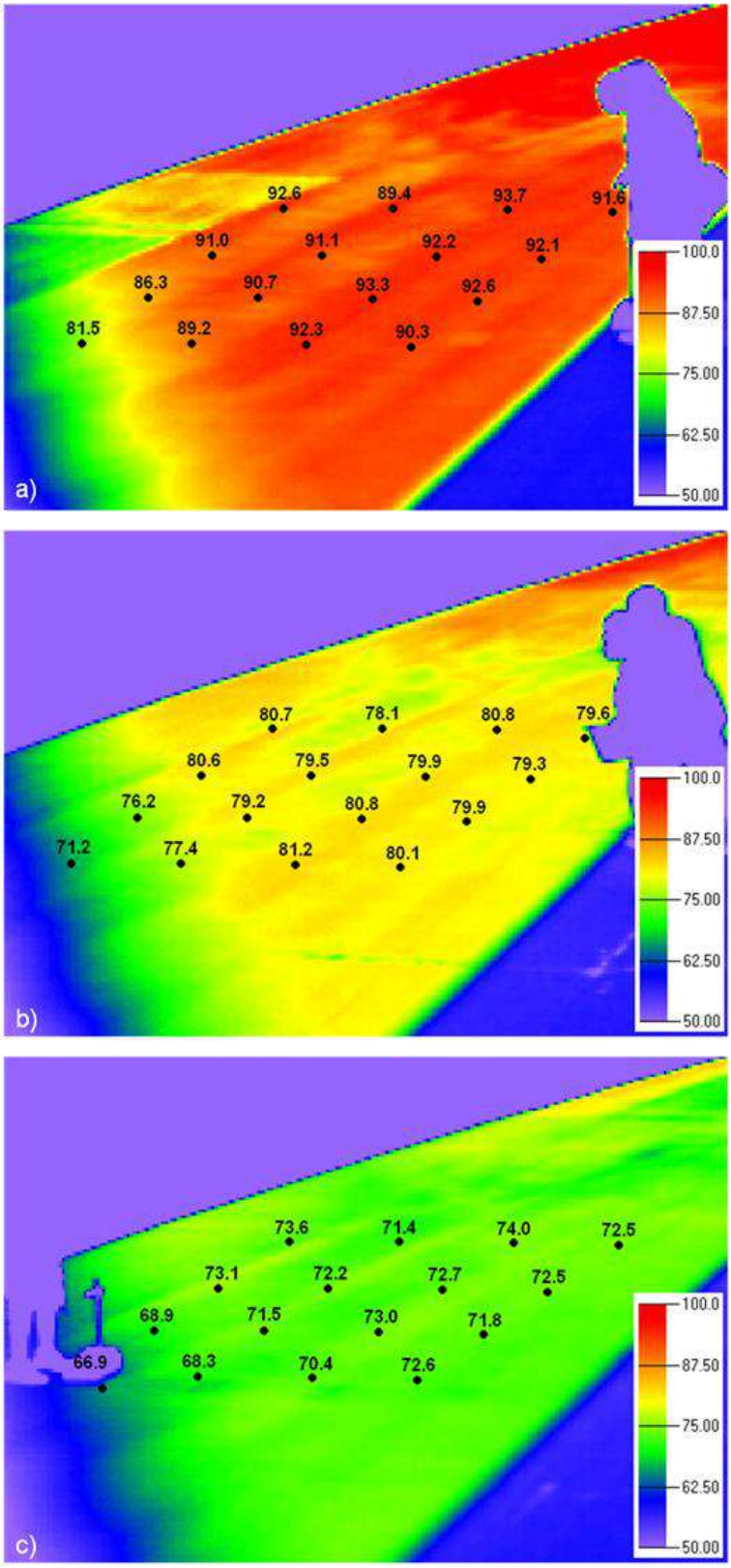

Fig. 4.39 Mat surface temperatures of base course mixture

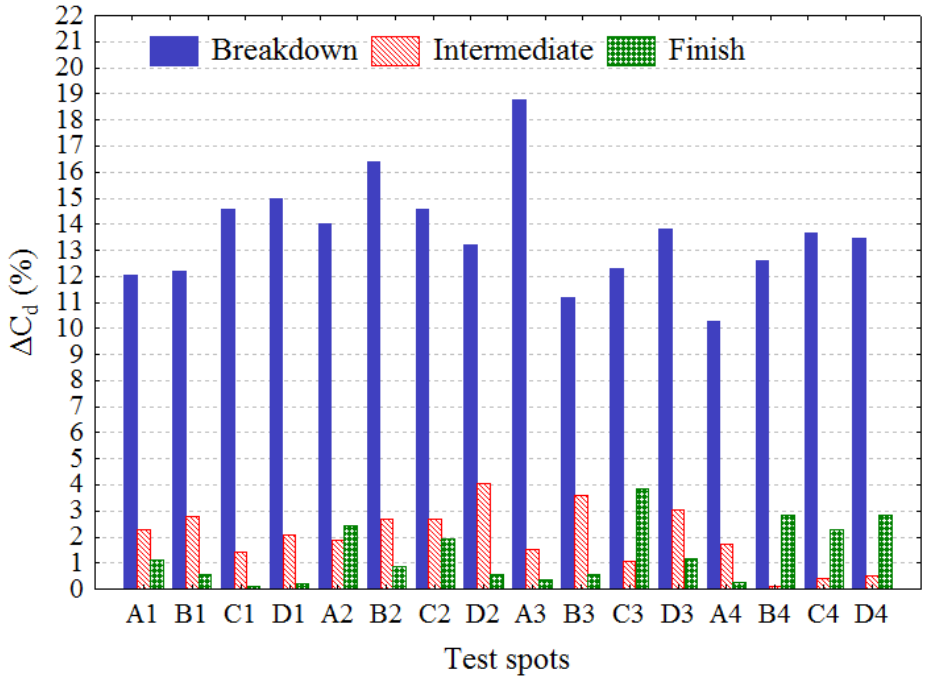

Fig.4.40 Density growth values during compaction of base course mixture

Figure 4.40 shows that the higher values of density growth, ranging from 10.3-18.8%, were observed after the breakdown phase, when mat surface temperatures were quite high. With the progression of compaction, density growth decreases sharply. The decrease in density growth is partially due to temperature, but is also partially due to the fact that as the mixture is compacted, it takes more effort to further compact it. However, considering that the same steel roller used for both breakdown and finish compaction, thus the operating weight is almost identical, it can be argued that the density growth differences observed in Fig. 4.40 are greatly associated with the decrease in temperature. For instance, the finish roller passes, made at lower temperatures for final leveling, have the least contribution (0.1-4.0%) to the final measured density.

Similar to the case of the base course mixture, Fig. 4.41 illustrates the temperature readings on the surface course mixture at the a) breakdown, b) intermediate and c) finish phase of compaction. In addition, Fig. 4.42 summarizes the density growth values of the surface course mixture due to the different compaction phases for each station. The roller compaction train of the HMA surface course layer used two identical 10-ton steel double drum rollers with 1.8 m drum width operating in echelon. The initial rolling was

performed using static mode, followed by a number of passes in vibratory mode. At the end of compaction process the static mode was used for final leveling.

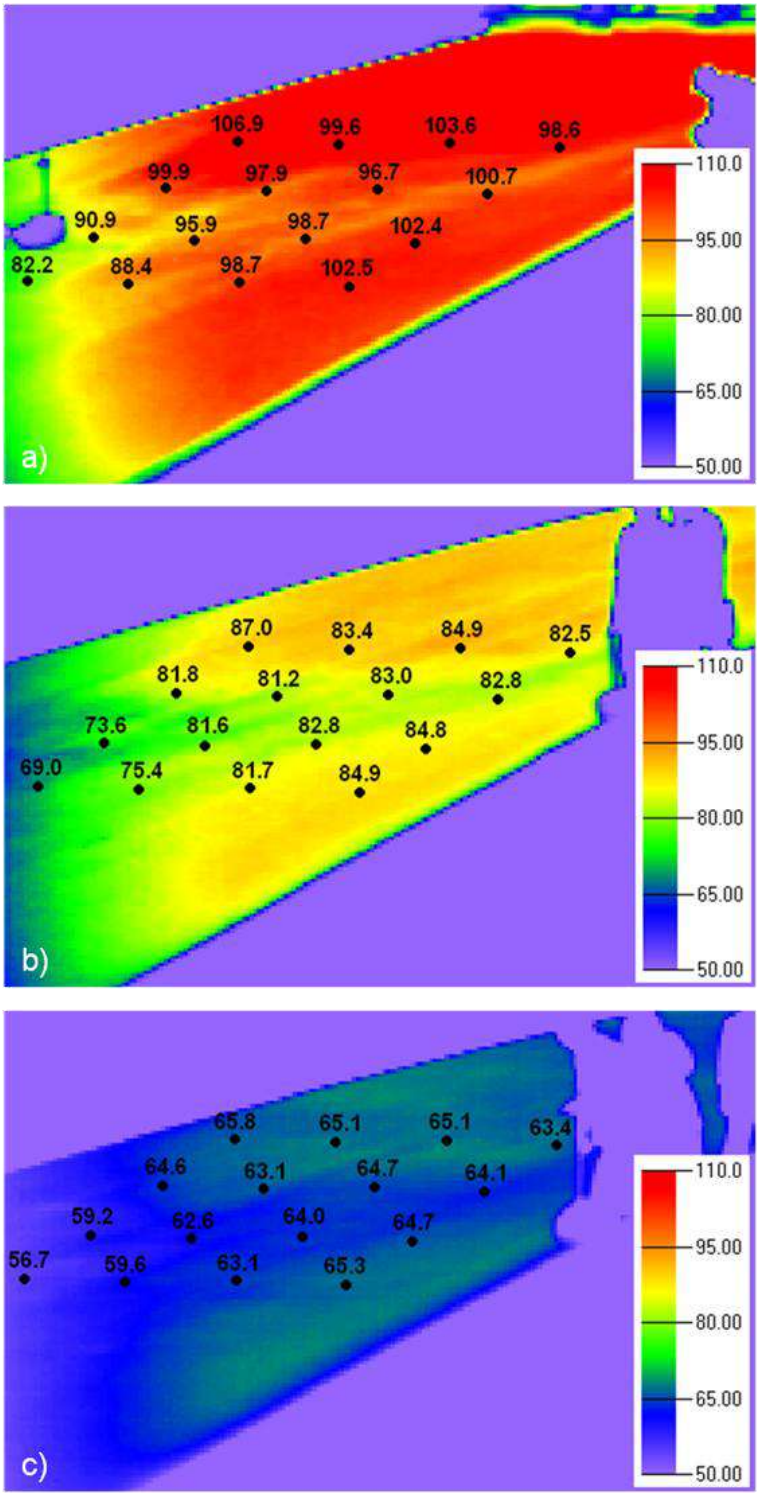

Fig. 4.41 Mat surface temperatures of surface course mixture

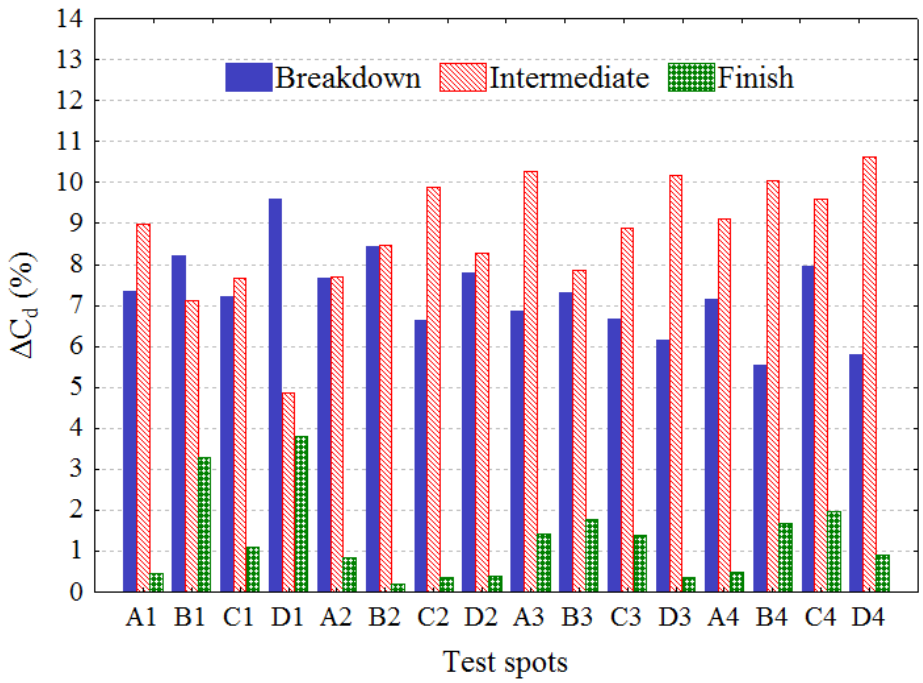

Fig. 4.42 Density growth values during compaction of surface course mixture

From Fig. 4.42, the general observation is that density increases significantly after both the breakdown and intermediate phase. It is interesting to note that the density growth at the fourteen out of the sixteen stations was greater after intermediate phase, when mix temperature was significantly lower compared to the breakdown phase. However, considering again that the applied compaction energy (i.e. roller passes) at the intermediate compaction phase is three-fold compared with the breakdown phase and the difference in density growth is not proportionate, temperature seems to be the most significant factor affecting density growth. The finish roller passes, made at lower temperatures for final leveling, have the least contribution (0.2-3.8%) to the final measured density.

To substantiate the observations relating to the influence of the mat surface temperature (T_{surf}) and applied compaction effort in terms of the Accumulated Compaction Pressure (*ACP*) on the density growth of asphalt mixtures, a statistical analysis was undertaken. The goal was to fit a reliable model that can describe or explain the experimental data. Considering the sixteen test stations, an adequate sample of data was collected and used for statistical analysis. It should be noted that ACP is a well-documented indicator for field compactability that quantifies the total applied

compaction effort to the HMA mat (Leiva et al. 2008). In the light of the above, the contact pressure of steel rollers was estimated for each roller pass (and compaction phase) using the methodology presented in Delgadillo et al. (2008), while for pneumatic rollers it was assumed to be equal to the tire pressure. Taking into consideration that finish compaction phase remotely contributes to the gained density growth, the related data were eliminated from statistical analysis of both mixtures. Tables 4.14 and 4.15 tabulate the results of the applied linear regression for the base and surface course mixtures, respectively.

Table 4.14 Statistical analysis results of base course mixture

Variables	Coefficient	Std. error	*t*-Stat.	*p*-value	Significant at a=0.05
Regression summary					
ACP	.000547	.000920	.593828	.562099	No
T_{surf}	.151866	.034502	4.401696	.000603	Yes
ANOVA	Sum of squares	df	Mean squares	*F*	*p*-value
Regression	3904.919	2	1952.460	367.178	.000000
Residual	74.445	14	5.317		
Total	3979.364				
Goodness of fit statistics					
r	.991				
R^2(adj.)	.979				
Std. error	2.306				

Table 4.15 Statistical analysis results of surface course mixture

Variables	Coefficient	Std. error	*t*- Stat.	*p*-value	Significant at a=0.05
Regression summary					
ACP	.000362	.000336	1.076951	.299710	No
T_{surf}	.137006	.024305	5.636996	.000061	Yes
ANOVA	Sum of squares	df	Mean squares	*F*	*p*-value
Regression	4072.706	2	2036.353	1119.170	.000000
Residual	25.473	14	1.820		
Total	4098.179				
Goodness of fit statistics					
r	.997				
R^2(adj.)	.993				
Std. error	1.349				

According to the ANOVA results of Table 4.14 the F-test with a *p*-value of almost zero shows a strong relation between the density growth and the variables selected. Moreover, the high R^2 of 97.9% indicates that almost full of variation in density growth is explained by the ACP and mat surface temperature T_{surf}. However, the mat surface temperature has a significant effect on the density growth, while ACP has a marginal effect for 95% confidence level. In the light of the above the practical finding that could be derived is that higher compaction temperatures yield greater increases in density growth, as expected. At lower compaction temperatures more roller cumulative passes (i.e. ACP) may be not efficient enough to gain the desired level of density growth.

Similar findings were derived with respect to the surface course mix. Again, the ACP variable is insignificant, suggesting no statistical difference in the gained density growth. The statistical results of Table 4.15 indicate that 99.3% of variation in density growth is explained mainly by the mat surface temperature.

The above results demonstrate that a density-growth curve must be developed for the specific mixture and compaction train being used. To accomplish this goal, it seems that the emerging IRT technology provides a powerful advantage as it makes the measurement of HMA temperature during construction routine work.

4.4.3 Influence of compaction mode on HMA compactability

To explore the relationship between the HMA compactability and the compaction mode, GPR surveys utilizing a 2 GHz air-coupled GPR system were conducted (Plati et al. 2016). Preliminary surveys investigated the feasibility of using ε_{HMA} as HMA compactability indicator. For this purpose, two full-scale pavement test sections were selected in which stationary GPR scans, as illustrated in Fig. 4.43, combined with PQI measurements at the same test locations were conducted. The pavement construction sites involved the paving and compaction of a 50 mm thick new asphalt overlay surface course, using different dense-graded mixtures, over the existing flexible pavement structure.

Fig. 4.43 GPR field data collection

During the asphalt construction process of test section No. 1, stationary GPR measurements data were collected at three spots across the mat width. GPR measurements were conducted immediately after paving of AC12.5 surf 50/70[a] and successively after each roller pass (a pass corresponds to one forward or backward motion). As seen in Fig. 4.44, the PQI density progressively increases as the number of roller passes for each test point increases respectively. A similar trend is observed with respect to the ε_{HMA} and the number of roller passes, which indicates asphalt mixture densification. When asphalt mix material is compacted the volumetric proportion of air,

which has a low dielectric value, is squeezed out of the mixture and thus the dielectric value of the asphalt mixture increases.

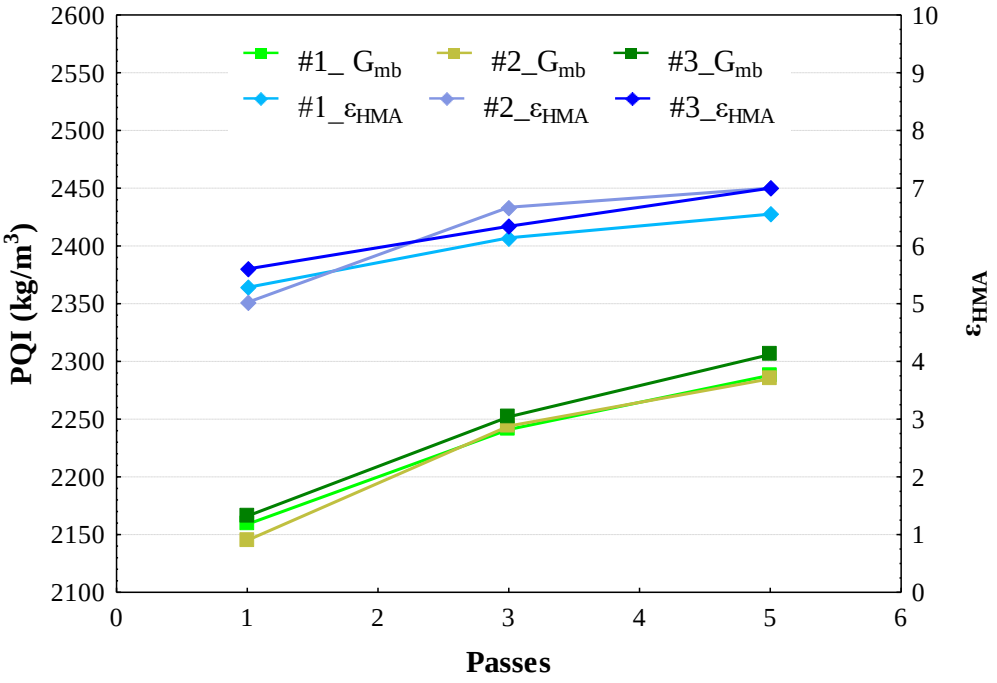

Fig. 4.44 Evolution of ε_{HMA} and bulk density of asphalt mix with respect to roller passes

To further verify the effectiveness of ε_{HMA} indicator test section No. 2, constructed using a similar surface course mix (i.e. AC12.5 surf 50/70^{b}) was monitored again by means of GPR and PQI testing. The idea was to assess the effect of preconstruction works (i.e. milling vs non-milling) on overlay HMA compactability. Figure 4.45 presents an example of the ε_{HMA}- PQI curves corresponding to three spots across the mat width of two subsections. While both Fig. 4.45a-b show that ε_{HMA} values increase with the number of roller passes, it is further demonstrated that higher ε_{HMA} and PQI density values are derived concerning the milled subsection. Given that the same compaction effort was applied to HMA, the enhanced compaction outcome for the milled subsection could be attributed to the milling process, as expected.

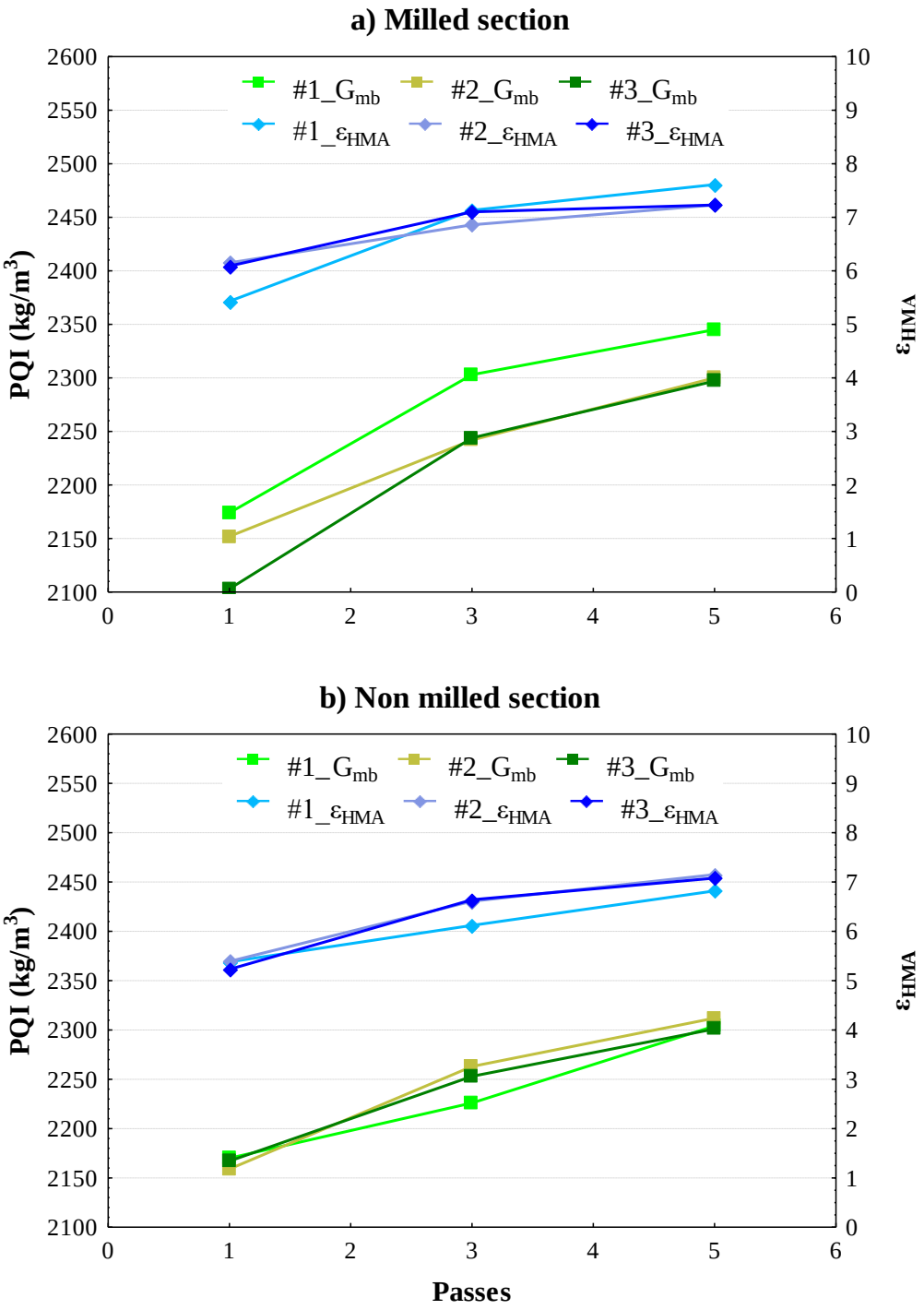

Fig. 4.45 Evolution of ε_{HMA} and bulk density of asphalt mix with respect to roller passes for different compaction techniques

The feasibility study results indicate that the estimated ε_{HMA} value during the compaction process could be considered as a measure of the asphalt mix field compactability.

Given the above, a new test section (No.3) which also included the overlay construction of a surface course mix (i.e. AC20 surf 50/70) over the same existing flexible pavement structure, was monitored by means of GPR testing to investigate the effect of compaction mode on in-situ HMA compactability. For this purpose, the test section was divided into four subsections that were compacted using different compaction methods, as illustrated in Fig. 4.46.

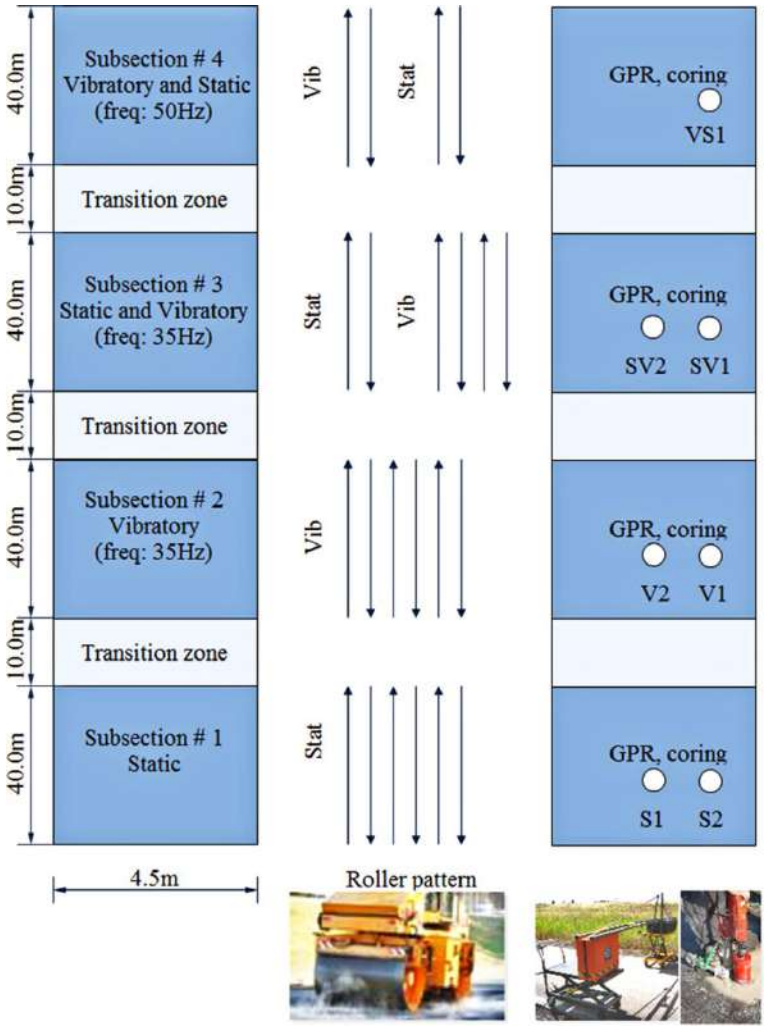

Fig. 4.46 Schematic layout of test section

A 10-ton steel double drum roller, able to operate in a vibratory or static mode was utilized to construct these test subsections. Each subsection (approximately 40m long)

was compacted using a varying number of roller passes. Subsection # 1 was compacted in a static mode. Subsection # 2 was compacted using a vibratory steel roller at a medium frequency of 35Hz. Subsection # 3 was compacted using a static steel roller for breakdown and then a vibratory mode with a 35Hz frequency was implemented. Subsection # 4 was compacted using a vibratory steel roller at a high frequency (i.e. 50Hz) for breakdown and then a static mode for finishing.

Figure 4.47 illustrates the evolution of ε_{HMA} per test spot and roller pass for the various subsections (i.e. Static, Vibratory, Static-Vibratory and Vibratory-Static). From Fig. 4.47 it can be seen that after paving (i.e. roller pass # 1), deviation -with respect to ε_{HMA} values (ranging from 4.2 to 5.0) among the four subsections- is observed and thus it could be stated that the finisher screed provides a non-uniform precompaction. A more uniform precompaction seems to be achieved across the mat width, if we compare the ε_{HMA} values from the two test spots.

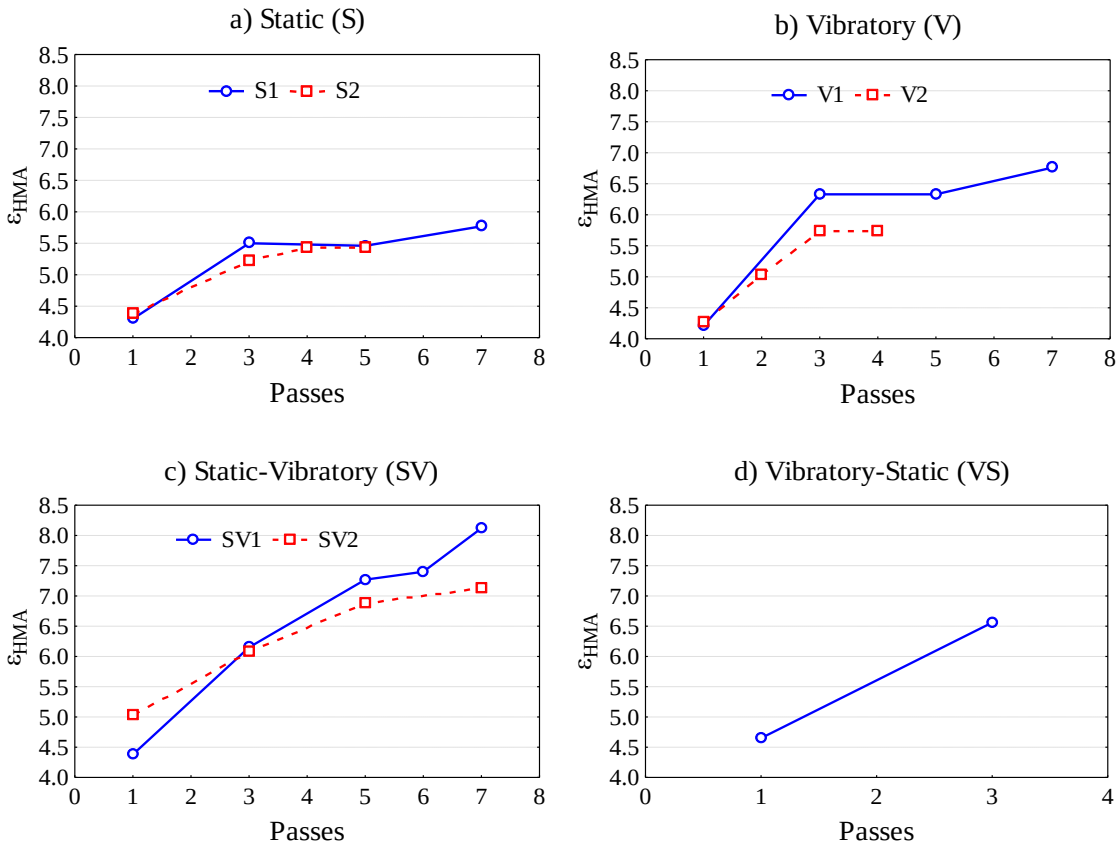

Fig. 4.47 Evolution of ε_{HMA} values with respect to roller passes and compaction mode

A comparative analysis between the four subsections shows that the compaction curve slope of the Static-Vibration subsection increases at a changing rate, even after seven roller passes. Regarding the remaining subsections, the ε_{HMA} starts experiencing a slow rate of increase after the fifth roller pass, almost tapering off beyond this point, and it is thus expected to reach a steady-state condition. After finish compaction stage, the subsections final ε_{HMA} values present a substantial deviation, thus providing an indication of differently achieved field compaction degree. Given the above, it is argued that this approach could be used to evaluate the efficiency of compaction modes and further set up the compaction pattern that is needed to achieve the desired asphalt pavement density.

A week after the construction process, repetitive GPR static measurements were performed in combination with coring/cutting at the same test locations for further evaluations. The aim was to investigate the effect of compaction temperature to GPR readings. Figure 4.48 presents the ε_{HMA} values from both after the finish compaction stage (where the mat temperature was still warm) and a week long period after construction (where the mat temperature had cooled down).

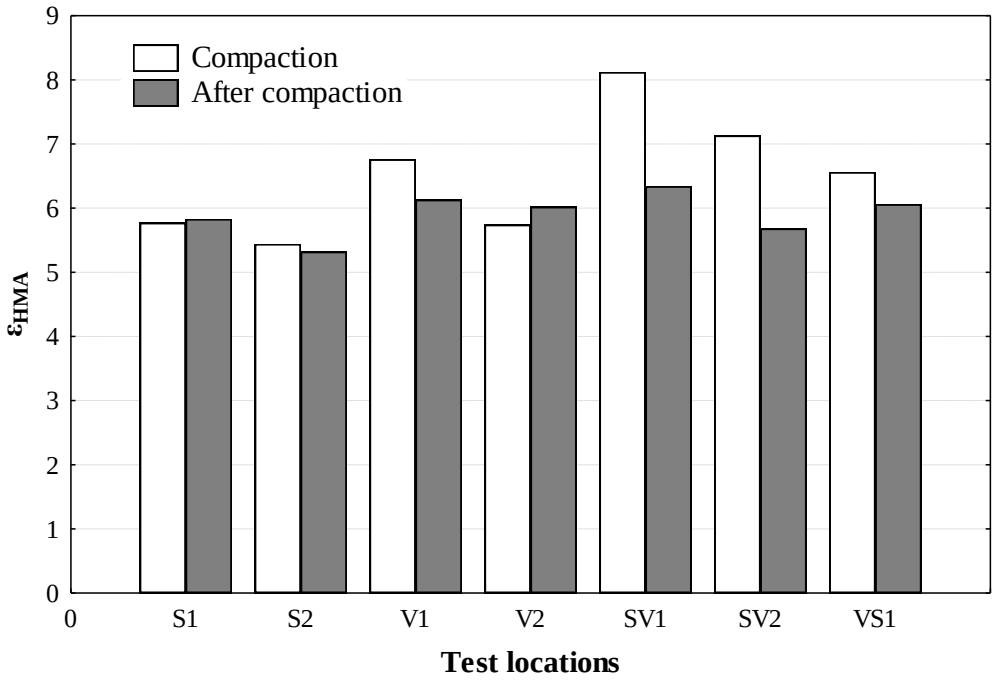

Fig. 4.48 Evaluation of ε_{HMA} values with respect to time period (temperature) of GPR measurements

In Fig. 4.48, substantial differences can be observed, except for Static, for all subsections. Generally, the overall trend was that ε_{HMA} values at the end of compaction process were higher than the values obtained a week period after construction; these differences ranged from +1.76 to -0.28. Based on the above results, it is evident that in place density prediction using GPR data during the compaction process can lead to overestimated values.

4.4.4 Evaluation of compactability indices

The compaction characteristics of the mixtures under investigation were also evaluated by means of indicators related to semi-logarithmic densification curves fitted to the field experimental data. Similar to the gyratory and roller compaction study, the slope *b* and the number of passes to achieve 8 and 15 percent air voids, (N_8) and (N_{15}) respectively, were used. The evolution of the air void content, covering the full spectrum of compaction modes, in relation to the number of passes is expressed as follows:

$$v(n_{fp}) = a - b\ln(n_{fp}) \quad (4.17)$$

where $v(n_{fp})$ is the air void content for a number of field roller passes (%), *a* and *b* are regression-based constants, and n_{fp} is the number of field roller passes.

It should be pointed out that the air void content with respect to roller passes for all mixtures, in general, indicate little variation, as demonstrated from the statistical results of Table 4.16. In that respect, the mean value of air void contents may be considered appropriate for the purpose of the analyses regarding the determination of compactability indicators.

Table 4.16 Statistical results

Mix type	Passes	Air voids (%)	
		Mean	StDev
AC12.5 surf 50/70[a]	1	12.6	.6
	3	8.8	.2
	5	6.7	.6
	7	6.3	.5
	9	5.5	.6
AC12.5 surf PmB (SBS)	1	31.4	.6
	3	25.2	1.0
	5	20.7	.9
	10	17.7	.8
	12	16.7	.8
	15	14.2	1.1
AC20 base 50/70	1	23.4	1.6
	4	10.4	.8
	6	8.5	1.0
	8	7.2	1.0
	11	5.9	1.0

Figure 4.49 illustrates the experimental compaction data for all mixtures, while Table 4.17 tabulates the analysis results of the above study.

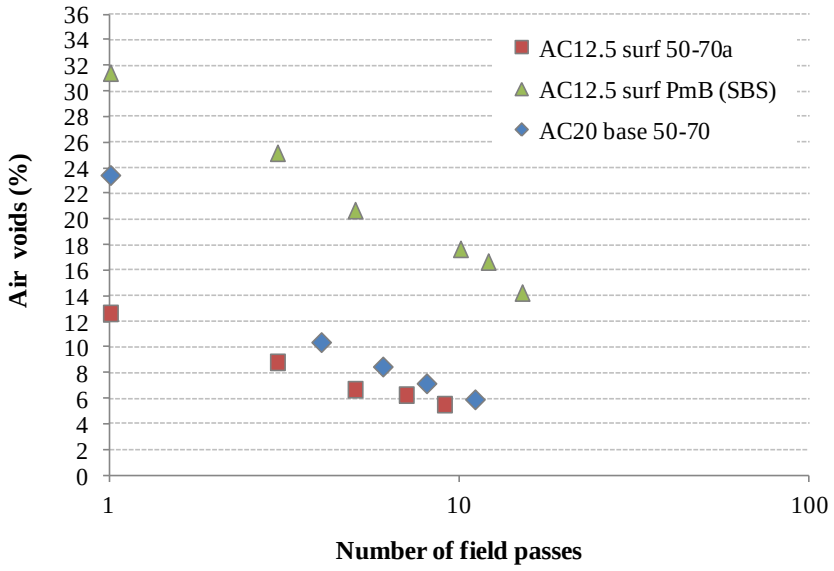

Fig. 4.49 Air voids variation as a function of compaction effort (all mixtures)

Table 4.17 Compactability indicators for all mixtures

Mixture	Regression equation	R^2	b factor	N_8/N_{15}
AC12.5 surf 50/70[a]	y= 12.50- 3.29lnx	.988	3.29	4
AC12.5 surf PmB (SBS)	y= 31.45- 6.16lnx	.991	6.16	14
AC20 base 50/70	y= 22.53- 7.49lnx	.969	7.49	7

Table 4.17 shows that the experimental data fit well to the regression equations; the R^2 values are higher than 0.97. It can also be stated that the higher value of slope *b* indicates greater ease of compaction for the AC20 base 50/70 mix. However, the required number of passes to achieve 8% air voids is higher, compared to the AC12.5 surf 50/70[b]. This may be attributed to the different percentages of initial air voids, as obtained from the paver screed. Also, the AC12.5 surf PmB (SBS) mix seems to need more compactive effort compared to the other mixtures, which may be attributed to its mixture properties and the rather low pre-compaction level delivered from the finisher.

4.4.5 Estimation of in-situ density

This section discusses the study results related to the effort devoted for the estimation of the in-situ HMA density using two different methodologies. As previously mentioned, researchers have demonstrated the potential of GPR coupled with the use of novel algorithms to predict the in-situ field density. On this basis, the prediction performance of these models is evaluated.

Also, building on previous findings which demonstrated the significant effect of temperature on compaction, a formulation to describe the compaction process is studied. For this purpose, a closed formula found in the literature (Huh and Nam 2000) which quantifies the relationship between density and number of roller passes, taking into consideration the temperature evolution (cooling) with respect to roller passes is verified using experimental compaction data.

4.4.5.1 GPR-based density prediction models

Primarily, the prediction performance of the three recently developed EM-based density models, as described in Eq. 4.7-4.9, was evaluated using different methodological approaches (Plati et al. 2016). Particularly, a laboratory-based methodology and a field-

based methodology were followed with respect to the backcalculation of ε_s of the mix aggregates, which are to be discussed in the subsequent sections. Also, a comparative assessment was conducted between the CRIM, Rayleigh and ALL models to illustrate the performance of these density prediction models.

Based on the findings of this study, the best EM-based model was selected for further evaluation. Particularly, a comparative assessment of predictions obtained using also other GPR-based algorithms, PQI results and field cores densities. Moreover, a parametric analysis was performed to evaluate the error performance of density models with respect to the number of calibration cores and GPR antenna frequency.

For these purposes, the experimental data obtained through the construction of the three full-scale test sections, as described in section 4.4.3, were further analyzed. The mixtures information needed for the course of this study are tabulated in Table 4.18.

Table 4.18 Mix design

Mix design properties	AC12.5 surf 50/70[a]	AC12.5 surf 50/70[b]	AC20 surf 50/70
Aggregate type	Limestone	Limestone	Limestone
Aggregate bulk specific gravity (G_{sb})	2.735	2.710	2.648
Aggregate effective specific gravity (G_{se})	2.746	2.750	2.650
Bitumen type	50/70pen	50/70pen	50/70pen
Bitumen content (P_b)	4.3%	4.3%	4.3%
Bitumen specific gravity (G_b)	1.02	1.02	1.01
Maximum specific gravity (G_{mm})	2.560	2.563	2.480

4.4.5.1.1 Laboratory-based approach

Laboratory tests were conducted on HMA slabs to evaluate the three EM-based density models. Tests included the fabrication and compaction of asphalt slabs, corresponding to AC20 surf 50/70 mix, and GPR measurements with a 2-GHz antenna. The aim was to investigate the prediction performance of the density models based on GPR laboratory-measured dielectric constants. For this purpose, determination of bulk densities by means of coring of asphalt slabs coupled with the asphalt slabs measured ε_{HMA} values were used to backcalculate the ε_s of mix aggregates in order to be employed as input in the density models for the assessment of field density.

Laboratory compaction was performed using the steel segmented roller compactor, for which multiple research studies argue that it simulates in-situ compaction (Renken 2000; Sousa et al. 1991). Particularly, laboratory compaction was meant to mirror field compaction, as illustrated in Fig. 4.46, adopting four compaction modes (i.e. Static: S, Vibratory: V, Static-Vibratory: VS and Vibratory-Static: VS). Also, the main compaction energy and vibration frequency reflected the operational characteristics of the steel wheel rollers used in the field compaction. After cooling of the RC slabs to ambient temperature, GPR testing was performed over the laboratory-compacted slabs implementing several test configurations. In addition, three 100mm diameter specimens were cored from the top of each slab. The volumetric properties of the cored specimens were evaluated with the saturated surface dry (SSD) method. The bulk densities results combined with the GPR measured ε_{HMA} values were utilized to backcalculate the ε_s of mix aggregates. The results of this approach are presented in Table 4.19.

Table 4.19 Backcalculated ε_s of mix aggregates based on laboratory-based approach

RC Slab	G_{mb} measured (mean)	ε_{HMA}	Backcalculated ε_s		
			CRIM	Rayleigh	ALL
S	2.373	6.6	7.5	7.8	7.8
V	2.375	4.6	5.0	5.1	5.3
SV	2.407	4.8	5.2	5.3	5.4
VS	2.377	4.2	4.6	4.6	4.8

Utilizing the mean ε_s obtained from the different laboratory compaction modes and the parameters values of Table 4.18, the three density models were employed to predict the G_{mb} of field cores. From the results, rather poor prediction performance was observed for all models. The mix aggregates ε_s – RC-based value seems to be unrealistic and thus the models over predict G_{mb} values of field cores, as illustrated in Fig. 4.50.

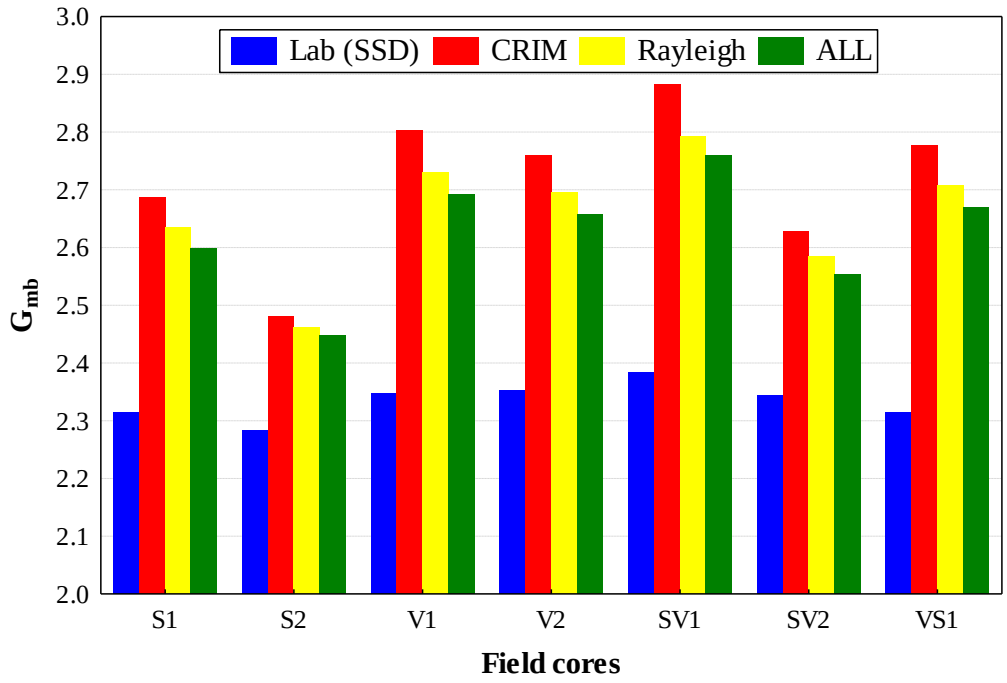

Fig. 4.50 EM model prediction performance (laboratory approach)

The overall trend showed that the ALL model exhibited the best prediction performance. However, this model still provided rather high prediction errors and thus further investigation should be attempted.

4.4.5.1.2 Field-based approach

Within this methodology, the bulk densities of two out of seven field cores, namely V1, V2 corresponding to Vibratory subsection of test section illustrated in Fig. 4.46, were utilized in combination with the related GPR measured ε_{HMA} to backcalculate the electric permittivity ε_s of mix aggregates, as described in detail by Leng et al. (2011). The criterion for selecting the specific cores for the backcalculation of ε_s was that the related ε_{HMA} had the lowest variation compared to the remaining subsections. After the value of ε_s was obtained, the three density models were applied to predict the G_{mb} for each test location and subsection. Note that the model parameter values utilized to employ the density algorithms are listed in Table 4.18. Based on the previous findings of the current study, it is worthwhile to mention that the predicted G_{mb} values were based on the ε_{HMA} values obtained a week after construction. Table 4.20 presents the backcalculated ε_s of

the three density EM models with respect to the measured G_{mb} values of the extracted cores.

Table 4.20 Backcalculated ε_s of mix aggregates based on field-based approach

Field cores	G_{mb} measured	ε_{HMA}	Backcalculated ε_s		
			CRIM	Rayleigh	ALL
V1	2.347	6.1	7.0	7.3	7.3
V2	2.352	6.0	6.8	7.1	7.2

Figure 4.51 illustrates the predicted G_{mb} values from the three EM models with respect to the 'ground truth' measured G_{mb} values of the remaining cores.

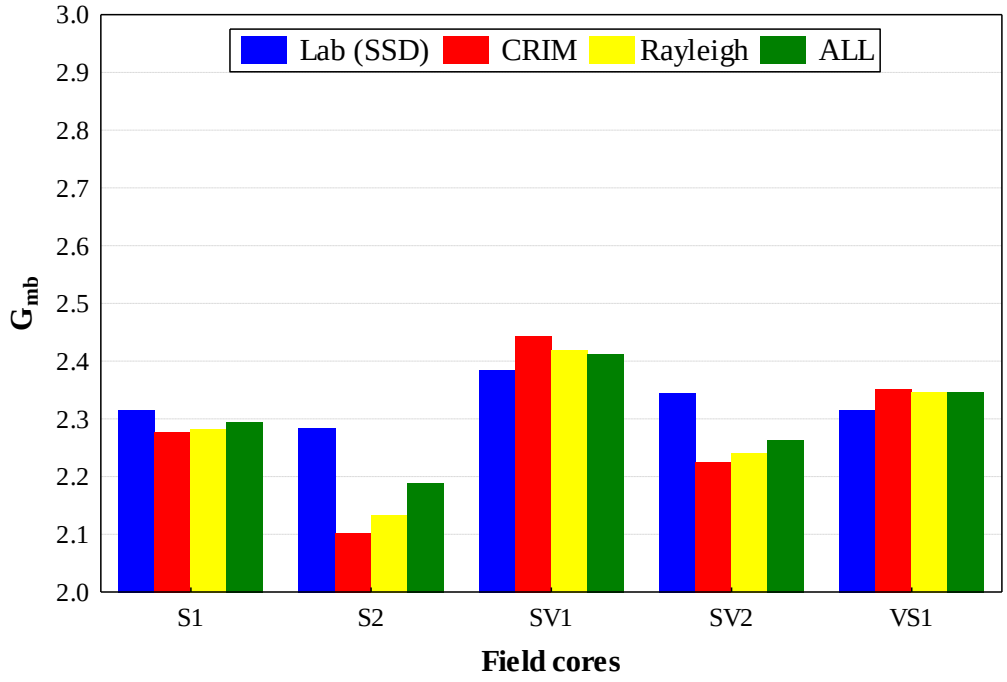

Fig. 4.51 EM model prediction performance (field approach)

It can be observed that the predicted G_{mb} values closely approach the 'ground truth' field cores densities. From the comparative analysis with the previous laboratory-based methodology results it is evident that the prediction performance of the EM density models based on the electric permittivity ε_s of mix aggregates, as assessed from field data, is superior. Moreover, the ALL model exhibits the best prediction performance among the three models.

To further verify the prediction performance of the ALL model, GPR data collected from test section No. 2 were also analyzed. The in-situ densities as predicted from the GPR data were compared to the laboratory measured densities of field cores. Figure 4.52 illustrates the measured and predicted data of the field cores.

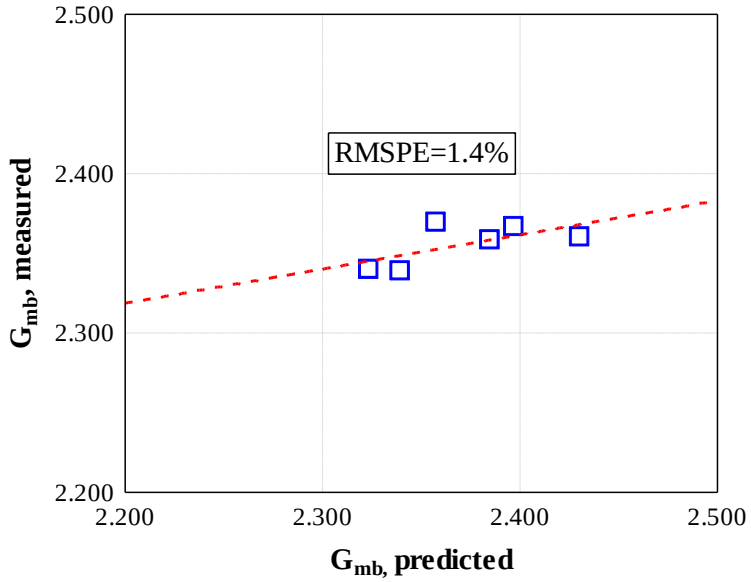

Fig. 4.52 Verification of ALL model prediction performance

The prediction error in terms of the root mean square percentage error (RMSPE) is 1.4%, hence indicating that the predicted values are close to the measured ones.

4.4.5.1.3 Comparative evaluation of density models

Building on previous findings, a further study was employed to evaluate the effectiveness of GPR methodology to estimate the in-situ compaction degree. The aim was to evaluate the error performance of density models with respect to the number of calibration cores and GPR antenna frequency, as shown schematically in Fig. 4.53. For this purpose, a field GPR survey was conducted on a pavement test section which involved the construction of an overlay course layer using AC12.5 surf 50/70^{b} mix. GPR measurements along six lanes of a 2.8km-long pavement section were conducted with both a 1-GHz and 2-GHz antennae. Then, the collected GPR data were analyzed and predictions of the in-place densities were obtained using the dielectric-properties based algorithms, as described in Eq. 4.9-4.11. PQI measurements were conducted per 200m

and field cores (in total 20) were also retrieved from an adequate number of these test locations.

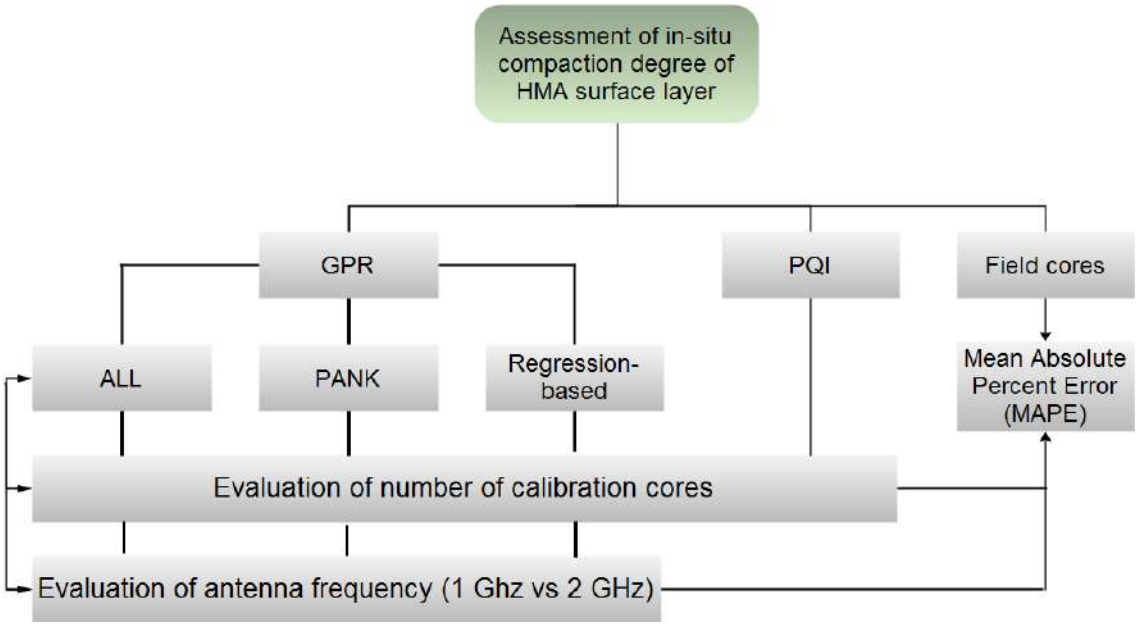

Fig. 4.53 Methodology layout

Data analysis included the determination of density algorithms coefficients, namely the ε_s, k, and a-b, with respect to the number of calibration cores and GPR antenna frequency. Using these coefficients, the density prediction models -namely ALL; PANK; and regression-based- were employed and the in-place density for the remaining cores was estimated. The error performance of these models was then evaluated with respect to the remaining field cores densities based on mean absolute percentage error (MAPE).

Figures 4.54-4.55 illustrate the variation of MAPE with respect to the number of drill cores used for calibration purposes concerning the PQI and GPR data collected using 1 and 2-Ghz antennae, respectively.

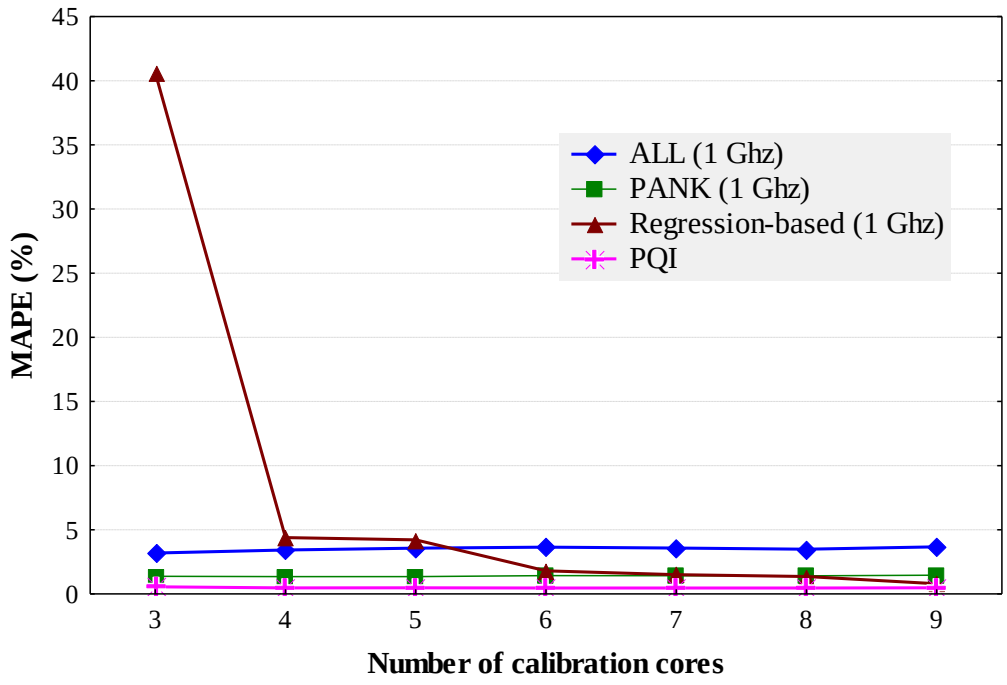

Fig. 4.54 Variation of MAPE vs number of calibration cores (1 Ghz antenna)

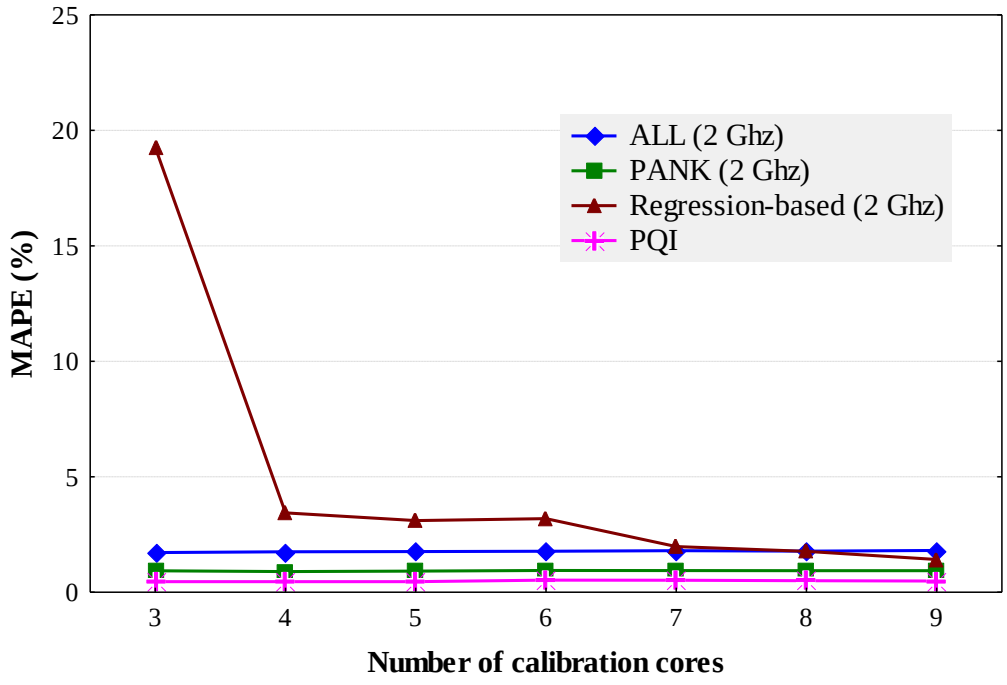

Fig. 4.55 Variation of MAPE vs number of calibration cores (2 Ghz antenna)

As shown above, the parametric analysis indicates that the GPR-based prediction algorithms, except for the regression-based, in general do not show significant error variation increasing the number of calibration cores. Hence, it could be claimed that a number of 3 cores is sufficient for calibration purposes. On the contrary, the error prediction performance of the regression-based method is improved significantly with the increase of number of calibration cores. Particularly, a number of 7 cores are needed to improve the predictions accuracy. From the comparative analysis of the results obtained using the two antennae, it can be also stated that using 2-Ghz antenna for GPR surveys more accurate predictions are obtained independently of the density model applied. Also, the PQI method was found to outperform the GPR-based methods, although this method provides information only at discrete test locations.

Figure 4.56 summarizes the (mean) error prediction results as a function of the GPR-based algorithms applied.

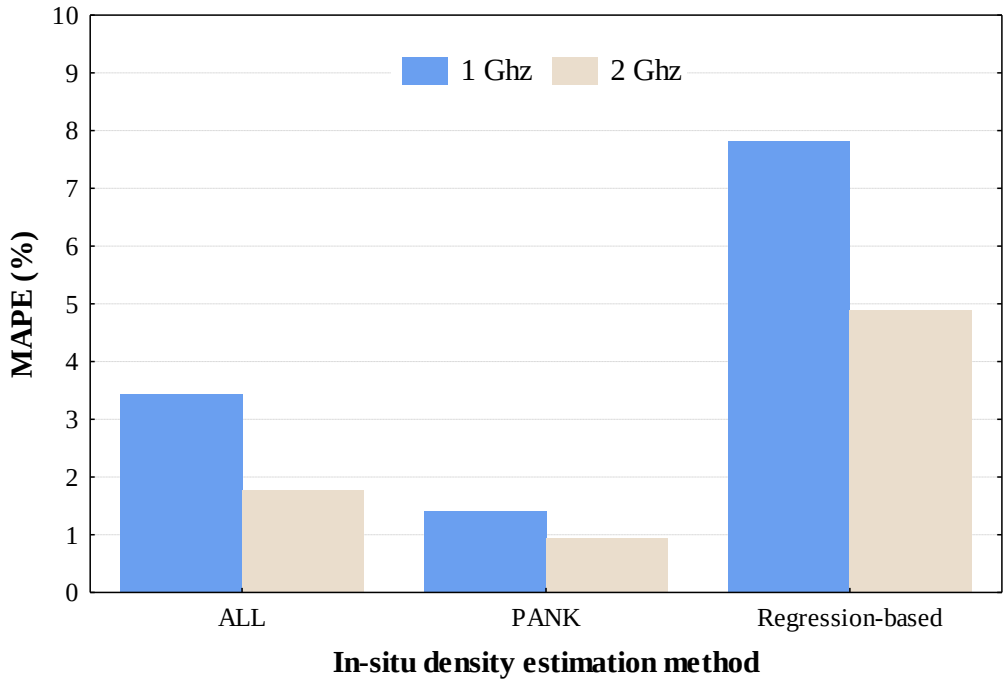

Fig. 4.56 MAPE (mean) vs GPR-based prediction models and antenna frequency

It can be seen that both the ALL and PANK prediction models provided reasonably accurate predictions on the basis of the 2 Ghz antenna data collected. The average prediction errors of the models with respect to the ‘ground truth’ data are 1.8% and

0.9%, respectively. This is more clearly demonstrated in the example of Fig. 4.57. This Figure shows the density profile of the HMA surface, as estimated implementing the GPR-based prediction models, throughout a lane of the pavement section along with PQI and field cores densities.

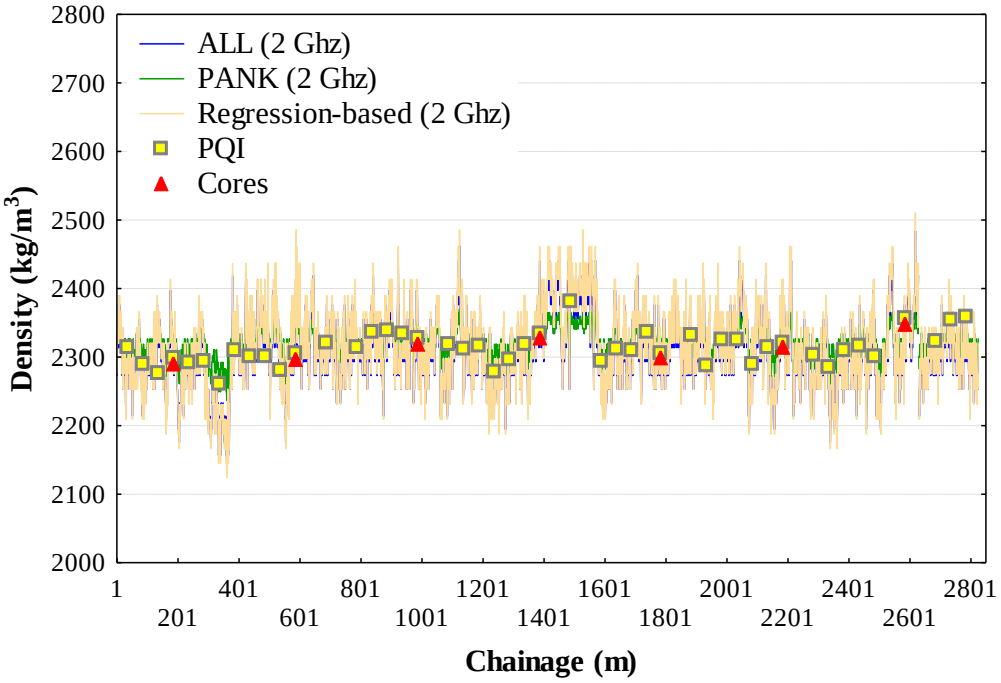

Fig. 4.57 MAPE (mean) vs GPR-based prediction models and antenna frequency

Comparing the data obtained from the GPR and PQI methods and measured density of core samples, it can be concluded that the GPR-based algorithms could be used to assess rather accurately the in-situ density of HMA pavement surface layer.

4.4.5.2 Closed form equation for density prediction

This subsection discusses the study results related to the effort devoted for the estimation of the in-situ HMA density using compaction density functions. As previously demonstrated, temperature influences significantly the compaction process. On this basis, a closed formula (Huh and Nam 2000) which quantifies the relationship between density and number of roller passes, taking into consideration the temperature evolution (cooling) with respect to roller passes is verified in terms of its prediction performance using experimental compaction data. This equation is expressed as follows:

$$\rho = \rho_0 + (\rho_m - \rho_0)\left\{1 - \exp\left[-Vexp(\frac{-W}{T})\right]N\right\} \quad (4.18)$$

where

$$V = \frac{b}{\eta_0^{0^k}} exp\left[\frac{W}{T_0}\right] \quad (4.19)$$

$$W = \frac{kE_a}{R} \quad (4.20)$$

where ρ is the density of a mix, ρ_0 is the initial density value obtained with no roller passes, ρ_m is the upper limit of density obtained with an infinite number of roller passes, η_0 is mixture's zero shear viscosity, T-T_0 are temperature and reference temperature, respectively, b-k are constants, E_α is the activation energy for flow, and R is the universal gas constant.

The closed form Eq. 4.18 describes density changes between the obtained finisher-based precompaction ρ_0 (with no roller passes) and the upper limit obtained with an infinite number of roller passes ρ_m as a function of both roller passes and temperature. Note that solidification by cooling is represented by a temperature-dependent factor [$exp(-W/T$)] and that consolidation by rolling compaction is denoted by a temperature independent factor V. This equation can be simplified inserting one more relationship expressing the cooling of mix temperature with respect to roller passes, for example, in terms of a quadratic form. Then, the compaction density can be expressed by a single variable of roller passes.

The experimental data used for this investigation was obtained during the construction of a full-scale test section which involved the paving of a 50 mm thick new asphalt overlay surface course, namely the AC12.5 surf 50/70[b], over the existing flexible pavement structure. The test section was divided into two subsections subjected to different compaction modes, namely vibratory and a combination of static-vibratory mode using a 10-ton steel double-drum roller. To fulfill the aim of this study, five spots were located across the mat width, at a fixed distance of 0.8m, and measured immediately after finisher paving and successively after each roller pass (a pass corresponds to one forward or backward motion). Monitoring of roller operations was conducted by means of PQI testing given its practicability. It should be pointed out that PQI is also equipped with an infrared temperature probe and hence mat surface

temperature can be easily measured simultaneously with density. Although surface temperature is generally lower than the in-asphalt temperature, it can be accepted as a reliable indicator of mat asphalt temperature (Delgadillo and Bahia 2008). In that respect, the infrared-based temperature was used for the purpose of this study analyses.

Figure 4.58 shows the effect of mix cooling on compaction density evolution with respect to field roller passes for the static-vibratory compaction mode. The counterpart results related to the vibratory compaction mode mix are illustrated in Fig. 4.59.

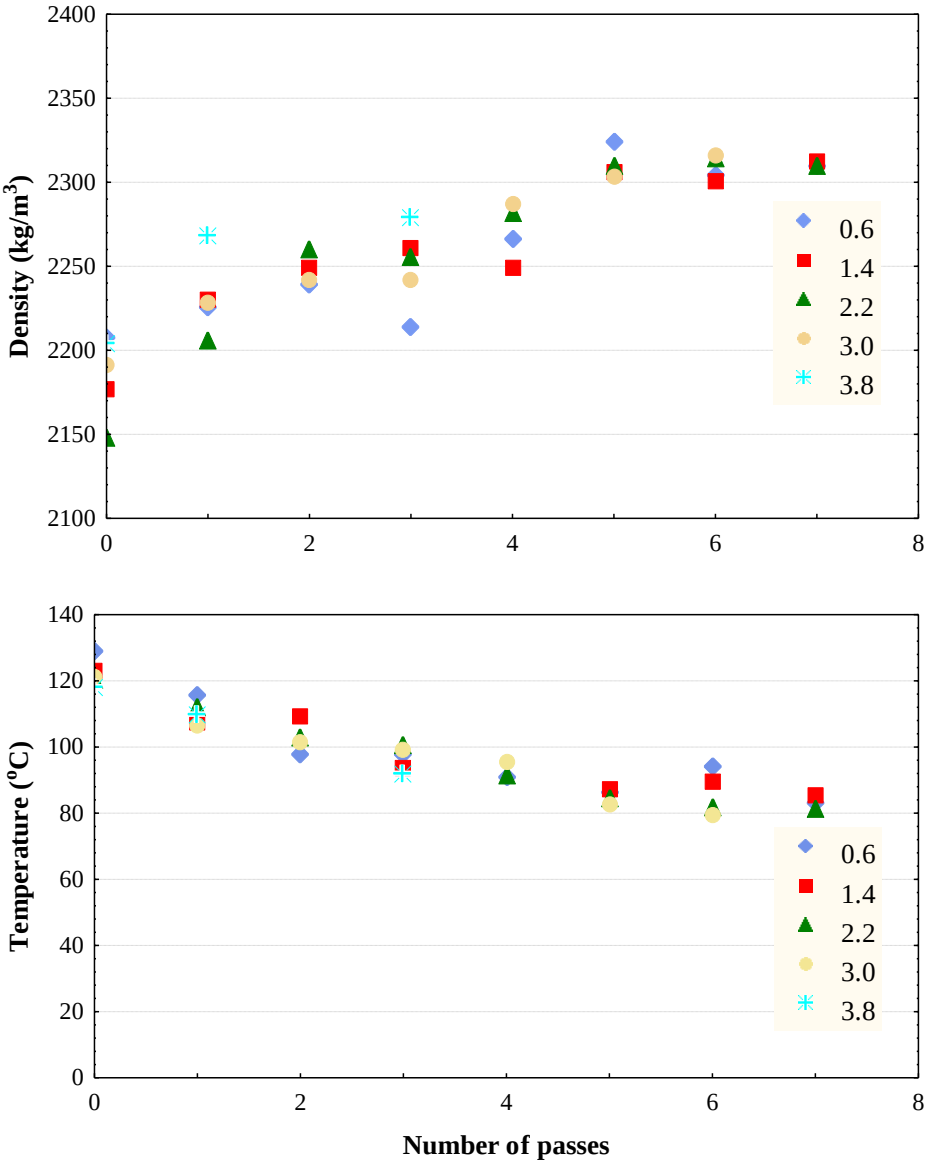

Fig. 4.58 Effect of mix cooling on compaction density for static-vibratory compaction mode

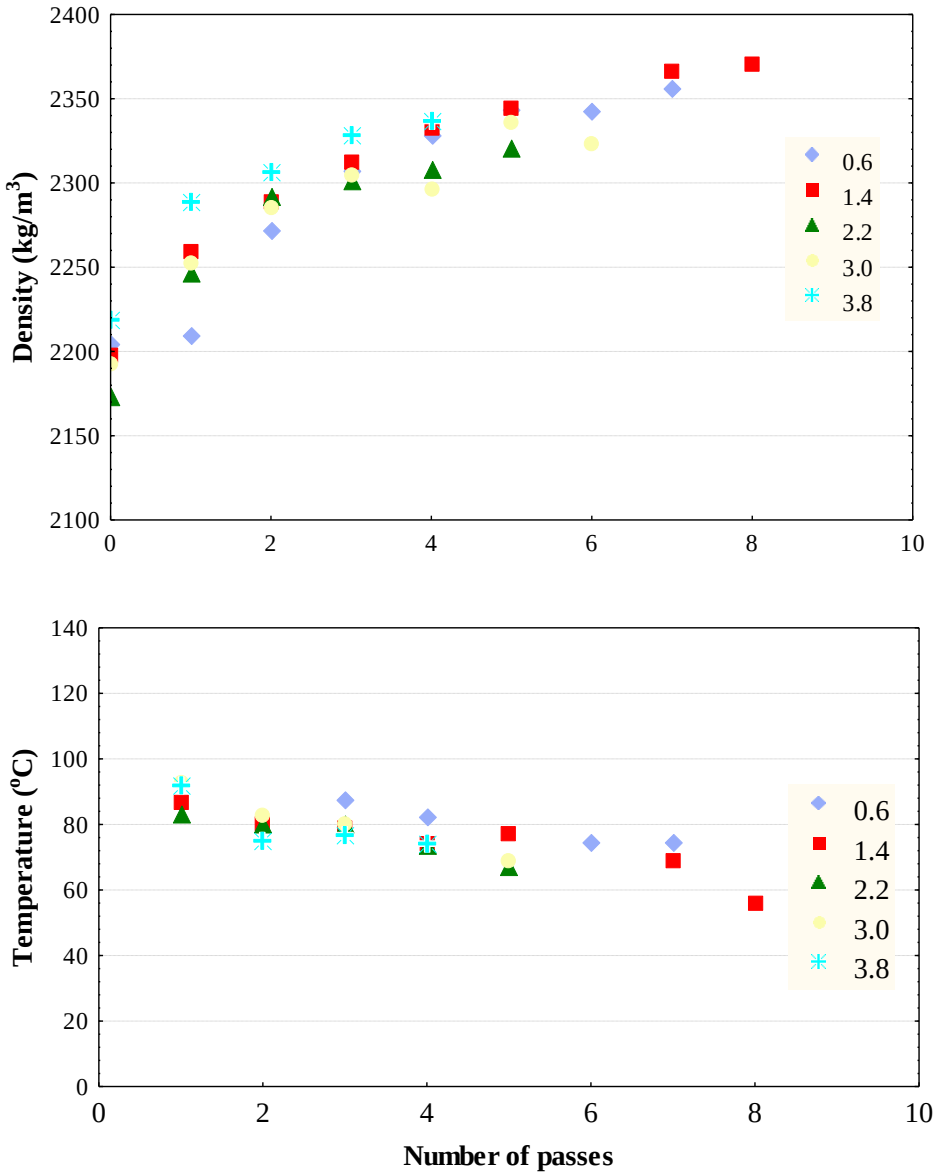

Fig. 4.59 Effect of mix cooling on compaction density for vibratory compaction mode

As shown in Fig. 4.58-4.59, the compaction density of paving layer increases rapidly at the beginning. With the increase of rolling passes and mix cooling, it increases slowly. Generally, when the mat surface temperature falls below 80°C it seems that additional compaction causes insignificant mat density increase.

The experimental compaction data, in terms of the average values of the five test spots, were then fit into the closed form (Eq. 4.18). Figures 4.60-4.61 show the predicted compaction data for each subsection, respectively.

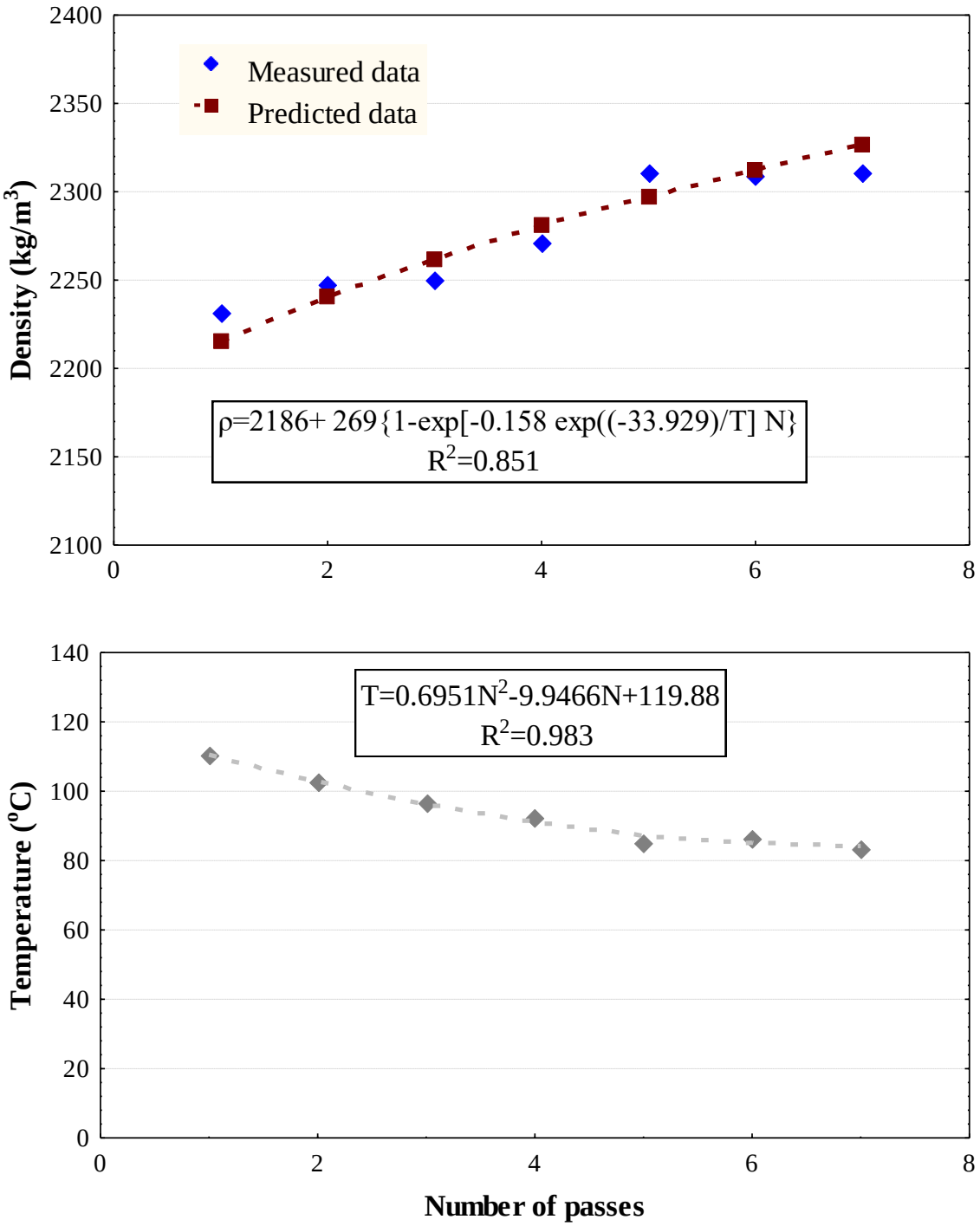

Fig. 4.60 Effect of mix cooling on compaction density for static-vibratory compaction mode

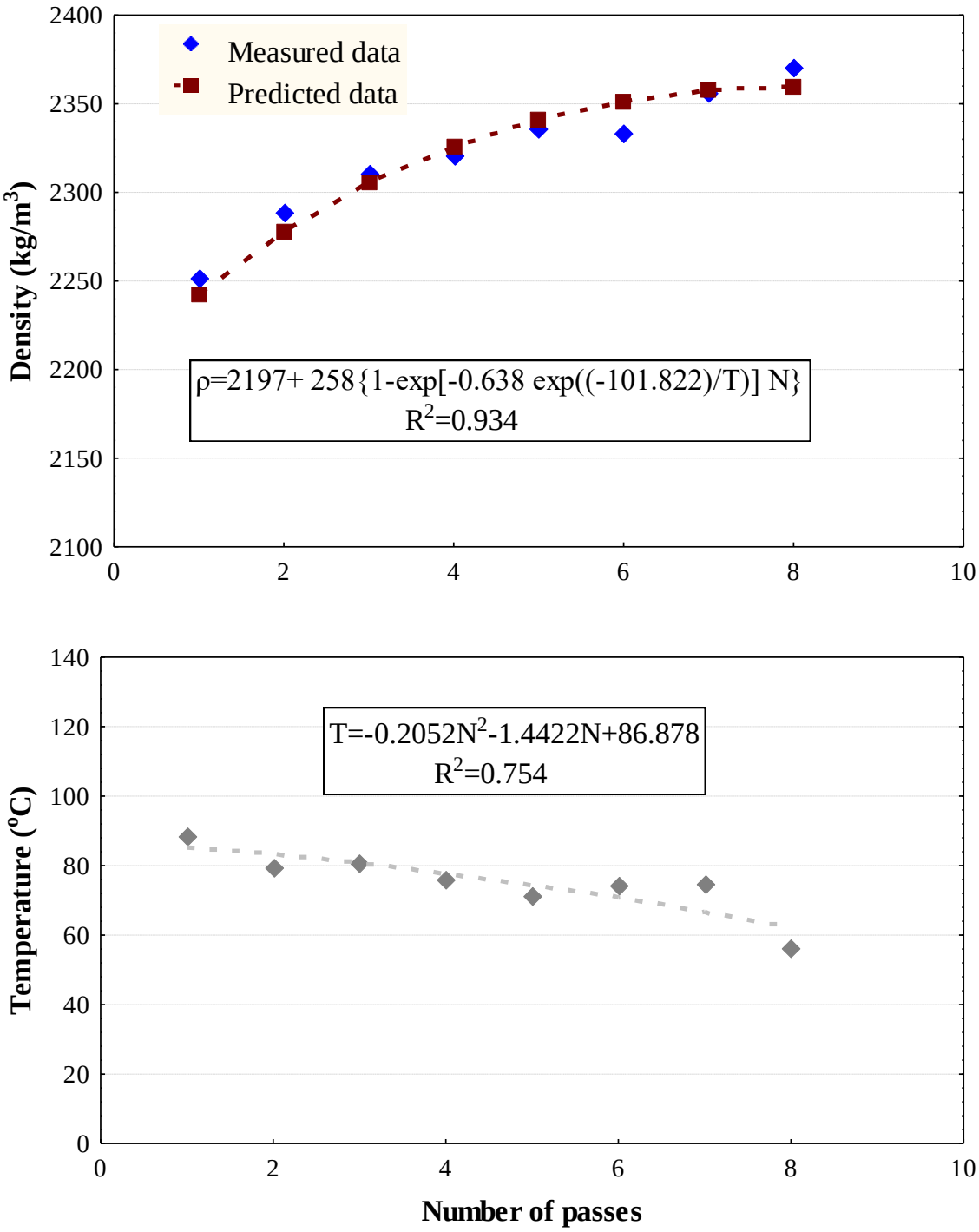

Fig. 4.61 Effect of mix cooling on compaction density for vibratory compaction mode

Figures above demonstrate a good fit to the experimental data. The high R^2 values, which exceed the 0.9, as well as the low mean absolute error (MAE) values ranging from 8.3-11.1 kg/m^3 and mean absolute percentage error (MAPE) of the order of 0.03%

indicate that the Eq. 4.18 can successfully predict density evolution with respect to roller passes.

Also, Fig. 4.62 summarizes the compaction curves related to each subsection and compaction mode. The results show that vibratory compaction mode is preferred compared to the static-vibratory mode, as manifested from the superior compaction density achieved for the same number of roller passes.

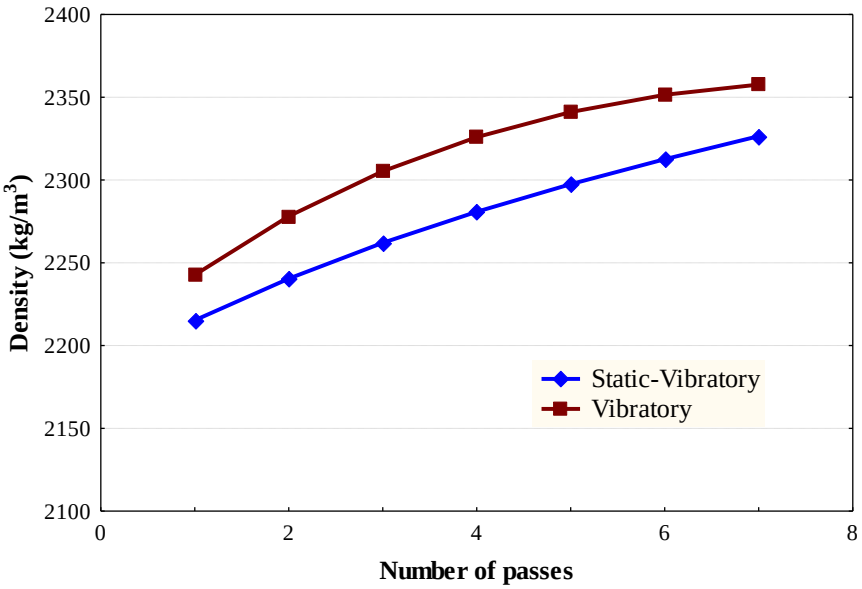

Fig. 4.62 Effect of compaction mode on HMA compactability

Summarizing, it could be stated that the mathematical formulation of the compaction process on the basis of Eq. 4.18, in lieu of sophisticated but complex computational models (Masad et al. 2016), may be an effective tool for suggesting the number of roller passes required to achieve the desired compaction level.

4.5 Relationship between laboratory compaction and field compaction

This section discusses the relationship between laboratory compaction and field compaction. The evaluation is based on the compactability indicators, namely the slope *b* and N_8/N_{15}. On the basis of the obtained results, as tabulated in Tables 4.7, 4.12-4.13 and 4.17, a comparative assessment is performed with respect to gyratory, roller and field compaction. Figures 4.63-4.65 summarize the results of the compactability indicators for the three mixtures studied. With regards to the gyratory compaction

results, the mean values -excluding the results concerning the 100-170 type specimens- have been considered for the evaluation.

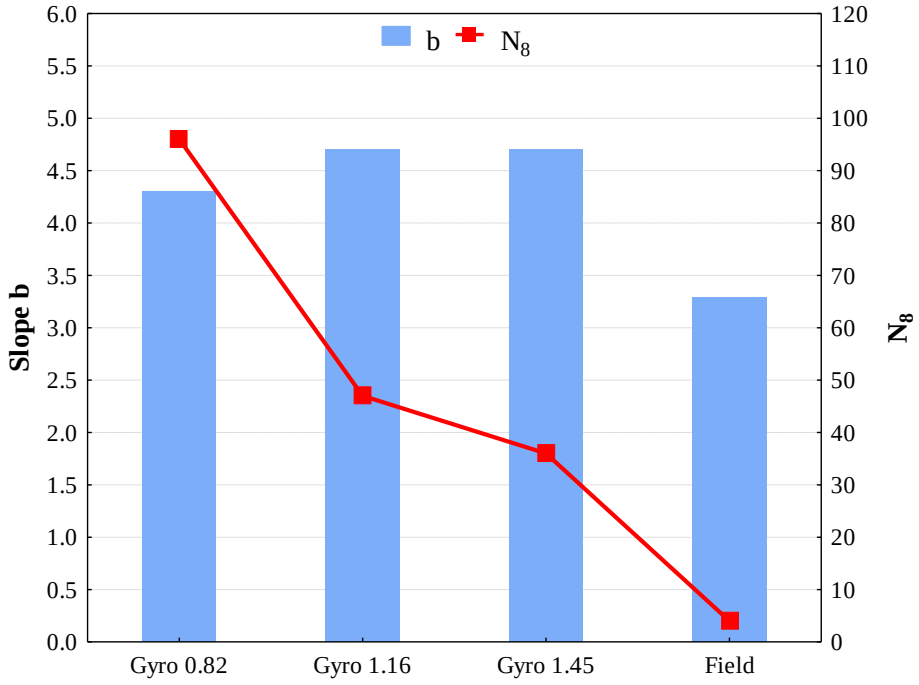

Fig. 4.63 Laboratory vs field compactability indicators (AC12.5 surf 50/70[a])

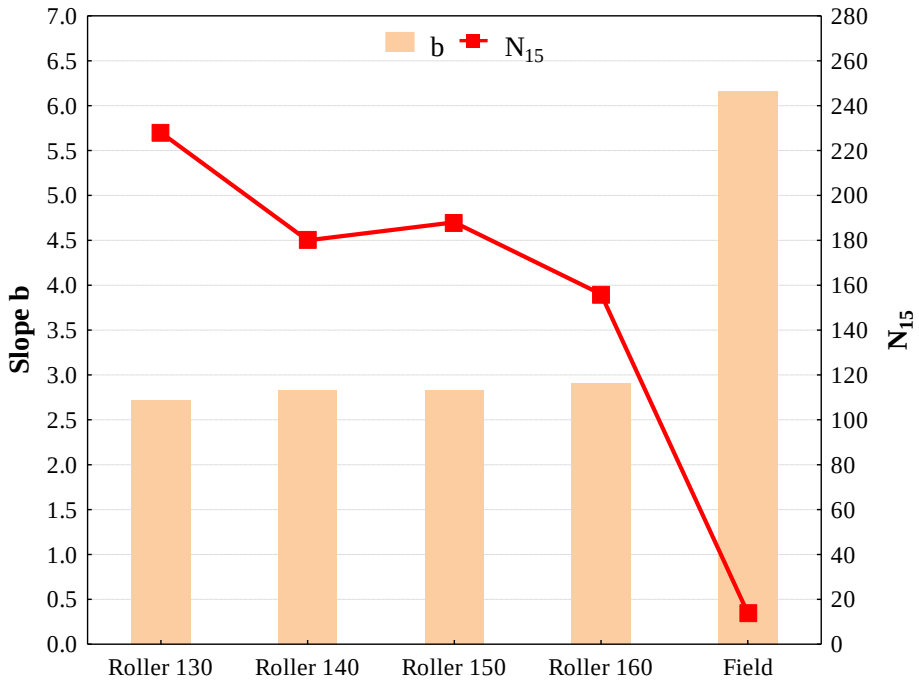

Fig. 4.64 Laboratory vs field compactability indicators (AC12.5 surf PmB (SBS))

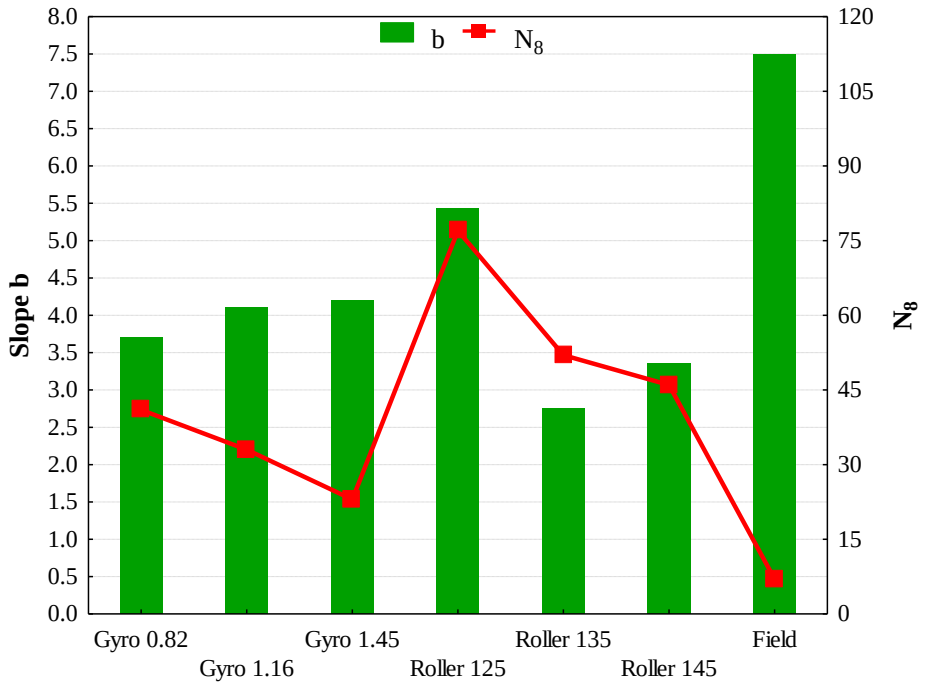

Fig. 4.65 Laboratory vs field compactability indicators (AC20 base50/70)

Generally, different compaction characteristics are obtained comparing laboratory and field compaction methods. It can be seen from Fig. 4.63-4.65 that the slope *b* of laboratory compaction curves differs significantly from the field. Particularly, higher slopes, generally speaking, by a factor of two were assessed for the field compaction compared to the laboratory methods. With regards to gyratory compaction, it seems that field compaction is better resembled using the 0.82^{o}. No clear trend could be found with regards to roller compaction. Regarding the compaction effort to achieve the same compaction level, simple relationships can be derived between the gyrations and field roller passes. For instance, in this study the ratio between gyrations and field roller passes to achieve 8% air voids is estimated to be eight. Similarly, an equivalent number of field roller passes by roughly a factor of eight and thirteen is required to achieve the specified field compaction level for the dense and open-graded mixtures, respectively.

5. Stiffness

5.1 Introduction

This Chapter focuses on the study of stiffness properties of various HMA types. By means of laboratory tests carried out using the Indirect Tensile Stiffness Modulus (ITSM) method, the stiffness modulus for specimens compacted using different compaction methodologies is investigated.

Primarily, the influence of the most commonly used laboratory compaction methods -namely Marshall, gyratory and roller- relative to field compaction performance on the stiffness properties of various asphalt mixtures, is investigated with regards to the compaction degree. The aim is to capture the differences between the laboratory compaction-based stiffness and assess the laboratory compaction methods with regards to its capabilities to reproduce the field compaction-based stiffness.

The main step of this course encompassed a comprehensive parametric study to evaluate the influence of various compaction factors on the stiffness of the laboratory-compacted specimens. For this purpose, different including standardized compaction regimes were established for each laboratory compaction method with the aim to gain more insight to the factors that affect the HMA stiffness properties. In the following sections, the analysis results are demonstrated and discussed.

5.2 ITSM test method

The ITSM test was carried out in this study to determine the stiffness of the asphalt mixtures manufactured using the three different laboratory compaction methods and field compaction (EN 12697-26). This test, which is non-destructive, consists of sinusoidal load pulses applied along the vertical diameter of specimen and characterized by the rise-time and transient horizontal deformation measured along the horizontal diameter using linear variable differential transformers (LVDT). For 100-mm diameter specimens, the target peak transient horizontal deformation is 5 μm and the target load pulse rise time is 124 milliseconds.

Fig. 5.1 ITSM test equipment

In terms of temperature conditioning, each specimen is placed in a controlled temperature cabinet and monitored until it has attained the test temperature. After temperature conditioning, the specimen is placed in the ITSM testing equipment, as illustrated in Fig. 5.1. A preliminary conditioning of ten load pulses is applied to bed the test specimen on the loading platens and to enable the equipment to adjust the load magnitude and duration in order to give the specified horizontal diametral deformation. Then, stiffness modulus is determined as the average modulus corresponding to five load pulses and the specimen is rotated through 90˚ about its horizontal axis. A further five load pulses are then applied and the resulting mean stiffness modulus is obtained. The stiffness modulus is then calculated as the average of these two mean values.

5.3 Influence of compaction method on HMA stiffness modulus

Three hot-mix asphalt mixtures were used in this investigation. The three mixes include: a binder course mix with Selenizza (SLN) asphaltite modified bitumen, and two base course mixtures with the same bitumen varying the dosage of SLN. These mixtures, which were described in Chapter 3, are denoted, respectively, as AC12.5 binder 50/70+8%SLN, AC20 base 50/70+8%SLN and AC20 base 50/70+10%SLN. All mixtures represent ‘production’ mixes, sampled during placement along with field cores retrieved, where feasible, to be used as ground truth data for comparative evaluation.

Using the loose mixtures samples, laboratory compaction was carried out using the Marshall, gyratory and roller compaction aiming to achieve 97% compaction degree, as generally required from technical specifications. For each mixture, two specimens were fabricated using the Marshall hammer and varying the compaction effort to achieve the target density. Also, three replicate 150-mm diameter and 70-mm tall specimens were initially compacted using the CEN gyratory compaction protocol, which were then cored to obtain 100-mm diameter specimens. The approach of compaction by specified energy was followed during the roller compaction complying with CEN and four 100-mm specimens were cored from each slab for subsequent testing. After fabrication, all laboratory specimens were trimmed. A total of 45 specimens, both laboratory- and field-compacted, were tested to assess the volumetric and stiffness properties. Controlled deformation stiffness tests, at a target deformation of 5μm, were performed at a test temperature of 15˚C.

Figures 5.2-5.4 illustrate the stiffness modulus with respect to the compaction method and degree for the three mixtures.

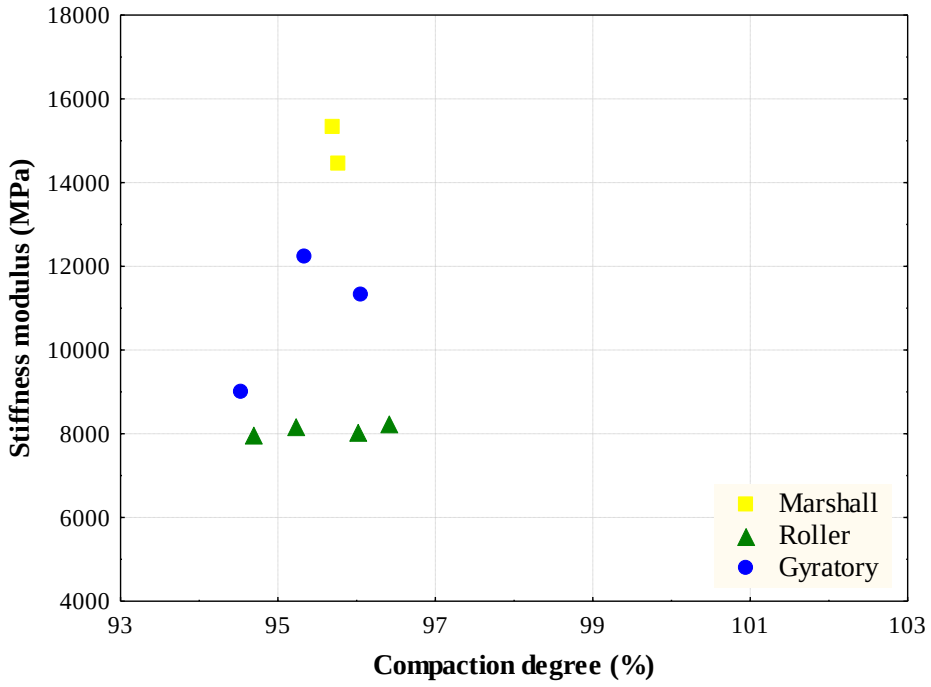

Fig. 5.2 Stiffness modulus as a function of compaction method and degree (AC12.5 binder 50/70+8%SLN)

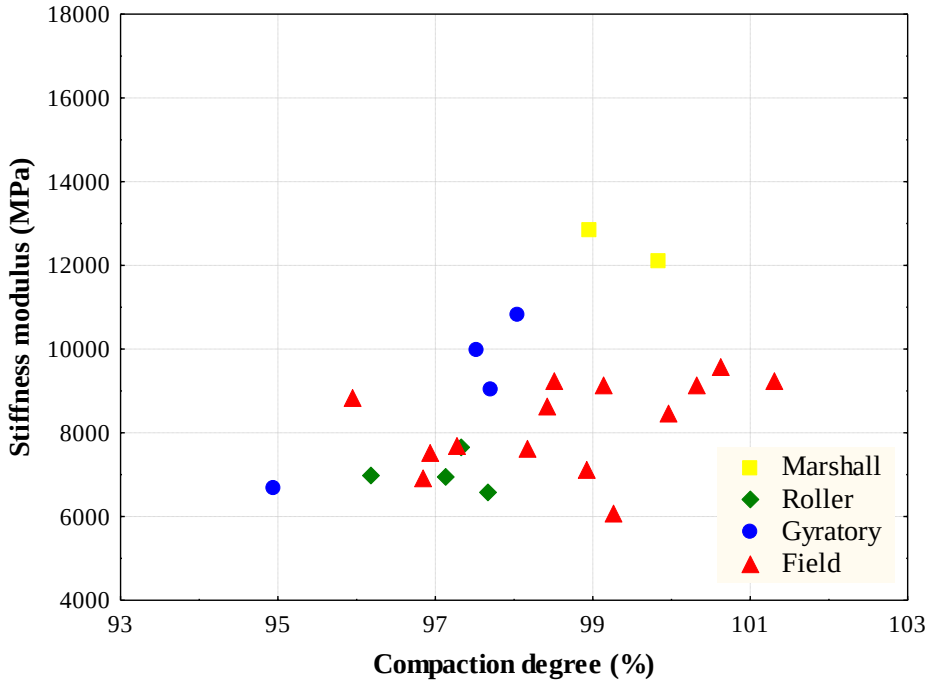

Fig. 5.3 Stiffness modulus as a function of compaction method and degree (AC20 base 50/70+8%SLN)

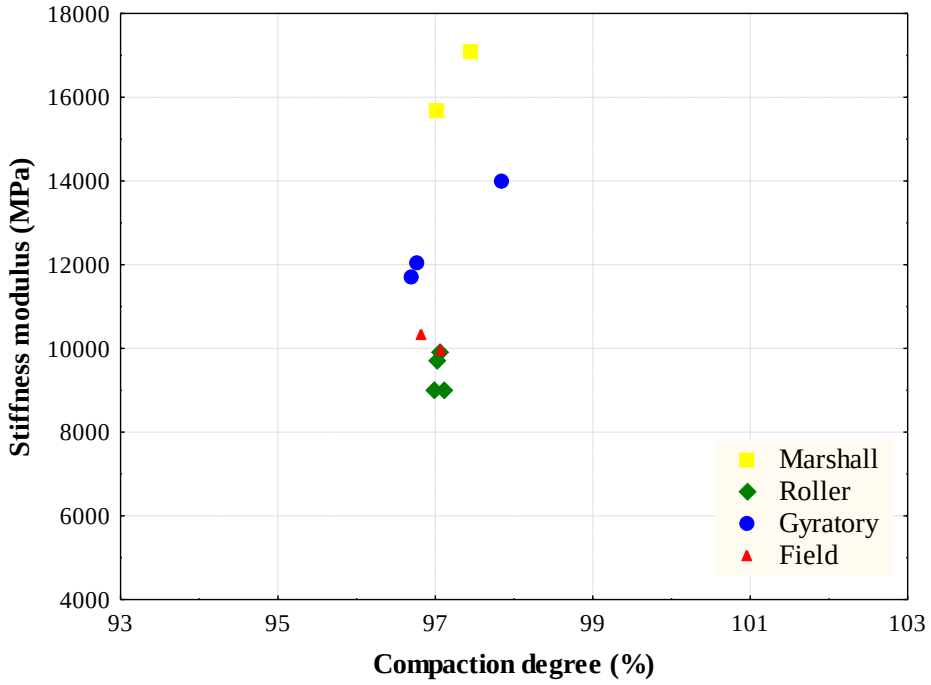

Fig. 5.4 Stiffness modulus as a function of compaction method and degree (AC20 base 50/70+10%SLN)

From the above figures, variability of the achieved compaction degree is observed with respect to the various HMA types. For instance, the mean compaction degree achieved is of the order of 96%, 98% and 97% concerning the AC12.5 binder 50/70+8%SLN, AC20 base 50/70+8%SLN and AC20 base 50/70+10%SLN mixtures, respectively. Particularly, concerning the AC20 base 50/70+8%SLN significant variability is observed with respect to the field compaction. This indicates that in general it is rather difficult to control HMA densification.

Moreover, it is interesting to note that significant differences, with regards to the stiffness modulus values, are observed for similar compaction degree achieved. This is clearly demonstrated in Fig. 5.4. The mould-based, namely Marshall and gyratory, compaction methods produce specimens with (mean) stiffness values reaching 16390MPa and 12570MPa, respectively. On the contrary, the roller compaction and field compaction-based modulus values are significantly lower, around 9400MPa. Similar conclusions can be drawn with respect to the other mixtures. From the comparative analysis of the laboratory compaction methods it is indicated that the Marshall compaction method tends to produce specimens with the highest stiffness modulus. On the contrary, the roller compaction produces specimens with the lowest stiffness modulus, which nonetheless is comparable to the field compaction-based stiffness.

It is also worth to mention that the achieved compaction degree influences the stiffness modulus. To clearly demonstrate the impact of compaction degree on stiffness modulus, a linear trend was fitted to the experimental results separately for each compaction method as graphically shown in Fig. 5.5-5.7.

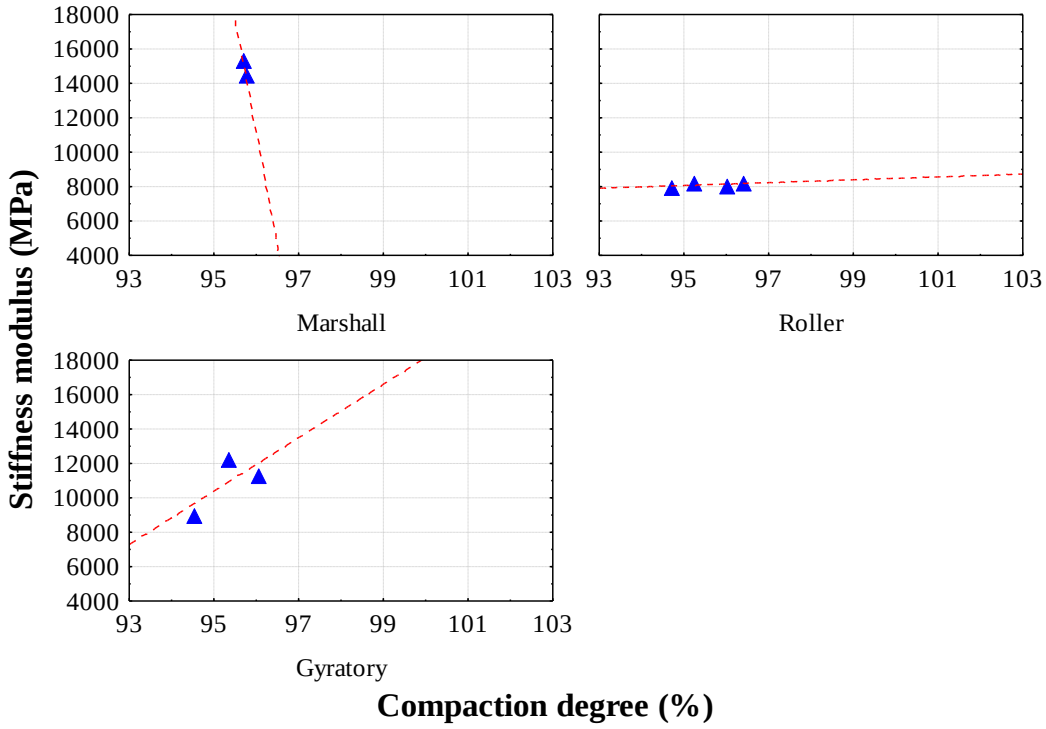

Fig. 5.5 Influence of compaction degree on stiffness modulus (AC12.5 binder 50/70+8%SLN)

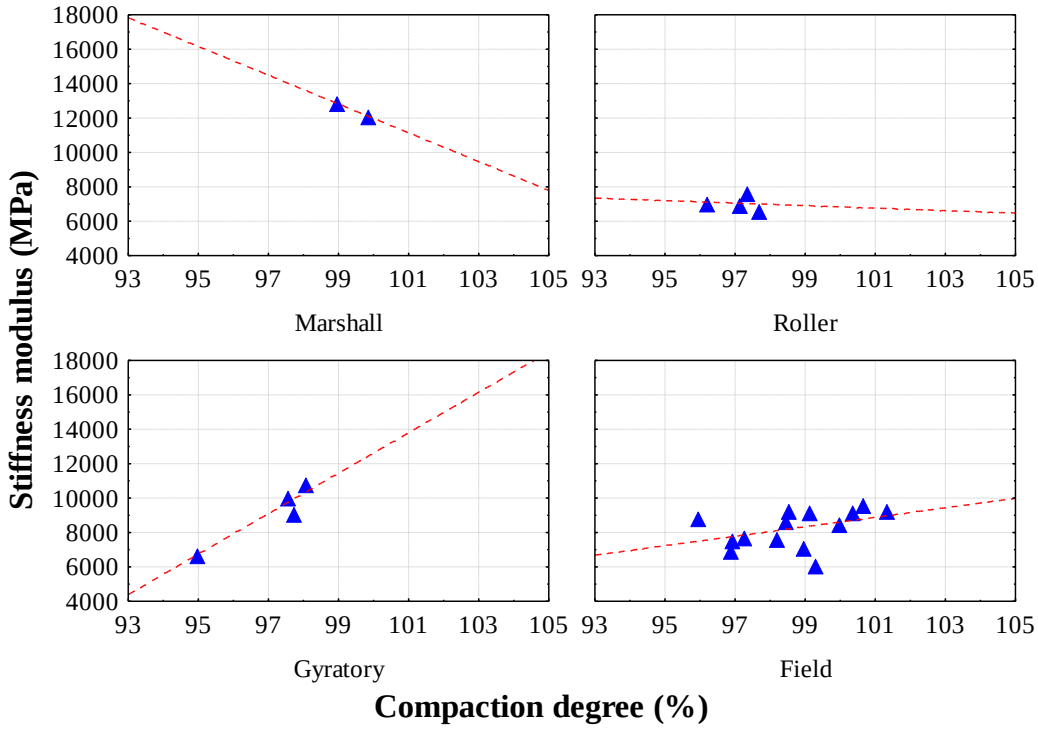

Fig. 5.6 Influence of compaction degree on stiffness modulus (AC20 base 50/70+8%SLN)

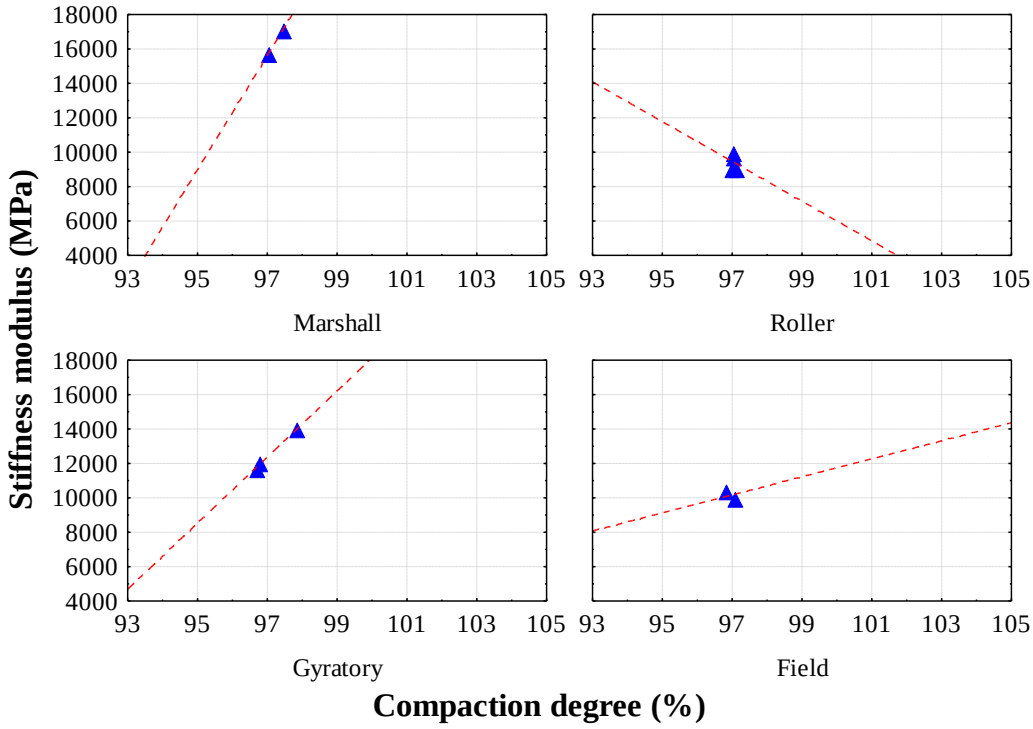

Fig. 5.7 Influence of compaction degree on stiffness modulus (AC20 base 50/70+10%SLN)

This study results indicate that an increase in the field compaction degree results in a stiffness modulus increase. For instance, complying with the minimum specified compaction degree of 97% the (mean) stiffness modulus reaches 7400MPa. Further densification to achieve 99% and 101% compaction degree, enhances significantly the HMA stiffness properties and an increase of modulus of the order of 7% and 28% is observed, respectively. A similar trend is observed with respect to the gyratory compaction results. On the contrary, the stiffness modulus of the roller-compacted specimens seems not to be affected from the compaction degree. No clear trend was observed with respect to the Marshall compaction.

5.4 Influence of compaction factors on HMA stiffness modulus

Three HMA mixtures were tested within this course, following the compactability laboratory studies presented in Chapter 4. The three mixes include: a surface course mix with 50/70 binder, a surface course mix with polymer modified bitumen (SBS) and a base course mix with 50/70 binder. These mixtures, which were described in Chapter 3,

are denoted, respectively, as AC12.5 surf 50/70[a], AC12.5 surf PmB (SBS) and AC20 base 50/70.

As mentioned before, all mixtures represent ‘production’ mixes, sampled during placement along with field cores retrieved to be used as ground truth data for comparative evaluation. Using the loose mixtures samples, laboratory compaction was carried out using the Marshall, gyratory and roller compaction. The field cores were also tested for air voids to be used as key parameter, linking laboratory to field compaction.

5.4.1 Marshall compaction

The asphalt mixtures were compacted using standard Marshall (impact) compaction, as described in CEN 12697-30, at compaction energy level of 75 blows per side. Varying compaction temperatures were used to fabricate the asphalt mixture specimens to evaluate the impact of compaction temperature on stiffness modulus (Georgiou et al. 2015). Particularly, the compaction was carried out at 125^{o}C, 135^{o}C and 145^{o}C for both the AC12.5 surf 50/70[a] and AC20 base 50/70 mixtures, while for the AC12.5 surf PmB (SBS) mixture, which consists of modified bitumen, compaction was performed at elevated temperatures 130^{o}C, 140^{o}C, 150^{o}C and 160^{o}C to cover a wider compaction range. Three replicates were fabricated at each temperature, which were subsequently subjected to volumetric and stiffness testing. Controlled deformation stiffness tests at a target deformation of 5μm were performed at a test temperature of 20˚C.

Figures 5.8-5.10 illustrate the stiffness modulus evolution with respect to compaction temperature for the specimens fabricated with the Marshall compaction.

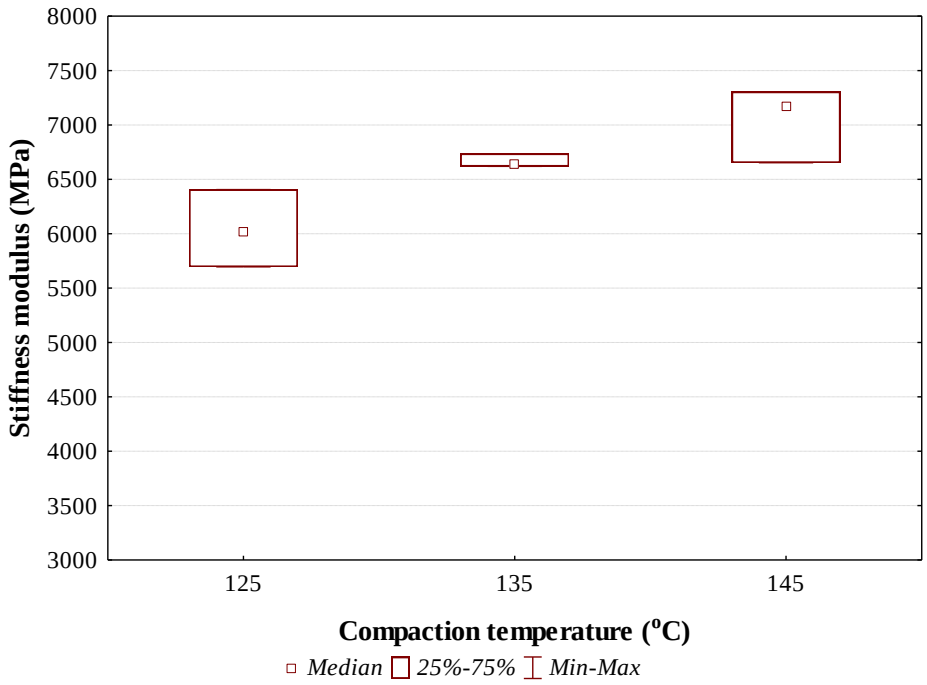

Fig. 5.8 Influence of compaction temperature on stiffness modulus (AC12.5 surf 50/70[a])

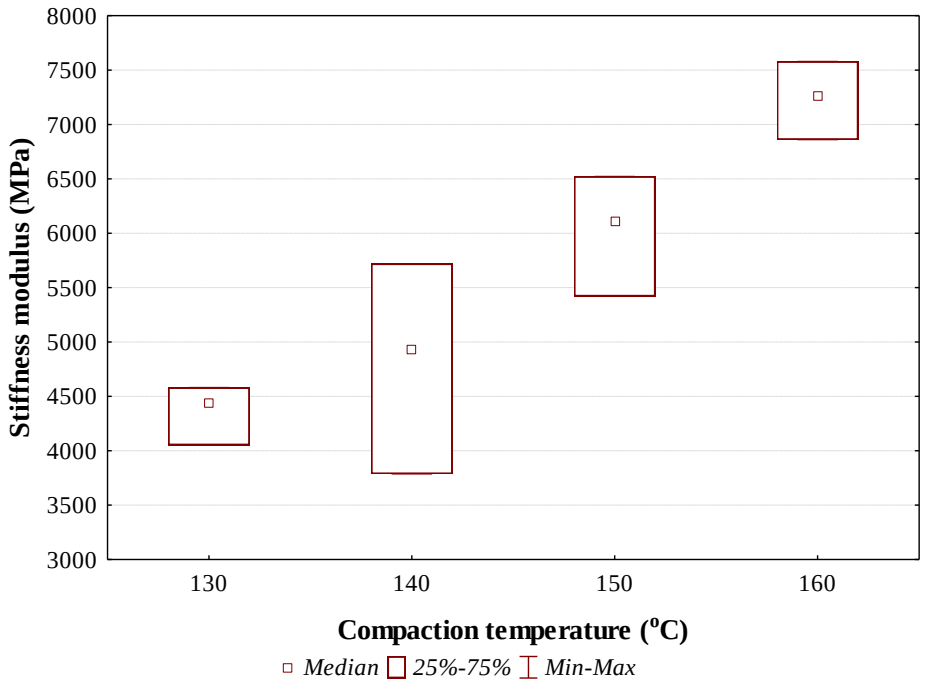

Fig. 5.9 Influence of compaction temperature on stiffness modulus (AC12.5 surf PmB (SBS))

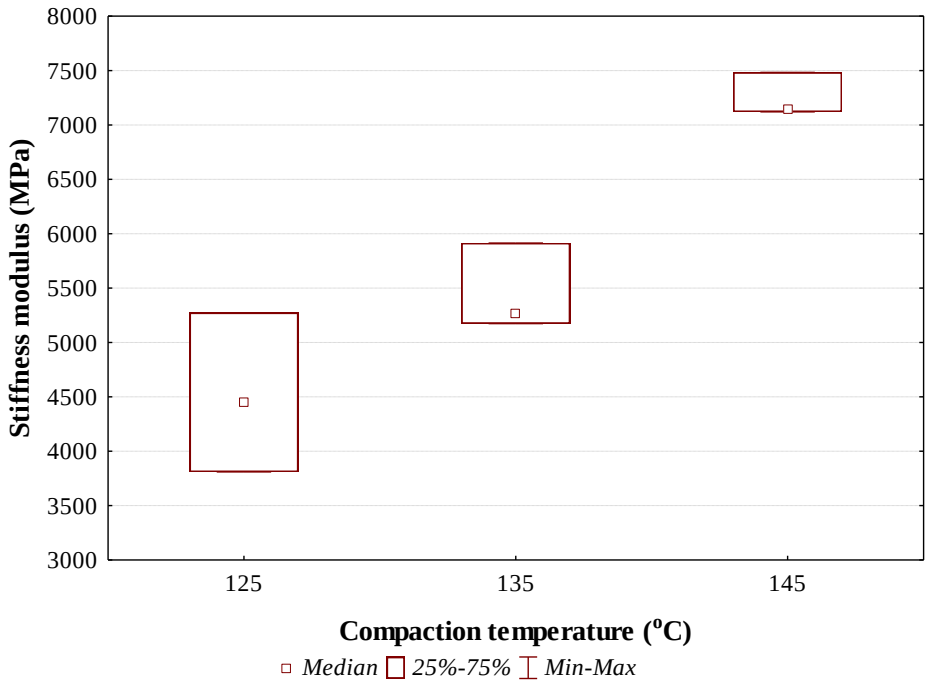

Fig. 5.10 Influence of compaction temperature on stiffness modulus (AC20 base 50/70)

From the above plots, the general trend observed is a modulus increase as the compaction temperature does. Concerning the AC12.5 surf 50/70[a] mix, the modulus at 125°C yields a median value around 6000 MPa, which is increased to around 6600 MPa and 7200 MPa for 135°C and 145°C compaction temperatures, respectively. Accordingly, in the AC12.5 surf PmB (SBS) mix, the modulus at 130ºC has a median value around 4500 MPa, at 140ºC close to 4900 MPa, while at 150ºC and 160ºC values of 6100 and 7250 MPa were yielded. In the AC20 base 50/70 mix, at 125ºC the modulus has a median value around 4500 MPa, at 135ºC the modulus has a median value close to 5300 MPa, whereas at 145ºC the modulus reaches 7100 MPa. Given the above, it is interesting to note that the % increase of modulus is more pronounced for the higher compaction temperatures.

The significance of the effect of compaction temperature on the stiffness of Marshall specimens was evaluated by means of Analysis of variance (ANOVA) test at 95% confidence interval (Table 5.1).

Table 5.1 ANOVA test results of stiffness (α = 0.05)

Mix type	Temperature
AC12.5 surf 50/70[a]	.000
AC12.5 surf PmB (SBS)	.000
AC20 base 50/70	.000

From the statistical analysis, it was demonstrated that the compaction temperature influences significantly the asphalt mix stiffness properties.

5.4.2 Gyratory compaction

Specimens compacted using the gyratory compactor and varying internal angle of gyration; compaction temperature; and (initial) diameter (100 mm and 150 mm), as already presented in Ch.4, were further tested to assess their stiffness properties (Georgiou et al. 2015). The stiffness modulus evolution with respect to these factors concerning the AC12.5 surf 50/70[a] is illustrated in Fig. 5.11-5.13, while Fig. 5.14-5.16 and Fig. 5.17-5.19 show the counterparts related to the AC12.5 surf PmB (SBS) and AC20 base 50/70 mix, respectively.

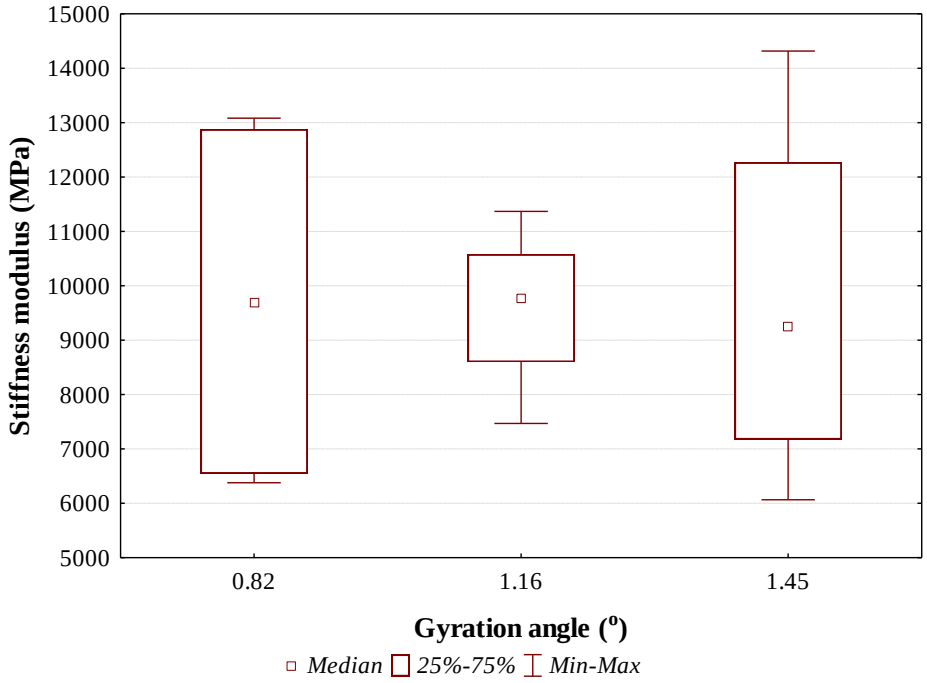

Fig. 5.11 Influence of gyration angle on stiffness modulus (AC12.5 surf 50/70[a])

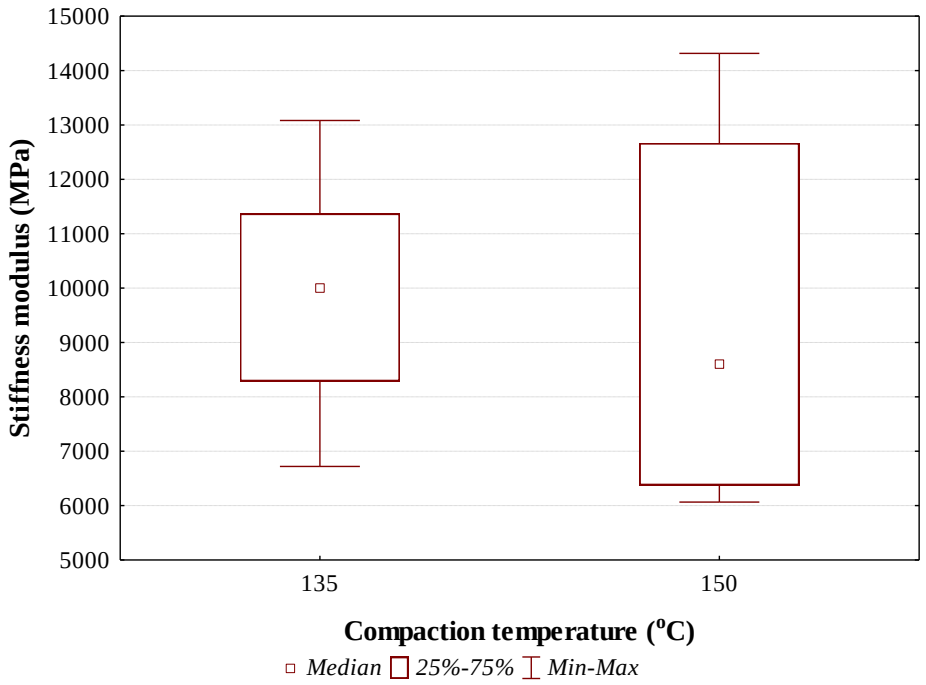

Fig. 5.12 Influence of compaction temperature on stiffness modulus (AC12.5 surf 50/70[a])

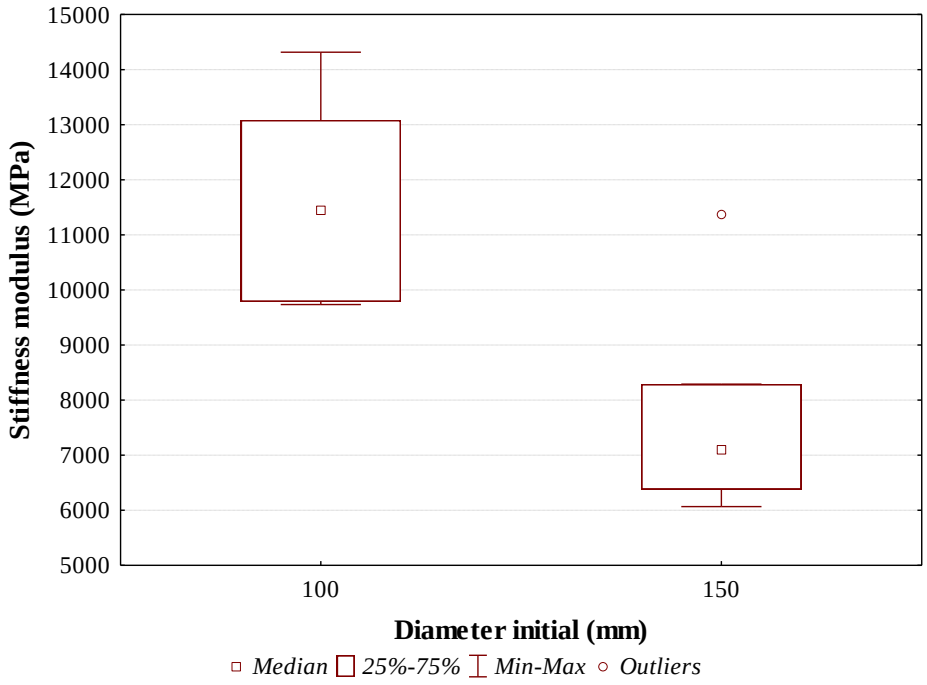

Fig. 5.13 Influence of specimen diameter (initial) on stiffness modulus (AC12.5 surf 50/70[a])

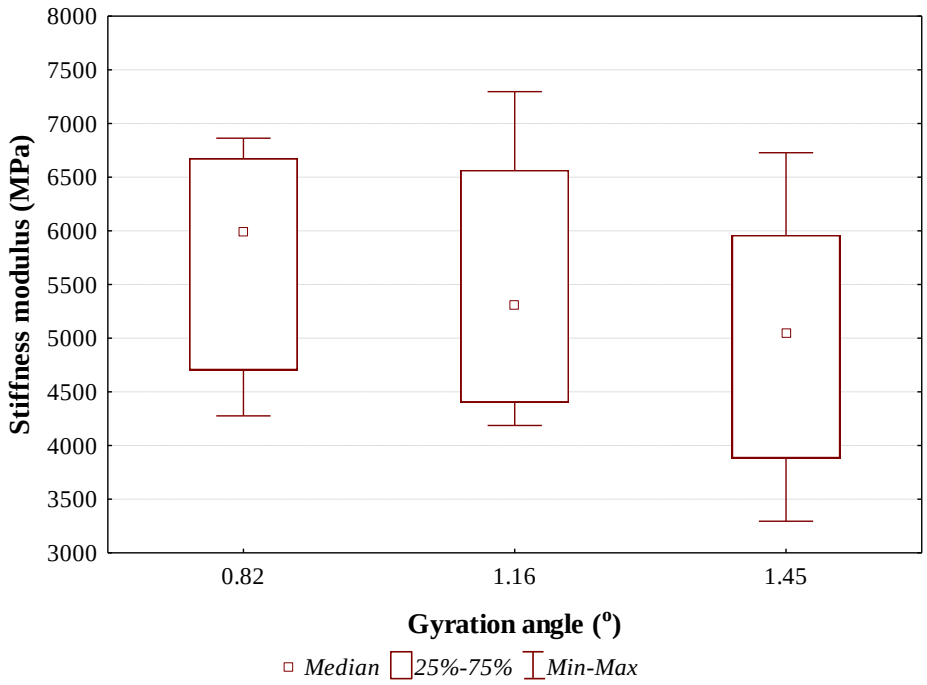

Fig. 5.14 Influence of gyration angle on stiffness modulus (AC12.5 surf PmB (SBS))

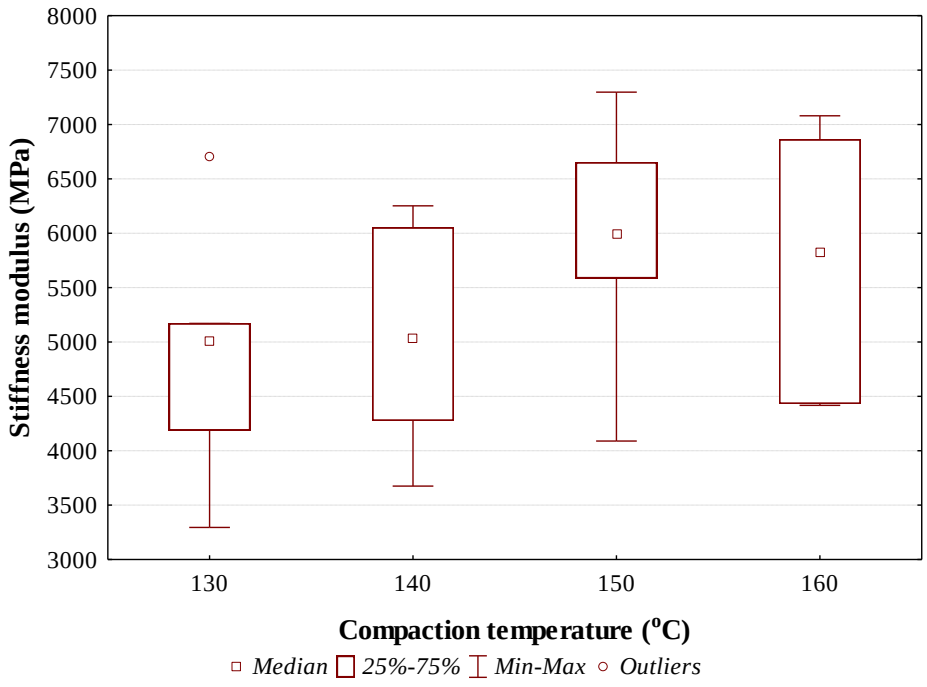

Fig. 5.15 Influence of compaction temperature on stiffness modulus (AC12.5 surf PmB (SBS))

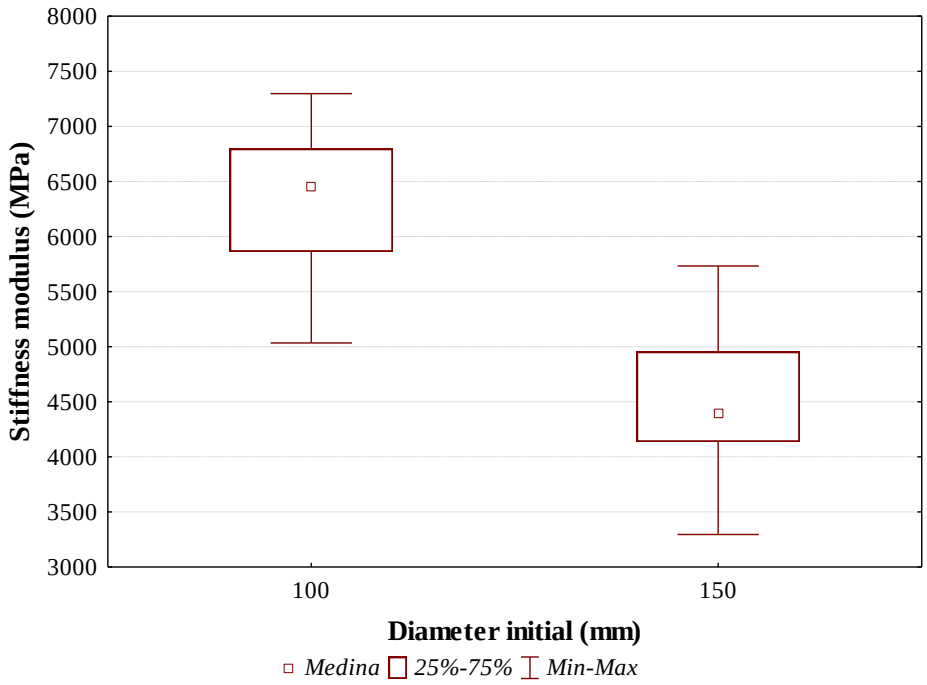

Fig. 5.16 Influence of specimen diameter (initial) on stiffness modulus (AC12.5 surf PmB (SBS))

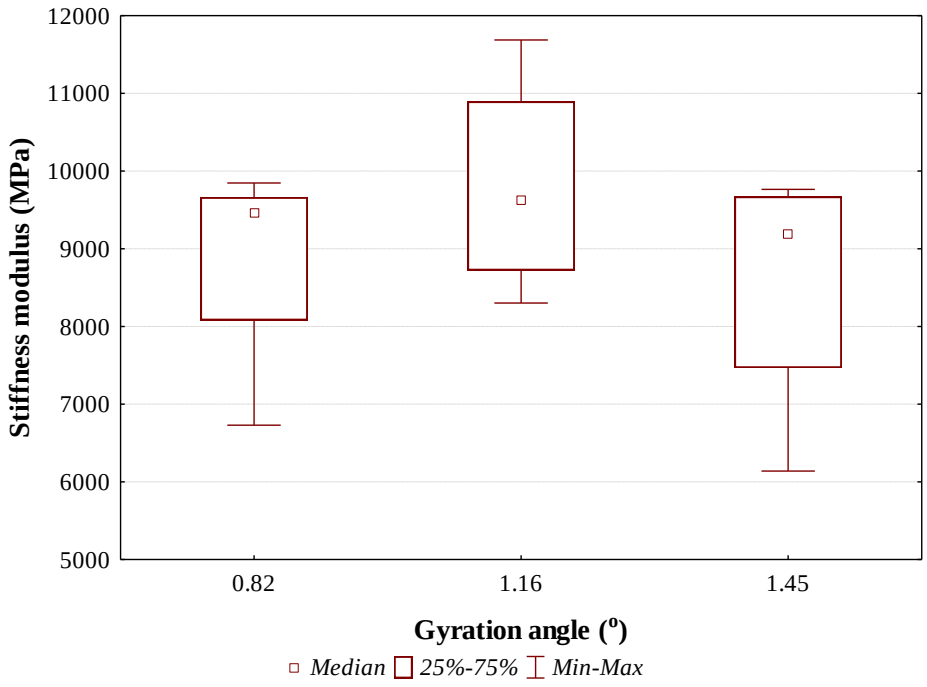

Fig. 5.17 Influence of gyration angle on stiffness modulus (AC20 base 50/70)

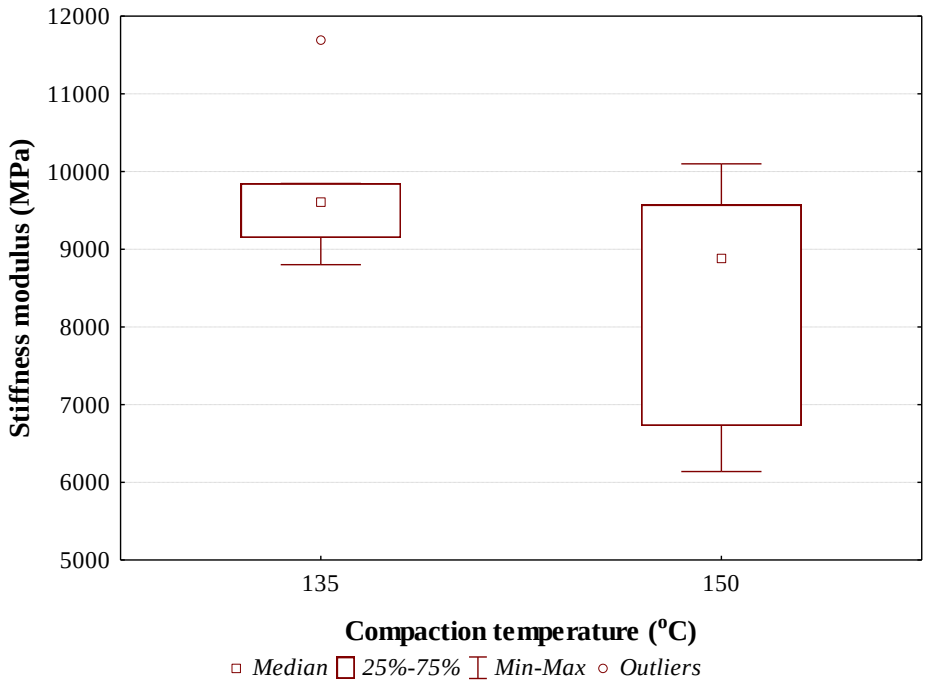

Fig. 5.18 Influence of compaction temperature on stiffness modulus (AC20 base 50/70)

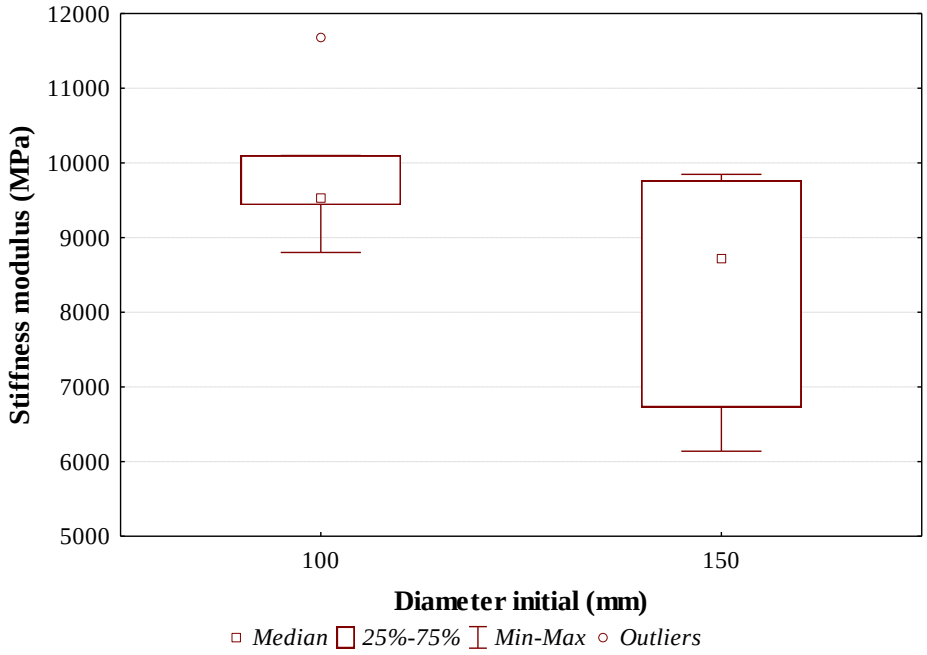

Fig. 5.19 Influence of specimen diameter (initial) on stiffness modulus (AC20 base 50/70)

The above results indicate that the angle of gyration influences the stiffness modulus. In general, the angle of 1.45^{o} produced the lowest modulus values. However, with respect to the angles specified in the CEN and AASHTO standards it can be stated that there is no significant difference among the stiffness modulus of the mixtures, except for the AC20 base 50/70 mix where increasing the gyration angle from 0.82˚ to 1.16˚ a higher modulus was obtained.

The temperature effect was found to be mixture dependent. Specifically, an increase in compaction temperature from 135ºC to 150ºC results in a decrease of modulus of the conventional bitumen based mixtures, namely the AC12.5 surf 50/70[a] and AC20 base 50/70; a modulus decrease of the order of 14% and 7% was calculated, respectively. On the contrary, for the AC12.5 surf PmB (SBS) mix stiffness modulus increases gradually with temperature. A modulus increase of the order of 17% is observed varying temperature from 130^{o}C to 160^{o}C.

In addition, it is interesting to note that by coring 100mm diameter from larger 150mm specimen a lower modulus is obtained compared to the as-compacted 100mm specimens. This effect is more pronounced with respect to the AC12.5 surf 50/70[a] and AC12.5 surf PmB (SBS), where a modulus decrease more than 30% is observed.

A detailed statistical analysis was performed to evaluate the significance of the effect of different variables on the stiffness modulus of gyratory specimens. Main compaction parameters were investigated at 95% confidence interval by means of Analysis of variance (ANOVA) test and the results are tabulated in Table 5.2.

Table 5.2 ANOVA test results of stiffness (α = 0.05)

Mix type	Compaction factors		
	Angle	Temperature	Diameter
AC12.5 surf 50/70[a]	.996	.735	.022
AC12.5 surf PmB (SBS)	.021	.005	.000
AC20 base 50/70	.300	.060	.044

The statistical analysis demonstrated that specimen diameter affects significantly the stiffness modulus; the parameters studied were ranked in order of significance as diameter, temperature and angle of gyration.

5.4.3 Roller compaction

Specimens compacted using the roller compactor and varying compaction mode; effort (number of passes) and temperature, as already presented in Ch.4, were further tested to assess their stiffness properties. The stiffness modulus evolution with respect to these factors concerning the AC12.5 surf PmB (SBS) is illustrated in Fig. 5.20-5.22, while Fig. 5.23-5.25 show the counterparts related to the AC20 base 50/70 mix (Plati et al. 2016; Georgiou et al. 2015).

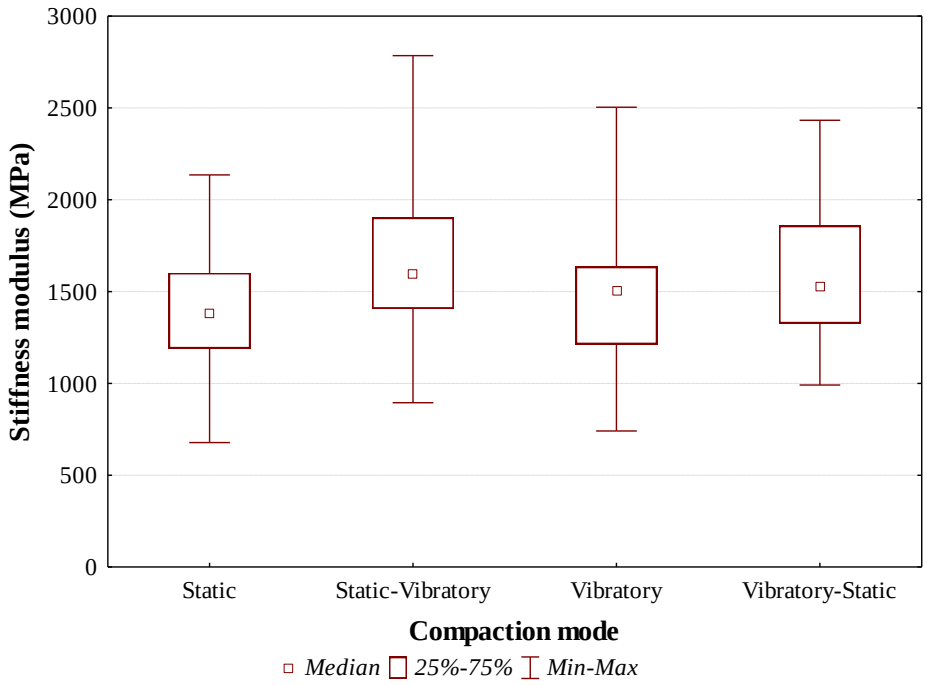

Fig. 5.20 Influence of compaction mode on stiffness modulus (AC12.5 surf PmB (SBS))

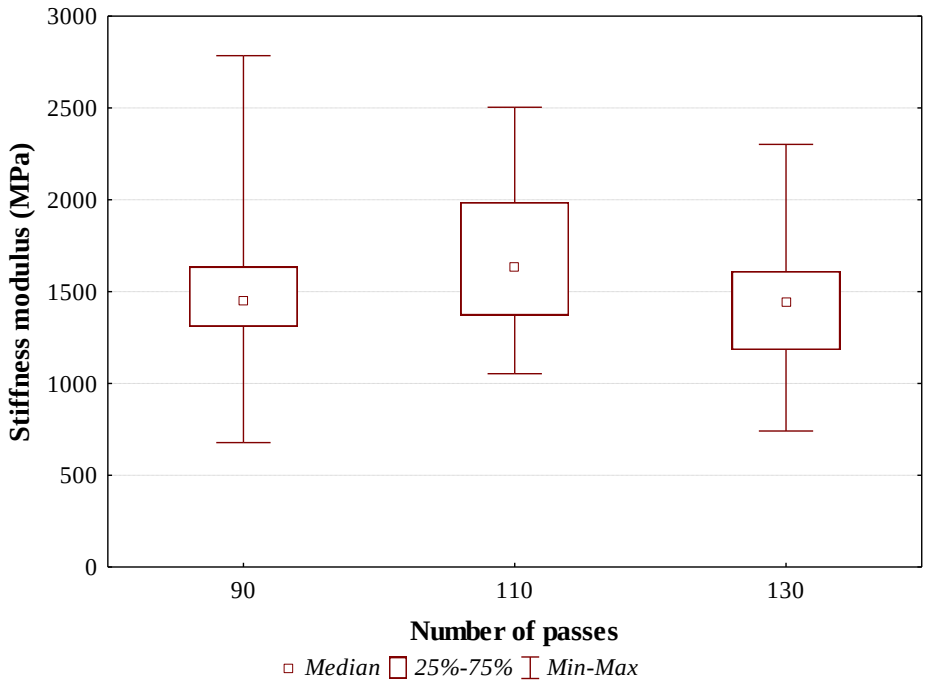

Fig. 5.21 Influence of compaction effort on stiffness modulus (AC12.5 surf PmB (SBS))

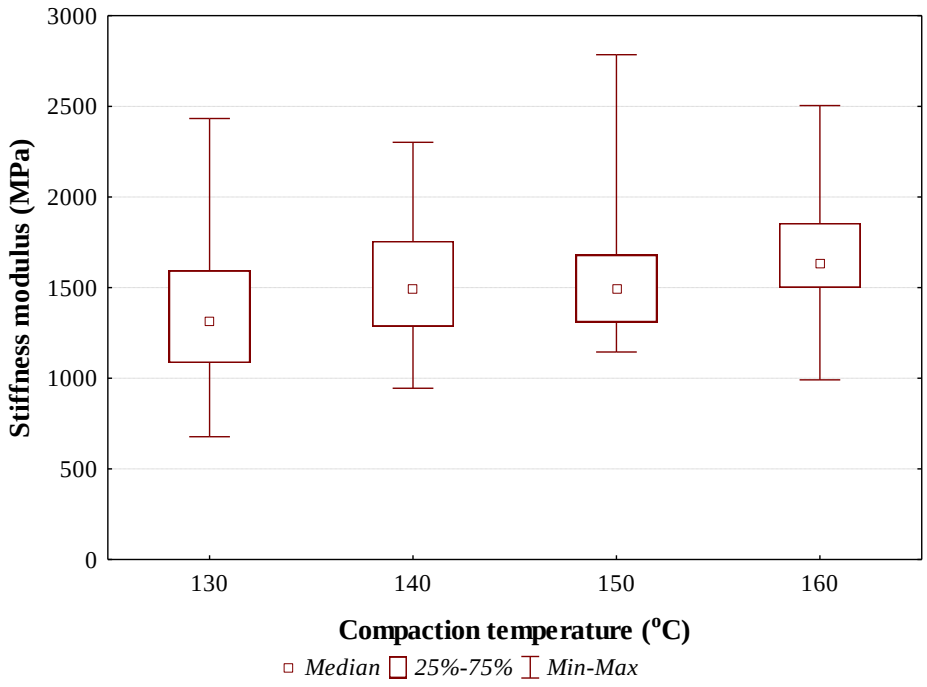

Fig. 5.22 Influence of compaction temperature on stiffness modulus (AC12.5 surf PmB (SBS))

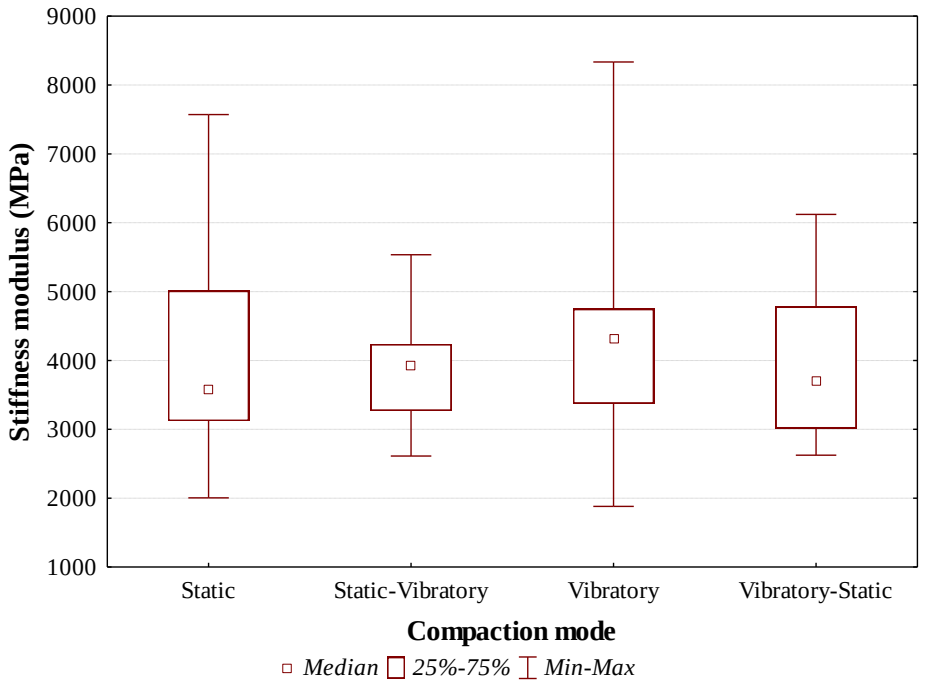

Fig. 5.23 Influence of compaction mode on stiffness modulus (AC20 base 50/70)

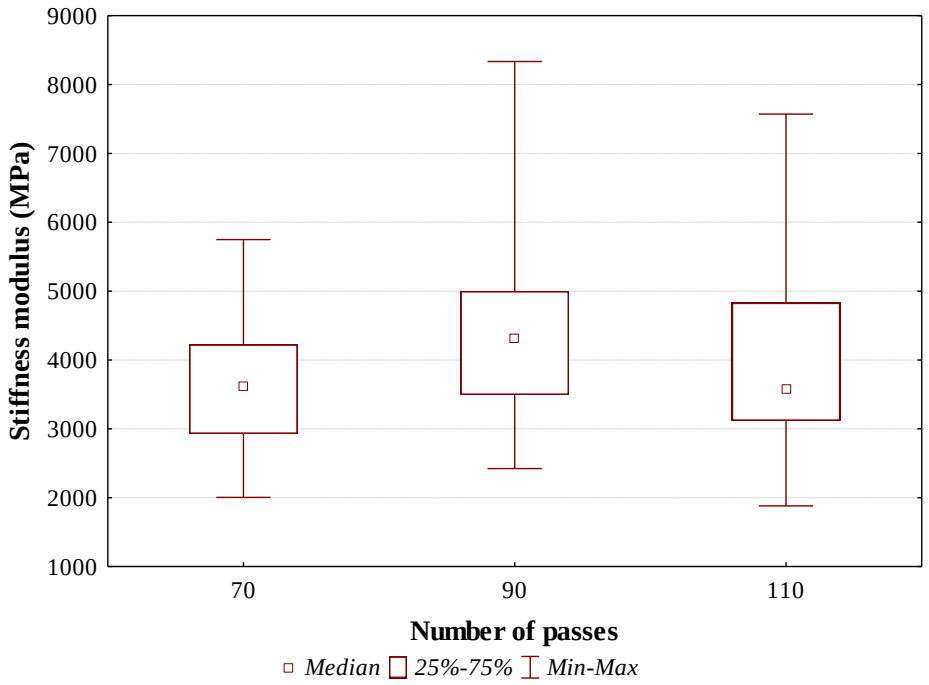

Fig. 5.24 Influence of compaction effort on stiffness modulus (AC20 base 50/70)

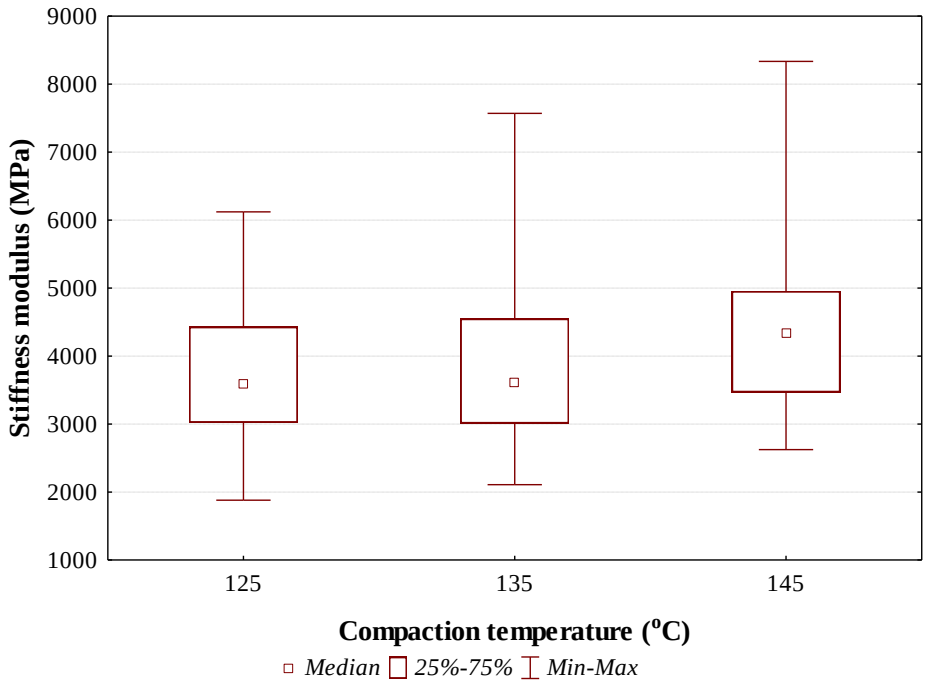

Fig. 5.25 Influence of compaction temperature on stiffness modulus (AC20 base 50/70)

The compaction mode seems to affect the modulus of the AC12.5 surf PmB (SBS) mix. Also, the results indicate some variability between the stiffness properties of the roller-compacted specimens of the AC20 base 50/70 mix.

In addition, compaction effort (in terms of roller passes) seems to affect both mixtures. Increasing the roller passes from 90 to 110 and from 70 to 90 for the AC12.5 surf PmB (SBS) and the AC20 base 50/70 respectively, an increase in modulus of the order of 13% and 19% is observed. Meanwhile, additional passes reduce the modulus to its initial state, possibly due to the reorientation and rearrangement of bitumen-coated aggregates.

In general, the results indicate a modulus increase with temperature. Concerning the AC12.5 surf PmB (SBS) the modulus increases by 14% when passing from 130ºC to 140ºC, and a further increase is observed when passing from 150ºC to 160ºC, hence indicating that similar moduli can be obtained for a wide temperature range of compaction temperature (140-160ºC). Also, significant increase of the order of 20% is appreciated for the AC20 base 50/70 when passing from 135ºC to 145ºC.

To substantiate the influence of roller compaction parameters on the stiffness properties of asphalt mixtures, the ANOVA test was performed.

Table 5.3 ANOVA test results of stiffness (α = 0.05)

Mix type	Compaction factors		
	Mode	Effort	Temperature
AC12.5 surf PmB (SBS)	.000	.000	.000
AC20 base 50/70	.456	.001	.003

From the statistical analysis results, as shown in Table 5.3, it was demonstrated that both the compaction effort (namely number of passes) and the temperature affect significantly the stiffness modulus; a lesser effect on stiffness is attributed to the compaction mode.

5.4.4 Comparison to field compaction

The air voids in HMA were used as a key parameter linking laboratory to field compaction. Figure 5.26 illustrates the compaction level achieved with respect to each compaction method covering the full spectrum of compaction factors considered (Georgiou et al. 2015).

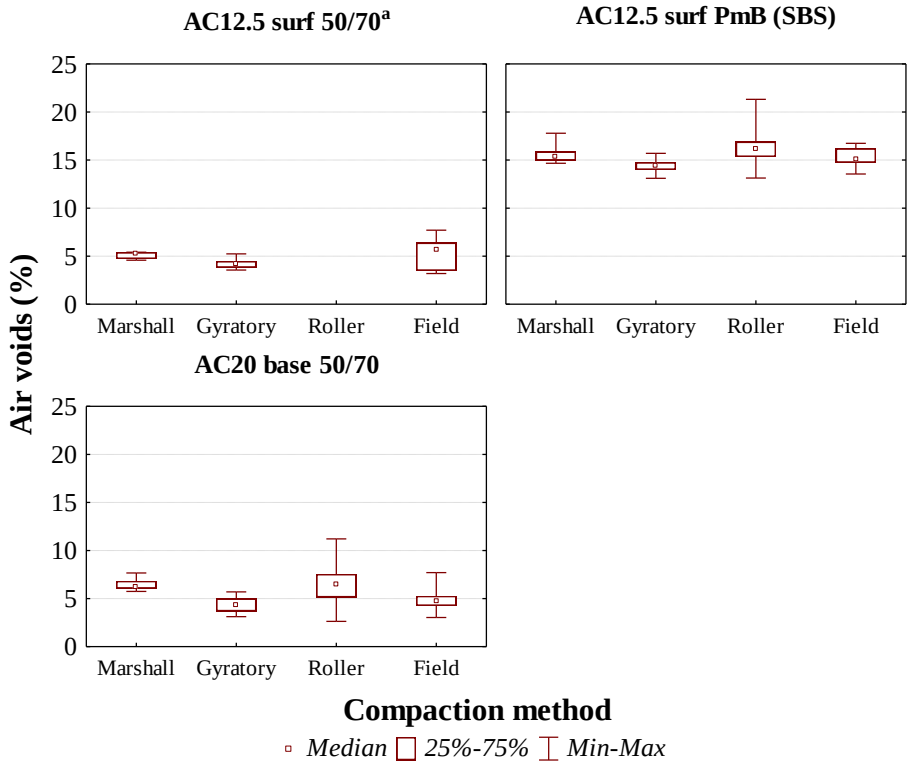

Fig. 5.26 Air voids as a function of compaction method

For the AC12.5 surf 50/70[a] mix, the air void content of field cores shows variability compared to the laboratory-compacted specimens. Also, specimens compacted using gyratory compaction show less air voids compared to field cores. The median values were calculated as 4.1%, 5.2%, and 5.6% for the gyratory, Marshall and field compaction method, respectively.

With regards to the AC12.5 surf PmB (SBS) mix, the air voids content varies among and within the various compaction methods. Increased variability is observed with respect to the roller compaction, relative to the other laboratory compaction methods, which can be attributed to the effect of compaction mode and effort. Compared to the field compaction variability, laboratory roller compaction method appears to show a similar performance. The median values were calculated as 15.3%, 14.4%, 16.1% and 15.1% for the Marshall, gyratory, roller and field compaction method, respectively.

More variability of air voids content is generally observed with respect to the AC20 base 50/70 mix, which can be attributed to the larger 20-mm nominal maximum aggregate size relative to the other mixtures. Again, similar variability is observed between the roller and field compaction method, hence indicating that the steel segmented roller compactor can simulate the in-situ performance of field rollers. The median values for all compaction methods are generally close to the average and were calculated as 6.2%, 4.4%, 6.5% and 4.7% for the Marshall, gyratory, roller and field compaction method. The above results, in general, indicate that the air void contents of the laboratory-compacted specimens fairly approximated the air voids content of the field cores.

Figure 5.27 summarizes the effect of each compaction method, including the field compaction, on the stiffness modulus (Georgiou et al. 2015).

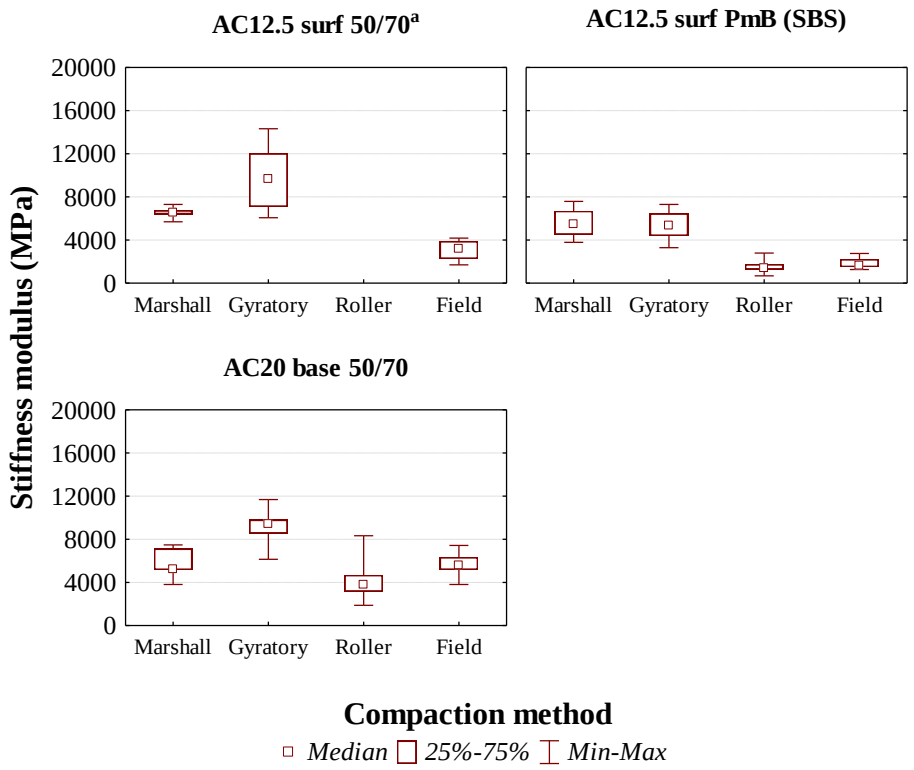

Fig. 5.27 Stiffness as a function of compaction methods

According to Fig. 5.27, field compaction seems to produce specimens with variability in terms of the ITSM values. Also, the median values were calculated as 3200, 1700 and 5600 MPa for the AC12.5 surf 50/70[a], AC12.5 surf PmB (SBS) and AC20 base 50/70 mix, respectively.

The combined results for the three studied mixtures indicate that, in general, the mould-based compaction methods (Marshall and gyratory) tend to produce specimens of higher stiffness than the roller-compacted specimens, as shown in Fig. 5.27. The gyratory-compacted specimens, with similar air void content to the field-compacted specimens, as shown in Fig. 5.26, have almost two and a half fold the stiffness modulus of the field cores. It is also observed that, although the air voids of Marshall specimens are higher than the field cores, the modulus is higher, especially, for the AC12.5 surf PmB (SBS) mix. On the contrary, the roller- and field-compacted specimens are of comparable stiffness if the difference in air void content is accounted for (increased air voids for roller specimens).

Using the above results, a preliminary study was carried out to investigate the impact of laboratory compaction-based HMA stiffness modulus on pavement response. Although such investigation would typically need more advanced calculations, a simplified approach using the BISAR (BISAR 1998) was adopted. For this purpose, pavement analyses were carried out in a typical flexible pavement taking into account the material characteristics of asphalt mixtures as measured in the lab. The pavement structure consists of a subgrade with a modulus of 200MPa, 400mm of a granular base with a modulus of 600MPa, 150mm of an asphalt base (type AC20 base 50/70) and 40mm of a surface mix (type AC12.5 surf PmB (SBS)), as shown in Fig. 5.28.

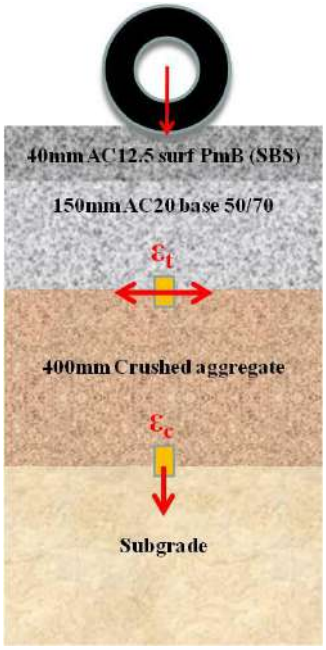

Fig. 5.28 Pavement structure

The aim was to calculate the tensile strain (ε_t) at the bottom of the asphalt layer and the compressive strain (ε_c) at the top of the subgrade soil under an Equivalent Standard Axle Load (ESAL) of 80 kN (single axle, double wheel, 20 kN load per wheel). In light of the above, four pavement structures associated to the laboratory and field compaction methods -namely Marshall, gyratory, roller and field- were analyzed using the BISAR. The critical strains ε_t and ε_c for the considered standard load was determined for each pavement structure using different inputs for the HMA material stiffness properties and assuming Poisson's ratio of 0.35 for all layers, except for the subgrade (v=0.40). The four different considered moduli selections were based on the mean values of the

measured stiffness modulus at temperature of 20°C with respect to the compaction method for both HMA mixes, as shown in Table 5.4. Prior to commencement of the strain analyses, the ITSM values of the two mixture types were used for the estimation of one composite modulus (SHRP 1993). The tensile strain ε_t at the bottom of the asphalt base and the vertical strain ε_c at the top of the subgrade for the different structures are illustrated in Fig. 5.29.

Table 5.4 Stiffness moduli for pavement analysis

Mix type	Stiffness modulus (MPa)			
	Marshall	Gyratory	Roller	Field
AC12.5 surf PmB (SBS)	5610	5410	1540	1870
AC20 base 50/70	5740	9080	3990	5720

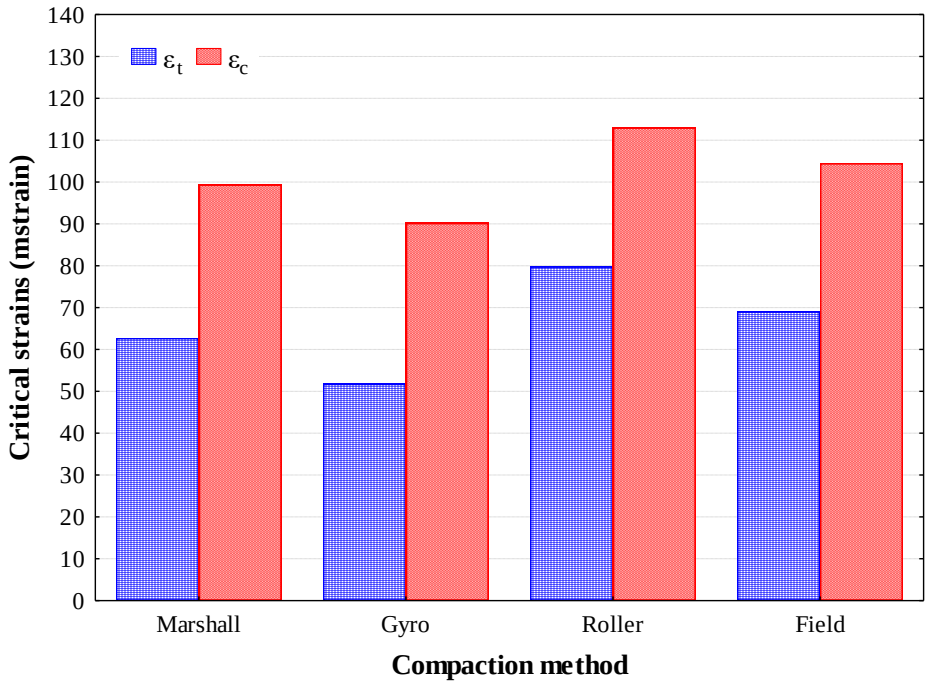

Fig. 5.29 Critical strains

The results indicate that that the lowest critical strains are estimated using the gyratory compaction-based stiffness for the asphalt mixtures. Conversely, the highest values are associated to the roller compaction, whereas the Marshall compaction-based results fall in between. Comparing with the field results, both Marshall and gyratory underestimate the field pavement strains. In contrast, it is demonstrated that roller

compaction-based results are greater than the field results, which in turn implies that by using these results for the purpose of predicting the pavement performance the estimated life span, especially fatigue, is conservative and from the safe side compared to the as-built pavement service life. Exemplifying the impact of the compaction-based stiffness modulus on pavement prediction performance would offer meaningful information, however this is beyond the scope of this study. In any case, it is unequivocal that the prediction of pavement performance is affected by the choice of compaction method and relative modulus. Therefore, closing the gap between the laboratory- and field compaction-based stiffness the differences in strains and the resulting pavement life span will be definitely lower. This implies that for analytical design purposes conversion factors should be established between laboratory- and field compaction-based stiffness.

In the light of the above, the stiffness ratio for each laboratory compaction method relative to field compaction was calculated, as presented in Fig. 5.30.

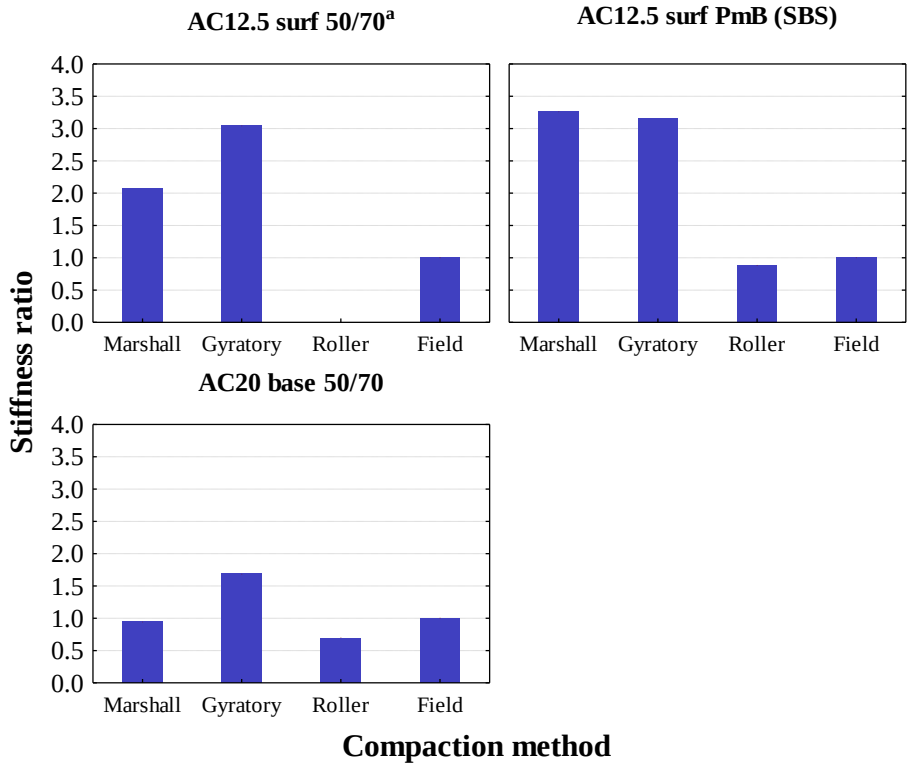

Fig. 5.30 Stiffness ratio of laboratory compaction methods relative to field compaction

For the interpretation, the median values- although not significantly differentiated from the mean- were used for the analysis and the results in terms of the ITSM ratios (i.e. Marshall/field, gyratory/field and roller/field) are presented in Fig. 5.30. The results indicate that the modulus values of Marshall-compacted specimens differentiate from the respective modulus values of field-compacted specimens by a factor ranging from 0.9 to 3.3. Also, this factor ranges from 1.7 to 3.2 with regards to gyratory and field compaction. On the contrary, the modulus values of roller-compacted specimens are generally lower but comparable to the field-compacted specimens with ratios calculated ranging from 0.7 to 0.9. On average, the stiffness modulus of laboratory-compacted specimens (namely Marshall, gyratory and roller) is approximately 2.1, 2.6 and 0.8 times, respectively, the stiffness modulus of field cores.

6. Rut resistance

6.1 Introduction

This Chapter focuses on the evaluation of rut resistance characteristics of various HMA types. By means of laboratory tests carried out using the Indirect Tension (IDT) Strength test method, the rut resistance of specimens fabricated using different compaction methodologies is investigated.

Following the stiffness study presented in the previous chapter, this study further examines the influence of various compaction factors on the high temperature IDT strength of the laboratory-compacted specimens with the aim to gain more insight to the factors that affect the HMA rut resistance characteristics. In addition, the magnitude of differences between the laboratory- and field compaction-based IDT strength is evaluated. In the following sections, the analysis results are demonstrated and discussed.

6.2 IDT Strength test method

In principal, the IDT strength test involves the application of a loading diametrically along the direction of the cylinder axis of a specimen with a constant speed of displacement until it breaks. The IDT strength is the maximum tensile stress calculated from the peak load applied at break and the dimensions of the specimen. Further, the IDT strength test performed at high temperatures has been found to be a simple and effective test for evaluating the rut resistance of asphalt mixtures (Christensen and Bonaquist 2007; Christensen et al. 2004). The recommended test protocol suggests applying the load at a rate of 50mm/min, hence offering the capability for the test to be performed using a commercial Marshall test frame. In addition, the test temperature should be 9°C lower than the yearly, 7-day average, maximum pavement temperature 20 mm below the pavement surface.

Taking into account available climatic data and pavement temperature models the design high pavement temperature was calculated, based on which the test temperature of asphalt mixtures was selected to be 50^{o}C. Prior to testing, each specimen was placed in a controlled temperature chamber and monitored until it attained the test temperature.

After conditioning, the specimen was removed from the chamber, then placed in the testing apparatus and immediately loaded to failure at 50mm/min, as illustrated in Figure 6.1.

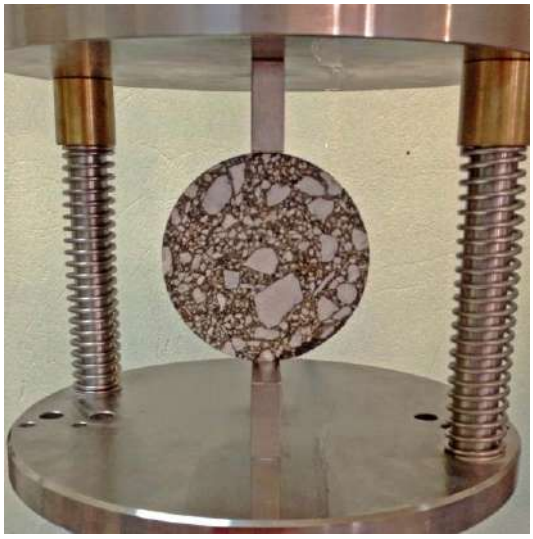

Fig. 6.1 IDT Strength test

Considerable attention was given so that specimen failure occurred within 60s of removal from the chamber, to ensure the specimen temperature did not significantly change during testing. The IDT strength was then calculated using the following formula:

$$\sigma_{IDT} = \frac{2P}{\pi t D} \quad (6.1)$$

where $\sigma_{(IDT)}$ is the IDT strength (KPa), P is the maximum applied load (kN), t is the thickness of the specimen (m), D is the diameter of the specimen (m).

6.3 Influence of compaction factors on HMA rut resistance

Three HMA types were tested within this course. Mixtures studied include a surface course mix with 50/70 binder, a surface course mix with polymer modified bitumen (SBS) and a base course mix with 50/70 binder and are denoted, respectively, as AC12.5 surf 50/70[a], AC12.5 surf PmB (SBS) and AC20 base 50/70.

6.3.1 Marshall compaction

Specimens compacted using the Marshall compactor and varying compaction temperatures were further tested to assess their rut resistance characteristics. IDT strength tests were performed at a test temperature of 50^{o}C and the results with respect to compaction temperature for the various HMA types are illustrated in Figures 6.2-6.4.

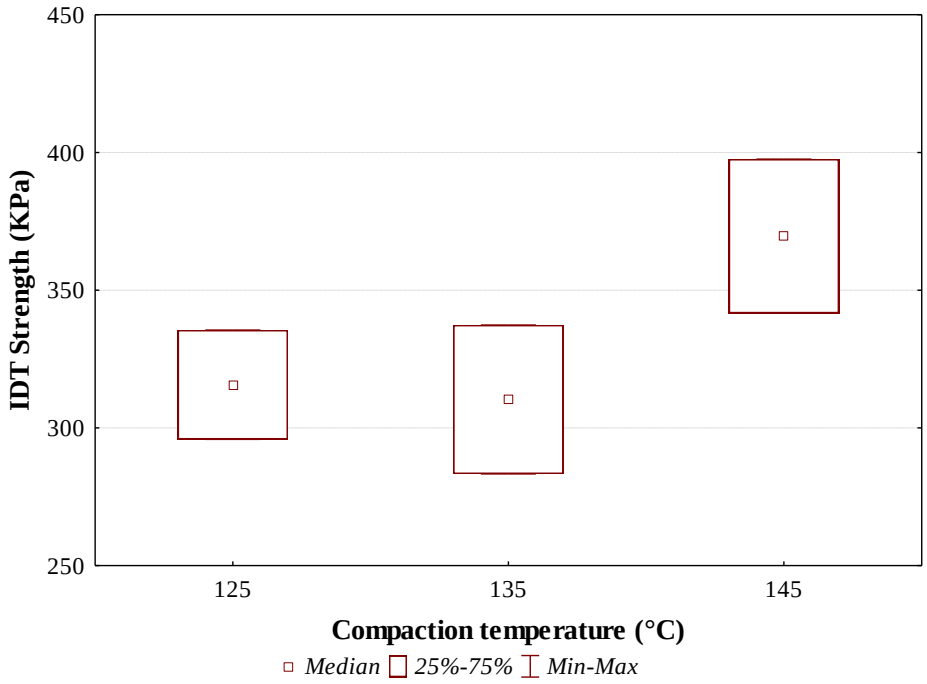

Fig. 6.2 Influence of compaction temperature on IDT strength (AC12.5 surf 50/70[a])

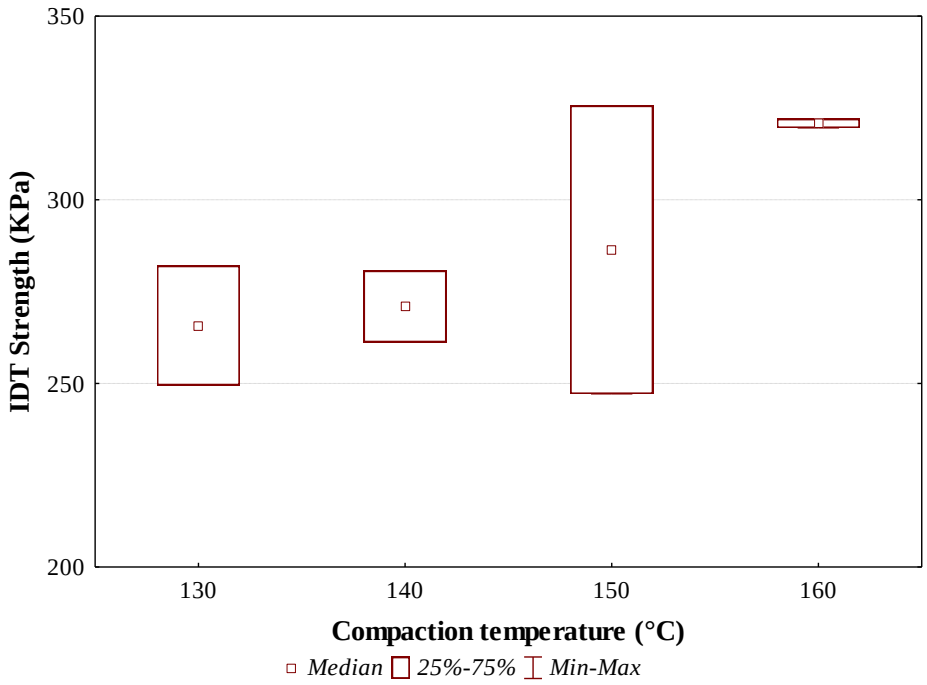

Fig. 6.3 Influence of compaction temperature on IDT strength (AC12.5 surf PmB (SBS))

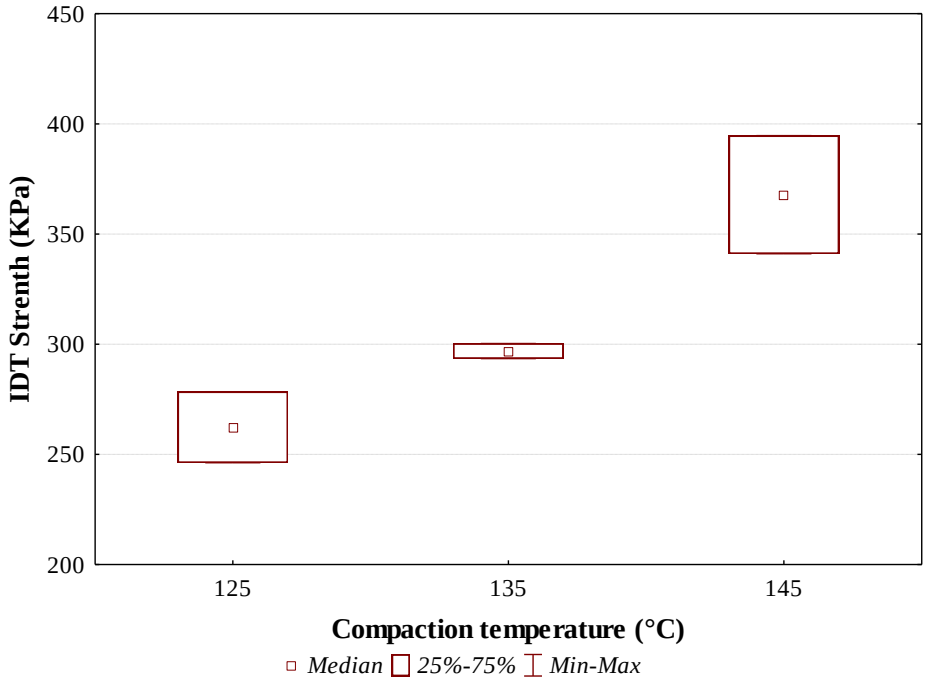

Fig. 6.4 Influence of compaction temperature on IDT strength (AC20 base 50/70)

From the above plots, the general trend observed is an increase of high temperature IDT strength with the increase of the compaction temperature. This indicates an improved rut resistance of Marshall specimens at elevated compaction temperatures. For instance, concerning the AC12.5 surf 50/70 mix, the IDT strength yields similar values for compaction at 125 ^{o}C and 135^{o}C, however specimens compacted at 145^{o}C show an increased IDT strength of the order of 20%. Accordingly, in the AC12.5 surf PmB (SBS) mix, the IDT strength value of specimens compacted at 160^{o}C is 12% and 17% higher than those of specimens compacted at 150^{o}C and 140^{o}C, respectively. Also, a gradual increase of IDT strength of the order of 13% and 24% is observed regarding the specimens of the AC20 base 50/70 mix when compaction temperature rises consecutively from 125 ^{o}C to 135 ^{o}C and 145^{o}C.

Table 6.1 ANOVA test results of rut resistance (α = 0.05)

Mix type	Temperature
AC12.5 surf 50/70[a]	.001
AC12.5 surf PmB (SBS)	.000
AC20 base 50/70	.000

The significance of the effect of compaction temperature on the rut resistance of Marshall specimens was evaluated by means of Analysis of variance (ANOVA) test at 95% confidence interval. From the statistical analysis, it was demonstrated that the compaction temperature influences significantly the Marshall specimens rut resistance characteristics (Table 6.1).

6.3.2 Gyratory compaction

Specimens compacted using the gyratory compactor and varying internal angle of gyration; compaction temperature; and (initial) diameter were also tested to assess their rut resistance characteristics. The high temperature IDT strength evolution with respect to these factors concerning the AC12.5 surf 50/70[a] is illustrated in Fig. 6.5-6.7, while Fig. 6.8-6.10 and Fig. 6.11-6.13 show the counterparts related to the AC12.5 surf PmB (SBS) and AC20 base 50/70 mix, respectively.

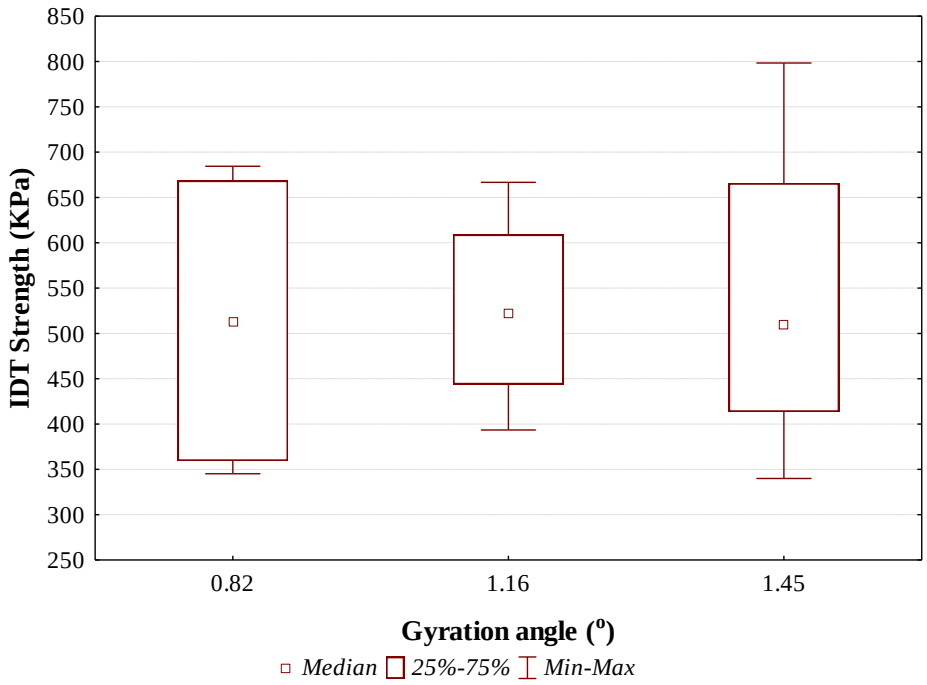

Fig. 6.5 Influence of gyration angle on IDT strength (AC12.5 surf 50/70[a])

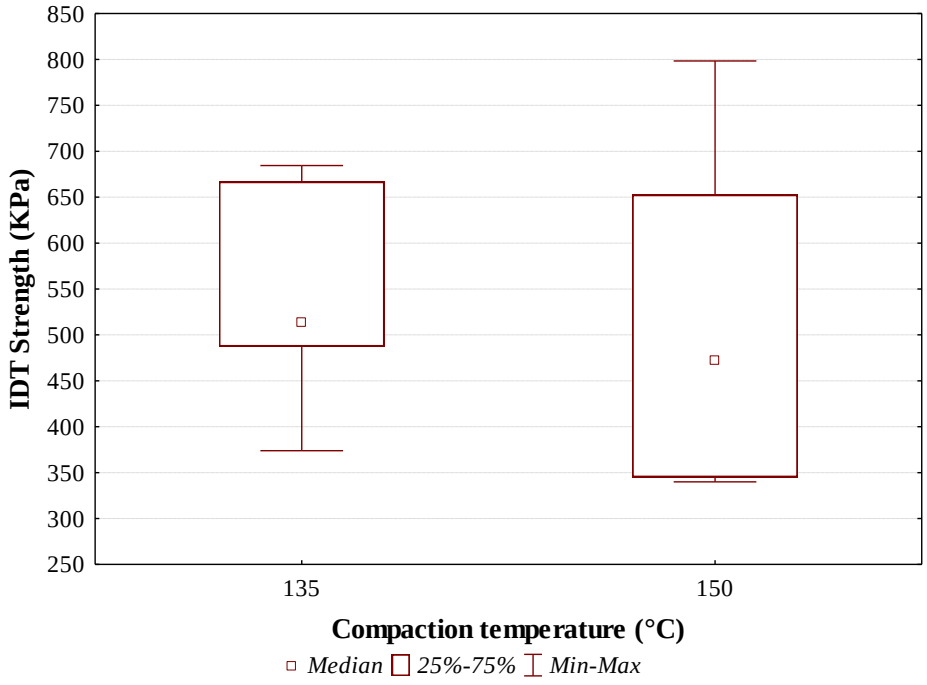

Fig. 6.6 Influence of compaction temperature on IDT strength (AC12.5 surf 50/70[a])

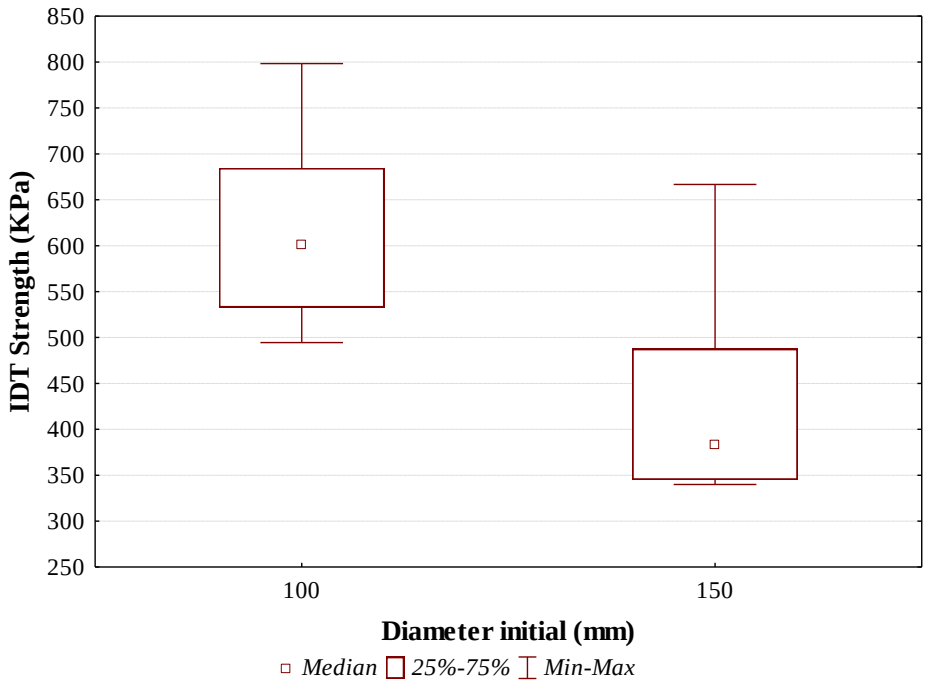

Fig. 6.7 Influence of specimen diameter (initial) on IDT strength (AC12.5 surf 50/70[a])

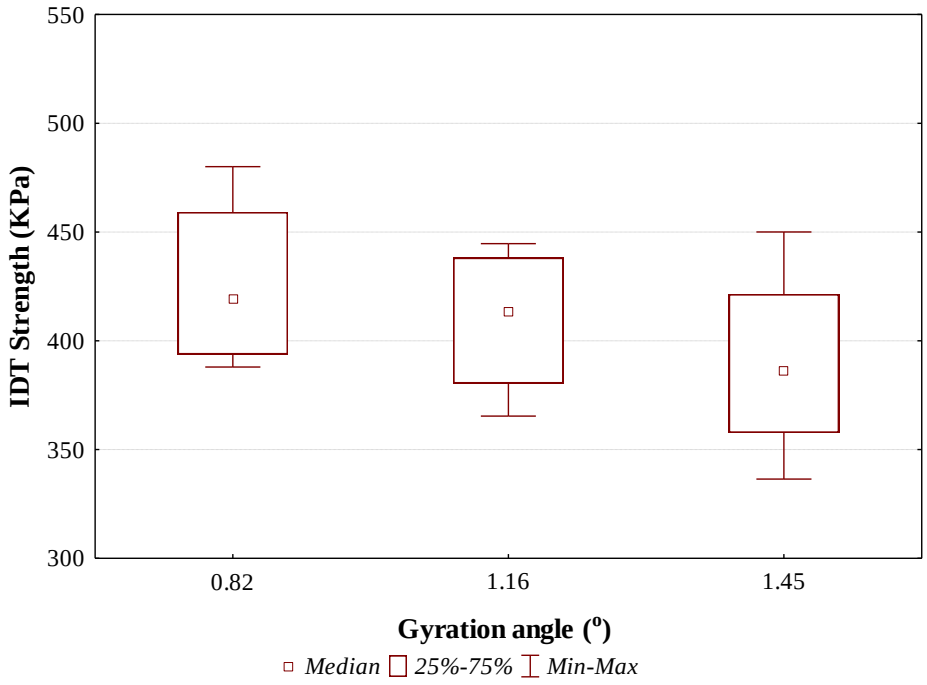

Fig. 6.8 Influence of gyration angle on IDT strength (AC12.5 surf PmB (SBS))

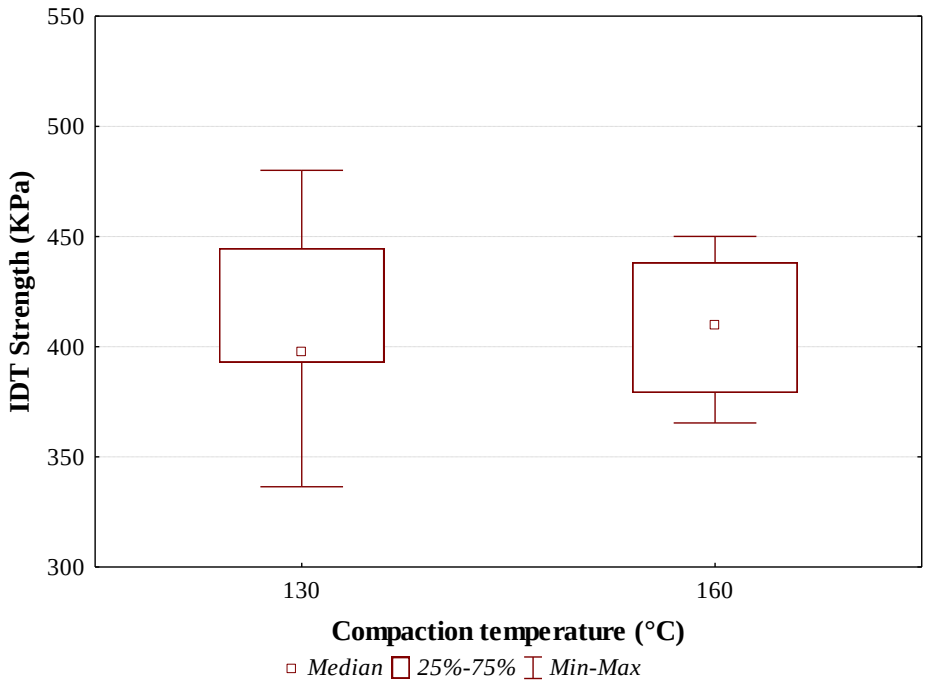

Fig. 6.9 Influence of compaction temperature on IDT strength (AC12.5 surf PmB (SBS))

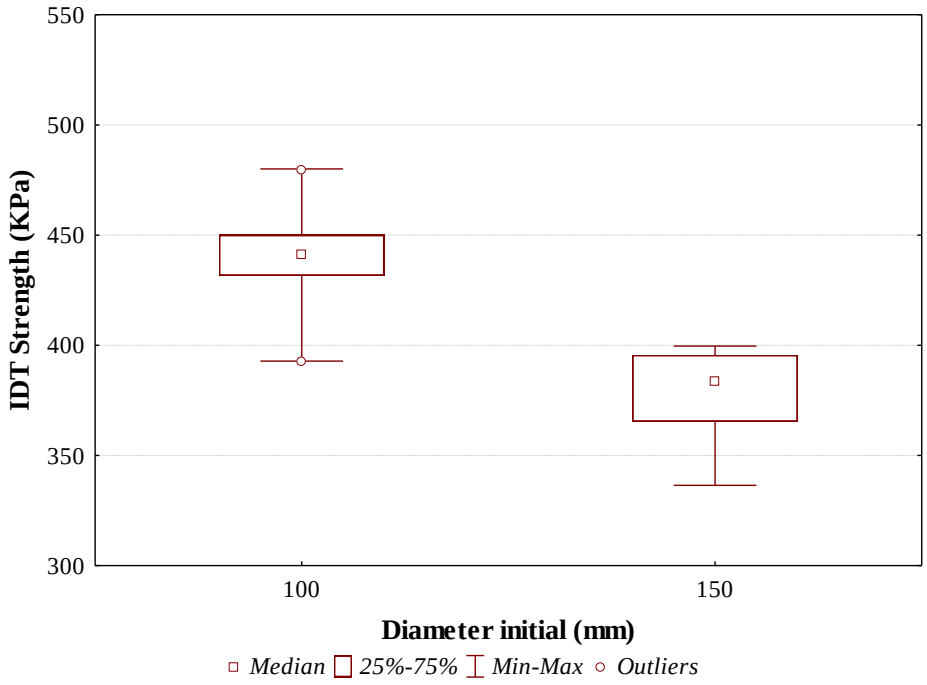

Fig. 6.10 Influence of specimen diameter (initial) on IDT strength (AC12.5 surf PmB (SBS))

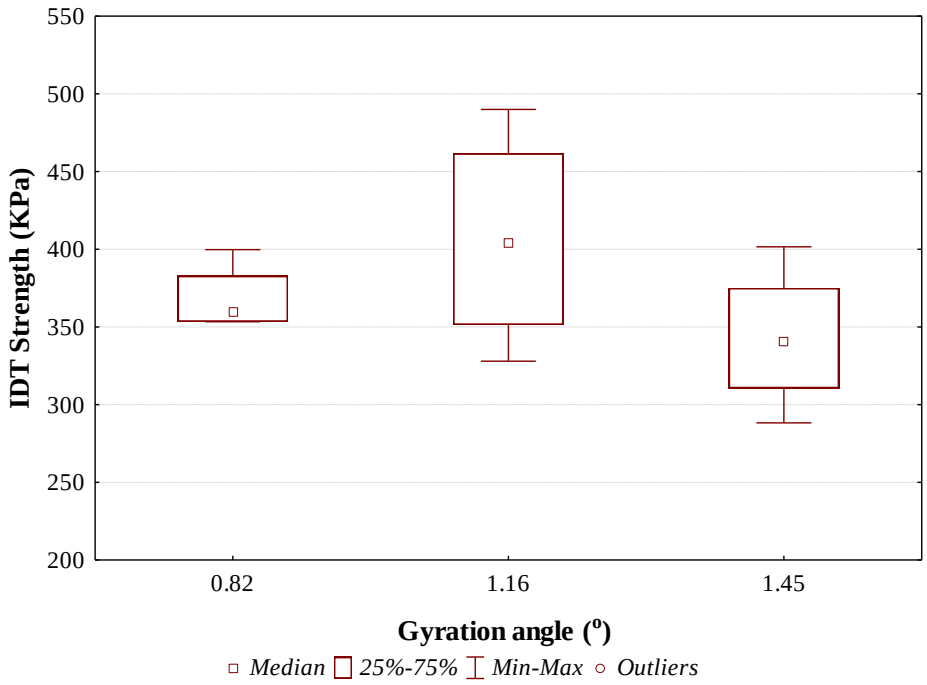

Fig. 6.11 Influence of gyration angle on IDT strength (AC20 base 50/70)

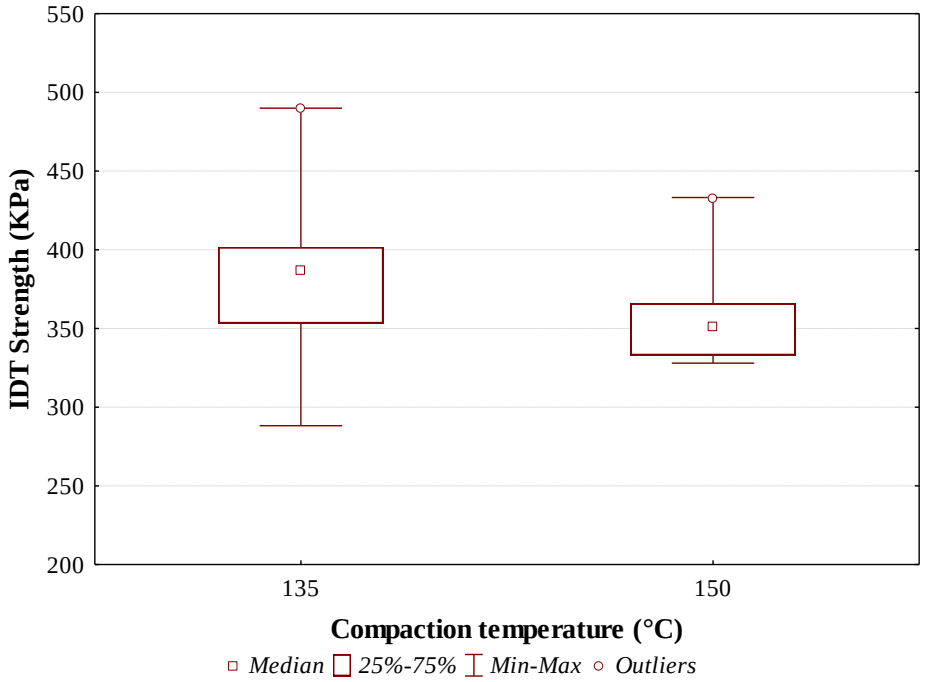

Fig. 6.12 Influence of compaction temperature on IDT strength (AC20 base 50/70)

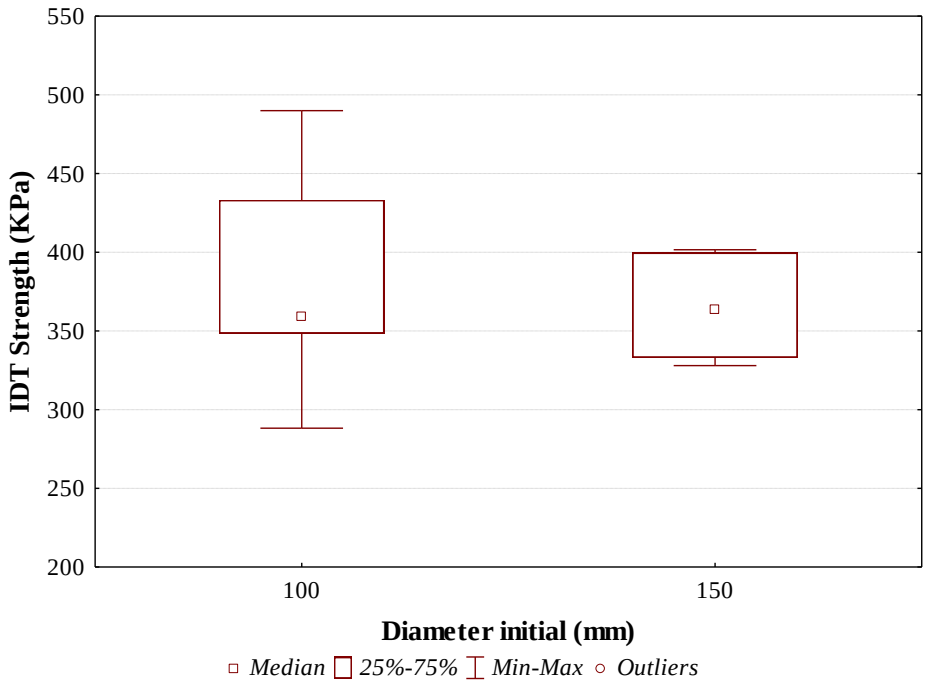

Fig. 6.13 Influence of specimen diameter (initial) on IDT strength (AC20 base 50/70)

The above results indicate that the angle of gyration influences the high temperature IDT strength. In general, the angle of 1.45^{o} produced the lowest IDT strength values. However, with respect to the angles specified in the CEN and AASHTO standards it can be stated that there is no significant difference among the high temperature IDT strength of the mixtures, except for the AC20 base 50/70 mix where increasing the gyration angle from 0.82˚ to 1.16˚ a higher IDT strength was obtained. It is worth mentioning that similar conclusions with respect to the effect of gyration angle were drawn from the stiffness study results.

The temperature effect was found to be mixture dependent. Specifically, an increase in compaction temperature from 135ºC to 150ºC results in a decrease of IDT strength of the conventional bitumen based mixtures, namely the AC12.5 surf 50/70^{a} and AC20 base 50/70; a IDT strength decrease of the order of 5% and 6% was calculated, respectively. On the contrary, similar IDT strength values are obtained concerning the AC12.5 surf PmB (SBS) mix when varying compaction temperature from 130^{o}C to 160^{o}C.

In addition, it is interesting to note that by coring 100mm diameter from larger 150mm specimen a lower IDT strength is obtained compared to the as-compacted

100mm specimens. This effect is more pronounced with respect to the AC12.5 surf 50/70[a] and AC12.5 surf PmB (SBS), where IDT strength decrease reach up to 30%.

Table 6.2 ANOVA test results of rut resistance (α = 0.05)

Mix type	Compaction factors		
	Angle	Temperature	Diameter
AC12.5 surf 50/70[a]	.968	.754	.059
AC12.5 surf PmB (SBS)	.166	.982	.003
AC20 base 50/70	.307	.462	.660

A detailed statistical analysis was performed to evaluate the significance of the effect of different variables on the rut resistance of gyratory specimens. Main compaction parameters were investigated at 95% confidence interval by means of ANOVA and the results in terms of the p-values are tabulated in Table 6.2. The statistical analysis demonstrated that, in general, specimen diameter affects significantly the high temperature IDT strength.

6.3.3 Roller compaction

Specimens compacted using the roller compactor and varying compaction mode; effort (number of passes) and temperature were also tested to assess their rut resistance characteristics. The high temperature IDT strength evolution with respect to these factors concerning the AC12.5 surf PmB (SBS) is illustrated in Fig. 6.14-6.16, while Fig. 6.17-6.19 show the counterparts related to the AC20 base 50/70 mix.

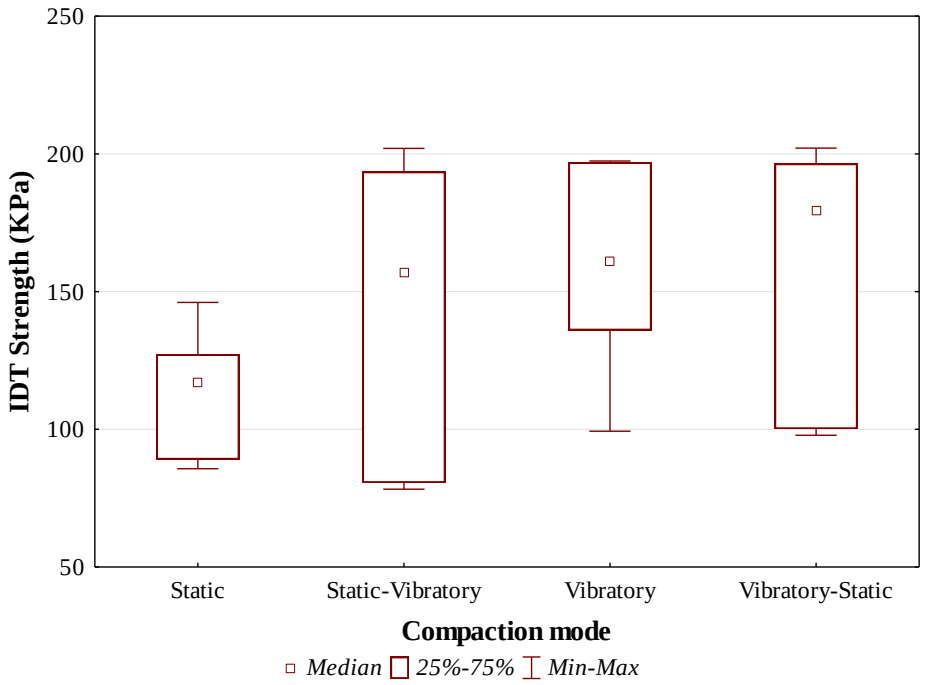

Fig. 6.14 Influence of compaction mode on IDT strength (AC12.5 surf PmB (SBS))

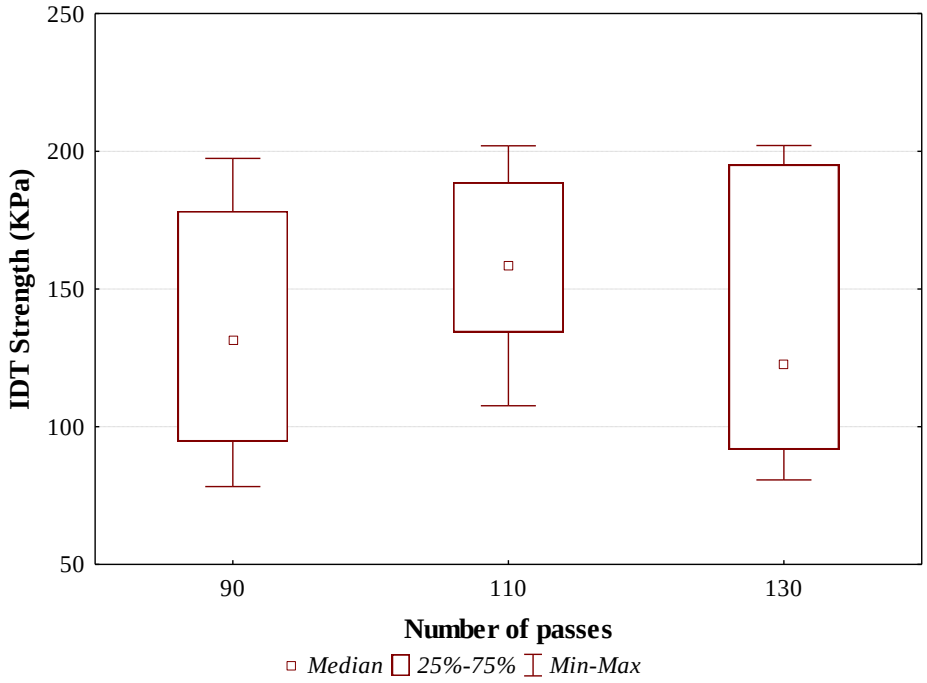

Fig. 6.15 Influence of compaction effort on IDT strength (AC12.5 surf PmB (SBS))

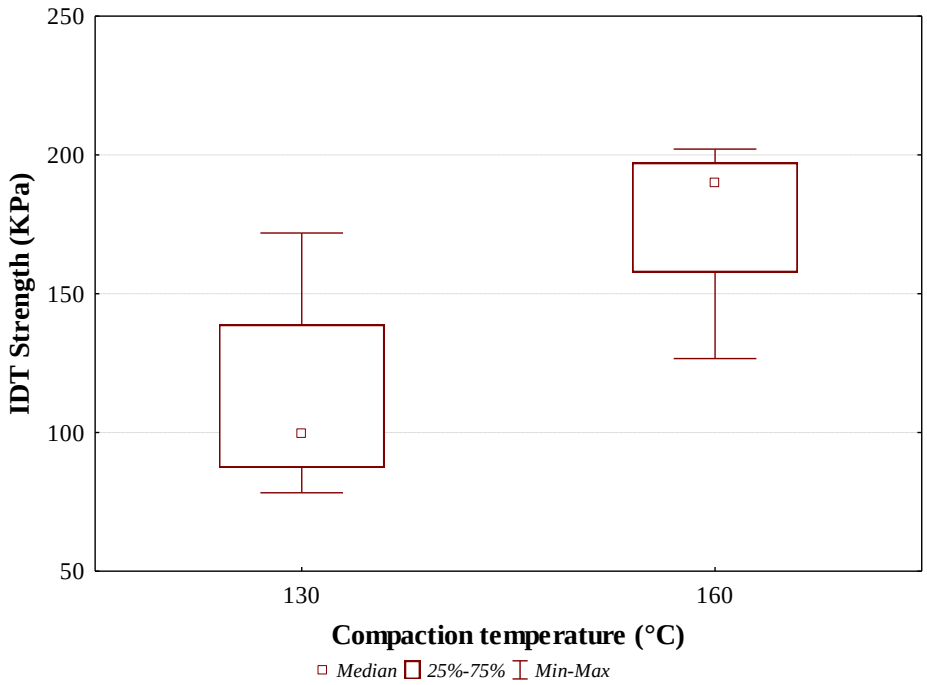

Fig. 6.16 Influence of compaction temperature on IDT strength (AC12.5 surf PmB (SBS))

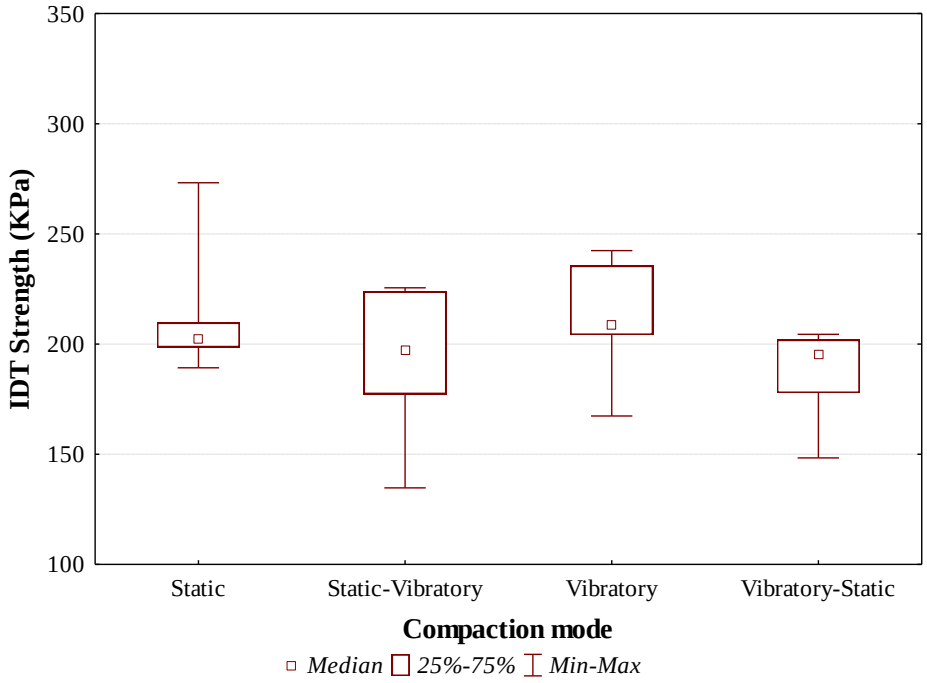

Fig. 6.17 Influence of compaction mode on IDT strength (AC20 base 50/70)

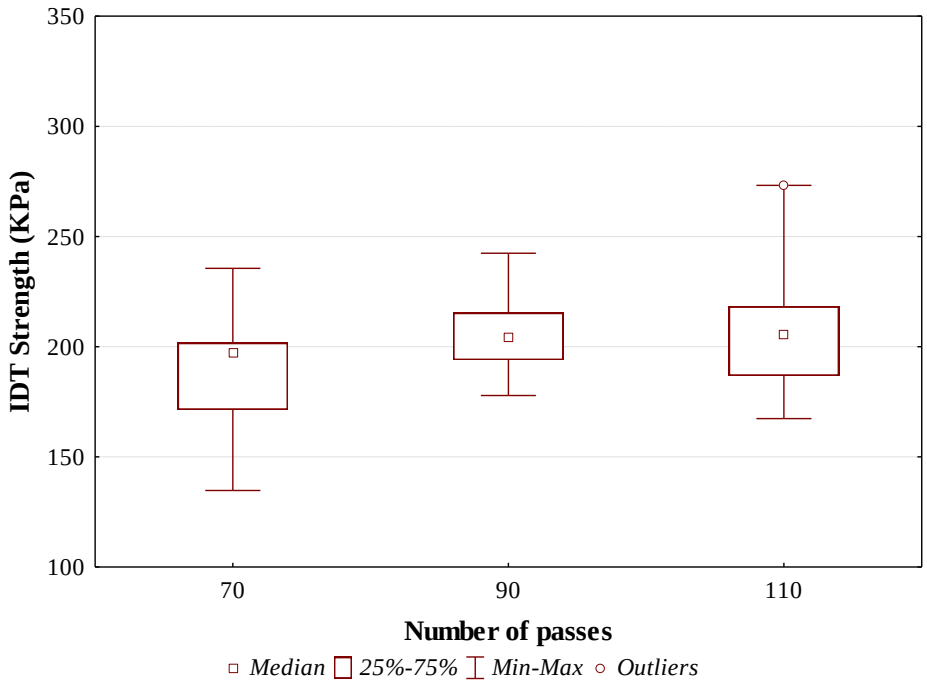

Fig. 6.18 Influence of compaction effort on IDT strength (AC20 base 50/70)

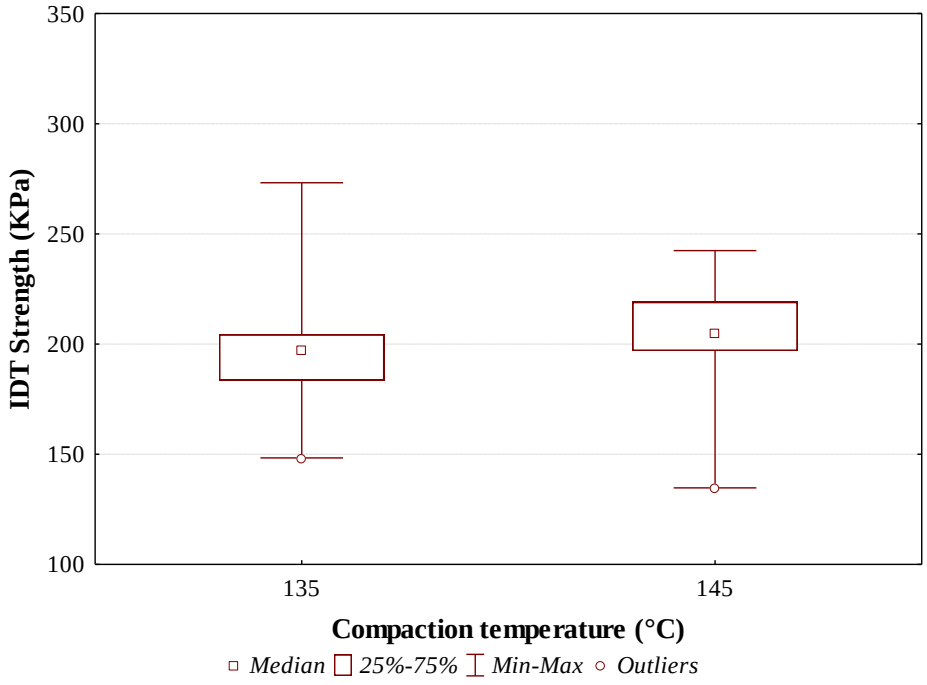

Fig. 6.19 Influence of compaction temperature on IDT strength (AC20 base 50/70)

The compaction mode seems to affect the high temperature IDT strength of the AC12.5 surf PmB (SBS) mix. Less variation of the IDT strength with respect to the compaction mode is observed for the AC20 base 50/70 mix.

In addition, the results indicate that for both mixtures increase of compaction effort (namely roller passes) up to a certain level (i.e. 110 and 90 passes for AC12.5 surf PmB (SBS) and AC20 base 50/70 mix, respectively) results in IDT strength increase of the order of 17% and 13%. Further compaction effort does not improve the rut resistance of mixtures.

Moreover, the results indicate that although similar IDT strength values can be obtained when compacting AC20 base 50/70 mix at 135ºC and 145ºC, significant increase of IDT strength of the order of 60% is achieved for the AC12.5 surf PmB (SBS) with the increase of compaction temperature from the 130ºC to 160ºC.

To substantiate the influence of roller compaction parameters on the rut resistance of asphalt mixtures statistical analysis was performed. Table 6.3 summarizes the ANOVA results in terms of the p-values for the three main compaction factors at 95% confidence interval.

Table 6.3 ANOVA test results of rut resistance (α = 0.05)

Mix type	Compaction factors		
	Mode	Effort	Temperature
AC12.5 surf PmB (SBS)	.000	.082	.006
AC20 base 50/70	.648	.382	.350

The analysis reveals that both the compaction mode and temperature affect significantly the high temperature IDT strength of AC12.5 surf PmB (SBS) mix; a lesser effect on IDT strength is attributed to the compaction effort (namely number of passes). Less significant effect of compaction factors on the IDT strength was found for the AC20 base 50/70 mix.

6.3.4 Comparison to field compaction

Field-compacted specimens were also tested to evaluate their rut resistance characteristics and to compare them with the laboratory-compacted specimens. Figure

6.20 summarize the high temperature IDT strength results with respect to the compaction methods, both laboratory and field.

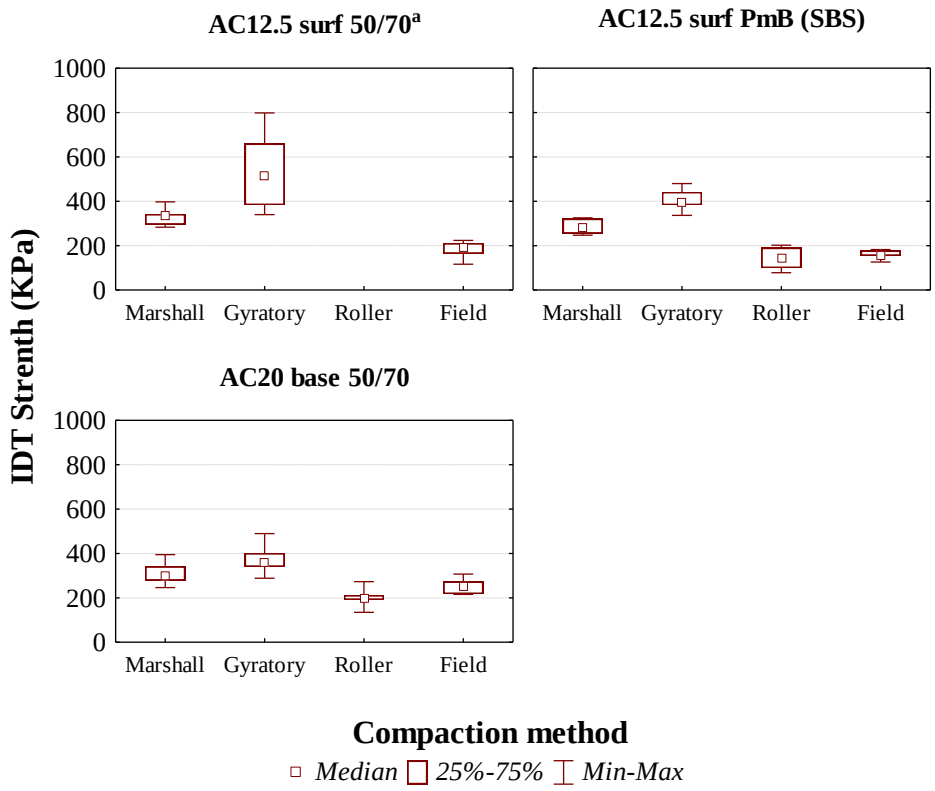

Fig. 6.20 IDT strength as a function of compaction methods

According to Fig. 6.20, field compaction seems to produce specimens with some variability in terms of the IDT strength values, which is more pronounced for the AC12.5 surf 50/70[a] mix. Also, the median values were calculated as 189, 158 and 251 KPa for the AC12.5 surf 50/70[a], AC12.5 surf PmB (SBS) and AC20 base 50/70 mix, respectively.

The combined results for the three studied mixtures indicate that the mould-based compaction methods (Marshall and gyratory) tend to produce specimens of higher rut resistance than the field-compacted specimens, as shown in Fig. 6.20. Particularly, the high temperature IDT strength values of Marshall- and gyratory-compacted specimens are higher than the respective strength values of field-compacted specimens by a factor of the order of 1.6 and 2.2, respectively. It is interesting to note that for the pure bitumen-based mixtures the magnitude of IDT strength differences between laboratory and field compaction methods becomes larger for smaller NMAS (i.e. 12.5mm). On the

contrary, the rut resistance of field-compacted specimens seems to be aligned with the roller-compacted specimens. Particularly, the IDT strength values of roller-compacted specimens are lower compared to field cores by a factor of the order of 0.9, as also found from the stiffness study results.

7. Internal structure

7.1 Introduction

In the course of the stiffness- rut resistance studies presented in the previous chapters, significant differences were manifested with respect to the compaction factors and regimes considered. As already underlined during the literature review, the differences in engineering properties of asphalt mixtures compacted using various compaction methods may be associated to the variation of specimen's internal structure. In this regard, this chapter focuses on the evaluation of the internal structure by means of 2-D imaging analysis, as described hereinafter, of various HMA types compacted both in the lab (using Marshall, gyratory and roller compaction) and field.

The aim was to investigate the impact of various laboratory compaction factors on asphalt mix microstructure and assess the laboratory compaction methods with regards to its capabilities to reproduce the field compaction-based microstructure. In a follow up level, the interrelation between the asphalt mix microstructure and engineering properties will be discussed; hence to gain a better insight, image analysis was focused on specimens representing significant variation in mechanical properties. Also, it should be mentioned that the 2-D imaging analysis was performed at horizontal cross-sections of the compacted specimens. This approach was supported given that the loading and, mostly, the corresponding load-induced stress distribution within the mixture during the mechanical testing (both stiffness and rut resistance) was in the same direction. Therefore, it was reasonably hypothesized that, in such case, more meaningful results will be obtained on the purpose to assess subsequently the microstructure and its relation to asphalt mix performance.

7.2 Imaging technique

Generally, imaging techniques consist of three main stages: i) image acquisition, in which a physical object is converted to digital form, ii) image processing, which involves application of various filters on the image, in order to enhance its visual appearance and define its features for subsequent measurement and iii) image analysis,

which refers to the acquisition of specific information by measuring certain image characteristics (regions of interest) via the appropriate mathematical procedures (Russ 2011). In this subsection, the imaging technique used in this study to capture and analyze the internal structure of asphalt mixes is described.

Internal structure characterization of laboratory- and field-compacted specimens was performed by means of 2-D imaging, which is considered to be a cost-effective and efficient method. A flatbed scanner was used for capturing the internal structure in terms of RGB (Red-Green-Blue) colored images. All specimens were cut at two sections, 10 mm from the top and the bottom and digital images of the two cut surfaces for each specimen were taken. Figure 7.1 illustrates a representative scanned raw image for each mixture studied.

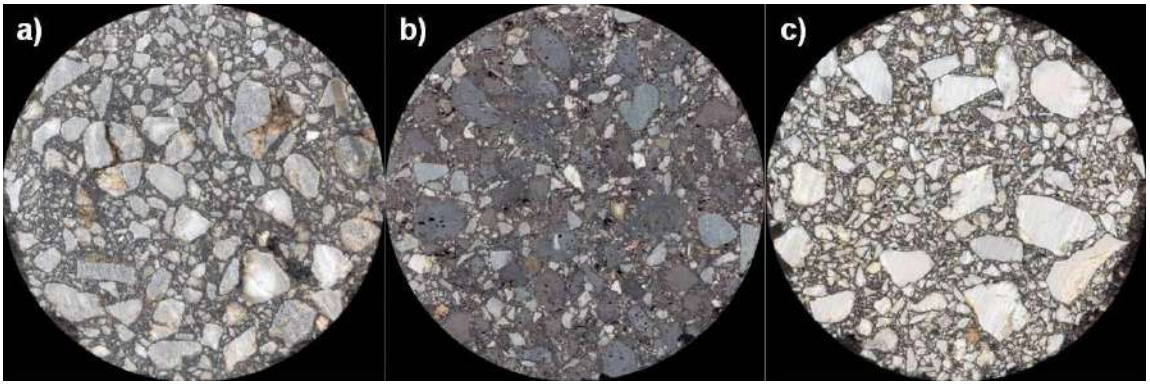

Fig. 7.1 Scanned images of mixtures; (a) AC12.5 surf 50/70[a], (b) AC12.5 surf PmB (SBS) and (c) AC20 base 50/70

The processing stage, along with the image analysis was performed using iPas software (Coenen et al. 2012), which has been developed as part of the RILEM Technical Committee 237-SIB TG2 activities and applied effectively for the internal structure characterization of HMA samples (Sefidmazgi et al. 2014; Sefidmazgi et al. 2012). In this stage, the color image is converted into a binary image (i.e., black and white) to facilitate the analysis towards separation of the phases of mixture in terms of their color intensity differences.

The main target of image processing is to detect the aggregate areas in the image accurately and isolate them from the rest of the mixture's constituents. To accomplish this goal primarily the image resolution and mix volumetrics are entered in the iPas software. Then, the filters described hereinafter are applied in the scanned image (Fig.

7.2a) as: i) median filter, to reduce the noise in the image, as shown in Fig. 7.2b; ii) Hmax filter, in order to smooth the color variation in aggregate areas (Fig. 7.2c); iii) watershed transformation, to separate the aggregates (Fig. 7.2d); and iv) thresholding, to convert the grey scale image into a binary one where white pixels represent the aggregates (Fig. 7.2e). The filter values are adjusted properly verifying that the obtained images are representative of the actual mixture.

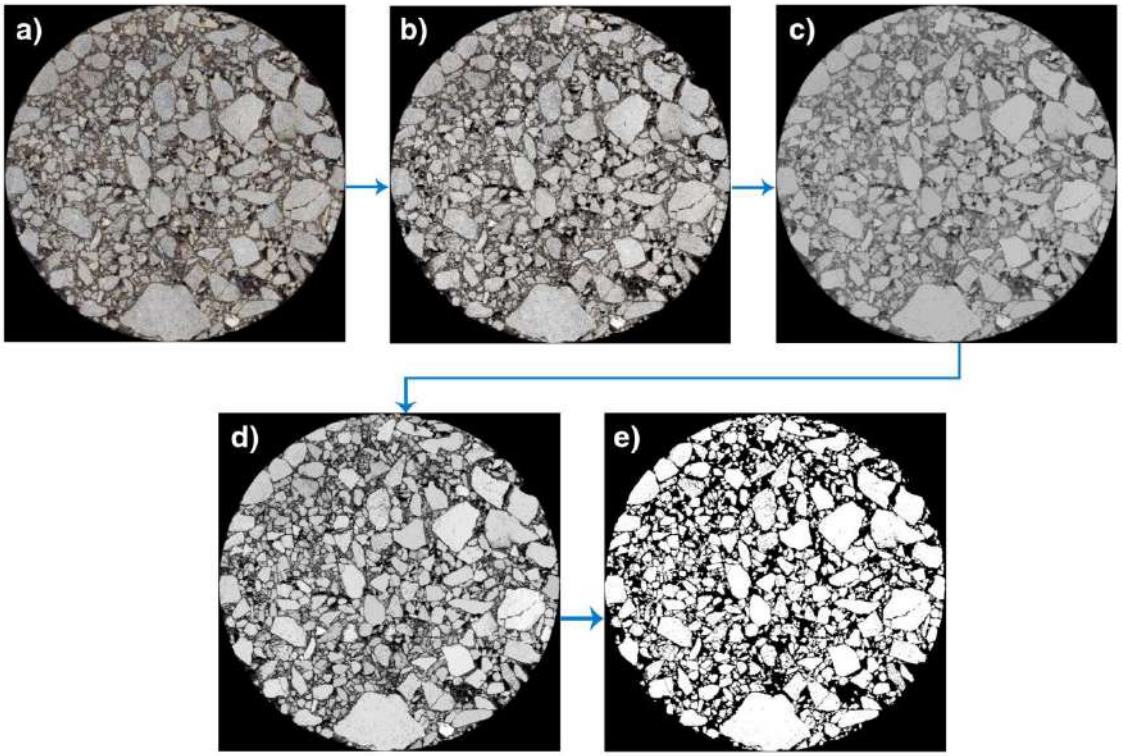

Fig. 7.2 Image processing procedure

It is worthwhile to point out that the images of mixture AC12.5 surf 50/70[a] and AC20 base 50/70 specimens, which contain light-colored limestone aggregates, were very accurately processed hence the output image was close to the original physical image as shown in Fig. 7.3. Processing of the planar images of mixture AC12.5 surf PmB (SBS) proved to be very challenging due to the low contrast between bitumen and steel slag aggregates. Nevertheless, the obtained output images seem to represent rather accurately the original ones, as illustrated in Fig. 7.4.

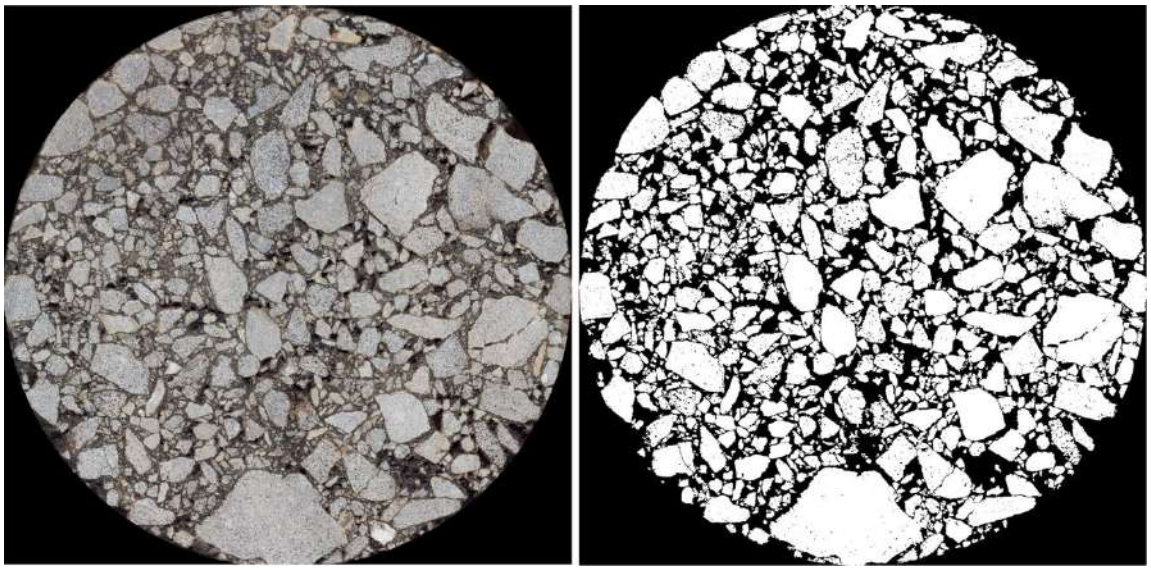

Fig. 7.3 Image processing of limestone-based mixtures

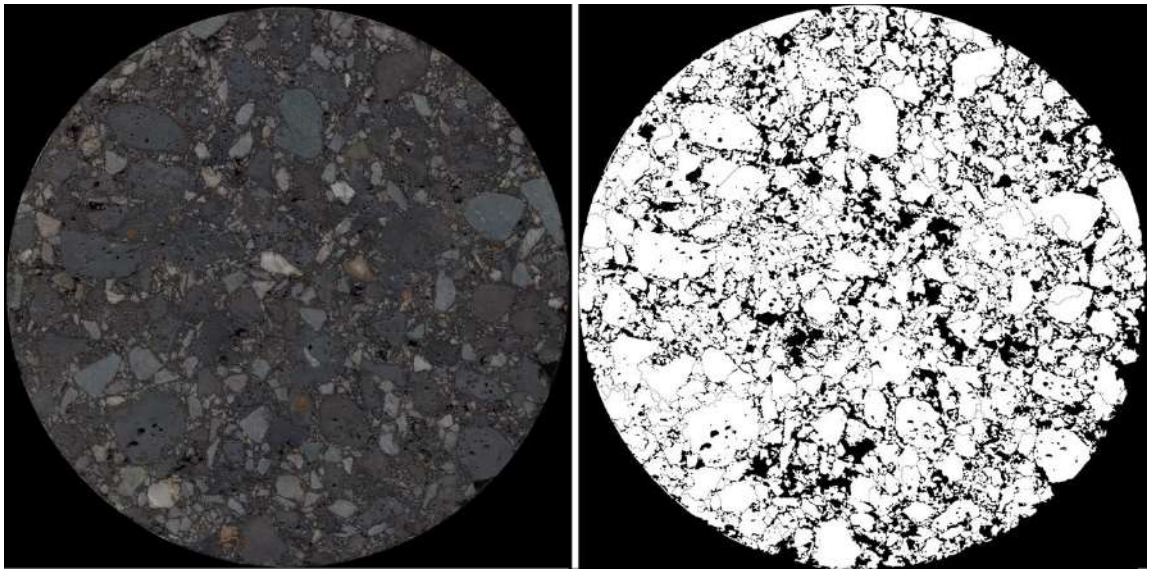

Fig. 7.4 Image processing of steel slag-based mixture

After processing, the internal structure can be quantified by means of various indicators related to aggregate contact points, orientation and segregation, which are described hereinafter. The minimum aggregate size used for calculations, distinguishing coarse aggregates from sand, was set to 2.36 mm. This threshold was determined based on the capacities of the image analysis software. Target was to identify the smallest clearly visible aggregate within the mixture image, while including the maximum percentage of total aggregates.

Number of contact points (CP). Neighboring aggregates separated by distance less or equal to 0.5 mm, defined as surface distance threshold (SDT) and illustrated in Fig. 7.5a, are considered in contact. By defining the contact distance and the minimum aggregate size, the locations that meet the criteria are determined and the total number of contact points is reported. For each specimen the average contact points of the top and bottom image were averaged- this was also applied for each of the indicators described below- to be used for further analysis.

Contact length (CL). Moreover, capturing aggregates' perimeter pixels that are within the specified SDT, the total pixels form a contact line between the two aggregates and subsequently the contact length can be assessed, as illustrated in Fig. 7.5b.

Contact length in branches (CLB). The aggregates that are inter-connected (i.e., contacted) along the sample, as assumed to form the aggregate skeleton, were also considered to define the contact length in branches (Fig. 7.5c).

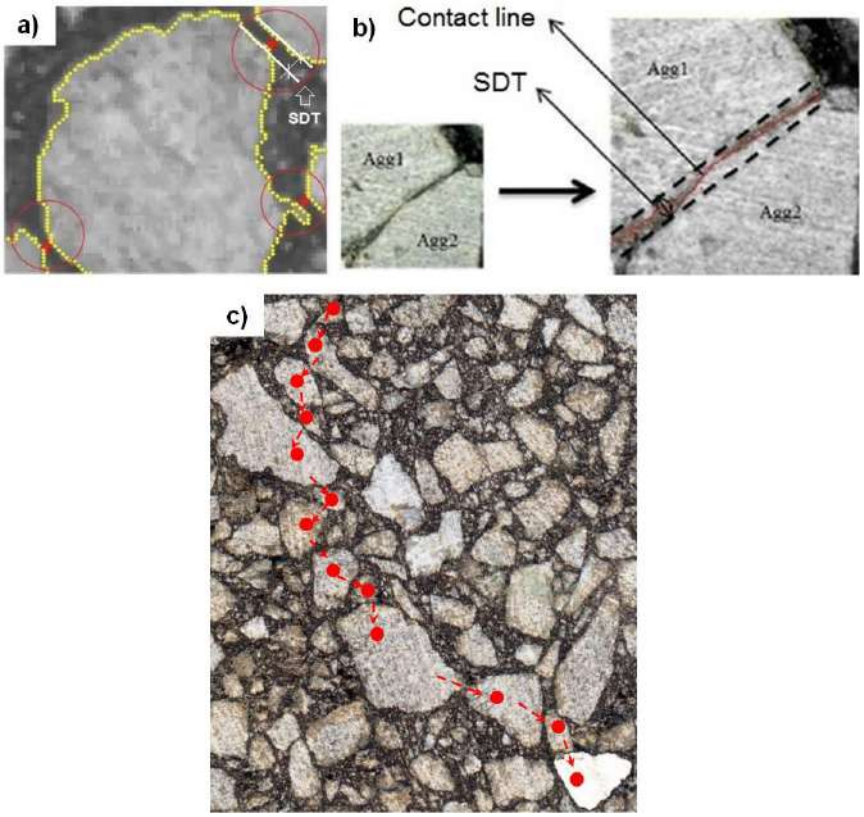

Fig. 7.5 a) Contact between aggregates, b) contact line and c) branches in aggregate skeleton

It is worthwhile to mention that the above indices represent the connectivity of the aggregate structure, which is believed to be associated to the load-induced stress distribution within the mixture.

Orientation. Orientation was characterized in terms of the orientation angle θ_k, which is defined as the angle between each aggregate's major axis and the radius of the cross section (Fig. 7.6). Orientation angle was calculated with respect to the center of the cross sectional area, so that the rotation of the specimens does not affect the results and ranges from 0 to 179^o.

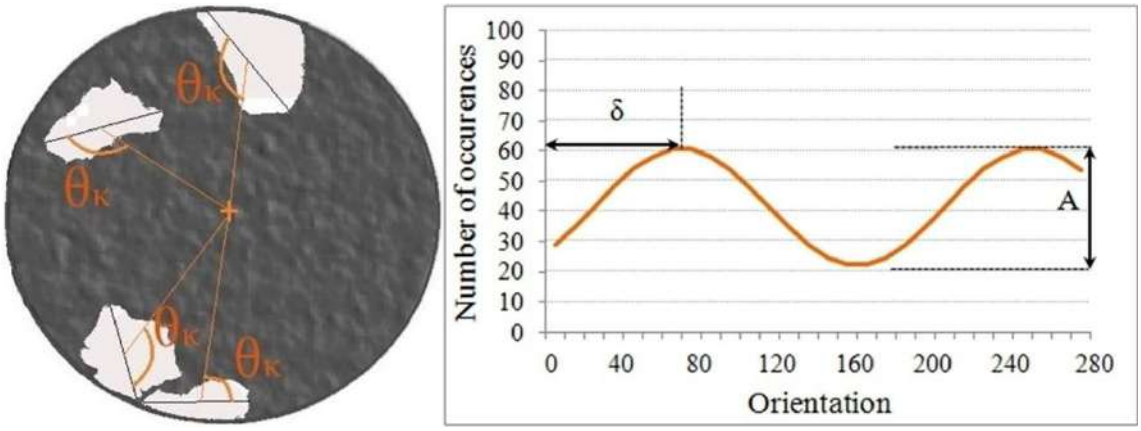

Fig. 7.6 Orientation angle (left); harmonic fit parameters (right)

Due to the large number of aggregates within an asphalt mixture, the distribution of aggregate orientation needs to be concisely described. For this purpose, in this study a harmonic function, which has been well documented in literature (Partl et al. 2013; Coenen et al. 2012; Tashman et al. 2001), was assigned to the aggregate orientation angle distribution expressed as follows:

$$n(\theta_i) = n_a(1 + acos^2\theta_i + 2bsin\theta_i cos\theta_i - asin^2\theta_i) \quad (7.1)$$

where

$$n_a = N/N_d \quad (7.2)$$

$$a = [2\sum_{k=1}^{N} \cos(2\theta_k)]/N \quad (7.3)$$

$$b = [2\sum_{k=1}^{N} \sin(2\theta_k)]/N \quad (7.4)$$

where $n(\theta_i)$ is the number of aggregates oriented at an angle of θ_i and n_a is the number of aggregates randomly oriented within an image.

Then, quantification of aggregate orientation was based on parameters δ and A of the harmonic function. Parameter δ corresponds to the first maximum value of the harmonic and identifies the predominant orientation angle, while A is the amplitude of the harmonic and indicates the tendency of the aggregates to orientate towards orientation angle δ (Fig. 7.6). A uniform orientation is indicated by value of zero for parameter A, while the higher the value the more variance from the uniform distribution within the mixture is considered.

Segregation. To calculate aggregate segregation, the circular cross section image was separated in two regions; the inner and the outer region. The inner region is defined as the circular section whose radius is the 2/3 of the total radius of the image, while the outer region is the rest of the initial cross sectional image, as illustrated in Fig. 7.7.

Fig. 7.7 Inner and outer region definition for segregation analysis

Determining the aggregates whose centroids are within each region, quantification of lateral segregation was based on parameter S_L, which is defined as the percentage change in the average aggregate diameter in the outer region to that in the inner region (Saadeh et al. 2002) and expressed as follows:

$$S_L = \left(\frac{D_{out}}{D_{in}} - 1\right) 100 \ [\%] \quad (7.5)$$

Consequently, a S_L value of zero indicates uniform aggregate spatial distribution. A positive value of S_L indicates distribution of coarse aggregates in the outer region, while a negative value indicates the opposite.

7.3 Influence of compaction factors on HMA internal structure

Three HMA mixtures were tested within this course, following the compactability, stiffness and rut resistance laboratory studies presented in Chapters 4, 5 and 6. The three mixes include: a surface course mix with 50/70 binder, a surface course mix with polymer modified bitumen (SBS) and a base course mix with 50/70 binder. These mixtures, which were described in Chapter 3, are denoted, respectively, as AC12.5 surf 50/70[a], AC12.5 surf PmB (SBS) and AC20 base 50/70.

7.3.1 Marshall compaction

Internal structure characteristics derived from the image analysis of Marshall specimens are summarized in Tables 7.1-7.3. Table 7.1 tabulates the analysis results regarding the aggregates contact points as a function of compaction temperature for the various mixtures.

Table 7.1 Contact points as a function of compaction temperature

Mix type	Temp (°C)	CP		CL		CLB	
		Mean	StDev	Mean	StDev	Mean	StDev
AC12.5 surf 50/70[a]	125	145	12	328	23	168	45
	135	159	17	359	106	165	79
	145	149	15	339	16	172	3
AC12.5 surf PmB (SBS)	130	88	25	633	358	554	319
	140	87	2	511	84	424	57
	150	103	10	740	132	637	104
	160	99	12	751	109	697	122
AC20 base 50/70	125	164	16	374	36	231	32
	135	155	6	316	18	170	10
	145	171	3	348	4	196	20

Although the results show some variation, in general, the contact-based indices seem to follow the same trend for all mixtures. This indicates that each indicator may explain the differences in internal structure due to the compaction temperature. The effect of compaction temperature on connectivity between aggregates seems to be mixture dependent. For instance, in regard to the AC12.5 surf 50/70[a] mix the results showed that by increasing the compaction temperature from 125°C to 135°C the

aggregate packing increased, and then began to slightly decrease at higher temperature of 145^{o}C. Moreover, in regards to the AC12.5 surf PmB (SBS) mix which is composed of an open gradation, it is demonstrated that higher connectivity between aggregates is achieved in the highest compaction temperatures (ranging from 150-160^{o}C). On the contrary, in regard to the AC20 base 50/70 mix, the contact points evolution follows a parabolic curve where the fewest aggregates contacts seem to be obtained at the intermediate compaction temperature of 135^{o}C. Surprisingly, for this mix the most contact points are yielded for the lower compaction temperature (namely 125^{o}C).

Aggregates orientation was quantified by the parameters δ and A of the harmonic fit function, whose variations with respect to compaction temperature is summarized in Table 7.2.

Table 7.2 Orientation as a function of compaction temperature

Mix type	Temp (^{o}C)	δ		A	
		Mean	StDev	Mean	StDev
AC12.5 surf 50/70[a]	125	99	14	5	0
	135	94	4	6	0
	145	105	2	5	1
AC12.5 surf PmB (SBS)	130	84	12	2	0
	140	85	13	3	2
	150	71	6	1	0
	160	88	38	2	0
AC20 base 50/70	125	104	11	2	1
	135	83	18	3	2
	145	119	5	3	3

In general, the mixtures designed with pure bitumen (namely AC12.5 surf 50/70[a] and AC20 base 50/70) follow the same trend. Particularly, the results indicated lower orientation angles as going from 125^{o}C to 135^{o}C followed by an increase in orientation angle for further increase of compaction temperature up to 145^{o}C. For 135^{o}C, the aggregates tend to orientate to angle close to 90^{o} for both mixtures, which implies that the particles are aligned in a circumferential direction. Also, for these mixtures the greatest values for amplitude A correspond to the higher compaction temperatures, hence indicating a narrow distribution of aggregate orientation values and tendency of aggregates orientation to a particular angle. With regard to the AC12.5 surf PmB (SBS)

mix no clear trend is identified for the harmonic fit parameters δ and A in respect to the compaction temperature variation. Predominant angles close to 90^o are observed for all compaction temperatures, except for the 150^oC; also examining the orientation parameter A results, in general rather low values are noted indicating little influence on the aggregate orientation.

Segregation was evaluated based on the distribution of aggregates in the two regions, as defined in Fig. 7.7, in terms of the parameter S_L. The effect of compaction temperature on the radial segregation for the three study mixtures is shown in Table 7.3.

Table 7.3 Segregation as a function of compaction temperature

Mix type	Temp (^oC)	S_L		$\|S_L\|$	
		Mean	StDev	Mean	StDev
AC12.5 surf 50/70[a]	125	4	4	4	4
	135	0	14	10	0
	145	-1	13	9	1
AC12.5 surf PmB (SBS)	130	10	9	10	9
	140	0	14	10	0
	150	-4	5	4	5
	160	0	13	9	0
AC20 base 50/70	125	15	15	15	15
	135	9	6	9	6
	145	18	0	18	0

Segregation parameter S_L values show variation and range, in general, up to about ±10% for the 12.5-mm surface course mixtures. For these mixtures, it should be noted that the almost equal number of positive and negative S_L values implies that there is no specific trend for the coarser aggregates' movement towards the inner or outer region of the Marshall specimens. Considering the above, along with the fact that the use of mean S_L values might give a misleading perception of homogeneity due to counterbalance, it makes more sense that the absolute values of S_L are also included for consideration. Regarding the AC20 base 50/70 mix, in general the higher S_L values compared to the surface course mixes indicate more segregation which may be attributed to the higher NMAS. Significant variation in aggregates' spatial distribution is also observed with respect to the upper and lower compaction temperature. It should be noted that for this mixture only positive S_L values were calculated, which indicates that coarser aggregate

is distributed in the outer region. In general, the data suggest that Marshall compaction produce rather non homogeneous specimens.

Table 7.4 P-values of compaction temperature for image indicators in each mixture

Mix type	Contact points			Orientation		Segregation
	CP	CL	CLB	δ	A	S_L
AC12.5 surf 50/70[a]	.642	.893	.991	.514	.696	.912
AC12.5 surf PmB (SBS)	.652	.644	.532	.848	.847	.643
AC20 base 50/70	.404	.191	.154	.142	.650	.622

To further evaluate the impact of compaction temperature on the internal structure indices statistical analysis was also carried out. Table 7.4 tabulates the analyses results in terms of p-values at 95% confidence interval. The statistical results suggest that the internal structure indicators of asphalt mixtures did not differ significantly in respect of the compaction temperature.

7.3.2 Gyratory compaction

Specimens compacted using the gyratory compactor and varying the internal angle of gyration, compaction temperature, and (initial) diameter (100 mm and 150 mm), as already presented in Ch.4, were further tested to assess their microstructure's properties (Georgiou et al. 2016). The analysis results are presented hereinafter.

Tables 7.5-7.7 tabulate the analysis results regarding the aggregates contact points, orientation and segregation as a function of gyration angle for the various mixtures.

Table 7.5 Contact points as a function of gyration angle

Mix type	Angle (°)	CP		CL		CLB	
		Mean	StDev	Mean	StDev	Mean	StDev
AC12.5 surf 50/70[a]	0.82	245	34	581	130	396	195
	1.16	226	16	523	74	328	100
	1.45	204	20	433	62	254	62
AC12.5 surf PmB (SBS)	0.82	91	11	420	100	344	72
	1.16	78	24	389	159	268	177
	1.45	87	10	415	78	288	77
AC20 base 50/70	0.82	118	28	260	100	115	119
	1.16	116	13	267	39	118	37
	1.45	110	11	230	30	106	28

Table 7.6 Orientation as a function of gyration angle

Mix type	Angle (°)	δ		A	
		Mean	StDev	Mean	StDev
AC12.5 surf 50/70[a]	0.82	104	14	9	4
	1.16	98	8	12	5
	1.45	75	16	11	6
AC12.5 surf PmB (SBS)	0.82	102	19	7	1
	1.16	91	12	8	5
	1.45	92	8	9	2
AC20 base 50/70	0.82	111	6	4	2
	1.16	83	12	5	2
	1.45	72	19	5	1

Table 7.7 Segregation as a function of gyration angle

Mix type	Angle (°)	S_L		$\|S_L\|$	
		Mean	StDev	Mean	StDev
AC12.5 surf 50/70[a]	0.82	1	4	3	2
	1.16	7	9	10	4
	1.45	-2	5	4	3
AC12.5 surf PmB (SBS)	0.82	0	5	5	2
	1.16	0	5	5	1
	1.45	-5	4	5	4
AC20 base 50/70	0.82	-7	10	10	6
	1.16	-3	9	6	7
	1.45	0	11	9	2

In general, the contact-based indices seem to follow the same trend for all mixtures, although results present some variance. Also, the effect of gyration angle on stone-to-stone contact seems to be mixture dependent. For instance, in regard to the AC12.5 surf 50/70[a] mix the results demonstrated that when increasing the angle, the contact points were successively decreased; the lowest number of proximity zones between aggregates was reported for the angle of 1.45°. Mixed results were obtained in regards to the remaining mixtures. Particularly, in regards to the AC20 base 50/70 the higher connectivity between aggregates seems to be achieved for the angle of 1.16°, as specified in the AASHTO standard, while using the same angle for the AC12.5 surf PmB (SBS) mix less contact points seem to be obtained, compared to the other angles.

With respect to predominant orientation angle (δ), it was found that the increase in gyration angle leads to reduction of the orientation angle; this trend was more pronounced with respect to the AC12.5 surf 50/70[a] and AC20 base 50/70 mixtures. Moreover, the transition from the standard angles of 0.82^o and 1.16^o, where aggregates tend to align in a circumferential direction, results in a more random orientation of aggregates towards 70^o. Examining the orientation parameter A results, generally high values were noted, except for the AC20 base 50/70 mix, hence further indicating the aggregates tendency to orientate towards the identified angles.

Segregation parameter S_L values range up to about ±10% for most gyratory specimens, whereas in few cases values up to ±15% were observed. The above results indicate that the gyratory compaction produces rather non homogeneous specimens, while the almost equal number of positive and negative S_L values implies that there is no specific trend for the coarser aggregates' movement towards the inner or outer region of the specimen. Also, the effect of the gyration angle was found to be dependent on the mixture's type.

Tables 7.8-7.10 tabulate the analysis results regarding the aggregates contact points, orientation and segregation as a function of compaction temperature.

Table 7.8 Contact points as a function of compaction temperature

Mix type	Temp (^{o}C)	CP		CL		CLB	
		Mean	StDev	Mean	StDev	Mean	StDev
AC12.5 surf 50/70[a]	135	232	30	557	106	378	144
	150	218	28	467	92	273	108
AC12.5 surf PmB (SBS)	130	87	14	444	83	321	96
	160	84	19	372	123	279	133
AC20 base 50/70	135	126	14	275	67	141	82
	150	104	13	230	49	85	33

The contact-based indices seem to follow the same trend for all mixtures, although results present some variance. The results indicate that the increase in compaction temperature reduces the proximity zones between aggregates.

Table 7.9 Orientation as a function of compaction temperature

Mix type	Temp (°C)	δ		A	
		Mean	StDev	Mean	StDev
AC12.5 surf 50/70[a]	135	95	18	9	4
	150	89	18	11	6
AC12.5 surf PmB (SBS)	130	101	12	7	3
	160	88	13	9	2
AC20 base 50/70	135	89	26	5	1
	150	89	16	5	2

Table 7.10 Segregation as a function of compaction temperature

Mix type	Temp (°C)	S_L		$\|S_L\|$	
		Mean	StDev	Mean	StDev
AC12.5 surf 50/70[a]	135	1	6	5	3
	150	3	8	6	6
AC12.5 surf PmB (SBS)	130	-2	7	6	3
	160	-2	4	4	1
AC20 base 50/70	135	-3	11	9	6
	150	-4	9	8	5

Specimens compacted at higher temperatures presented lower orientation angles, although temperature didn't seem to influence significantly the aggregates directional distribution. Moreover, compaction at higher temperatures led to a more pronounced preferred aggregate orientation within the mix. Also, variation of compaction temperature did not seem to have substantial effect on lateral segregation.

Tables 7.11-7.13 summarize the analysis results regarding the aggregates contact points, orientation and segregation as a function of specimen (initial) diameter.

Table 7.11 Contact points as a function of specimen (initial) diameter

Mix type	Dia (mm)	CP		CL		CLB	
		Mean	StDev	Mean	StDev	Mean	StDev
AC12.5 surf 50/70[a]	100	241	28	567	108	401	139
	150	208	19	457	76	251	79
AC12.5 surf PmB (SBS)	100	95	10	474	68	373	74
	150	76	15	342	101	227	98
AC20 base 50/70	100	123	16	290	62	144	81
	150	106	15	215	31	82	31

Table 7.12 Orientation as a function of specimen (initial) diameter

Mix type	Dia (mm)	δ		A	
		Mean	StDev	Mean	StDev
AC12.5 surf 50/70[a]	100	83	16	9	4
	150	102	14	12	5
AC12.5 surf PmB (SBS)	100	97	9	8	2
	150	93	18	8	4
AC20 base 50/70	100	79	24	4	1
	150	98	14	6	1

Table 7.13 Segregation as a function of specimen (initial) diameter

Mix type	Dia (mm)	S_L		$\|S_L\|$	
		Mean	StDev	Mean	StDev
AC12.5 surf 50/70[a]	100	2	7	5	5
	150	2	7	6	4
AC12.5 surf PmB (SBS)	100	-1	5	6	2
	150	-3	6	6	3
AC20 base 50/70	100	-6	10	9	7
	150	-1	9	8	4

With respect to the specimen diameter, the results have indicated a significantly higher number of contact points and longer contact lengths for the as-compacted 100mm specimens, compared to the cored 100mm -from larger 150mm- specimens. Regarding the dense-graded mixes, namely the AC12.5 surf 50/70[a] and AC20 base 50/70 mixtures, the aggregates in the cut/cored specimens were orientated at a higher angle, while the opposite was found for the open-graded mix. A narrow distribution of aggregate orientation values and tendency of aggregate orientation to a particular angle was observed for these specimens as well, as suggested by the higher values of parameter A. The segregation analysis results indicate minor variations with respect to the specimen diameter.

A detailed statistical analysis was performed to evaluate the significance of the effect of different variables on the gyratory specimens' internal structure indices. Main compaction parameters were investigated at 95% confidence interval by means of

Analysis of variance (ANOVA) test and the results are tabulated in terms of p-values in Table 7.14.

Table 7.14 P-values of gyratory compaction factors for image indicators in each mixture

Mix type	Factor	Contact points			Orientation		Segregation
		CP	CL	CLB	δ	A	$\|S_L\|$
AC12.5 surf 50/70[a]	Angle	.020	.014	.141	.001	.736	.073
	Temp	.147	.020	.077	.179	.448	.858
	Dia	.007	.008	.021	.001	.265	.842
AC12.5 surf PmB (SBS)	Angle	.422	.875	.501	.480	.542	.847
	Temp	.662	.206	.448	.122	.199	.196
	Dia	.037	.039	.026	.654	.934	.381
AC20 base 50/70	Angle	.620	.514	.963	.001	.392	.541
	Temp	.009	.132	.163	1.000	.456	.749
	Dia	.026	.026	.134	.009	.031	.724

The analysis reveals that the specimen's diameter affects significantly both the aggregates' contact points and its orientation; in general this was consistent for all mixtures tested. Moreover, gyration angle was found to influence significantly the orientation angle, and to a lesser extent the contact points (only for the case of AC12.5 surf 50/70[a] mix). The compaction temperature seems to have some effect on contact points, particularly for the dense-graded mixtures.

7.3.3 Roller compaction

Specimens compacted using the roller compactor and varying the compaction mode, effort (number of passes) and temperature, as already presented in Ch.4, were further tested to assess their microstructure's properties.

Tables 7.15-7.17 tabulate the analysis results regarding the aggregates' contact points, orientation and segregation as a function of compaction mode.

Table 7.15 Contact points as a function of compaction mode

Mix type	Mode	CP		CL		CLB	
		Mean	StDev	Mean	StDev	Mean	StDev
AC12.5 surf PmB (SBS)	S	82	23	460	120	330	154
	SV	98	28	499	114	416	147
	V	95	11	600	100	506	140
	VS	102	15	587	115	520	131
AC20 base 50/70	S	189	79	468	242	321	235
	SV	181	41	453	150	292	155
	V	182	24	431	75	273	95
	VS	158	36	362	126	195	128

Table 7.16 Orientation as a function of compaction mode

Mix type	Mode	δ		A	
		Mean	StDev	Mean	StDev
AC12.5 surf PmB (SBS)	S	96	34	2	1
	SV	87	26	2	1
	V	71	27	2	1
	VS	93	20	2	1
AC20 base 50/70	S	93	16	4	1
	SV	104	22	3	1
	V	86	16	3	1
	VS	65	15	3	1

Table 7.17 Segregation as a function of compaction mode

Mix type	Mode	S_L		$\lvert S_L \rvert$	
		Mean	StDev	Mean	StDev
AC12.5 surf PmB (SBS)	S	-3	4	5	2
	SV	0	10	7	5
	V	2	4	3	2
	VS	-11	8	11	7
AC20 base 50/70	S	0	5	4	2
	SV	0	4	3	2
	V	-6	8	7	6
	VS	-2	7	4	5

The results regarding the contact-based indices indicate slight variability with respect to the compaction mode. It is worth noting that, regarding the AC12.5 surf PmB (SBS), the highest and lowest proximity zones were induced respectively by the vibratory-static and static mode. Converse effect was observed for the AC20 base 50/70 mix, where the static mode was found superior compared to the other compaction modes in terms of aggregates connectivity. Hence, the mode of compaction appears to influence the contacts between aggregates of different mix designs (namely dense- and open-graded mixtures).

With respect to predominant orientation angle (δ), considering the wide variation of results it can be concluded that the different compaction modes did not induce a substantial effect on aggregates arrangement. In general, for all modes of compaction average predominant angles close to 90^o were reported; combined with the low severity A values, this is fairly indicative of aligning the aggregates concentric to the perimeter. Departure from this trend showed the vibratory and vibratory-static mode regarding, respectively, the AC12.5 surf PmB (SBS) and AC20 base 50/70 mixtures, which tend to orient the aggregates to around 70^o.

Segregation parameter S_L values range up to about ±10% for most roller-compacted specimens. No discernible trend was observed with respect to the compaction modes independent of the mixture type studied.

Tables 7.18-7.20 tabulate the analysis results regarding the aggregates contact points, orientation and segregation as a function of compaction effort (namely number of passes).

Table 7.18 Contact points as a function of compaction effort

Mix type	Effort	CP		CL		CLB	
		Mean	StDev	Mean	StDev	Mean	StDev
AC12.5 surf PmB (SBS)	90	96	13	583	104	522	96
	110	87	24	466	130	361	184
	130	100	20	560	120	447	166
AC20 base 50/70	70	167	47	398	134	248	143
	90	185	54	451	181	281	182
	110	181	51	436	179	281	182

Table 7.19 Orientation as a function of compaction effort

Mix type	Effort	δ		A	
		Mean	StDev	Mean	StDev
AC12.5 surf PmB (SBS)	90	96	26	2	1
	110	79	26	2	1
	130	85	31	2	0
AC20 base 50/70	70	89	27	3	1
	90	95	20	3	1
	110	77	15	4	1

Table 7.20 Segregation as a function of compaction effort

Mix type	Effort	S_L		$\|S_L\|$	
		Mean	StDev	Mean	StDev
AC12.5 surf PmB (SBS)	90	-2	7	5	4
	110	-4	12	9	7
	130	-4	5	5	4
AC20 base 50/70	70	-4	8	6	6
	90	-2	7	5	4
	110	0	4	3	2

In general, the compaction effort seems to have some influence on the contacts between aggregates. However, the trend observed is not similar for both mixtures. For instance, regarding the AC12.5 surf PmB (SBS) the highest proximity zones were induced for the low number of compaction passes (i.e. 90). Within the same mix, additional passes appear to affect negatively the aggregates contact formation. With regard to the AC20 base 50/70 mix the lowest compaction effort induced the lowest aggregate proximity zones; additional passes appeared to enhance the connectivity between aggregates.

The evaluation of the aggregates orientation was based on the parameters of the predominant angle of aggregate orientation (δ), and the level of severity (A) estimated from the harmonic fit of the orientation spectrum. This evaluation is tabulated in Table 7.19. Although variance is observed the reported (mean) predominant angles tend to approximate 90^o, indicating that aggregates tend to align circumferentially in a radial fashion.

Segregation parameter S_L values range up to about ±10% for most roller-compacted specimens. The degree of segregation decrease as the roller passes considered increases for the AC20 base 50/70 mix, while for the AC12.5 surf PmB (SBS) mix the highest degree of segregation is indentified for the intermediate compaction effort.

Tables 7.21-7.23 tabulate the analysis results regarding the aggregates contact points, orientation and segregation as a function of compaction temperature.

Table 7.21 Contact points as a function of compaction temperature

Mix type	Temp (^oC)	CP		CL		CLB	
		Mean	StDev	Mean	StDev	Mean	StDev
AC12.5 surf PmB (SBS)	130	88	22	503	120	423	141
	160	101	19	570	125	463	179
AC20 base 50/70	135	214	41	552	127	397	129
	145	140	30	305	98	143	97

Table 7.22 Orientation as a function of compaction temperature

Mix type	Temp (^oC)	δ		A	
		Mean	StDev	Mean	StDev
AC12.5 surf PmB (SBS)	130	103	27	2	1
	160	71	21	2	1
AC20 base 50/70	135	85	19	4	1
	145	89	25	3	1

Table 7.23 Segregation as a function of compaction temperature

Mix type	Temp (^oC)	S_L		$\|S_L\|$	
		Mean	StDev	Mean	StDev
AC12.5 surf PmB (SBS)	130	0	8	6	5
	160	-6	8	8	6
AC20 base 50/70	135	-1	6	4	4
	145	-3	7	5	5

From Table 7.21, considerable impact on aggregates contact points is observed for both mixtures in respect to the compaction temperature. However, mixed effect is identified. For the open-graded mix designed with PmB, the elevated compaction temperature (160^oC) considered in this study enhanced aggregate packing. In contrast,

for the conventional bitumen-based mix the increase of the compaction temperature from 135^{o}C to 145^{o}C led to a significant decrease of contact points.

The predominant angle of aggregate orientation (δ) and the level of severity (A) for all compaction temperatures were calculated. According to the results shown in Table 7.22, the orientation angles are significantly different for the different compaction temperatures considered for the AC12.5 surf PmB (SBS) mix, following a decreasing trend from 130^{o}C to 160^{o}C. The average angle values of around 100^{o} and 70^{o} indicate a more random directional distribution of aggregates. In case of the AC20 base 50/70 mix, the average orientation angles combined with the low severity A values indicate that the aggregates are aligned in a circumferential direction.

On the basis of segregation S_L values shown in Table 7.23, the results show no evidence of considerable segregation as the values range up to about ±5% for most roller-compacted specimens. Also, marginal increase of average S_L values is observed for compaction temperature increase for both mixtures.

A detailed statistical analysis was performed to evaluate the significance of the effect of different variables on the roller specimens' internal structure indices. Main compaction parameters were investigated at 95% confidence interval by means of Analysis of variance (ANOVA) test and the results are tabulated in terms of p-values in Table 7.24.

Table 7.24 P-values of roller compaction factors for image indicators in each mixture

Mix type	Factor	Contact points			Orientation		Segregation
		CP	CL	CLB	δ	A	$\|S_L\|$
AC12.5 surf PmB (SBS)	Mode	.951	.387	.285	.452	.111	.988
	Effort	.552	.157	.152	.412	.242	.330
	Temp	.189	.190	.533	.008	.737	.500
AC20 base 50/70	Mode	.785	.899	.885	.822	.345	.168
	Effort	.640	.704	.841	.366	.064	.454
	Temp	.000	.000	.000	.658	.173	.717

The analysis reveals that the compaction temperature affects significantly both the aggregates' contact points and orientation; this was particularly demonstrated for the dense-graded AC20 base 50/70 mix. For this mix, compaction effort also seems to

marginally affect the predominant orientation angle (δ) of aggregates. Moreover, it was found that the compaction mode did not have any statistically significant effect on the internal structure of roller-compacted specimens.

7.3.4 Comparison to field compaction

Field-compacted specimens were also analyzed to evaluate their internal structure's characteristics and to compare them with the laboratory-compacted specimens. The results derived from the image analysis regarding the contact points, orientation and segregation are summarized in Tables 7.25-7.27, respectively.

Table 7.25 Contact points of field cores

Mix type	CP		CL		CLB	
	Mean	StDev	Mean	StDev	Mean	StDev
AC12.5 surf 50/70[a]	99	15	178	34	43	13
AC12.5 surf PmB (SBS)	78	13	431	81	307	98
AC20 base 50/70	89	14	157	24	40	16

Table 7.26 Orientation of field cores

Mix type	δ		A	
	Mean	StDev	Mean	StDev
AC12.5 surf 50/70[a]	89	16	6	3
AC12.5 surf PmB (SBS)	90	12	8	3
AC20 base 50/70	88	17	6	4

Table 7.27 Segregation of field cores

Mix type	S_L		$\|S_L\|$	
	Mean	StDev	Mean	StDev
AC12.5 surf 50/70[a]	2	7	6	2
AC12.5 surf PmB (SBS)	0	7	6	2
AC20 base 50/70	-1	9	6	5

Examining the results, it can be argued that the variation of contact points observed between the mixtures studied, with the AC12.5 surf PmB (SBS) mix presenting significantly higher proximity zones between aggregates compared to the other mixtures, may be attributed to the mix gradations. However, orientation angle data indicate that

field compaction induces, in general, concentric orientation of the aggregates ($\delta \simeq 90^{o}$) for all mixtures. Furthermore, the spatial distribution of aggregates in field cores presented low levels of segregation, as the S_L values ranged up to ±6% independent of the mixture studied. In light of the above, it can be concluded that the field compaction produces similar internal structure in the paving mixtures studied.

To highlight the differences in microstructure induced due to various compaction methods, both lab and field, box-plot graphs were developed for each image-based indicator. Figures 7.8-7.10 illustrate the contact-based indicators with respect to the compaction methods.

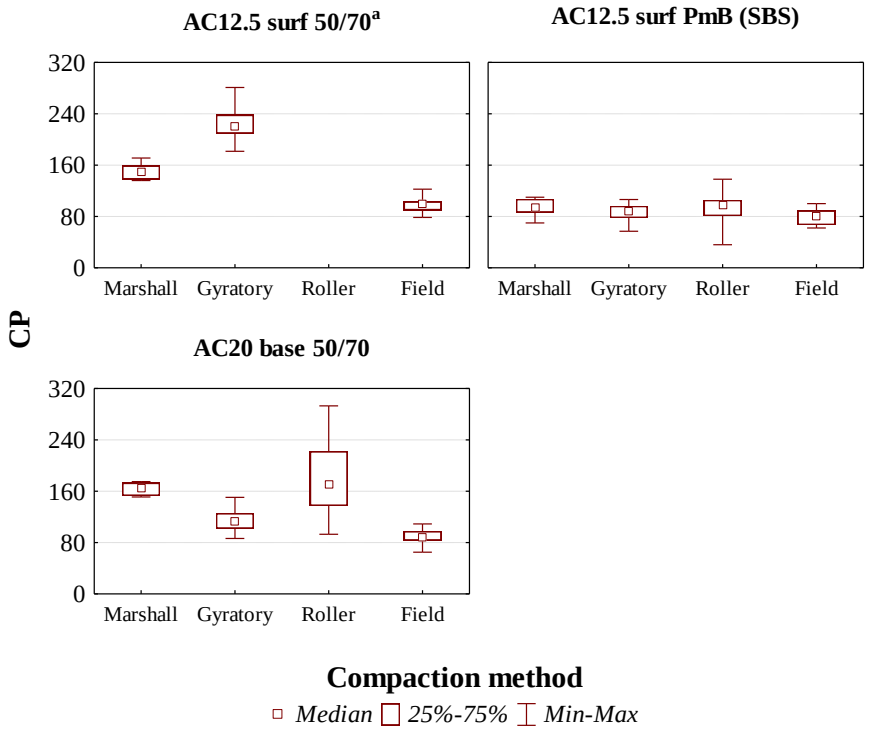

Fig. 7.8 Contact points as a function of compaction methods

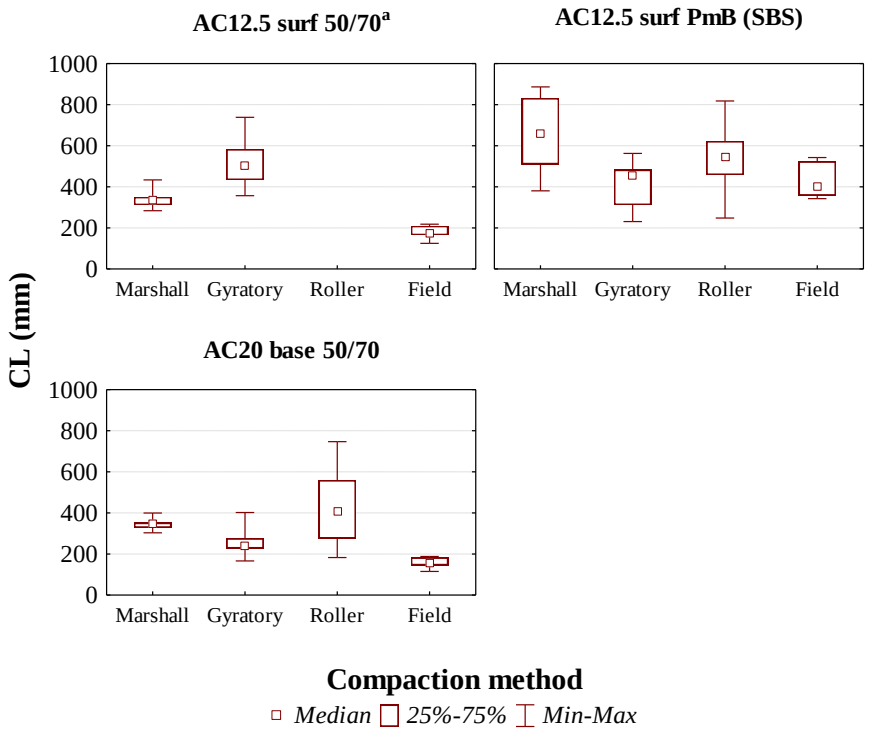

Fig. 7.9 Contact length as a function of compaction methods

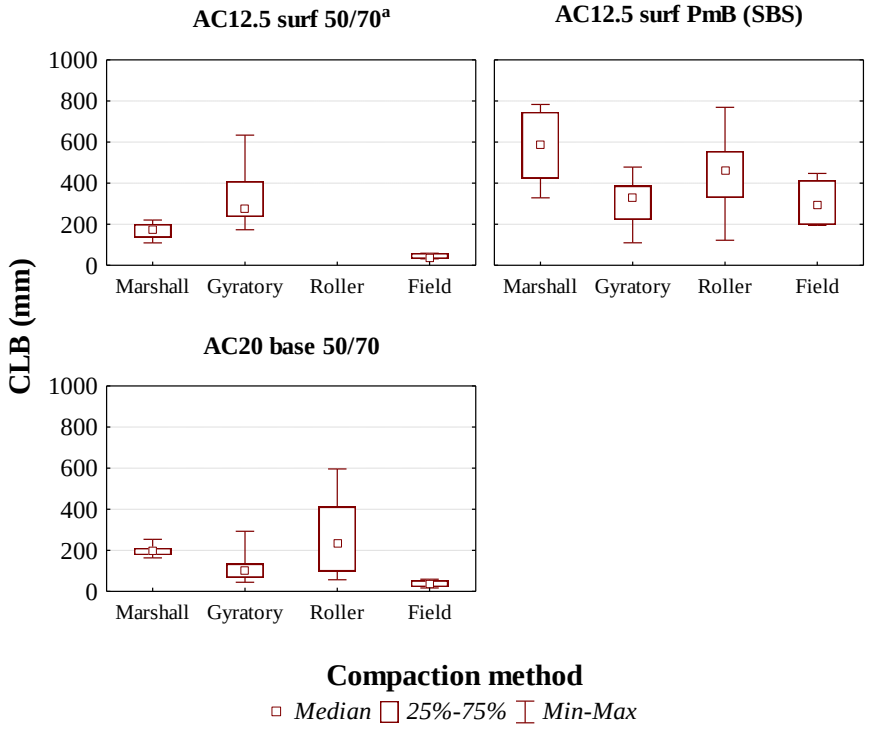

Fig. 7.10 Contact length in branches as a function of compaction methods

Clear differences in the aggregates contact-based indicators were identified between the field and laboratory compaction methods. Results indicated fewer contacts between aggregates in field-compacted specimens relative to laboratory-compacted specimens independent of the mixture type. In most cases, the aggregates proximity zones within the Marshall specimens appear to deviate from field cores more than the other laboratory-compacted specimens. Conversely, the gyratory specimens of mixtures AC12.5 surf PmB (SBS) and AC20 base 50/70 seem to better approximate the aggregate contacts identified within the field cores. Also, the aggregate structure parameters related to the roller-compacted specimens falling in-between and appear to be in some extent comparable to those of field cores, although the results show some variations.

Figures 7.11-7.12 illustrate the orientation indicators with respect to the compaction methods. Moreover, the segregation results are illustrated in Fig. 7.13.

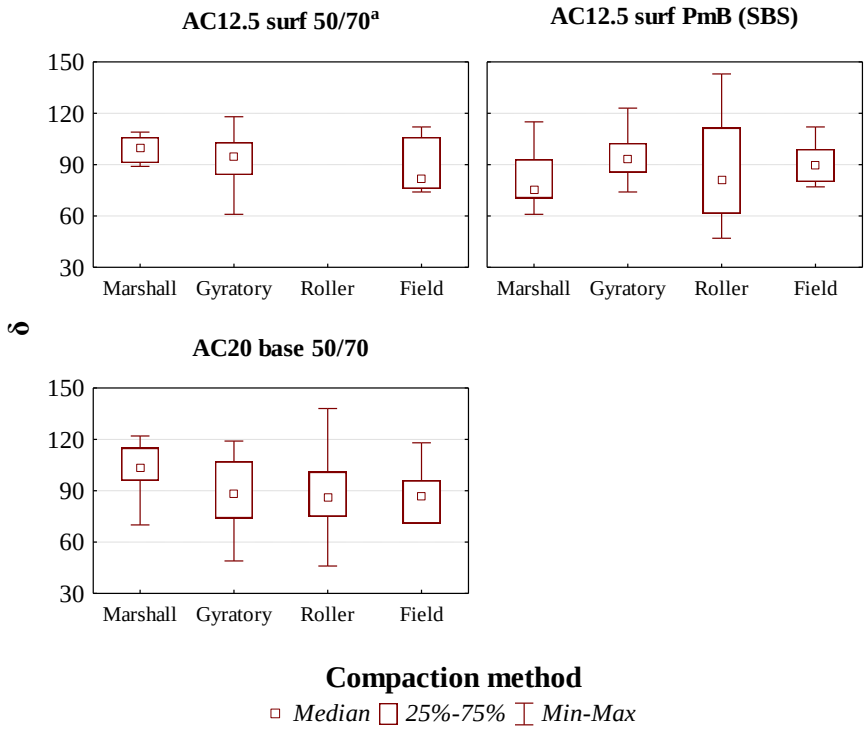

Fig. 7.11 Orientation angle (δ) as a function of compaction methods

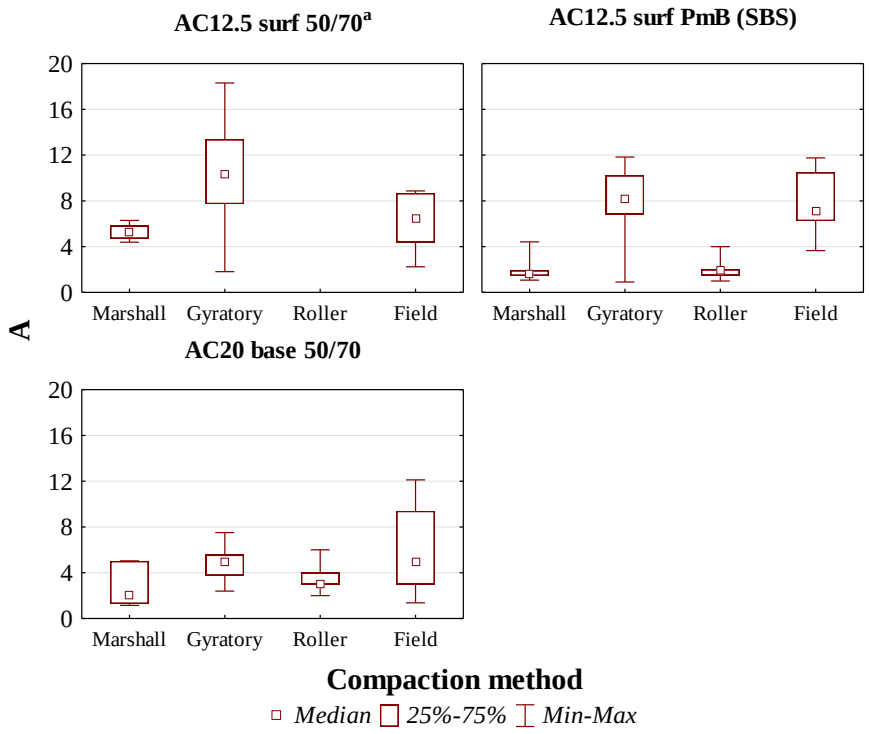

Fig. 7.12 Orientation severity (A) as a function of compaction methods

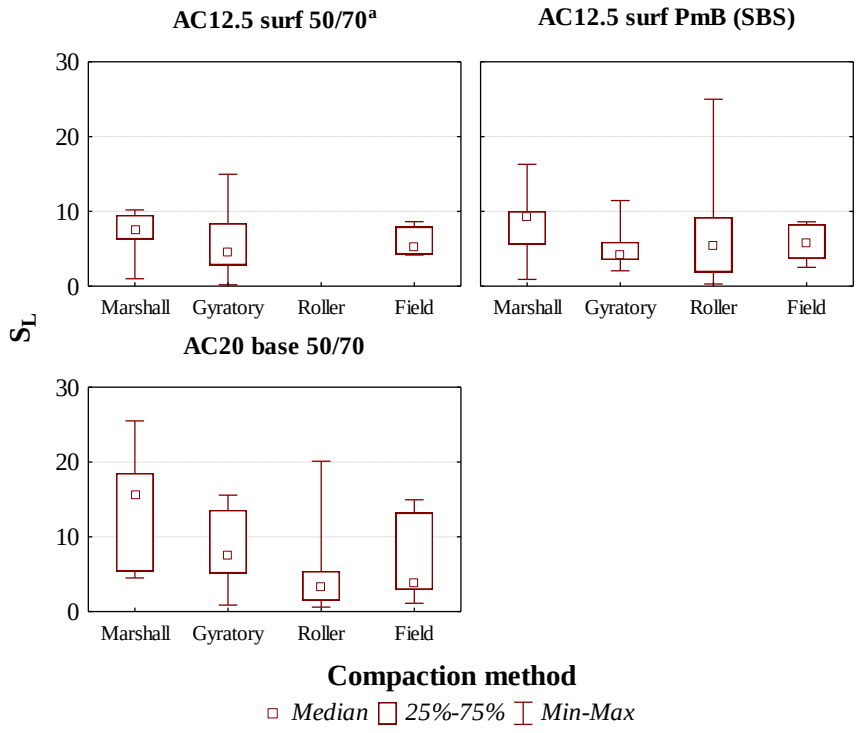

Fig. 7.13 Segregation (S_L) as a function of compaction methods

Comparative evaluation of the predominant angle (in terms of the median values) of approximately 86^o of field cores relative to the various laboratory compaction methods indicates that this aggregate orientation is most closely reproduced by the gyratory and roller compactors. Also, the severity A results (with a median value 6.1) indicated that field cores show preferred orientation towards the specified predominant angle of 86^o. This trend seems to be better represented from the gyratory compaction method with an average severity of 7.8. Both Marshall and roller show low severity values (close to 3), which imply that these methods have lower tendency to orient the aggregates towards particular angle.

Regarding the spatial distribution of aggregates, the overall results indicate that roller compaction better reproduced the field compaction in terms of the S_L values. Gyratory compaction seems to produce more segregated specimens than field cores, particularly with increasing NMAS, while more segregation of aggregates caused by using the Marshall compactor. It can be argued that the segregation observed in gyratory-compacted specimens is induced, mainly, from the rotational movement the gyratory. Also, it can be plausibly hypothesized that the specimen preparation plays some role in the spatial distribution of aggregates. This is more obvious for the mould-based compaction methods (namely gyratory and Marshall). For instance, when filling the moulds with asphalt material, clusters of coarser aggregates may be positioned across its perimeter without being able to move due to the mould wall restrictions. Correspondingly, it should be mentioned that the coring process in terms of the locations selected along the surface of the slab may has affected the results regarding the roller-compacted specimens.

It is worth noting that the above results correspond to the full spectrum of compaction variables considered for each laboratory method. In other words, various combinations of compaction parameters are included within this analysis. To find out the combination of compaction parameters that offer the best approximation of the aggregate structure induced by the field compaction a more detailed investigation is needed.

Figure 7.14 shows the comparison of Marshall and field compaction effect on each internal structure indicator. Line plots show the effect of the compaction temperature on the mean values of Marshall specimens' contact points, orientation and segregation,

while a horizontal line represents the field compaction as the mean value of field core specimens.

Accordingly, the comparative evaluation between the gyratory and field compaction is illustrated in Fig. 7.15. For this case, taking into consideration the statistical analysis results which demonstrated that the specimen (initial) diameter and angle of gyration were the most significant parameters in influencing the aggregate structure of gyratory specimens, evaluation of the interaction of these key parameters relative to the field compaction-based internal structures was performed (Georgiou et al. 2016). Also, the mixed effect of compaction temperature and effort on the internal structure of roller specimens relative to the field cores is illustrated in Fig. 7.16.

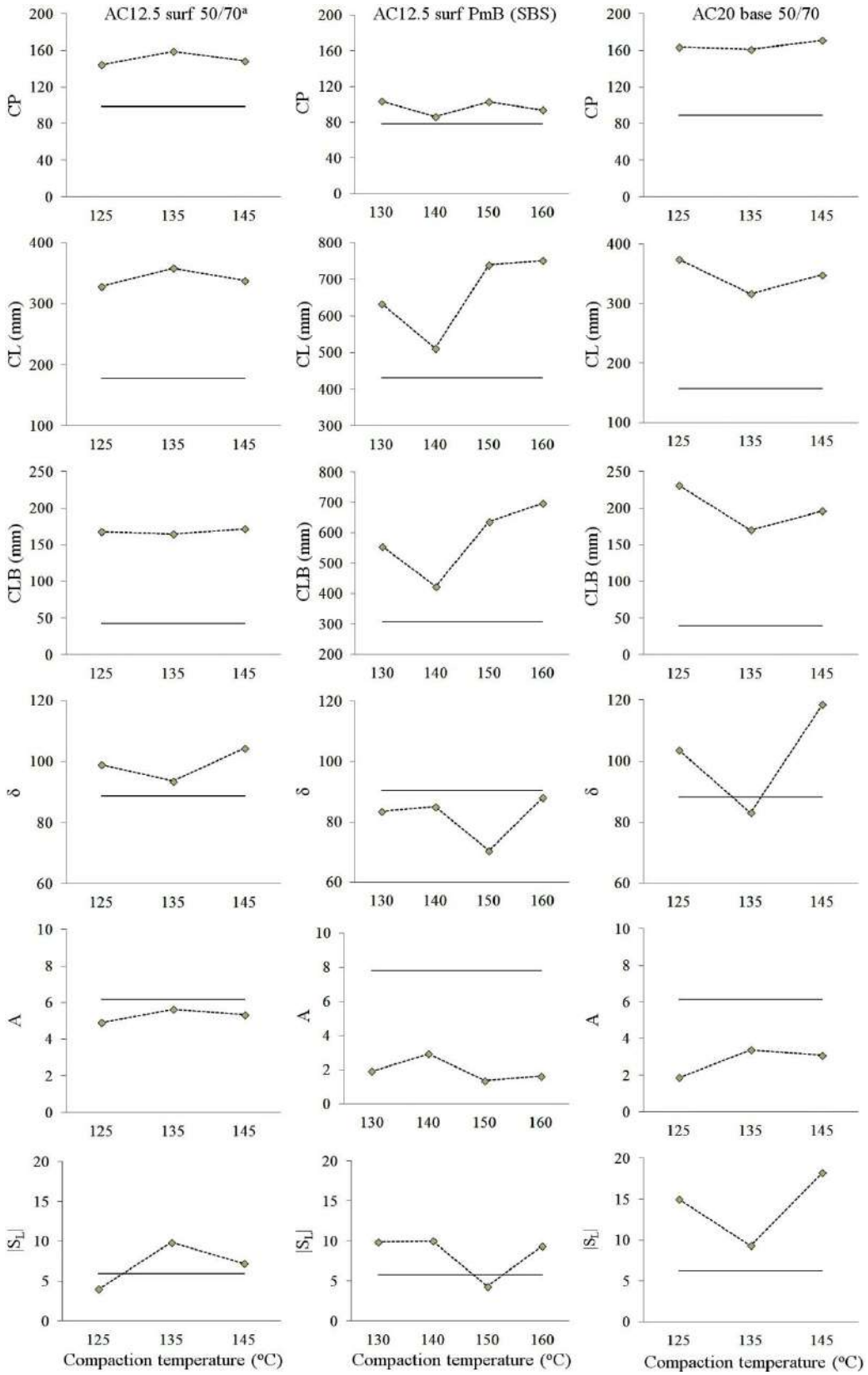

Fig. 7.14 Field and Marshall specimens' internal structure indicators

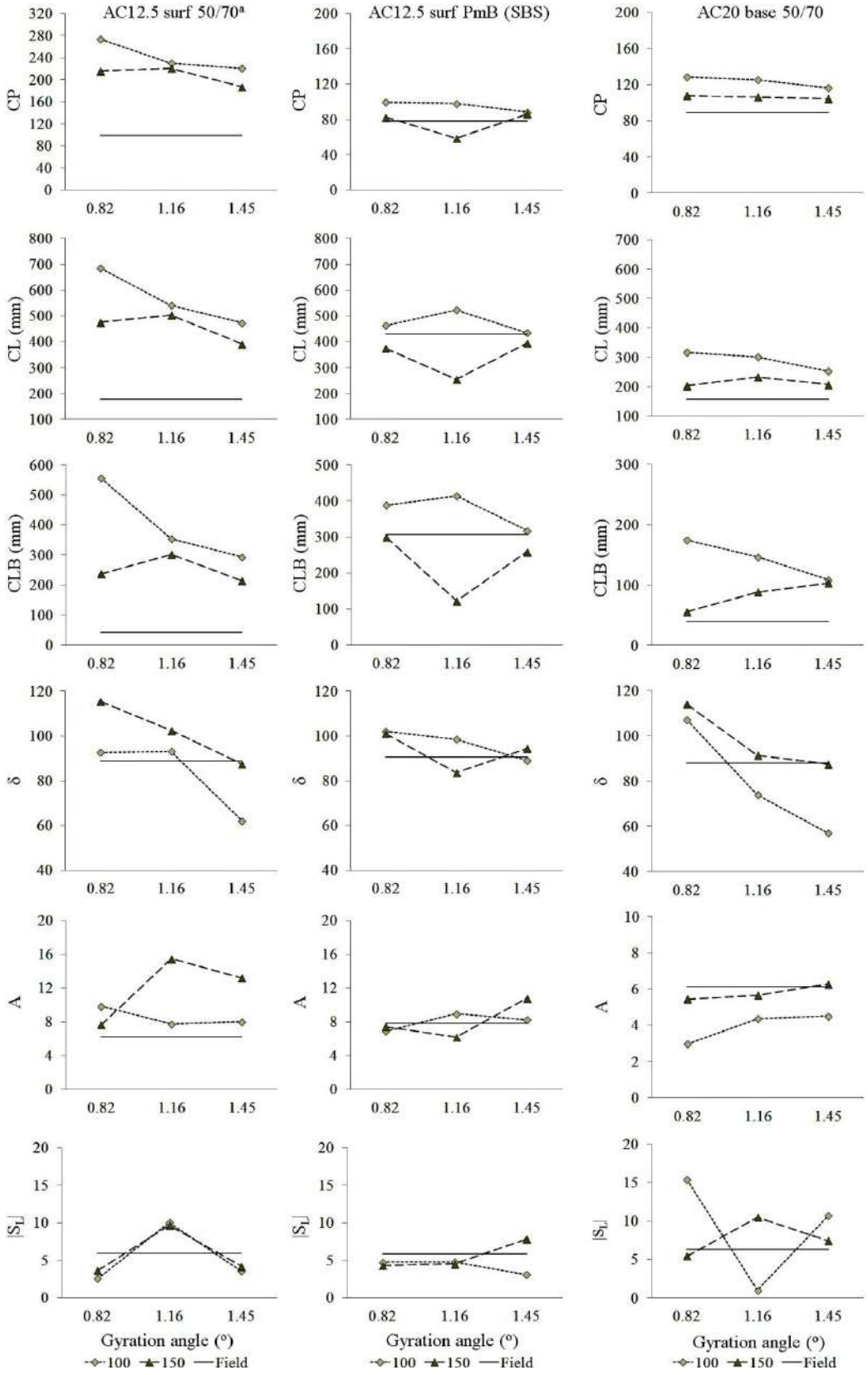

Fig. 7.15 Field and gyratory specimens' internal structure indicators

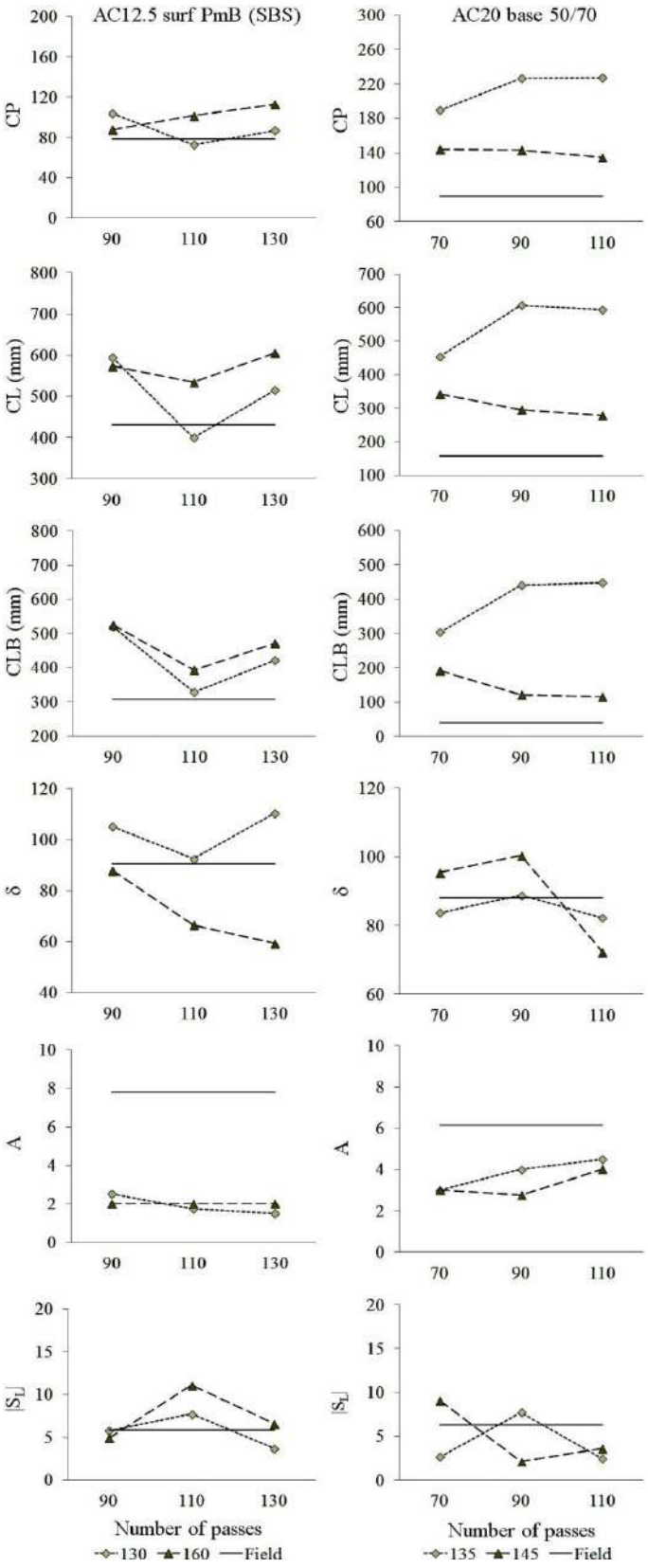

Fig. 7.16 Field and roller specimens' internal structure indicators

Overall, the results indicate that different compaction methods and regimes induce variable microstructures. Within each compaction method, variation of the compaction regime (temperature or/and effort) it appears to affect the mechanism related to the aggregate mobility during compaction and the corresponding aggregate packing formation. Researchers argue that mastic (bitumen and mineral filler) viscosity is the controlling factor for particle arrangement and packing level (Sefidmazgi and Bahia 2014). This explains, for instance, the diversity of aggregate packing evolution with compaction temperature increase for the dense-graded mixtures compacted using the Marshall compaction method. Particularly, at the same compaction temperature (i.e., 135^{o}C) the maximum and minimum packing level is achieved, respectively, for the AC12.5 surf 50/70^{a} and AC20 base 50/70 mixtures. This further indicates that for each mixture varying compaction regimes may be suggested, due to the impact of mastic viscosity and compaction conditions on aggregate structure, to simulate, as closely as possible, the aggregate structure induced by the field compaction.

Comparing Marshall specimens and field cores, the results indicate differences between aggregate contacts, as shown in Fig. 7.14. Particularly, more stone-to-stone contacts are identified in Marshall specimens. However, for some compaction temperatures the differences shall be reduced. For instance, compaction at 135^{o}C produces Marshall specimens that appear to approximate the aggregates contacts of field cores for the AC12.5 surf 50/70^{a} and AC20 base 50/70 mixtures. Compaction at 140^{o}C is better reproducing the aggregates contacts of field cores for the AC12.5 surf PmB (SBS) mix. Regarding the aggregates orientation, the best simulation to the field cores in terms of the parameters δ and A was achieved again for the temperatures discussed earlier. Mixed results were obtained with respect to the segregation analysis. Compaction at 145^{o}C, 150^{o}C and 135^{o}C induce similar aggregate spatial distribution of Marshall specimens relative to the field cores, respectively, for the AC12.5 surf 50/70^{a}, AC12.5 surf PmB (SBS) and AC20 base 50/70 mixtures. Summarizing, it can be argued that compaction at 135^{o}C for the AC12.5 surf 50/70^{a} and AC20 base 50/70 mixtures along with compaction at 140^{o}C for the AC12.5 surf PmB (SBS) mix results in the best approximation of field compaction.

Moreover, measurements of aggregate contact points have shown that, in most cases, gyratory specimens have more stone-to-stone contacts than field cores. This is more pronounced with respect to AC12.5 surf 50/70[a] mix, as illustrated in Fig. 7.15. However, differences are not significant for the remaining mixtures. The results indicate that cut/cored- from larger 150mm- gyratory specimens compacted at angle 1.45^{o} had the closest approximation to the aggregates contacts of field cores. Regarding the orientation angle, the best simulation to the field cores was achieved again following cutting/coring process of gyratory-compacted specimen at angle 1.45^{o}. Segregation analysis showed that compaction at angles 0.82^{o} and 1.45^{o} along with cutting/coring the 150mm specimens gave the best results in duplicating the field conditions. Overall, the results above demonstrated that the 1.45° angle of gyration along with coring a 150mm - to obtain a 100mm- diameter specimen would better simulate the internal structure of field cores.

Regarding the roller-compacted specimens, the results indicate some differences in terms of aggregate contacts compared to the field cores. However, there are several combinations which approximate the aggregates contacts occurrences of field cores, as demonstrated in Fig. 7.16. For instance, specimens subjected to compaction effort of 110 roller passes at temperature of 130^{o}C seem to better reproduce the internal structure of field cores for the AC12.5 surf PmB (SBS) mix. Field conditions may be also reproduced for compaction at 160^{o}C and 90 roller passes. With regard to the AC20 base 50/70 mix, the compaction effort of 110 passes along with compaction temperature of 145^{o}C was found to be the best compaction regime in approximating the aggregate contacts of field cores. Considering the low A values, it can be argued that the aggregates' orientation within the roller specimens of both mixtures is comparable to that of the field cores for the basic compaction regimes discussed earlier. Additionally, it could be stated that for the case of AC20 base 50/70 mix, specimens subjected to compaction effort of 90 passes at temperature of 135^{o}C also represent the aggregates orientation distribution within the field cores. Segregation analysis showed that using the roller compactor several combinations may be followed to approximate the field compaction in terms of the S_L values. This manifests that roller and field compaction methods induce similar aggregate spatial distribution. Based on the above, it can be

argued that compaction at 130^{o}C and 145^{o}C along with compaction effort of 110 passes better reproduces the aggregate structure induced by the field compaction. Alternatively, field conditions may be also approximated for compaction at 160^{o}C and 90 roller passes, and compaction at 135^{o}C and 90 roller passes, respectively, for the AC12.5 surf PmB (SBS) and AC20 base 50/70 mixtures.

8. Relationship between mixture internal structure and mechanical properties

8.1 Introduction

In a follow up level, this Chapter discusses the interrelation between the asphalt mix microstructure and mechanical properties. Particularly, the relationship between HMA stiffness (Chapter 5), rut resistance (Chapter 6) and microstructure properties in terms of image analysis-based indices (Chapter 7) is investigated. To achieve this objective the analysis methodology followed consists of simple correlations along with regression models, particularly General Linear Models (GLM). In the following sections, the analysis results are demonstrated and discussed.

8.2 Results and discussion

8.2.1 Effect of aggregate contact points on the mechanical properties

The correlation between the stiffness modulus and high temperature IDT strength and aggregates contacts in terms of the various microstructure indices for the Marshall specimens is shown, respectively, in Fig. 8.1 and 8.2. To clearly demonstrate the impact of connectivity between aggregates on the asphalt specimens' mechanical properties, a linear trend was fitted to the experimental results for each mixture. The correlation plots show that the increase in the number of proximity zones between aggregates (i.e., CP indicator) increases the stiffness modulus. In general, the results show variation and hence the R^2 values are very low, however the general trend observed seems to be reasonable. Similar findings were found with respect to IDT strength and aggregates' contact points. It is worth mentioning that the enhanced stiffness and rut resistance behavior of Marshall specimens due to the higher aggregate packing is more pronounced for the AC12.5 surf PmB (SBS) mixture, which consists of a semi-open aggregate gradation. Hence, for this mixture it seems that the stiffness and rut resistance performance due to Marshall compaction is controlled by the development of mechanical interlocking of the aggregate structure through stone-to-stone coarse aggregate contacts.

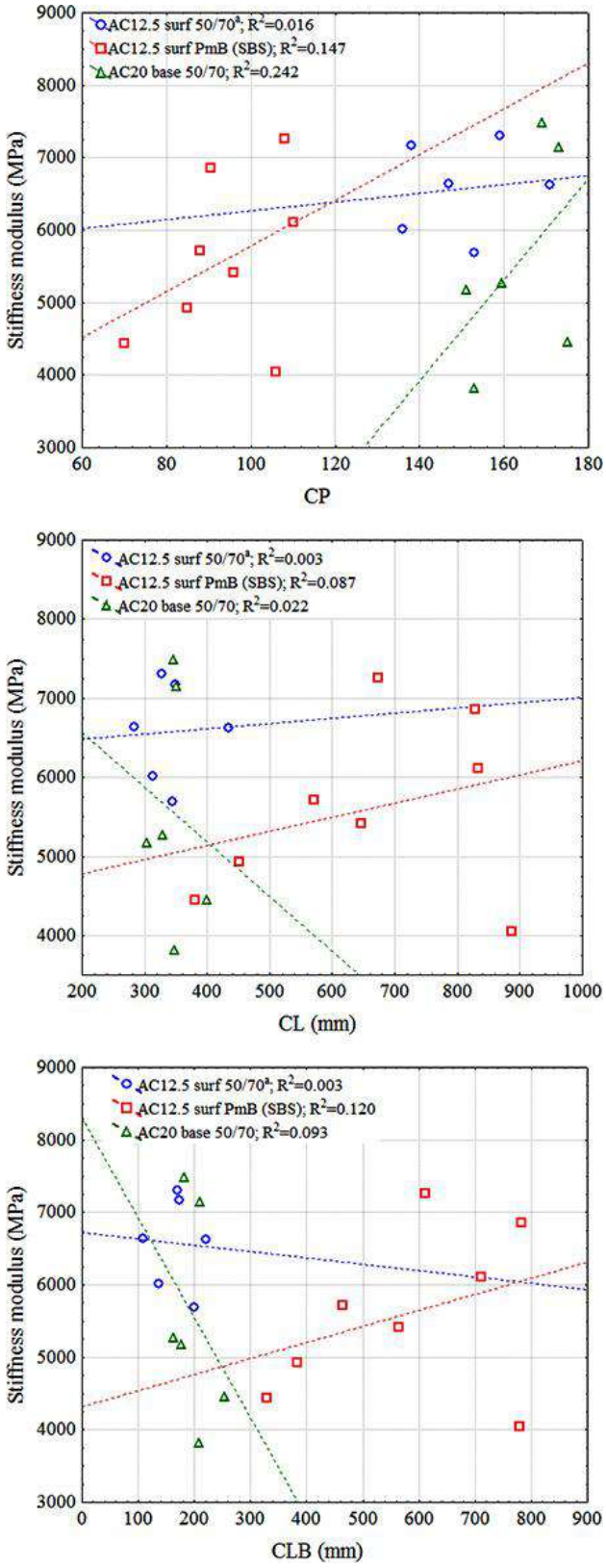

Fig. 8.1 Correlation of stiffness with indicators of aggregates' contacts for Marshall specimens

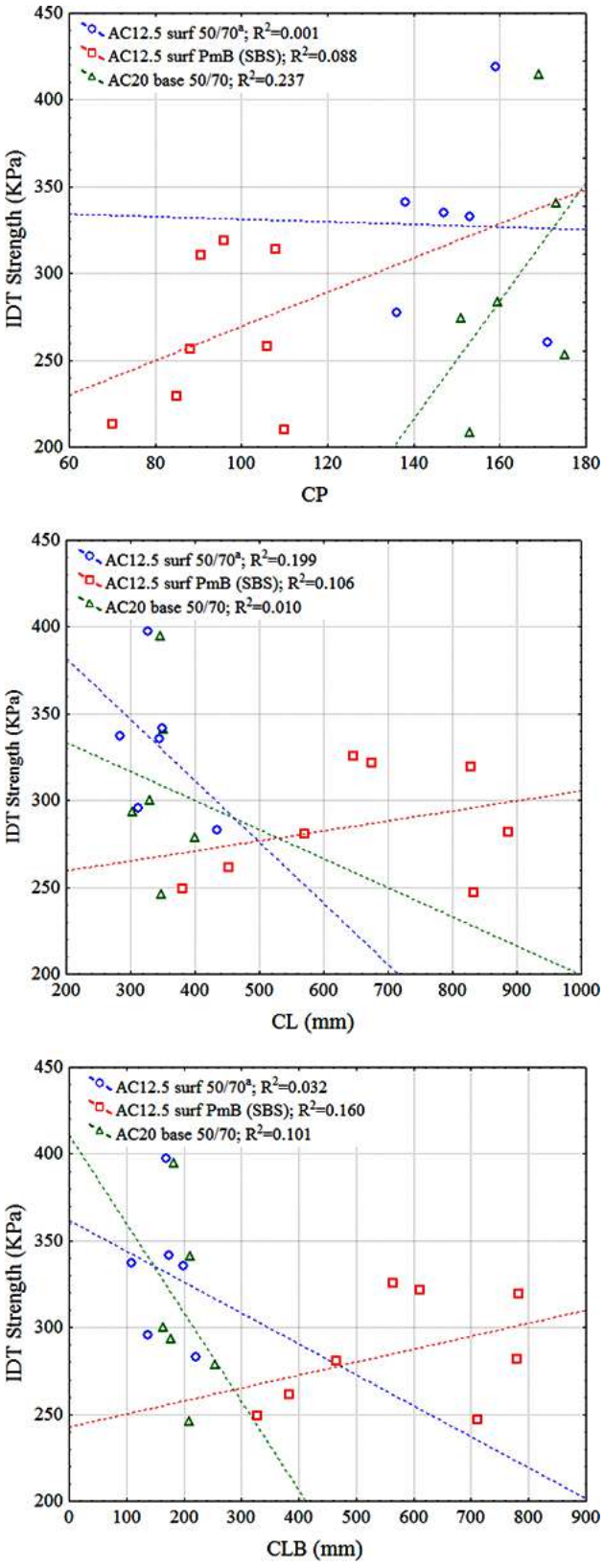

Fig. 8.2 Correlation of IDT strength with indicators of aggregates' contacts for Marshall specimens

Accordingly, Fig. 8.3-8.8 illustrate the correlations between the stiffness and IDT strength and the indicators of aggregates' contacts for the gyratory-, roller- and field-compacted specimens, respectively.

Regarding the gyratory specimens, the results indicate higher correlations compared to the Marshall specimens between the mechanical properties and indicators related to aggregates' contacts. This is supported from the increased R^2 values independent of the indicator considered. Hence, it is arguable between CP, CL and CLB, which index better characterizes the performance of mixtures. It is interesting to note that for some mixtures the stiffness modulus and high temperature IDT strength is very sensitive to the variation of proximity zones between aggregates. For instance, it can be seen that the increase of contact points from around 90 to 130 for the AC20 base 50/70 mix leads to an increase of modulus and IDT strength, respectively, from 6700 MPa to 11700MPa and 350 KPa to 490 KPa. Therefore, it can be concluded that the increase of aggregate packing and interlocking in the gyratory specimen results in significantly improving its mechanical performance.

No discernible trend is observed regarding the roller-compacted specimens of the various mixtures. Significant scatter of results is observed for both the aggregate contacts and mechanical properties within each mixture. However, by examining the contact points occurrences between the mixtures studied, it appears that the higher stiffness modulus and IDT strength values of AC20 base 50/70 are associated to the higher number of proximity zones identified.

Comparing the various compaction methods, the highest correlation between micro-structural aggregate contacts indices and mechanical properties of mixtures was observed for the field compaction. On the basis of the R^2 values obtained, variance of results up to 87% can be explained. The correlation plots show that there is an increasing trend between the aggregates contacts and stiffness-IDT strength especially for the AC12.5 surf 50/70[a] and AC20 base 50/70 mixtures. Results also demonstrate that a change of contact length indicators significantly changes the stiffness and rut resistance characteristics of the field-compacted specimens. No meaningful results were obtained with regards to the AC12.5 surf PmB (SBS).

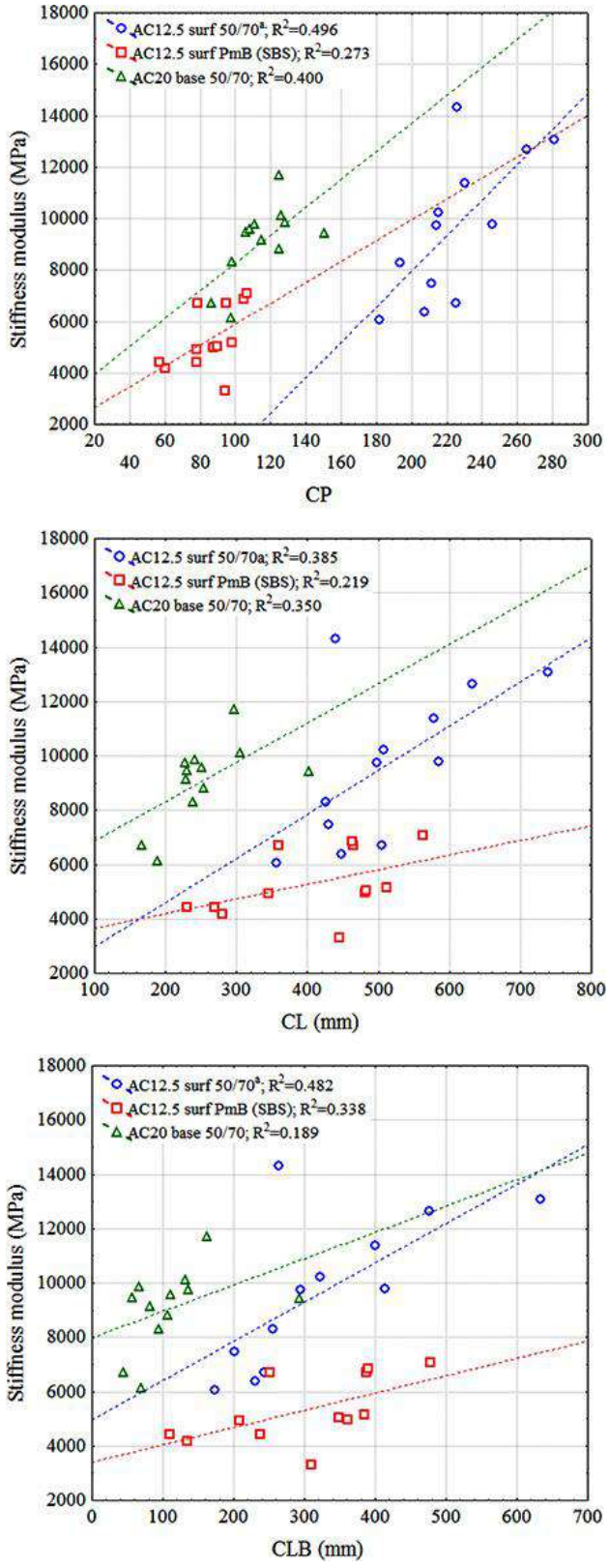

Fig. 8.3 Correlation of stiffness with indicators of aggregates' contacts for gyratory specimens

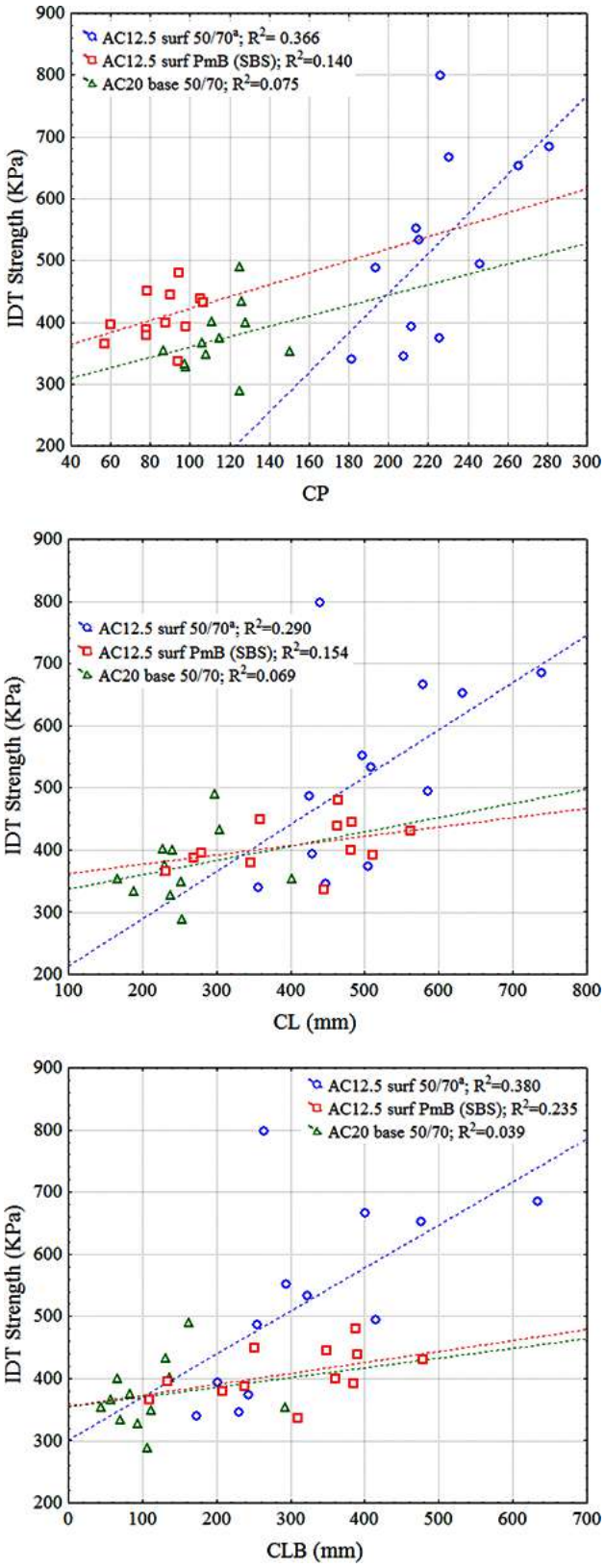

Fig. 8.4 Correlation of IDT strength with indicators of aggregates' contacts for gyratory specimens

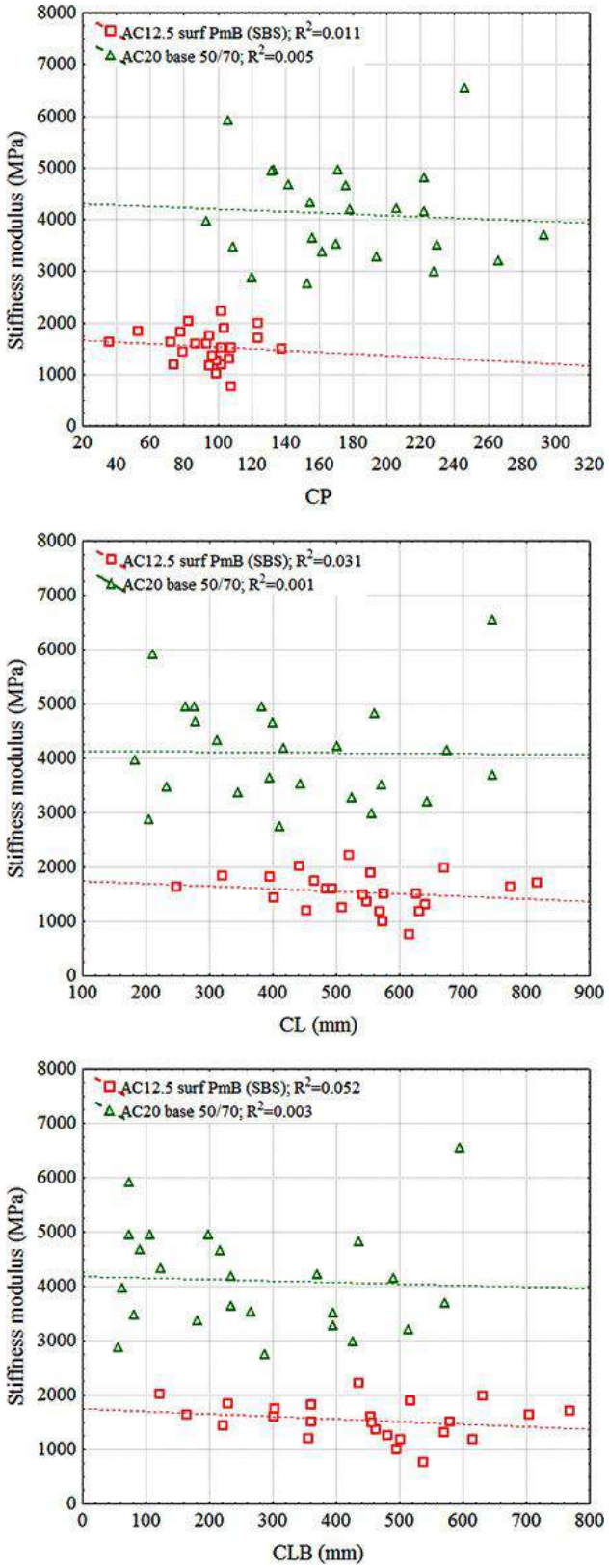

Fig. 8.5 Correlation of stiffness with indicators of aggregates' contacts for roller specimens

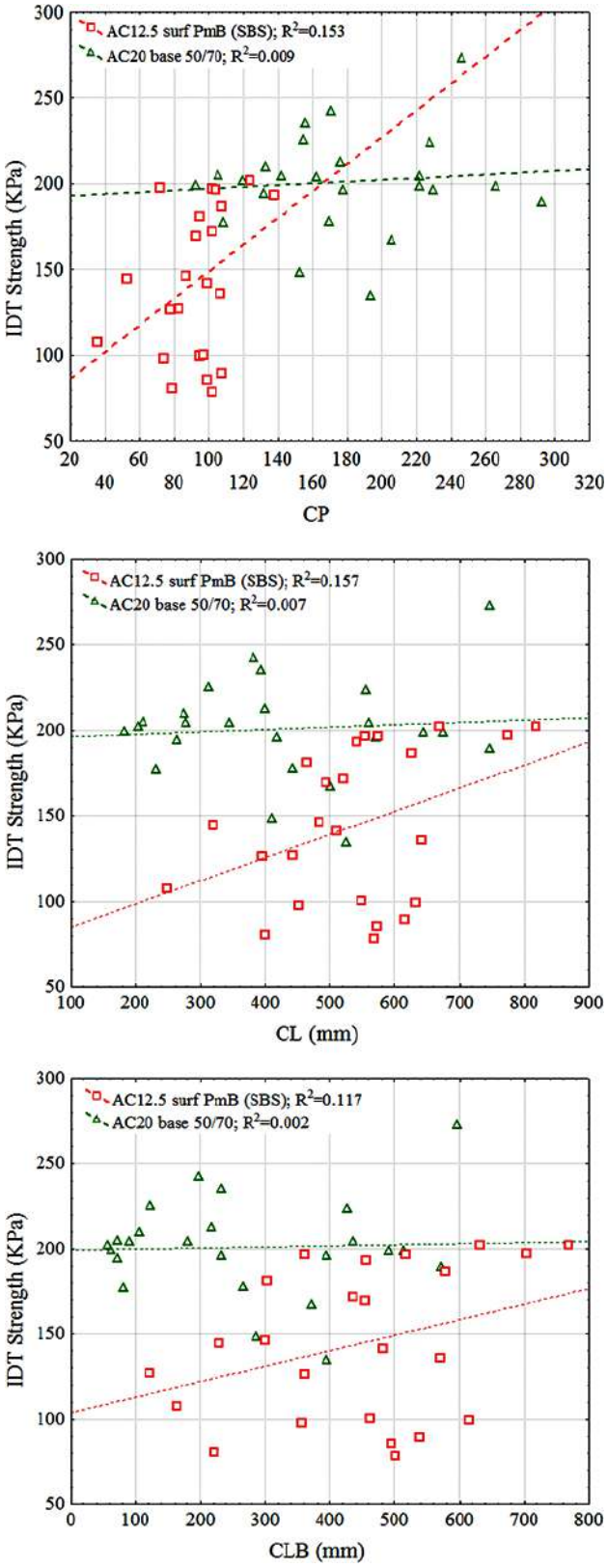

Fig. 8.6 Correlation of IDT strength with indicators of aggregates' contacts for roller specimens

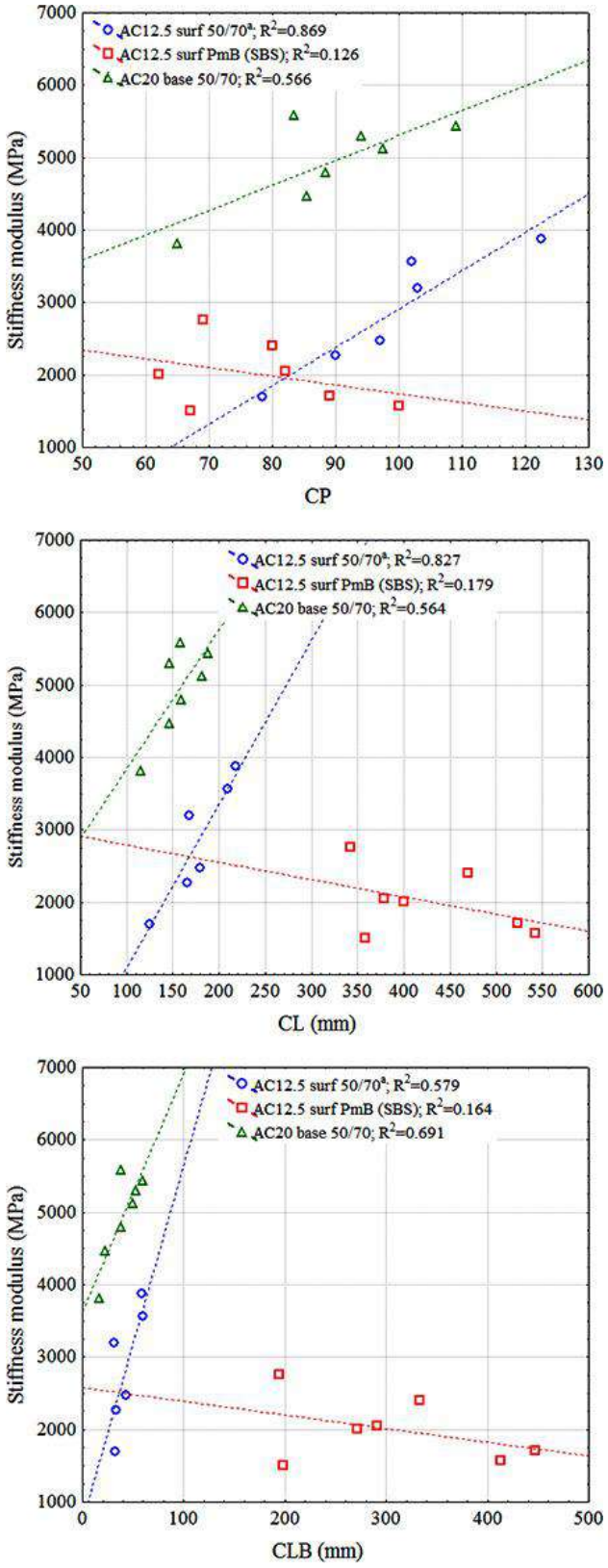

Fig. 8.7 Correlation of stiffness with indicators of aggregates' contacts for field cores

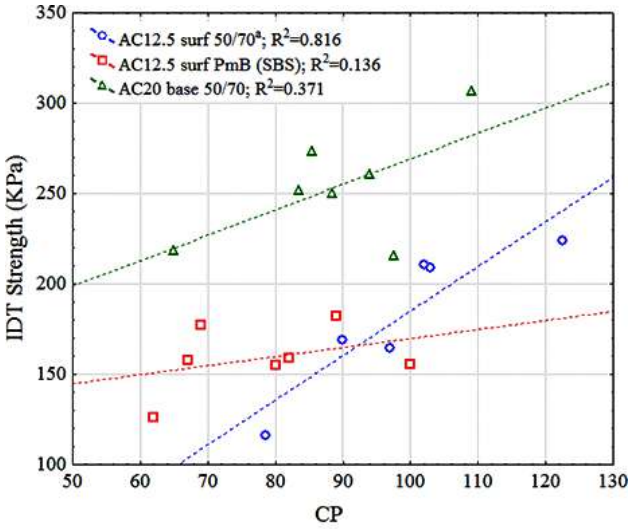

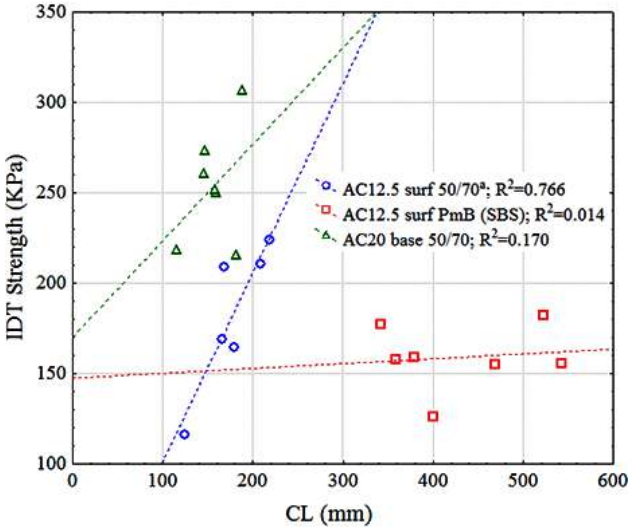

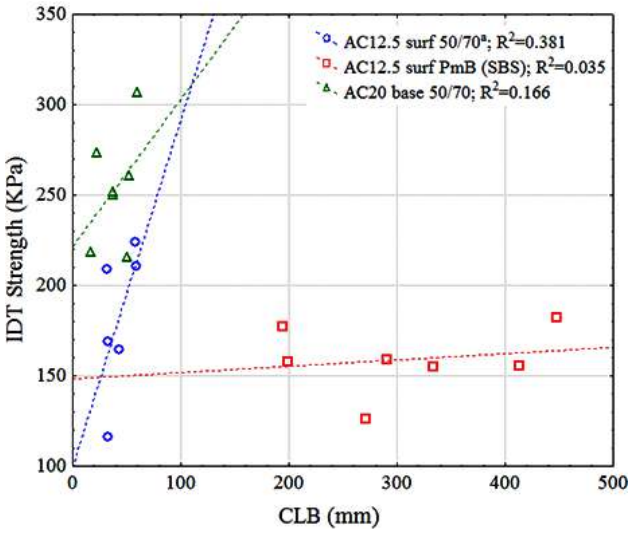

Fig. 8.8 Correlation of IDT strength with indicators of aggregates' contacts for field cores

8.2.2 Effect of horizontal orientation angle on the mechanical properties

The effect of horizontal orientation angle on the stiffness modulus and high temperature IDT strength for the Marshall specimens is shown respectively, in Fig. 8.9 and Fig. 8.10. The results show variation and hence the R^2 values are low; also, mixed effect is observed with respect to the various mixtures. The correlation plots demonstrate an increasing trend between the predominant orientation angle δ and mechanical properties for the AC12.5 surf 50/70[a] and AC20 base 50/70 mixtures; on the contrary a decreasing trend is shown for the AC12.5 surf PmB (SBS). However, it is interesting to note that the lowest values of stiffness and IDT strength for all mixtures correspond to specimens with aggregates orientated in circumferential direction (i.e., $\delta=90^{o}$). The range of A values of each mixture is very narrow and hence no valid conclusions can be drawn.

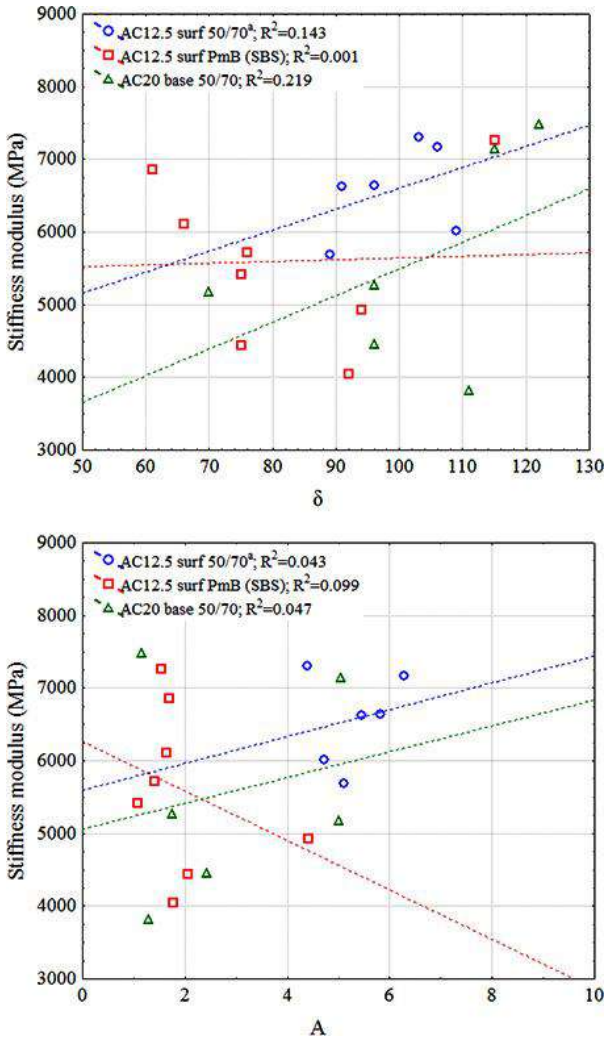

Fig. 8.9 Correlation of stiffness with indicators of aggregates' orientation for Marshall specimens

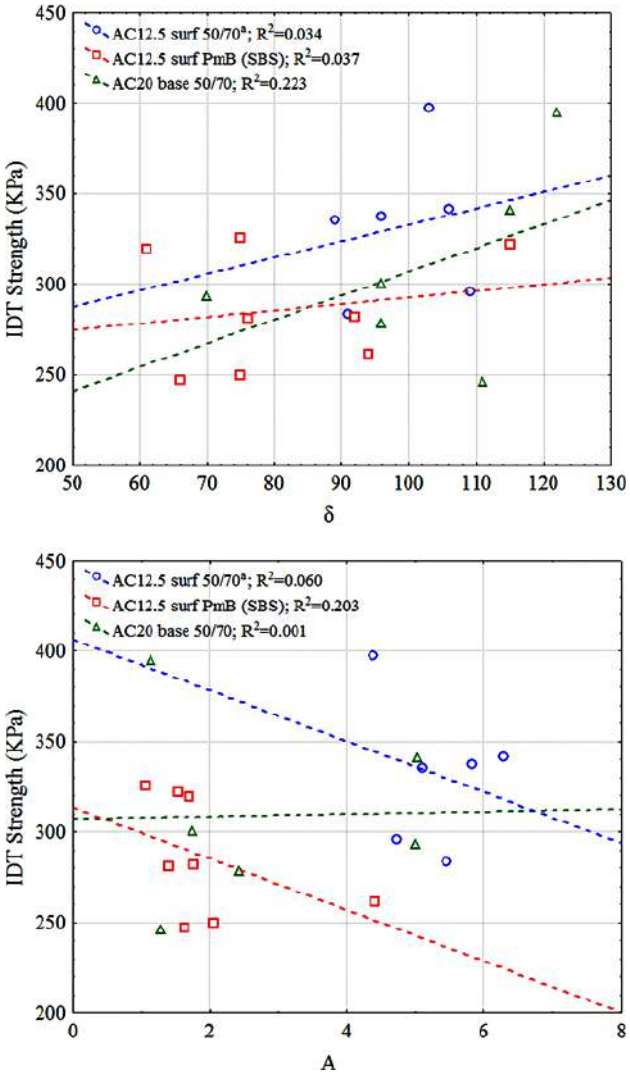

Fig. 8.10 Correlation of IDT strength with indicators of aggregates' orientation for Marshall specimens

The correlation between the stiffness and IDT strength and aggregates' orientation indicators, respectively, for the gyratory-, roller- and field-compacted specimens are illustrated in Fig. 8.11-8.16.

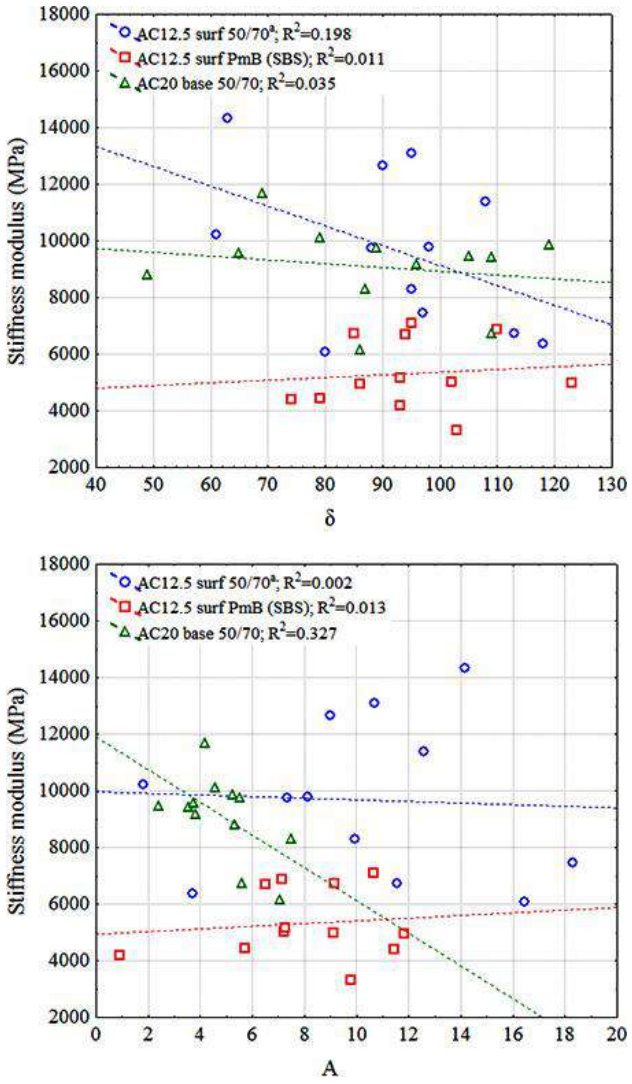

Fig. 8.11 Correlation of stiffness with indicators of aggregates' orientation for gyratory specimens

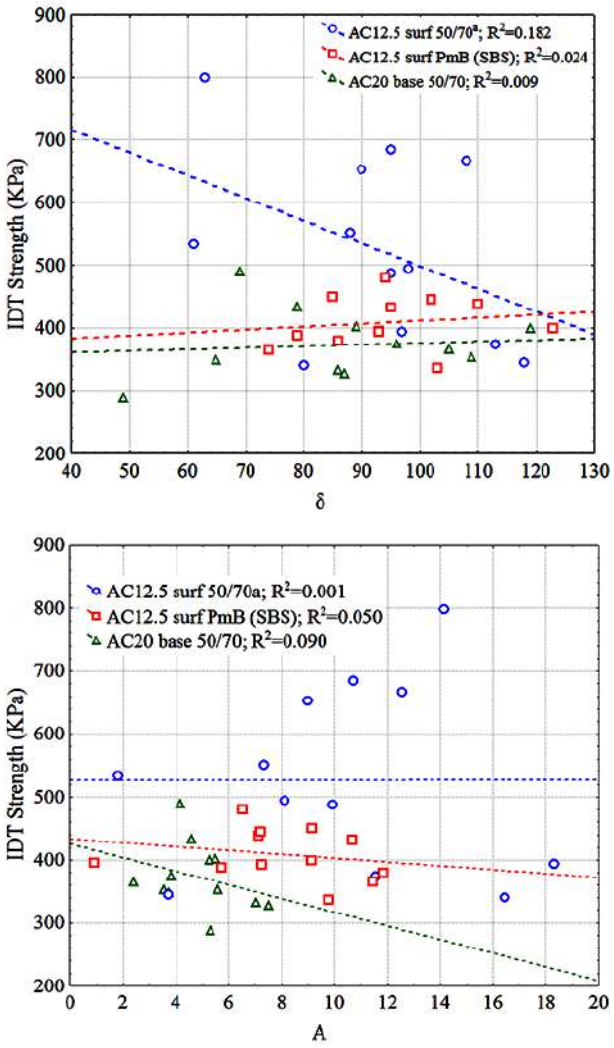

Fig. 8.12 Correlation of IDT strength with indicators of aggregates' orientation for gyratory specimens

Regarding the gyratory specimens, the results show scattering for all mixtures; this explains the low R^2 values obtained. Also, mixed effect is again observed with respect to the various mixtures. The correlation plots between the predominant orientation angle δ and stiffness- IDT strength show a decreasing trend for the AC12.5 surf 50/70^a as opposed to the AC12.5 surf PmB (SBS) mix. Moreover, variation of orientation angles in the specimens of AC20 base 50/70 mix seems to marginally influence their stiffness and rut resistance properties. As with Marshall specimens, the results do not reveal any specific trend regarding the severity A and stiffness- IDT strength values of gyratory specimens.

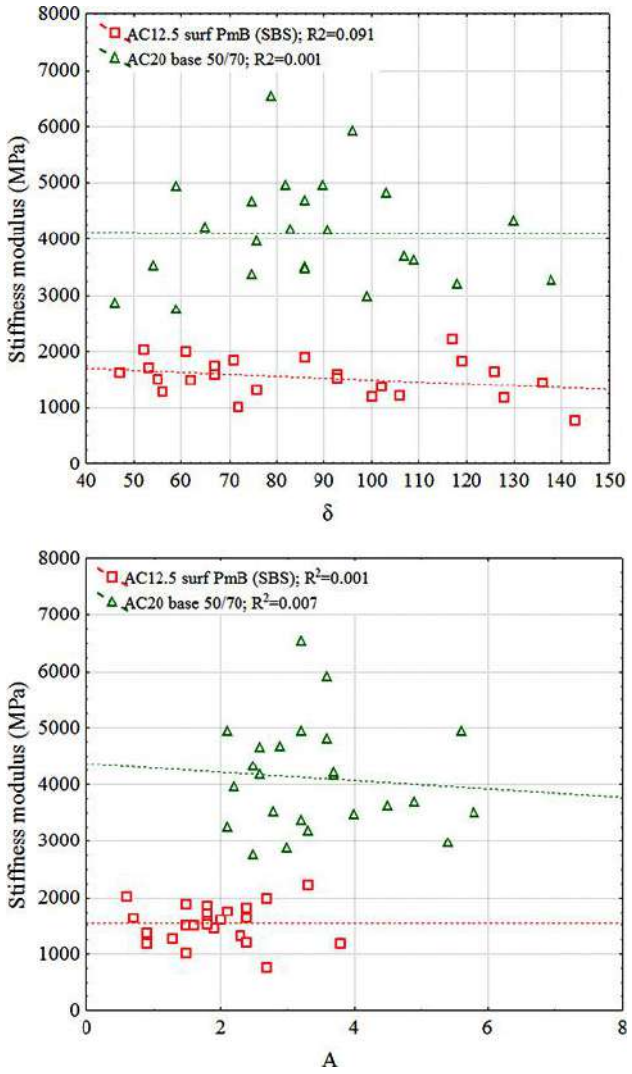

Fig. 8.13 Correlation of stiffness with indicators of aggregates' orientation for roller specimens

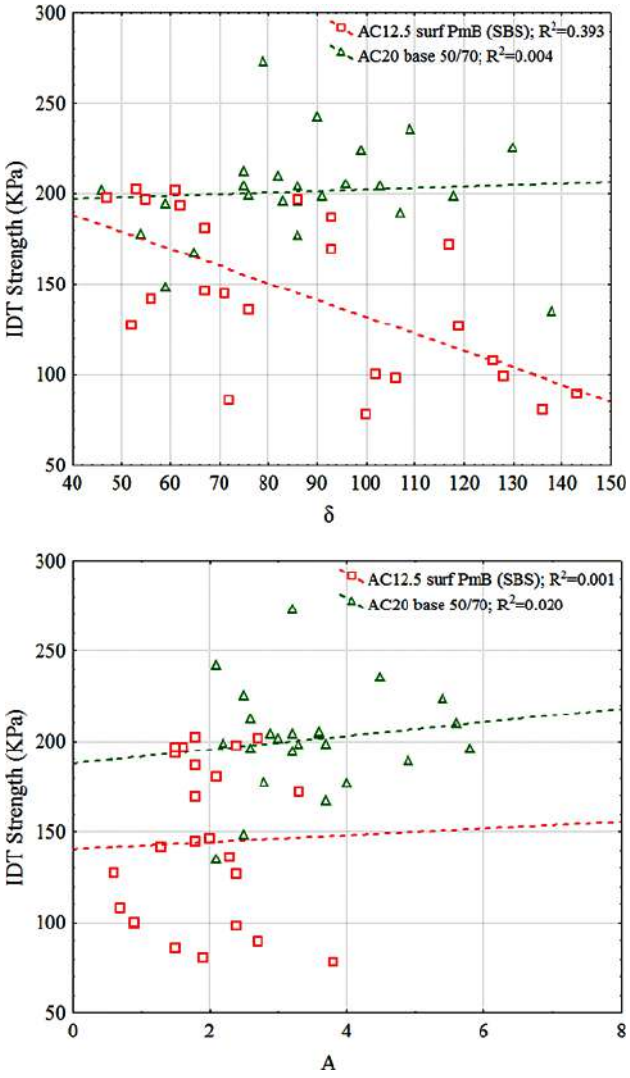

Fig. 8.14 Correlation of IDT strength with indicators of aggregates' orientation for roller specimens

Regarding the roller specimens, no clear trend can be identified between the mechanical properties and aggregates' orientation angles. Although directional distribution of aggregates in roller specimens varies widely, as also supported from the narrow range of severity A values, this variation does not seem to significantly influence the stiffness modulus of the various mixtures. This explains the almost zero values for the R^2. On the contrary, the results demonstrate that there is some influence of the preferred orientation angle on the high temperature IDT strength of the AC12.5 surf PmB (SBS) mix.

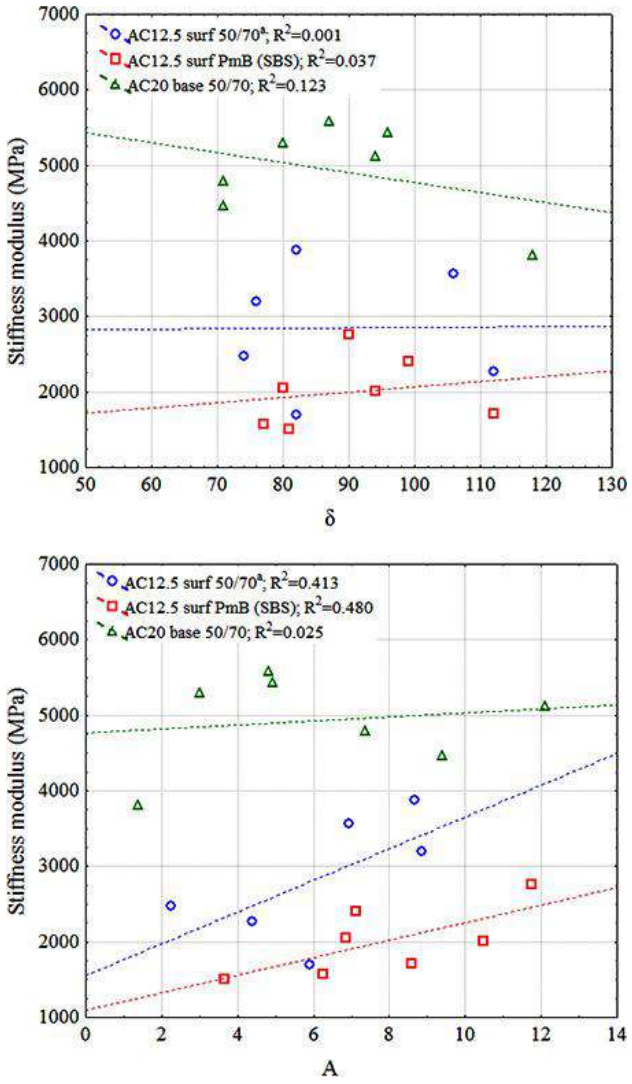

Fig. 8.15 Correlation of stiffness with indicators of aggregates' orientation for field cores

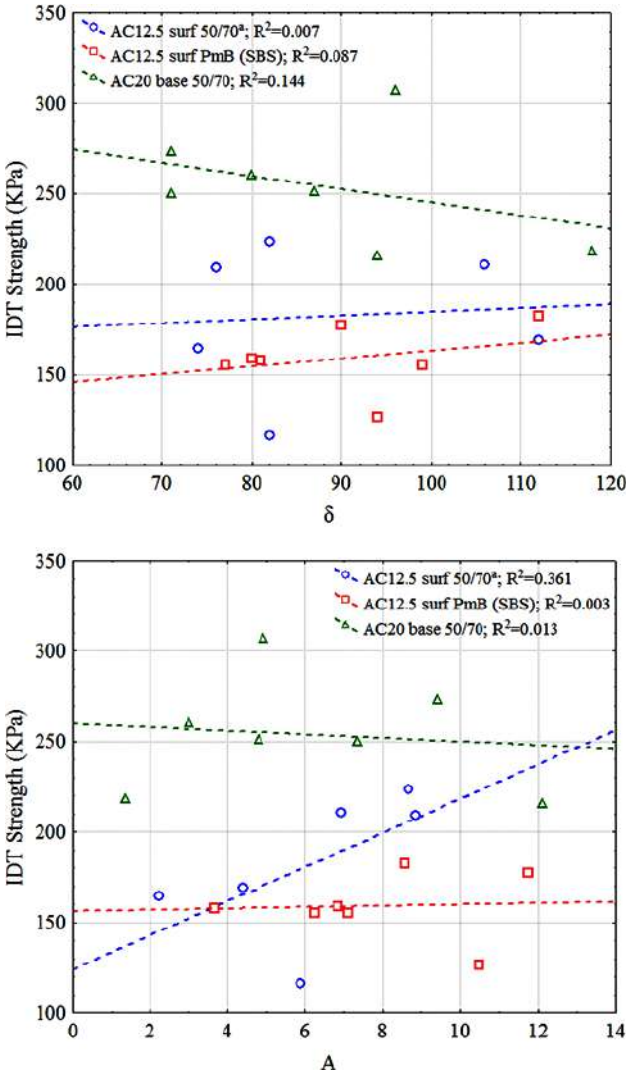

Fig. 8.16 Correlation of IDT strength with indicators of aggregates' orientation for field cores

No discernible trend is observed between the predominant orientation angle and mechanical properties of the field-compacted specimens. This is probably due to the narrow range of stiffness and IDT strength values of each mixture. However, it can be seen an increasing trend between the severity A and stiffness- IDT strength for the field cores.

8.2.3 Effect of radial segregation on the mechanical properties

The effect of radial segregation on the mechanical properties of specimens fabricated using Marshall, gyratory, roller and field compaction is shown in Fig. 8.17-8.24.

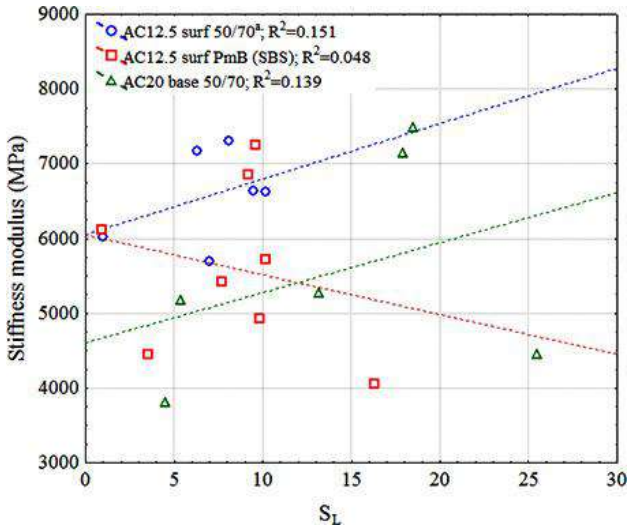

Fig. 8.17 Correlation of stiffness with aggregates segregation for Marshall specimens

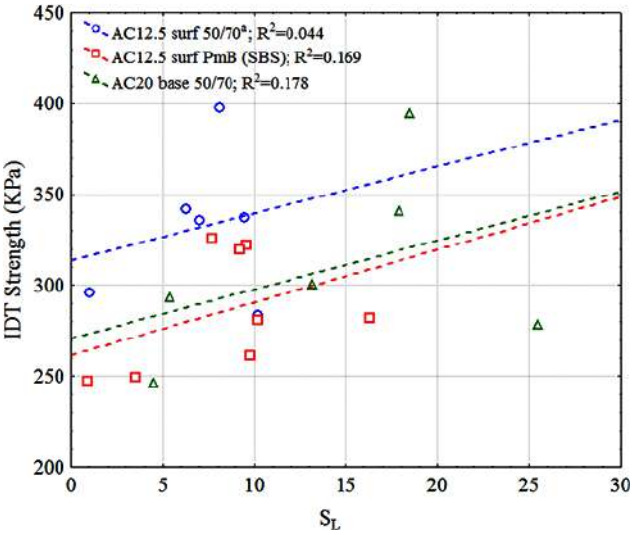

Fig. 8.18 Correlation of IDT strength with aggregates segregation for Marshall specimens

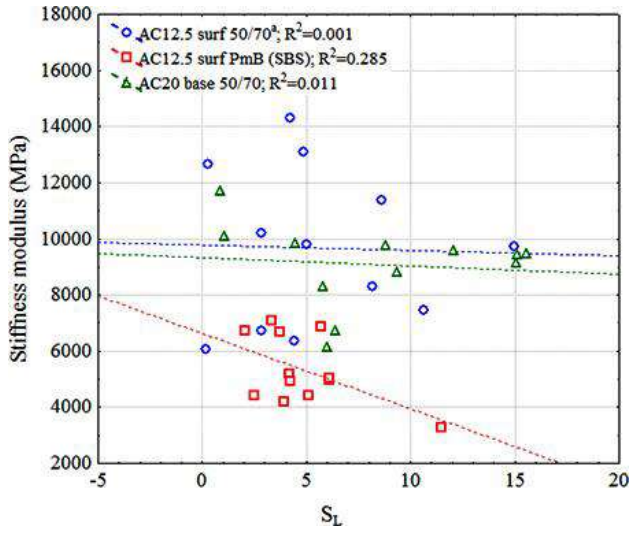

Fig. 8.19 Correlation of stiffness with aggregates segregation for gyratory specimens

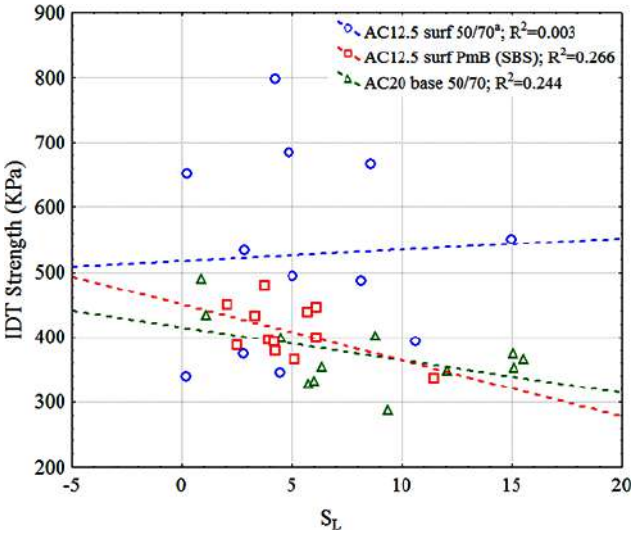

Fig. 8.20 Correlation of IDT strength with aggregates segregation for gyratory specimens

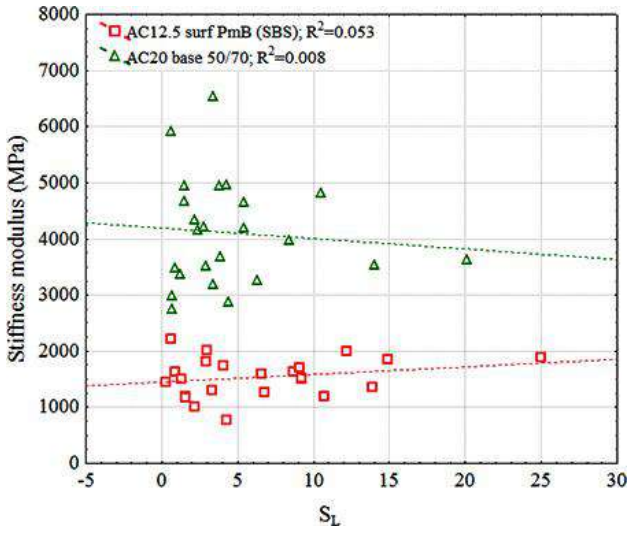

Fig. 8.21 Correlation of stiffness with aggregates segregation for roller specimens

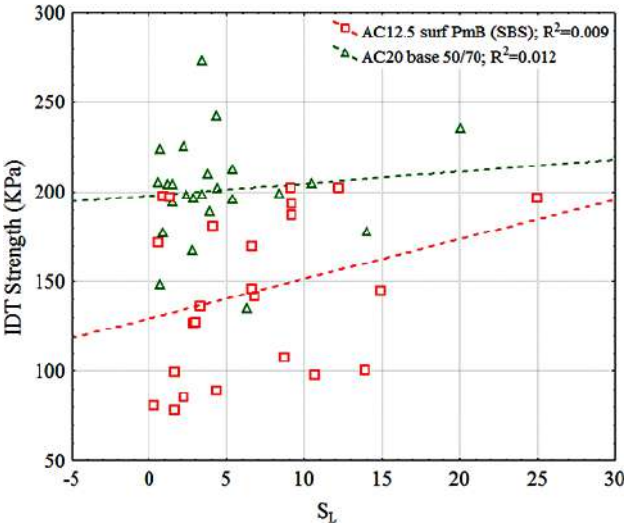

Fig. 8.22 Correlation of IDT strength with aggregates segregation for roller specimens

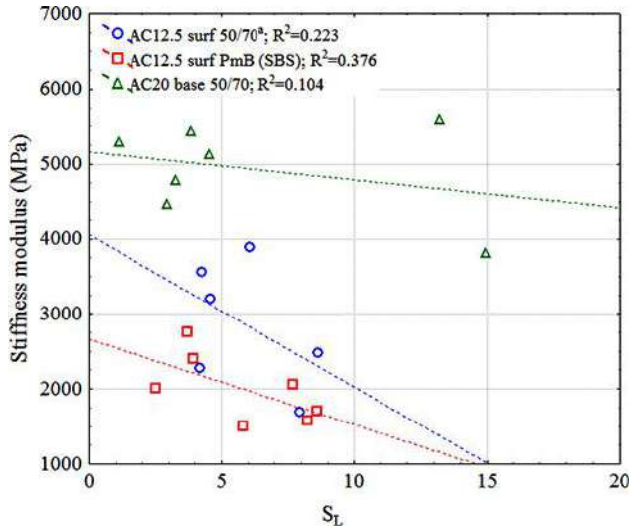

Fig. 8.23 Correlation of stiffness with aggregates segregation for field cores

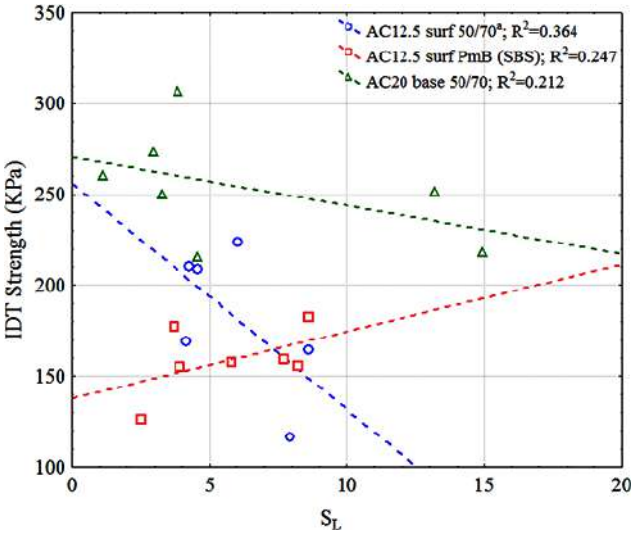

Fig. 8.24 Correlation of IDT strength with aggregates segregation for field cores

In general, the spatial distribution of aggregates in terms of the S_L parameter does not seem to influence the stiffness modulus irrespective of the compaction method used for specimen fabrication. Comparing the various compaction methods, it can be argued that the most influential method in stiffness modulus changes due to the aggregates spatial distribution seem to be the field compaction method. In this case, more segregation seems to affect negatively the stiffness modulus. This trend is more pronounced evaluating the relationship between the spatial distribution of aggregates and high temperature IDT strength for all compaction methods, except for the Marshall. For

this method, aggregates segregation within the specimen seems to positively affect the rut resistance characteristics.

8.2.4 GLM analysis

Furthermore, an analysis of variance (ANOVA) on the experimental datasets was performed using a general linear model to determine which internal structure indicators significantly contributed to the stiffness modulus and high temperature IDT strength results. The GLM fits a model to the variables that have been specified and tests the significance of a variable when entered in the model; in this study, analysis was performed at 95% confidence level. The p-values of all microstructure indicators with respect to stiffness and IDT strength independently for each compaction method are reported, respectively, in Tables 8.1 and 8.2. It should be noted that a variable is considered to be statistically significant at a 95% confidence level, when its p-value is lower than 0.05.

Table 8.1 Stiffness and internal structure GLM results (p-values) for all compaction methods

Compaction method	CP	CL	CLB	δ	A	S_L
Marshall	.631	.958	.876	.270	.221	.657
Gyratory	.000	.030	.047	.129	.104	.478
Roller	.000	.374	.535	.296	.568	.902
Field	.264	.384	.696	.857	.496	.879

Table 8.2 IDT strength and internal structure GLM results (p-values) for all compaction methods

Compaction method	CP	CL	CLB	δ	A	S_L
Marshall	.522	.693	.659	.332	.478	.803
Gyratory	.010	.343	.093	.208	.888	.613
Roller	.003	.678	.950	.003	.312	.164
Field	.129	.441	.649	.835	.966	.678

The analyses results indicate that several parameters have a statistically significant impact on the mechanical properties of compacted specimens. Regarding the Marshall specimens, none of the internal structure indicators considered seems to be significant in affecting the stiffness modulus and high temperature IDT strength. This was also

concluded for the field-compacted specimens. However, with regards to the gyratory-compacted specimens all parameters representing the connectivity between aggregates were found to significantly affect the stiffness modulus. For these specimens, it is also worth noting that the predominant orientation angle was found to be a marginally significant factor. Also, the number of proximity zones between aggregates was found to affect significantly the rut resistance characteristics of gyratory specimens. Significant impact of this indicator was also found with respect to the stiffness properties of roller-compacted specimens. In addition, it was further demonstrated that the rut resistance behavior of these specimens is strongly influenced by the number of contact points and the preferred orientation angle of aggregates.

Summarizing, it can be argued that the indicators representing the aggregate's contacts and packing within the mixtures structure, especially for the gyratory- and roller-compacted specimens, appear to provide essential information in terms of characterization of the stiffness and rut resistance performance of mixtures studied. Hence, it is believed that image analysis can assist in optimizing the compaction conditions on the purpose to improve the aggregate structure formation and the corresponding mechanical properties of asphalt mixtures.

9. Skid resistance

9.1 Introduction

Road agencies internationally specify that after final compaction on site the surface course of asphalt pavement shall be tested for compliance to construction specifications, including, among others, the surface macrotexture. Although macrotexture, which significantly contributes to the skid resistance during the pavement service life, has been recognized as an essential characteristic of asphalt material, so far no standardized methodology that enables the reliable estimation of pavement surface texture characteristics from laboratory testing is available. For instance, the European standard (EN 13108) is limited to provide guidance to fulfill requirements related only to grading envelope, binder content (minimum value) and void content (minimum-maximum values) of asphalt mixtures. Following these guidelines or through past experience practitioners and engineers involved with mixtures design assume that eventually after compaction on site of the surface course mixture the requirements for initial texture depth will be fulfilled. In this respect, practitioners and engineers, however, are not able *a priori*, during the mix design process, to quantify and assure the relative texture requirements. The importance to incorporate the skid resistance evaluation in the asphalt mix design practices implies that the asphalt surface characteristics of specimens produced in the laboratory may be considered representative of the real mixture in-situ. Therefore, a laboratory testing procedure capable of assessing reliably, as accurately as possible, the texture characteristics of a mixture in the laboratory before its installation as a surface course layer needs to be developed. In such framework, the laboratory compaction method seems to be a critical component to guarantee that the surface morphological properties of fabricated specimens are representative of the field values of the same mixture.

Under this view, it should be pointed out that the impact (Marshall) compaction method cannot be considered a potential candidate for such investigation. This method, which encompasses the asphalt mix to be placed into a defined mould and then compacted with the impact of a steel hammer, does not mimic the movement of a roller

during compaction and has been recognized as being the most severe mode of laboratory compaction in terms of potential aggregate degradation (Airey et al. 2008). This is supported from the higher connectivity between aggregates of Marshall specimens in the horizontal direction compared to field-compacted specimens, as demonstrated in Chapter 7. So, it seems reasonable to hypothesize that the aggregate degradation (breakdown) induced during compaction may affect the microtexture properties. Also, this research indicated the trend of this laboratory compaction method to induce lateral segregation of aggregates, as opposed to field compaction, which may be argued to affect the macrotexture properties. In light of the above, it can be speculated that the Marshall compaction cannot mimic the surface texture morphology induced from field compaction. Gyratory compaction could be potentially included as candidate, recognizing that this mould-based compaction method creates both normal and shear forces in the mixture which appears to better reproduce the field compaction conditions, as opposed to the impact compaction. However, it was previously demonstrated (in Chapter 7) that the distribution of aggregates induced by gyratory compaction method also differs, although clearly to a lesser extent compared to the impact compaction, from the field-compacted specimens. This possibly explains the findings from previous research which indicated that the gyratory compaction is not representative, from a frictional point of view, of the field compaction (Goodman et al. 2006; Boscaino et al. 2009). Hence, it was judged that the gyratory compaction method shall not be further studied. Besides, it is worth mentioning that the specimens fabricated with the mould-based compaction methods (namely impact and gyratory) have defined surface area, which is believed to be not sufficient to perform reliable characterization of the asphalt surface. Based on the above, this study focuses on roller compaction, for which this research findings support the argument that it best simulates the in-situ compaction (Iwama et al. 2007; Renken 2000; Sousa et al. 1991). Particularly, by means of laboratory fabrication of asphalt slabs and simple tests, it is investigated whether surfaces produced by a standardized laboratory compaction method may be used to simulate the frictional properties of the as-constructed pavement surfaces.

Starting with an overview of the test methods and skid resistance evaluation, this Chapter has been divided in two parts. In the first Part, the frictional characteristics of

asphalt mixtures with different aggregate sizes, mix gradations and binder contents were investigated in the laboratory to verify the concept. In the second part, based on new full-scale hot mix asphalt road test section constructed using several compaction modes, laboratory and field friction measurements were compared. The analysis results are demonstrated and discussed in the following sections.

9.2 Skid resistance evaluation

9.2.1 British Pendulum

A common device to measure friction characteristics of pavement surfaces is the British Pendulum Tester (BPT). The British Pendulum Tester produces a low speed sliding contact between a standard rubber slider and the pavement surface and measures frictional properties by determining the loss in kinetic energy of the slider when in contact with the pavement surface (ASTM 2013). The loss of kinetic energy is converted to a frictional force and thus pavement friction (i.e. BPN value). The BPT has the advantage of being easy to handle and provides friction and microtexture indicators at a low speed (i.e. 10 km/h) for any pavement, whether in the field or from laboratory analysis of cored or prepared samples. Furthermore, the BPT can be used to measure both longitudinal and lateral pavement– tire friction.

9.2.2 Sand patch method

Measuring the pavement microtexture and macrotexture and relating these measurements to pavement skid resistance has been a major concern for pavement researchers. The practice of measuring pavement macrotexture has been a common practice in recent years. Macrotexture data is generally measured using the sand patch method (ASTM 2006). Essentially, the sand patch method is a volumetric-based spot test method that assesses pavement surface macrotexture through the spreading of a known volume of sand or any fine-grained materials with uniform gradation onto a cleaned pavement surface. The material is then evenly distributed over a circular area and the diameter of the resulting circle is measured. The volume divided by the area of the circle is reported as the mean texture depth (MTD). This volumetric test is still used worldwide

as the reference ground truth standard (China and James 2012) and when combined with other data can provide friction information.

9.2.3 The IFI model

In this study, the frictional performance of asphalt mixes is reported in terms of the International Friction Index (IFI). The IFI represents a method for reporting both components of the tyre/ road pavement interaction in terms of friction and is often used for mix skid resistance evaluation (Fuentes et al. 2012; Fontes et al. 2008; Yeaman 2005). The IFI (ASTM 2011) consists of two parameters: the calibrated wet friction at 60 km/h (F60) and the speed constant of wet pavement friction (S_p), related to the surface macrotexture.

- Initially, the speed constant (S_p) parameter is calculated based on texture measurements:

$$S_p = a + bT_X \quad (9.1)$$

where *a* and *b* are calibration factors and different for each measuring device and T_x is a measure of pavement texture.

- The friction measurement at a slip speed *FR(S)* is then converted to a measurement at 60 km/h *FR(60):*

$$FR(60) = FR(S)exp^{\left(\frac{S-60}{Sp}\right)} \quad (9.2)$$

- Finally, the *F(60)* is recalculated by the use of speed adjusted friction value *FR(60)* and the following equation:

$$F60 = A + BFR(60) + CT_X \quad (9.3)$$

where *A*, *B*, and *C* are calibration constants for a selected friction device.

A transformation equation has also been established to allow for calculation of the IFI at speeds other than 60 km/hr, thus providing the potential of generating frictional curves.

9.3 Laboratory study

Initially, a preliminary laboratory study was conducted seeking to investigate the potential of using the standardized roller compaction method for ranking and efficient evaluation of the frictional performance of two HMA types (i.e. AC12.5 surf 50/70[c],

AC20 surf 50/70) with different NMAS, gradations and various binder contents (Georgiou and Loizos 2014). Specifically, this study included AC12.5 surf 50/70^{c} mix at the optimum Marshall binder content, also 0.5% less and 0.5%, 1.0% binder higher than the optimum. Moreover, AC20 surf 50/70 mix at the optimum Marshall binder content, also 0.5% less and 0.5% binder higher than the optimum were also evaluated. Note that the optimum Marshall binder content for each mix type was that which provided 4% air voids in the mix.

A total of seven mixtures were prepared and compacted (four Type AC12.5 surf 50/70^{c} mixes; and three Type AC20 surf 50/70 mixes) using a segmented roller compactor, which allowed aggregate particles to move relative to one another and orientate in a manner similar to the in-situ material. At the time of slab fabrication, the laboratory produced mixes were reheated gently to the compaction temperature and compacted into square steel moulds with dimensions (width and length) of 305 x 305 mm^{2}. Both asphalt concrete type mixes were compacted into 50 mm deep moulds. For the current test program, the approach of compaction by specified energy was followed to prepare the asphalt slabs. Compaction was accomplished in three phases and meant to mirror field compaction; pre-compaction and the main compaction phases. The pre-compaction phase comprised of five passes (each pass corresponded to one forward and one backward motion) applying a minimum compaction energy of 3 kN in order to avoid bow effects and achieve a smooth surface in the compacted slab. The main compaction phases comprised of ten passes applying compaction energy of 10 kN with vibration frequency of 35 Hz, followed by ten passes of 10 kN static compaction energy.

After the cooling of the roller-compacted (RC) slabs at ambient temperature, density measurements were performed to evaluate the achieved compaction degree (CEN 2007). As presented previously, the desirable air void content for each RC slab was varied based on the binder content (see Table 3.1). The results indicated that there is consistency between target and achieved density. It should also be noted that, based on preliminary tests, uniform compaction is usually generated in an area positioned about 4 cm far from the edges of the compacted RC slab. Hence, due to the segregation that occurs at the edges of the slab and the associated increase in air voids, it was decided to conduct the friction and macrotexture tests around the centre of the slab.

Friction measurements were commenced using the British Pendulum Tester. This test was performed on five different locations, within a rectangular area at the centre of each slab, in both the longitudinal and lateral directions of roller compaction. Five swings were recorded at each location and an average was calculated. Water was used as a lubricant to wet the sample surfaces. Surface temperatures were measured during each test as 20^{o}C and thus no correction in BPN values was applied. The results showed that the BPN20 values of Type AC20 surf 50/70 mixes were generally higher than those measured for Type AC12.5 surf 50/70^{c} mixes. Specifically, BPN20 values recorded for Type AC12.5 surf 50/70^{c} mixes ranged from 64 to 55, while for Type AC20 surf 50/70 mixes 81 to 79. Also, the overall trend showed that the BPN20 values decreased with an increase in binder content, while no significant deviation was observed between longitudinal and lateral to compaction direction measurements.

The sand patch method was used to measure the texture depth of the asphalt slabs. Two replicate measurements were performed and averaged to obtain the MTD value. Some interesting observations were made after analysis of texture results. Initially, higher magnitude of texture was achieved concerning Type AC20 surf 50/70 mixes as compared to Type AC12.5 surf 50/70^{c} mixes. This difference could be attributed to different NMAS; higher NMAS corresponds to higher texture depths. Moreover, an increase in the binder content leads in a decrease of achieved texture depth as demonstrated from MTD range values; 0.74mm to 0.51mm and 0.78mm to 0.80mm corresponding to Type AC12.5 surf 50/70^{c} and AC20 surf 50/70 mixes, respectively. Thus, it could be argued that the binder content and subsequently the air void level affect the surface macrotexture; minimizing the air void content lower textured surfaces are produced.

Friction and texture data were further analyzed to provide skid resistance information of the mixes under investigation. Essentially, skid resistance was quantified by the IFI (F60,Sp) which has been proposed in order to develop a universal method for the characterization of pavement surface friction (Wambold et al. 1995). The calculated IFI values with respect to type AC12.5 surf 50/70^{c} and AC20 surf 50/70 mixes are shown, respectively in Fig. 9.1 and 9.2.

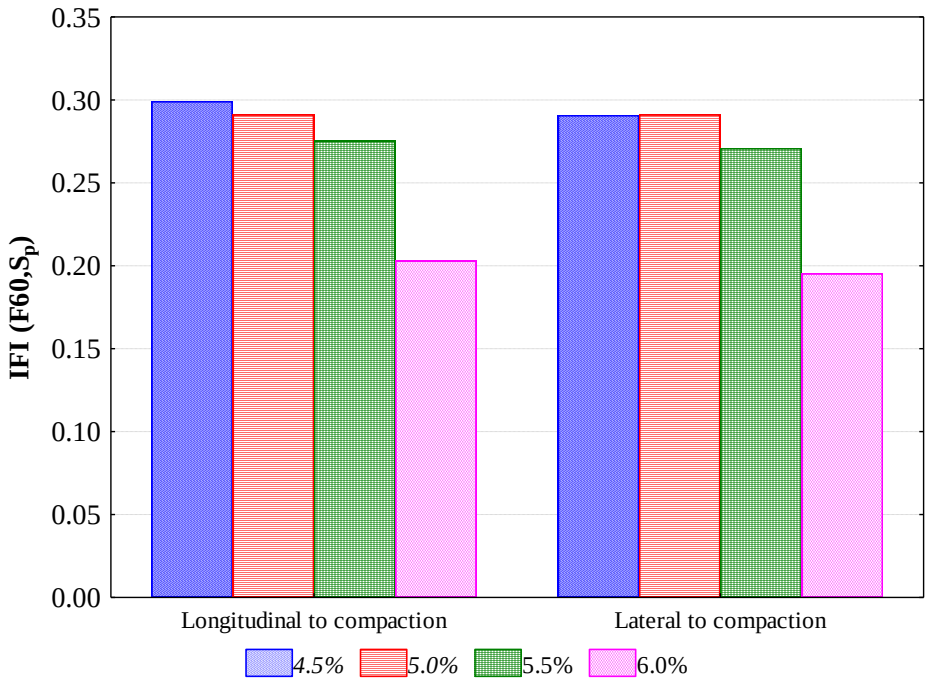

Fig. 9.1 IFI values corresponding to type AC12.5 surf 50/70[c] mixes

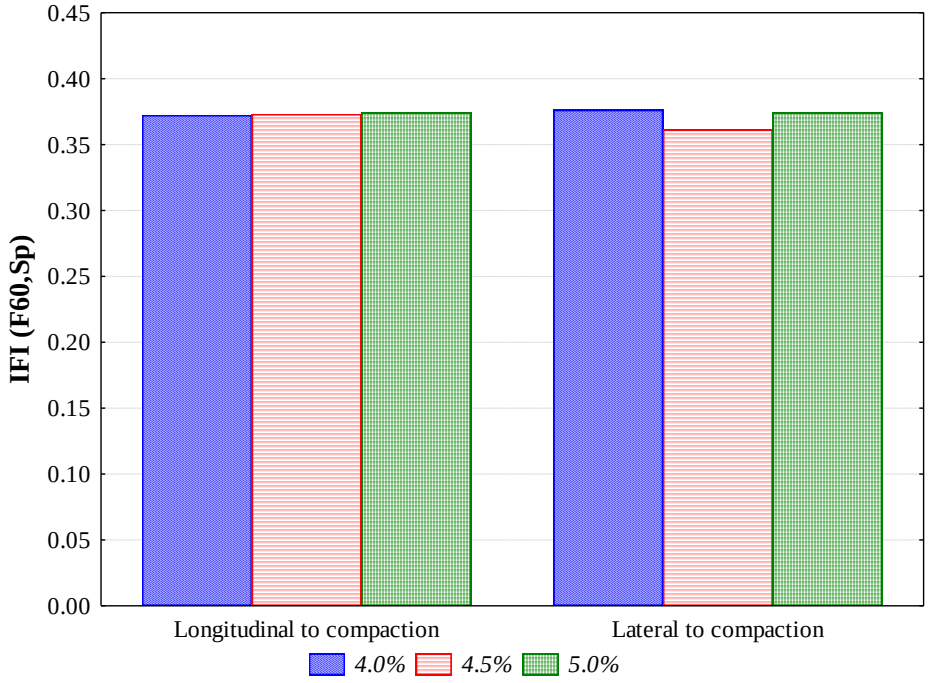

Fig. 9.2 IFI values corresponding to type AC20 surf 50/70 mixes

According to Fig. 9.1, it is evident that type AC12.5 surf 50/70^{c} mix with 4.5% binder content had the highest friction performance compared to the remaining mixes. On the contrary, type AC12.5 surf 50/70^{c} mix with 6.0% binder content showed the lowest friction performance, which is associated with its low MTD and BPN values. The IFI values between longitudinal and lateral measurements were almost identical, thus indicating that roller compaction results in homogeneous asphalt slab surfaces.

Also, the results demonstrate that type AC20 surf 50/70 mixes had almost the same friction performance, as shown in Fig. 9.2. Again, the IFI values between longitudinal and lateral measurements were found to be almost identical.

Comparing the IFI values between Type AC12.5 surf 50/70^{c} and AC20 surf 50/70 mixes it can be clearly seen in Fig. 9.1 and 9.2 that Type AC20 surf 50/70 mixes have superior friction performance. Both the macrotexture differentiation, as a result of changes in mix design practices (different NMAS), and the inferior physical aggregate properties of Type AC12.5 surf 50/70^{c} mixes seemed to be the key factors in mix types' friction performance differences. Based on the above findings it could be argued that methodologically the roller compaction method produces surfaces that discriminate in terms of friction due to the different mix properties; thus it could aid in ranking and evaluating the friction performance of different mixes.

9.4 Comparison to field compaction

The second part of this study aimed to investigate whether surfaces produced by roller compaction method, using several compaction modes, could be used to simulate the frictional properties of as-constructed pavement surfaces. For this purpose, type AC20 surf 50/70 mix designed with 4.5% binder content was selected for the field implementation. During construction, samples of plant-produced mix were collected for laboratory evaluation. For this mix, laboratory and field friction measurements were set up with the aim to correlate the laboratory and field performance (Georgiou and Loizos 2014).

9.4.1 Laboratory testing

The laboratory experiment included the fabrication and compaction of plant produced mix samples adopting four different compaction modes using the Roller Compactor. Specifically, four modes of roller compaction (i.e. Static: S, Vibratory: V, Static-Vibratory: VS and Vibratory-Static: VS) were established that might be implemented in the field. The main compaction energy and vibration frequency reflected the operational characteristics of the steel wheel rollers used in the field compaction. Based on density measurements conducted on the four RC slabs, after cooling to ambient temperature, air void content was determined as 4.5%, 4.3%, 3.0% and 4.4% for S, V, SV and VS compacted slab, respectively. Thus, it can be argued that achieved density fulfils the mix design requirements (target air void content 4.0%).

Moreover, each slab was tested for friction and texture. The British Pendulum test was utilized to measure friction on five different locations within the area of uniform compaction at the centre of each RC slab, in both the longitudinal and lateral direction of roller compaction. The average value of the five swings was recorded at each location. Surface temperature was also measured during each test as 20^{o}C and thus no correction in BPN values was applied. The BPN values were of the same order of magnitude (ranging from 75 to 79), irrespective to the compaction mode followed (i.e. S, V, SV and VS). Also, no significant deviation was observed between longitudinal and lateral to compaction direction measurements.

On the contrary, the MTD values (average of two replicate tests) measured on asphalt slabs differed significantly (ranging from 0.70 mm to 1.25 mm) and thus compaction mode seems to affect significantly surface texture. Specifically, adopting the Vibratory-Static mode the higher MTD value was yielded, while with the Static-Vibratory mode the lower MTD was obtained. Fig. 9.3 demonstrates the end result of sand patch tests on the four differently compacted asphalt slabs.

Fig. 9.3 Laboratory sand patch test results with respect to compaction mode

Friction and texture measurements were further analyzed to quantify skid resistance, in terms of the IFI (F60,Sp). The calculated IFI values with respect to different roller compaction modes are shown in Fig. 9.4.

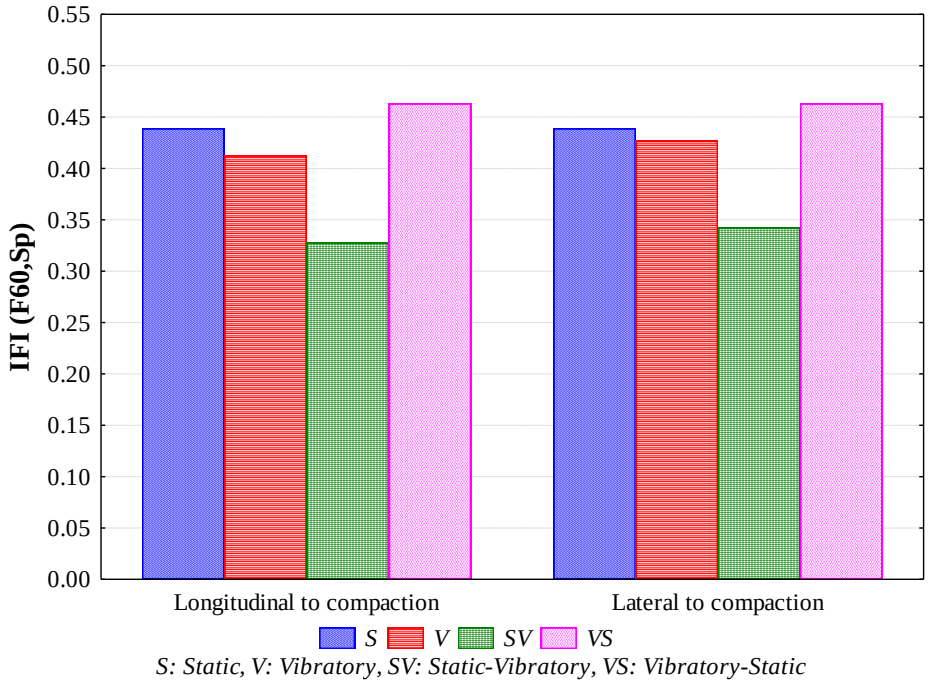

Fig. 9.4 IFI values corresponding to different laboratory roller compaction modes

From the results, it was demonstrated methodologically that the Vibratory-Static mode showed a significant effect on the asphalt mix friction performance, while the Static-Vibratory mode resulted in a reduced effect. Again, consistency was observed between longitudinal and lateral friction characteristics.

Given the above results friction values for different slip speeds, ranging from 20 to 100 km/h, were calculated based on the following equation:

$$F(S) = F60exp^{\left(\frac{60-S}{S_p}\right)} \quad (9.4)$$

where S is any slip of interest.

Fig. 9.5 illustrates the IFI curves for the various compaction modes for both longitudinal (designated as 'long') and lateral (designated as 'lat') measurements. As expected, a decreasing tendency of IFI values with increase in slip speed is observed. This decrease is more pronounced with respect to the Static-Vibratory compaction mode where an almost 50% decrease of skid resistance between 60 and 100 km/h slip speed is estimated.

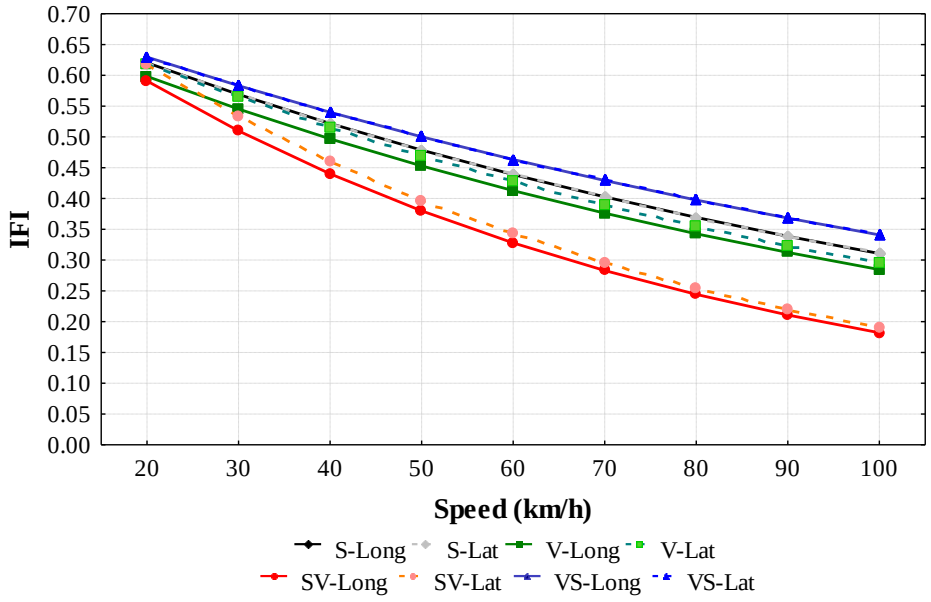

S: Static, V: Vibratory, SV: Static-Vibratory, VS: Vibratory-Static
Long: Longitudinal, Lat: Lateral

Fig. 9.5 Frictional curves corresponding to different laboratory roller compaction modes

9.4.2 Field testing

For the purpose of this study, skid resistance measurements were also conducted on a new full-scale HMA pavement test section. The test section was divided into four sub-test sections that were compacted using different compaction modes, as illustrated in Fig. 9.6. A 10-ton steel double drum roller, able to operate in vibratory or static mode was utilized to construct these test subsections. Subsection #1 was compacted at a static mode (i.e. S). Subsection #2 was compacted using vibratory steel roller at a medium frequency of 35 Hz (i.e. V). Subsection #3 was compacted using the static steel roller as a breakdown and then the vibratory mode with 35 Hz frequency was implemented (i.e. SV). Subsection #4 was compacted using the vibratory steel roller at a high frequency of 50 Hz as a breakdown and then static mode for finish (i.e. VS).

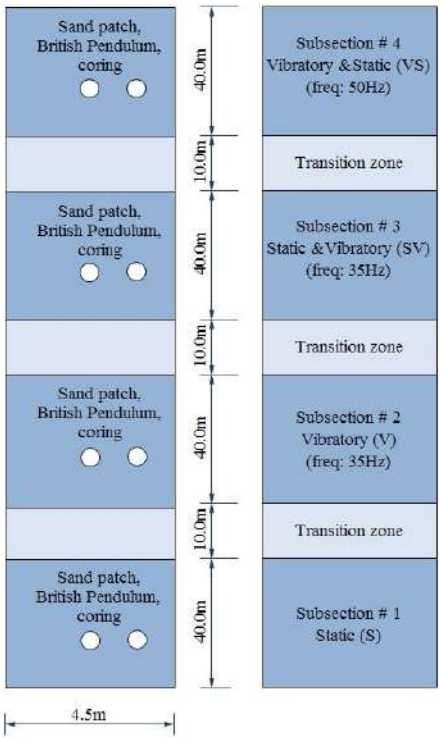

Fig. 9.6 Schematic layout of asphalt pavement subsections

A day after compaction was finished skid resistance measurements were performed on the various subsections. There are a wide range of devices for characterizing the skid resistance of a road pavement (SCRIM, Grip Tester etc) which are used to evaluate the macrotexture or the microtexture of the road. Although a wide range of these devices exists, the Sand patch method and British Pendulum were used again in the field

investigation so that comparable results to the laboratory experimental data would be derived (see Fig. 9.7). Two locations were selected across the test subsection width and were averaged to obtain the MTD value.

Fig. 9.7 Field microtexture and macrotexture measurements

Results demonstrated that the subsections had different texture properties (ranging from 0.45 mm to 0.89 mm) and thus the compaction mode affected the surface texture, as illustrated in Fig. 9.8. Ranking the field compaction in terms of macrotexture both the Vibratory- Static and Static mode showed the superior performance, while the Static-Vibratory the inferior performance. It is worth mentioning that a similar trend was observed during the laboratory texture measurements.

Microtexture measurements were conducted on the same test locations. Both longitudinal and lateral to compaction direction measurements were recorded as an average of five swings. Surface temperature was also measured during each test ranging from 33^{o}C to 40^{o}C. Consequently, a correction related to the temperature was applied in BPN values on the basis of a proper interpretation of the test data obtained at different temperatures (Steven 2009). The reference temperature was 20^{o}C and a correction was applied to the individual measured BPN values. Then, the corrected values (five readings per test spot) were averaged to give a single BPN20 value. Based on the results, BPN20 values ranged from 82 to 92, while the inherent variability among the four subsections was ±3 BPN20 and ±4 BPN20 units for the longitudinal and lateral measurements, respectively.

It should also be mentioned that after macrotexture and friction testing, cores were drilled from the test locations of each subsection, as illustrated in Fig. 9.6, in order to determine the achieved field densities. Based on the laboratory testing the air void

content (as an average of two cores) was determined as 6.5%, 4.4%, 3.8% and 4.4% for subsection S, V, SV and VS, respectively.

Skid resistance measurements were further analyzed and the IFI (F60,Sp) was calculated. The calculated IFI values with respect to different roller compaction modes are shown in Fig. 9.8. The IFI results demonstrated that Static and Vibratory- Static modes resulted in superior friction performance, while the Static- Vibratory mode had the opposite effect on the IFI values. Again, consistency was observed between longitudinal and lateral friction characteristics.

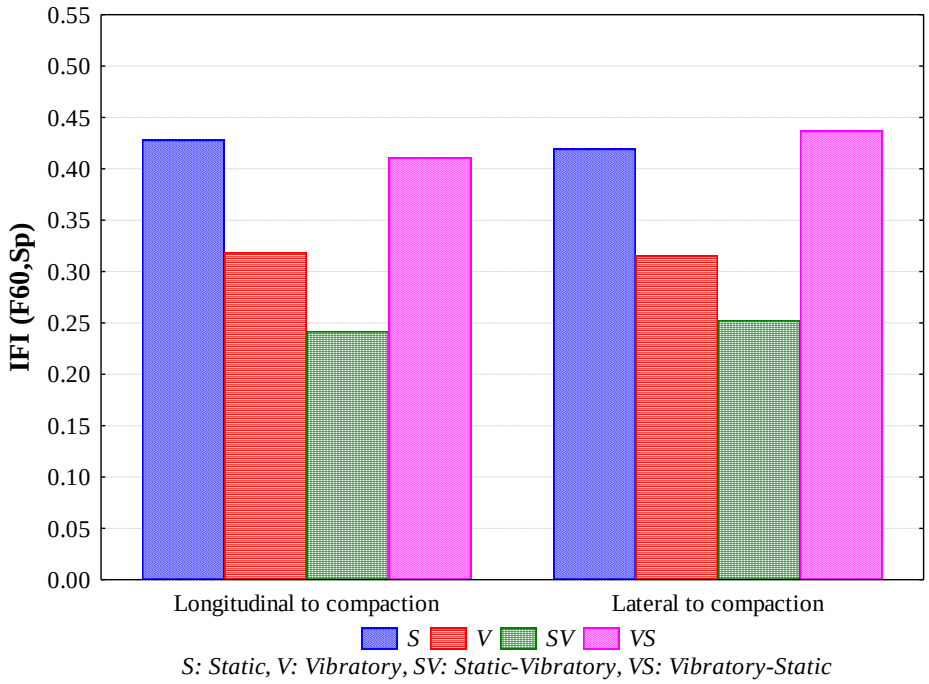

Fig. 9.8 IFI values corresponding to different field roller compaction modes

Friction values for different slip speeds, ranging from 20 to 100km/h, were also calculated to generate IFI curves which are presented in Fig. 9.9.

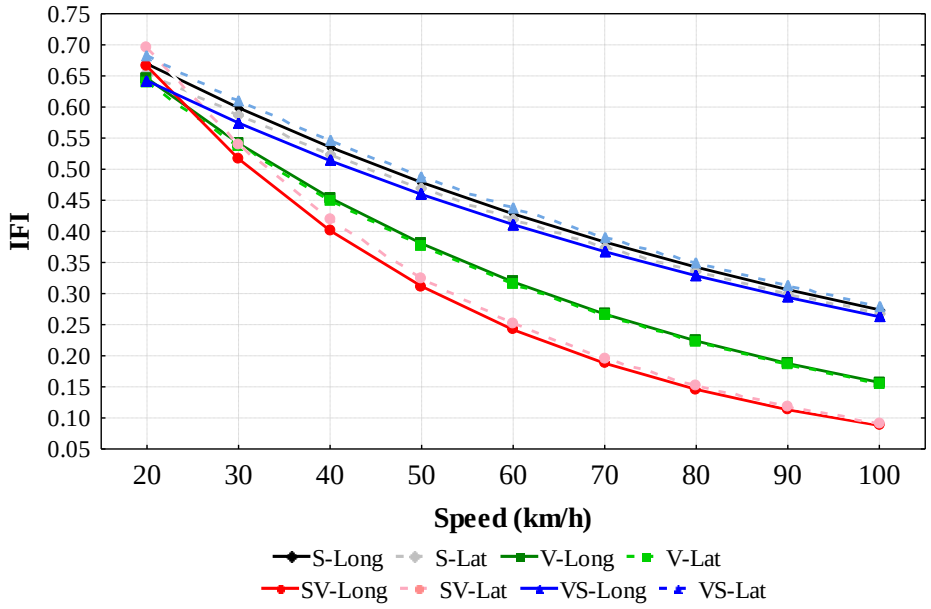

S: Static, V: Vibratory, SV: Static-Vibratory, VS: Vibratory-Static
Long: Longitudinal, Lat: Lateral

Fig. 9.9 Frictional curves corresponding to different field roller compaction modes

From Fig. 9.9, it could be concluded that both the Static and Vibratory-Static subsections showed a better skid resistance at low and high speeds compared to the Vibratory and Static-Vibratory subsections. Specifically, the high macrotexture values of former subsections resulted in good skid resistance at high speeds. On the contrary, the latter subsections presented a poor friction performance at high speeds, due to its lower macrotexture values. In such a case, all the subsections demonstrated high microtexture (i.e. BPN20 values) that contributes to good skid resistance at low speeds.

Following the above results, a statistical analysis was conducted to evaluate the correlation between laboratory and field measurements. Specifically, regression analysis was adopted between the skid resistance data of laboratory and field testing with respect to the various compaction modes (i.e. S, V, SV and VS) and measurements direction (i.e. longitudinal and lateral). Fig. 9.10 illustrates the results of the applied linear regression between field and laboratory data, in terms of the IFI (F60,Sp) values, for longitudinal and lateral measurements respectively.

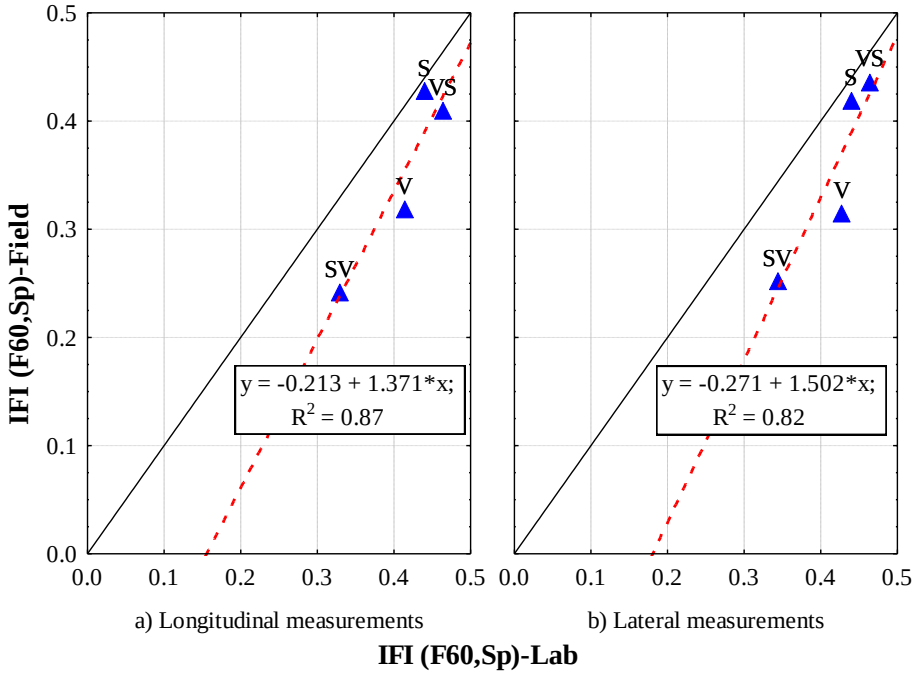

Fig. 9.10 Correlation between laboratory and field friction performance for different roller compaction modes

According to the results of Fig. 9.10 well-defined statistical relationships between field and laboratory friction can be established with coefficient of determination R^2 fair to good (i.e. 0.87, 0.82). Although, the analysis was based on limited data the initial findings from this investigation give promising results. The general trend shows that the laboratory roller compaction modes well characterize the field pavement surface friction performance. In particular, for this study the Static and Vibratory-Static mode, when adopted in the laboratory, seem to predict rather accurately the friction performance of the as-constructed (with the same compaction mode) field pavement surface.

10. Findings and conclusions

10.1 Summary

The aim of this Thesis was to contribute to a better simulation of in-situ conditions through laboratory compaction methods, so that reliable results can be obtained to assess, as accurately as possible, the on-site characteristics of field-compacted asphalt mixtures.

To achieve this aim, extensive laboratory experiments (based on impact (Marshall), gyratory and roller compaction methods) and field investigations on mixture performance have been performed which, collectively, allowed for the development of a methodological approach for the reliable assessment of asphalt field compaction-based characteristics. At first, the factors that control asphalt mixture compactability in both the laboratory and field were identified. Secondly, the influence of compaction methodology on asphalt stiffness, rut resistance and internal structure was evaluated. In a follow-up level, the interrelation between the asphalt mixture microstructure and the mechanical properties was investigated. Lastly, the relationship between the frictional properties of asphalt mixtures compacted in the laboratory and the field was assessed. Based on these, the main findings and the relative concluding suggestions of this study are presented hereafter and discussed along with recommendations for further research.

10.2 Findings

This section discusses the main findings within the methodological framework followed.

Regarding **Marshall compaction**, compaction temperature influences significantly the asphalt mixture stiffness and rut resistance characteristics. Although this factor found insignificantly affecting the internal structure in terms of aggregates contacts, as well as directional and spatial distribution, the results indicated that, in general, aggregates tend to be oriented in angles higher than 90^{o} and show evidence of segregation. Furthermore, an increase in the number of proximity zones between aggregates, results in stiffness modulus and high temperature IDT strength increase.

Regarding **gyratory compaction,** angle of gyration and specimen geometry were found to influence significantly the asphalt mixture compactability. To achieve the target compaction degree less compaction effort is needed when using the 1.45^{o} angle; between the CEN and AASHTO standard angles the slowest rate of mixtures densification is observed using the 0.82^{o} angle suggested by the European Standard. Also, when increasing the height to diameter ratio, density gradients generate within the specimen structure with the middle portion receiving less compaction energy. This implies that the gyratory specimens experience non-uniform air void distribution, as also indicated from several researchers (Thyagarajan et al. 2010; Partl et al. 2003; Tashman et al. 2002). However, it was demonstrated that the cutting and coring process on the as-compacted specimens tend to reduce this heterogeneity. Moreover, variation of compaction temperature from 135^{o}C to 150^{o}C does not have a great effect on densification properties of the conventional bitumen-based mixtures studied; hence indicating that in this range gyratory compaction is not sensitive to the mixture temperature.

Examining the stiffness properties of gyratory specimens, although the influence of compaction temperature is not statistically significant, the results indicate a decreasing trend of modulus with temperature for the conventional mixtures. On the contrary, concerning the AC12.5 surf PmB (SBS) mixture, stiffer specimens are produced at a higher temperature. Also, evaluating the relationship between the CEN and AASHTO standard angles of gyration and the stiffness, no discernible trend is observed, although it is clear that with the increased operation angle of 1.45^{o} lower modulus is reached. Significant influence of angle of gyration on stiffness was found only for the AC12.5 surf PmB (SBS) mixture. It is interesting to note that the stiffness is predominantly influenced by the specimen diameter, irrespective of the mixture type. By coring 100mm diameter from larger 150mm specimen, a lower modulus is obtained compared to the as-compacted 100mm specimen; this decrease may transcend 30%.

Similar conclusions were drawn evaluating the impact of gyratory compaction variables on the rut resistance of asphalt mixtures. Diameter was found again to be a statistically significant factor; coring from 150mm specimen results in decreasing high temperature IDT strength compared to the as-compacted 100mm specimens, which may reach up to 30%. Angle of gyration and temperature were found to have a lesser effect

on the rut resistance behavior of asphalt mixtures. Nevertheless, the results demonstrated a decreasing trend of high temperature IDT strength with temperature for the conventional bitumen-based mixtures and that specimens compacted using the 1.45^{o} angle, compared to the CEN and AASHTO standard angles of gyration, exhibited the lowest IDT strength values.

It is worth mentioning that similarly to the stiffness and rut resistance evaluation, specimen diameter also found to influence significantly the internal structure, especially aggregates' connectivity and directional distribution. The results indicated less aggregate interlocking for the cored 100 mm -from larger 150 mm- specimens; tendency was the same with the increase of compaction temperature. In addition, the angle of gyration was found to influence significantly the orientation angle, as also indicated from a previous study (Tashman et al. 2001); the results indicated a decreasing trend of the predominant orientation angle with gyration angle and aggregates oriented more randomly for specimens produced using the 1.45^{o} angle. Instead, the effect of gyratory compaction parameters on the spatial distribution of aggregates is insignificant; nonetheless, the results suggest that the gyratory compaction produces rather non homogeneous specimens. Several previous studies found that a slight non homogeneity is generated in a gyratory-compacted specimen (Coenen et al. 2012; Hassan et al. 2012; Hunter et al. 2004), although other studies reported that lateral non homogeneity is proven to be significant in gyratory specimens (Azari 2005).

One of the most noteworthy issues to consider is the high correlations between aggregates' contacts indicators and mechanical properties; an increased stiffness modulus and high temperature IDT strength is linked to higher number of proximity zones between aggregates. Predominant orientation angle also seems to affect the stiffness and rut resistance characteristics, although to a lesser extent.

Regarding **roller compaction,** compaction temperature and effort (in terms of roller passes) found to influence significantly the asphalt mixture compactability. In general, mixtures' densification is enhanced with the increase of compaction temperature and roller passes; however, there is a certain level of compaction effort up to which the impact on the degree of compaction is maximized. Although variability of air voids content is observed, this may not be attributed to the different compaction modes. In

addition, evaluation of air voids distribution indicates that roller compactor offers compaction homogeneity within the compacted slab.

It should be emphasized that compaction temperature and effort (in terms of roller passes) were identified also as the predominant parameters affecting the stiffness properties of roller-compacted specimens; stiffness is less influenced from the compaction mode. Particularly, a tendency to produce stiffer specimens with increase in compaction temperature is observed and this increase may transcend 20%. The trend is the same with respect to the roller passes, although the modulus increase is tapered off after a certain compaction effort, identically to compactability. The above findings indicate that the stiffness properties of roller-compacted specimens reflect their compactability characteristics.

It is interesting to note that the same trend was also found in evaluating the influence of compaction effort on the rut resistance behavior of these specimens. Compaction temperature was found to strongly affect the rut resistance characteristics of the AC12.5 surf PmB (SBS) mixture; the results indicated significant increase of high temperature IDT strength of the order of 60% with the increase of compaction temperature. For this mixture, compaction mode was also found to be a significantly influential factor. Less significant effect of compaction factors on the IDT strength was found for the conventional bitumen-based mixture.

Although mixed results were revealed with respect to the significance of the effect of compaction mode on stiffness and rut resistance characteristics of asphalt mixtures, it should be highlighted that this factor influences the macrotexture and in turn, the skid resistance-related characteristics of roller-compacted asphalt surfaces. This indicates that macrotexture is dependent not only on mixture grading and volumetric characteristics, but also on the compaction methodology.

Examining the internal structure, it was revealed that both the aggregates' contact points and orientation are mostly influenced from compaction temperature. However, the impact on each indicator was found to be mixture dependent. Compaction effort and mode did not have any statistically significant effect on the internal structure of roller-compacted specimens.

It is worth mentioning that, similarly to gyratory compaction, the number of proximity zones between aggregates has a statistically significant impact on the stiffness modulus of roller-compacted specimens. Correspondingly, the rut resistance behavior of these specimens is strongly influenced by the number of contact points and the preferred orientation angle of aggregates.

Comparing laboratory compaction methods to field compaction, different characteristics in terms of compactability was assessed in the laboratory relative to field. Although it is essential to relate field compaction to laboratory compaction in order to predict asphalt mixture compactability, the study results indicate that the in-situ compaction characteristics cannot be reliably predicted from laboratory testing. This may be attributed to several factors affecting field compaction such as environmental, laydown site and confinement conditions, compaction equipment and others, which cannot be simulated in the laboratory. However, the in-situ compaction characteristics of asphalt mixtures can be efficiently evaluated by means of modern NDT techniques. For instance, this study has demonstrated that the GPR technique not only provides measures of HMA compactability but also coupled with the use of novel algorithms based on the dielectric properties of asphalt mixtures (i.e., PANK and ALL models) may predict rather accurately the in-situ field density. The PQI method has been also found to provide useful real-time information regarding asphalt mixture compactability, although employing this method is not feasible to check the density of the entire surface of the pavement mat. Moreover, from the implementation of the infrared thermography during compaction it was demonstrated that this technique can offer possibilities to capture temperature differentials on the mat, evaluate the mix temperature evolution and develop density-growth curves.

Furthermore, from the assessment of the mechanical properties the test results revealed that the mould-based compaction methods (Marshall and gyratory) tend to produce specimens of superior stiffness and rut resistance characteristics compared to the field-compacted specimens. Although compaction using the steel segmented roller is a laborious method, requiring large quantities of asphalt material for specimen fabrication, it should be emphasized that the roller-compacted specimens show stiffness and rut resistance properties comparable to that of field cores. This pattern, in terms of

relative ranking of the asphalt mixtures compaction-based performance, is consistent with that presented in more recent and earlier research (Airey and Collop 2016; Mollenhauer and Wistuba 2016; Renken 2000), but contradicts with findings from Khan et al. (1998).

Trying to explain the differences between the laboratory- and field compaction-based stiffness and rut resistance characteristics, the mixtures' internal structure evaluation is utilized. In this sense, it can be concluded that regarding Marshall and field compaction, differences observed may be attributed mainly to aggregate contacts; particularly, when using Marshall compactor, it is likely that aggregate degradation occurs from impact compaction (Airey et al. 2008) and hence a significantly higher number of proximity zones between aggregates is induced compared to the field compaction. Regarding gyratory and field compaction, the analysis results demonstrated that the gyratory specimens can reproduce accurately the horizontal distribution and to some extent the spatial distribution of aggregates of field cores. Fairly good approximation was also observed in terms of the aggregate packing indicators. The best approximation of field conditions is achieved by means of compaction with gyration angle of 1.45^{o}, along with coring from 150 mm -to obtain a 100 mm- diameter specimen. It is worthwhile to highlight that this compaction regime not only comes in contrast to relative compaction procedures suggested from previous research (Peterson et al. 2004; Tashman et al. 2001), but also raises under criticism the gyration angles specified from the international standardization organizations (CEN and AASHTO). However, even for this compaction regime the mechanical properties of gyratory specimens still appear to deviate from field cores. As previously demonstrated, the stiffness and rut resistance characteristics of gyratory specimens, compared to field-compacted specimens, are highly sensitive to aggregate interlocking. This implies that a slight increase of aggregate interlocking results in significantly improving the mechanical performance of gyratory specimens. Therefore, for similar aggregate packing level induced from field- and gyratory compaction methods, it appears the latter compaction method to induce a more 'effective' aggregate skeleton to carry the stress intensities imposed during loading. Lastly, it can be inferred that the microstructure of roller-compacted specimens fairly well simulates that of field cores. Particularly, the aggregates contact-based indicators of

roller-compacted specimens are comparable to those of field cores. Also, the aggregates within the roller-compacted specimens tend to mimic the horizontal and spatial distribution of field-compacted specimens. Recalling that the number of contact points and the preferred orientation angle of aggregates contribute significantly to the mechanical behavior of roller-compacted specimens, this by extension may explain why the roller compaction-based stiffness and rut resistance approximates the mechanical characteristics of field-compacted specimens.

10.3 Concluding suggestions

The aim of this Thesis was to contribute to a better simulation of in-situ conditions through laboratory compaction methods, so that reliable results can be obtained to assess, as accurately as possible, the on-site characteristics of field-compacted asphalt mixtures. Based on the synthesis of the main findings methodological approaches, which constitute the scientific contributions of this Thesis, have been developed and suggested for the reliable assessment of asphalt field compaction-based mechanical and surface characteristics.

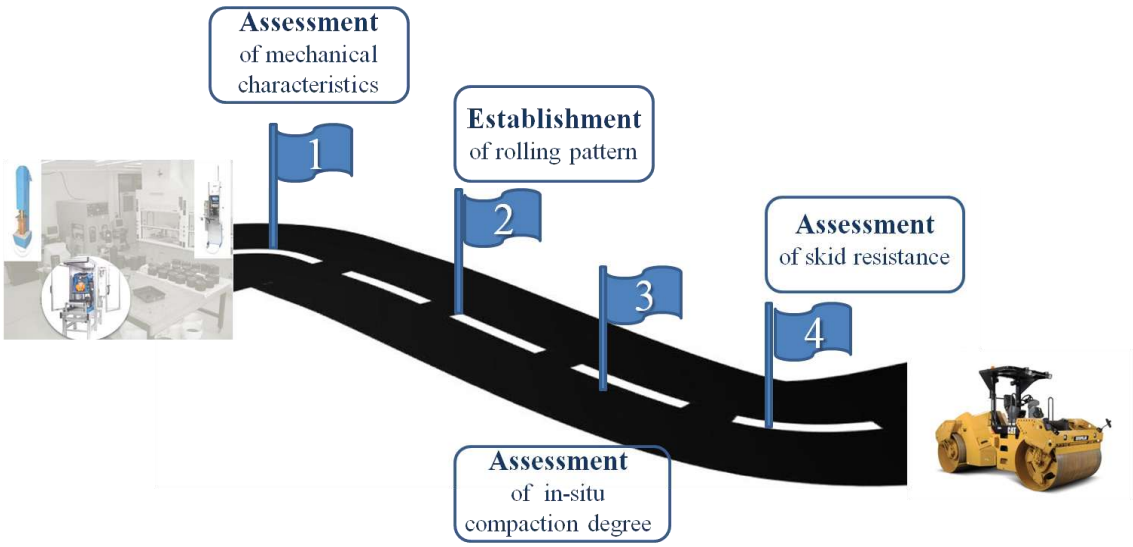

Fig. 10.1 Scientific contributions of this Thesis

Although it is acknowledged that the development of the methodological approaches, to be described hereafter, was relied upon a comprehensive research focused on typical mixtures used in the construction practice in Greece, it is anticipated for these

methods to be implemented on an international basis accounting for the local mixtures and conditions. It is strongly believed that these approaches, which have practical relevance for contractors, agencies and pavement engineers, will contribute significantly to improve not only the asphalt mixture and pavement design procedures but also the on-site compaction process and the quality control encouraging the implementation of modern NDT techniques, as presented hereafter.

10.3.1 Mechanical characteristics

Nowadays, the international standards related to bituminous mixtures specifications, including the European standards, contain a number of requirements for physical as well mechanical properties. Hence, during mixture design process fabrication of laboratory asphalt specimens shall be performed in order to be subjected to performance-based testing. This implies that among a multitude of options available a compaction methodology shall be followed, which in turn has a pronounced influence on the outcome of asphalt mixture performance-based testing. Moreover, when evaluating asphalt concrete mixtures in the laboratory it is desirable to fabricate compacted specimens that closely duplicate the properties of asphalt mixtures compacted in the field to ensure the proper behavior of asphalt layers and subsequently of the road pavement. To the best of the author's knowledge, little research effort has been devoted in the past to suggest guidelines for the compaction procedure in respect to the laboratory compaction method employed, namely impact, gyratory or roller, for the best simulation of in-situ compaction in terms of the mixtures' mechanical properties. This Thesis offers significant input towards this perspective.

Particularly, to bridge the gap between the lab- and field compaction-based mechanical characteristics of asphalt mixtures with reference to the same compaction degree (or air void content) **compaction regimes** are suggested, based on the typical greek mixtures studied, for each laboratory compaction method, as outlined hereinafter.

- Regarding **Marshall compaction**, it is suggested that the fabrication of laboratory specimens for performance-based testing should be performed within temperature window of 125-135^{o}C for conventional dense-graded

mixtures. Slightly higher temperatures (of the order of 5-10^{o}C) should be established for the compaction of SBS modified asphalt mixtures.

- Regarding **gyratory compaction**, from the various compaction protocols evaluated, including standard CEN and AASHTO, the best approximation of field conditions is achieved by means of compaction with gyration angle of 1.45^{o}, along with coring from 150 mm -to obtain a 100 mm- diameter specimen.
- Regarding **roller compaction**, several laboratory compaction regimes (in terms of combinations of compaction temperature and effort) were found to reflect the field compaction-based characteristics. In essence, applying a fixed load (to represent the field roller), and establishing the compaction temperature (higher temperature is preferred) or effort interchangeably the remaining variable to achieve the target compaction degree can be determined.

It is also believed that these guidelines form a good basis to further improving the compaction regimes towards achieving harmonization between the available laboratory compaction methods.

Further, recognizing the modern trend towards the use of mechanistic-empirical pavement analyses methods that encompass asphalt mixture characteristics as design inputs, such as stiffness, it shall be emphasized that material properties obtained from laboratory testing have profound influence on the pavement response, as demonstrated in Chapter 5. Therefore, in an attempt to improve the pavement analysis towards better representing the as-built pavement performance a two-level hierarchical approach is proposed, which is illustrated schematically in Figure 10.2. This approach allows estimating the stiffness modulus of the as-built material (i.e., field core) from mixture collected during production.

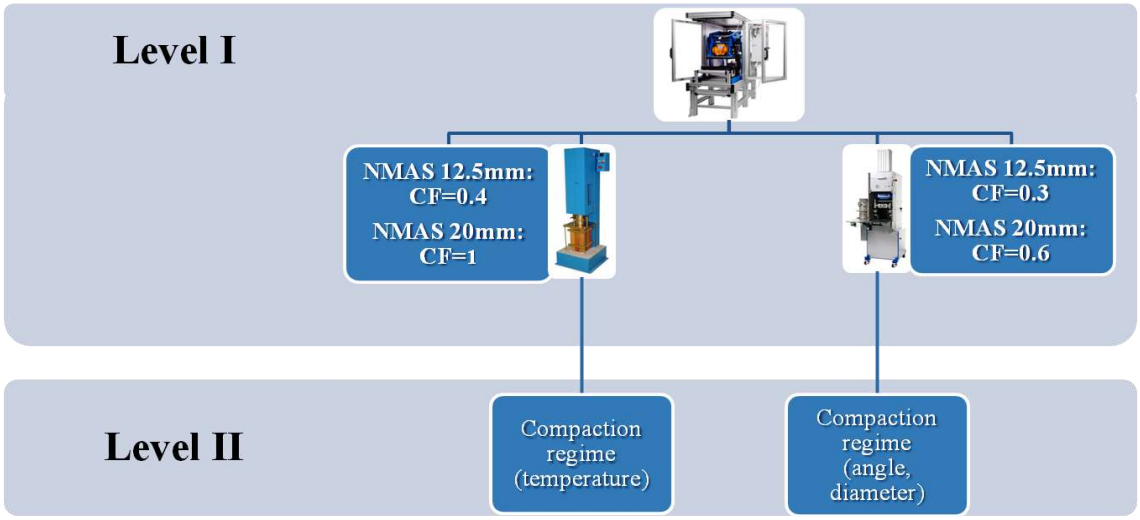

Fig. 10.2 Proposed two-level hierarchical approach for stiffness assessment

The two levels refer to the significance of the HMA stiffness when used as input in the analysis, with Level I representing the case of requirement for increased reliability of results. The two levels are outlined hereafter:

- Level I: stiffness obtained through testing a) of roller-compacted specimen or b) Marshall- and gyratory-compacted specimens and use of conversion factors (CF) with respect to NMAS.
- Level II: stiffness obtained through testing of Marshall and gyratory specimens compacted using the above-suggested compaction regimes.

More specifically, a pavement engineer can adopt the suggested compaction regimes, as previously described, for the specimen fabrication followed by stiffness testing or implement conversion factors, developed on the basis of our experimental results, to the stiffness results obtained from the mould-based compacted specimens. Of course, for those agencies using solely the gyratory compaction, the process of changing the standard angle being used to evaluate the volumetric properties of asphalt mixtures to a different angle for the purpose of assessing their stiffness properties may be not feasible, so in that case the use of conversion factors may be inevitable.

10.3.2 Compactability

Based on our findings, laboratory compaction testing during mixture design process cannot reliably reflect the compactability of asphalt mixtures in the field and hence

provide essential input to be used for the construction process. In practice, achieving on-site the target compaction degree is still a heuristic process. Prior to commencement of permanent works, road agencies specify the installation of a trial section so that evaluation of the contractor's construction techniques is possible. Within this process, the contractors seek, among others, to establish the rolling pattern that ensures the quality acceptance specifications are met. To accomplish this goal, contractors generally try several different combinations of equipment, and numbers of passes with each combination, to determine the most effective rolling pattern. In-place density, defined by nuclear/ non nuclear density gauges, is the measure of rolling pattern effectiveness. With this procedure, compaction curves relating density and number of passes are developed, which enable to define the required compactive effort to achieve the target density. Although this procedure concerns a general guide described, in some instances, in the construction specifications, the outcome of this procedure reflects only the site conditions met during the installation of the trial section. Besides, it is noteworthy to point out that this procedure lacks dominant factors affecting compactability, such as mixture temperature. In this respect, for the scenario that the mixture temperature after placement departs from its relevant value during the installation of the trial section, it is likely that a different number of roller passes to achieve the target density will be needed, which however cannot be assessed. This implies that a more effective methodology based on mixture temperature properties shall be followed to establish the rolling pattern, thus making due allowance for the variability in construction conditions.

Under this view, the scientific contribution of this Thesis concerns **the development of an improved and practical methodology to establish effectively the rolling pattern** and maximize the benefits from the installation of a trial section. This methodology, which is shown schematically in Fig. 10.3, involves, during the installation of the trial section, the implementation of modern NDT techniques, namely Infrared Thermography and PQI techniques, and roller pass-by-pass measurements of mat temperature and in-place density, respectively, for each compaction strategy to be evaluated.

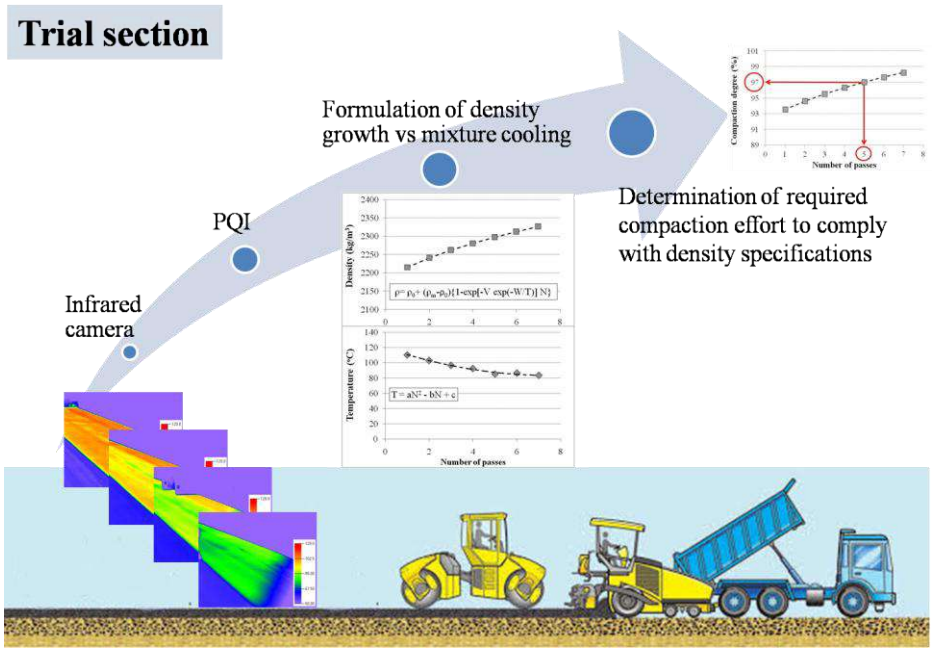

Fig. 10.3 NDT-based methodology to establish the rolling pattern during installation of trial section

With the implementation of these methods a clear understanding of the impact of asphalt mixture temperature on densification is gained. This understanding may be further enhanced commencing rolling at a) typical and b) the lowest allowable mixture temperature on delivery at site, which will thus enable to define necessary modifications to be conducted due to the diversity of mixture temperatures on delivery at site. Hence, the proposed methodology is superior to the procedure commonly followed in practice by offering the potential to capture the density growth in respect to the temperature drop curve, which is crucial to define an effective rolling pattern. The measured in-situ data may be further reclaimed to describe mathematically the compaction process. A closed formula, described in Chapter 4 and verified with our experimental data, has been found to very effective for such analysis. The fitted model describes the compaction density evolution with respect to mixture temperature cooling and number of passes; by controlling these two parameters it is expected to become easier to achieve the desired compaction density. This comprehensive approach, which offers the possibility to make due allowance for the variability of construction conditions, enables to establish not only the most effective compaction strategy but also the required compaction effort to ensure compliance with density specifications. It is therefore believed that this model offers essential information for contractors to enhance the compaction process. Considering

also that the quality of paving and compaction conditions of individual asphalt mix layer has a major impact on the life-time and durability of the pavement, with this methodology a proper pavement initial condition, according to design criteria, will be ensured. In this case, the positive influences through enhanced field compaction will therefore be not only a substantial decrease in needs for maintenance works and thereby in the total life cycle cost, but also less disruption to road users.

However, the effectiveness of the established rolling pattern to achieve the target density needs to be verified within production rolling. In this respect, the as-built compaction quality should be evaluated with reference to the density specifications (mostly compaction degree). In practice, nearly all agencies specify either cored samples or nuclear/ non nuclear density gauges to provide in-place density measurement of the constructed pavement. Typically, a small number of spot tests (with either cores or nuclear gauges) are performed and a judgment about the density level of the entire roadway is made, based on the results of this spot testing. However, density measurement from a small number of spots may not be representative of the density of the pavement mat and therefore full coverage evaluation of compaction quality of the pavement mat is needed. This perspective can be attained by implementing the GPR technique and HMA dielectric properties-based novel algorithms. Building on prior knowledge, **this Thesis introduces an integrated methodology to reliably assess the in-place density**. Based on the experimental parametric investigations conducted, which explored the influence of various available algorithms, the antenna frequency and number of calibration cores on the assessment of the in-place compaction density, the methodology shown schematically in Figure 10.4 is recommended.

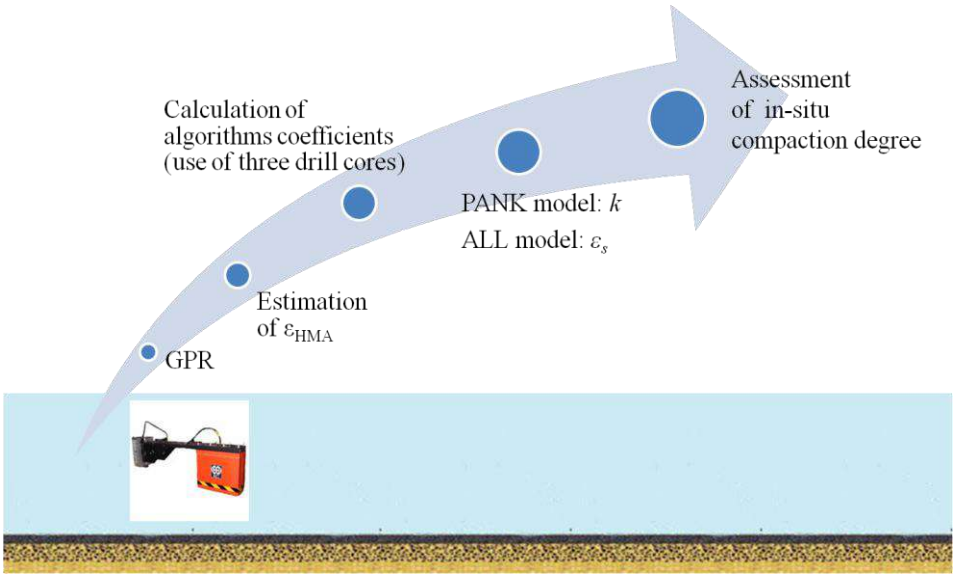

Fig. 10.4 Verification of rolling pattern effectiveness during production rolling using an NDT-based methodology to assess the in-place compaction density

This methodology consists of a) GPR measurements with a 2 GHz antenna, b) assessment of asphalt mixture electric permittivity ε_{HMA} based on GPR, c) extraction of three cores to determine its bulk density, d) back-calculation of algorithms coefficients and e) activation of the novel algorithms (i.e., PANK and/or ALL models) to estimate the in-situ compaction degree. It should be noted that this methodology offers reasonably accurate prediction capabilities of in-place density as well as the benefit of full coverage nondestructive evaluation of the pavement mat compared to more traditional destructive test methods. In light of the above, it is believed that this methodology may be considered a surrogate tool for pavement compaction quality purposes.

10.3.3 Skid resistance

Road agencies internationally specify that after final compaction on site the surface course of asphalt pavement shall be tested for compliance to general requirements, including, among others, the surface macrotexture. However, practitioners and engineers are not able *a priori*, during the mix design process, to quantify and assure the relative texture requirements. Therefore, a methodology that enables the reliable estimation of pavement surface texture characteristics from laboratory testing is of utmost importance.

Given the above concern, **in this Thesis a practical-oriented methodology was introduced based on laboratory roller compaction method**, as illustrated schematically in Fig. 10.5. This methodology includes primarily fabrication of laboratory asphalt specimens of the same thickness to be laid on site using the steel segmented roller, which accommodates also a vibration assembly to simulate the field rollers operation. It follows assessment of surface texture indicators by means of typical laboratory tests (such as the sand patch method and the British Pendulum test).

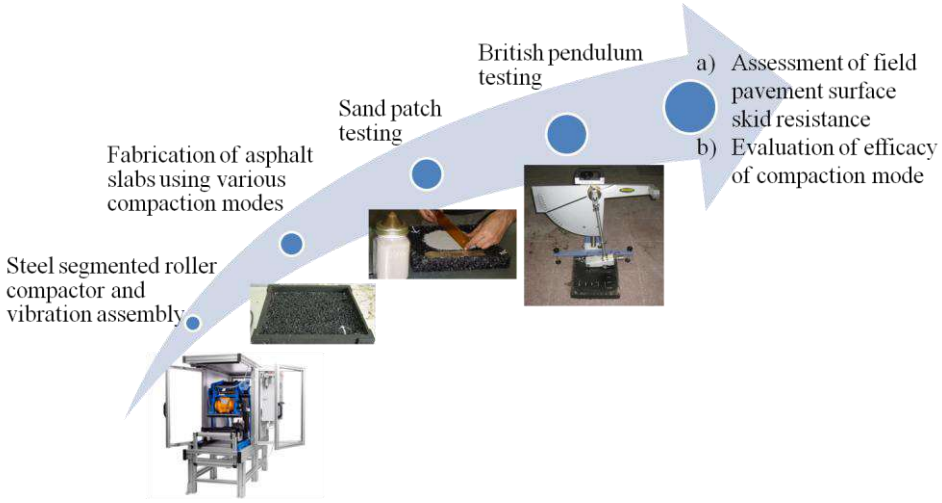

Fig. 10.5 Proposed methodology for skid resistance assessment

Based on the experimental results, this Thesis highlighted that the laboratory roller compaction method can be a reliable method to represent, from a frictional point of view, the field compaction; it is noteworthy to be mentioned that this methodology has been validated from recent study results (Ramirez et al. 2015). The controlling factors for the skid resistance of the as-built pavement surface, namely the macrotexture as set out in the construction acceptance specifications as well as the microtexture, may be reliably assessed from laboratory measurements on the basis of roller-compacted asphalt slabs. Also, the efficacy of various compaction modes can be laboratory evaluated in a competent manner. Hence, this methodology can benefit pavement engineers offering them the possibility to quantify and optimize the skid resistance-related characteristics of asphalt mixtures during the laboratory design process, as well as helpful information that may be potentially used to assess the safety of road users at the early stage of pavement in service. Further, this methodology offers essential information for contractors to

establish an effective field compaction mode to achieve conformity with construction requirements. Of course, field verification of the laboratory texture measurements on roller-compacted asphalt slabs may be conducted in terms of a trial section, thus further maximizing the benefits from its installation.

It is clearly pointed out that adopting the suggested roller compaction methodology, to take the benefit for the skid resistance evaluation of asphalt mixtures, does not premises that for the assessment of mechanical characteristics this methodology shall be also followed. Another possibility would be to alternatively use the compaction regimes related to impact or gyratory compaction methods (as described in section 10.3.1).

10.4 Recommendations for further research

The research conducted in this Thesis raises some questions that can be further investigated in future research.

Firstly, given the wide spread of gyratory compaction along with advantages attributed to its controlled and straight forward use, further research should be devoted to identify other significant compaction parameters, in an attempt to better mimic the aggregate packing and interlocking induced by field compaction. It is then likely to further improve the suggested compaction regime and produce specimens showing similar mechanical characteristics to field-compacted specimens.

Secondly, it was anticipated that by matching the direction for the 2-D image analysis with the loading direction imposed during the mechanical testing of laboratory-compacted specimens and field cores a clear understanding will be attained with regard to the aggregate microstructure and its relation to the asphalt mechanical behavior. However, it is likely that differences in mechanical properties between laboratory-compacted specimens and field cores may be also associated to the microstructure anisotropy (aggregates and air voids distribution) induced by each compaction method. In other words, the aggregates and air voids distribution in the vertical direction within the internal structure of asphalt specimens appear to affect in some extent its behavior in the stress-induced loading. Therefore, it is suggested that 2-D vertical cut surfaces of laboratory and field-compacted specimens (or a higher number of 2-D horizontal cross-sections) be also analyzed to explore potential relationship and add further insight.

Lastly, the relationship between the laboratory compaction-based and the field roller compaction-based frictional characteristics may be further improved. Therefore, it is recommended that additional types of HMA and different compaction methods should be investigated. Moreover, skid resistance of asphalt surfaces decrease during pavement service life due to polishing and hence it would be valuable for pavement engineers and road managers to estimate this variation during the laboratory mix design process. Hence, to the future steps consists the extension of the current proposed laboratory roller compaction-based methodology by incorporating as well the laboratory characterization of asphalt mixture friction evolution with respect to the polishing mechanism.

11. References

AASHTO (2012). Preparing and determining the density of Hot-Mix Asphalt (HMA) specimens by means of the Superpave Gyratory Compactor. AASHTO T312, American Association of State Highway and Transportation Officials.

Airey GD, Collop A, Zoorob SE, Hunter AE (2006). Comparison of field and laboratory compacted asphalt mixtures. In: Proceeding of 10th international conference on asphalt pavements, 12–17 Aug Quebec City, Canada.

Airey GD, Hunter AE, Collop AC (2008). The effect of asphalt mixture gradation and compaction energy on aggregate degradation. Constr Build Mater 22(5): 972–980.

Airey GD, Collop A (2016). Mechanical and structural assessment of laboratory and field-compacted asphalt mixtures. Int J Pavement Eng 17(1): 50-63.

Al-Qadi IL, Lahouar S, Loulizi A (2001). In situ measurements of hot-mix asphalt dielectric properties. NDT & E International 34:427-434.

Al-Qadi IL, Lahouar S (2004). Ground penetrating radar: state of the practice for pavement assessment. Mater Eval 62: 759–763.

Al-Qadi IL, Lahouar S (2005). Measuring layer thicknesses with GPR—theory to practice. Constr Build Mater 19: 763–772.

Al-Qadi IL, Leng Z, Lahouar S, Baek J (2010). In-place Hot-Mix Asphalt density estimation using Ground-Penetrating Radar. Transp Res Rec 2152: 19-27.

Arndt RW (2010). Square pulse thermography in frequency domain as adaptation of pulsed phase thermography for qualitative and quantitative applications in cultural heritage and civil engineering. Infrared Phys 53(4): 246–253.

ASTM (2005). Standard test method for density of bituminous concrete in place by nuclear methods. ASTM D2950 / D2950M, West Conshohocken, Pa.

ASTM (2006). Standard test method for measuring mavement macrotexture depth using a volumetric technique. ASTM E965, West Conshohocken, Pa.

ASTM (2009). Standard test method for preparation and determination of the relative density of Hot Mix Asphalt (HMA) specimens by means of the Superpave Gyratory Compactor. ASTM D6925, West Conshohocken, Pa.

ASTM (2010). Standard test method for density of bituminous paving mixtures in place by the electromagnetic surface contact methods. ASTM D7113 / D7113M, West Conshohocken, Pa.

ASTM (2011). Standard practice for calculating International Friction Index of a pavement surface. ASTM E1960, West Conshohocken, Pa.

ASTM (2013). Standard test method for measuring surface frictional properties using the British pendulum tester, ASTM E303, West Conshohocken, Pa.

Bell C, Hicks R, Wilson J (1989). Effect of percent compaction on asphalt mixture life. ASTM, STP829 Placement and Compaction of Asphalt Mixtures, 107-130.

Benedetto A and Pensa S (2007). Indirect diagnosis of pavement structural damages using surface GPR reflection techniques. Journal of Applied Geophysics 62: 107-123.

Benedetto A (2010). Water content evaluation in unsaturated soil using GPR signal analysis in the frequency domain. Journal of Applied Geophysics 71: 26-35.

BISAR (1998). User Manual. Bitumen Business Group

Boscaino G, Celauro B, Celauro C, Amadore A (2009). Evaluation of the laboratory prediction of surface properties of bituminous mixtures. Constr Build Mater 23: 943-952.

Brown R (1990). Density of asphalt concrete – How much is needed? NCAT Report No. 90-3, Auburn, Alabama.

Brown ER, Hainin MR, Cooley LA (2005). Determining minimum lift thickness for Hot Mix Asphalt (HMA) mixtures. J Assoc Asphalt Paving Technol 74: 23-66.

Button J, Little D, Jagadam V, Pendleton O (1994). Correlation of selected laboratory compaction methods with field compaction. Transp Res Rec 1454: 193-201.

CEN (2001). Bituminous mixtures. Test methods for hot mix asphalt. Part 10: Compactability, EN 12697-10: 2001.

CEN (2006). Bituminous mixtures - Material specifications - Part 1: Asphalt Concrete, EN 13108-1.

CEN (2006). Bituminous mixtures - Material specifications - Part 20: Type Testing, EN 13108-20.

CEN (2007). Bituminous mixtures - Test methods for hot mix asphalt - Part 5: Determination of the maximum density, EN 12697-5: 2007.

CEN (2007). Bituminous mixtures - Test methods for hot mix asphalt - Part 6: Determination of bulk density of bituminous specimens, EN 12697-6: 2007.

CEN (2007). Bituminous mixtures - Test methods for hot mix asphalt - Part 8: Determination of void characteristics of bituminous specimens, EN 12697-8: 2007.

CEN (2007). Bituminous mixtures - Test methods for hot mix asphalt - Part 30: Specimen preparation by impact compactor, EN12697-30.

CEN (2007). Bituminous mixtures - Test methods for hot mix asphalt - Part 31: Specimen preparation by gyratory compactor, EN12697-31.

CEN (2007). Bituminous mixtures - Test methods for hot mix asphalt – Part 32: Laboratory compaction of bituminous mixtures by vibratory compactor, EN 12697-32.

CEN (2007). Bituminous mixtures - Test methods for hot mix asphalt – Part 33: Specimen prepared by roller compactor, EN 12697-33.

China S, James D (2012). Comparison of laser-based and sand patch measurements of pavement surface macrotexture. J Transp Eng 138 (2012): 176–181.

Christensen D, Bonaquist R (2007). Using the indirect tension test to evaluate rut resistance in developing Hot-Mix Asphalt Mix designs. In: Transp Res Circ E-C124. Transp Res Board, 62-77.

Christensen D, Bonaquist R, Anderson D, Gokhale S (2004). Indirect tension strength as a simple performance test. In: Transp Res Circ E-C068. Transp Res Board, 44-57.

Choubane B, Upshaw P, Sholar G, Page G, Musselman J (1999). Nuclear density readings and core densities: A comparative study. Transp Res Rec 1654: 70-78.

Coenen A, Kutay E, Sefidmazgi N, Bahia H (2012). Aggregate structure characterization of asphalt mixtures using two-dimensional image analysis. Road Mater Pavement Des 13(3): 433-454.

Commuri S, Mai AT, Zaman M (2011). Neural network–based intelligent compaction analyzer for estimating compaction quality of hot asphalt mixes. Journal of Construction Engineering and Management 137(9): 634-644.

Consuegra A, Little DN, Quintus HV, Burati J (1989). Comparative evaluation of laboratory compaction devices based on their ability to produce mixtures with engineering properties similar to those produced in the field. Transp Res Rec 1228: 80-87.

Corps of Engineers (2000). Hot-Mix Asphalt paving handbook 2000. US Army Corps of Engineers, Washington, D.C.

Crispino M, Rampini R, Pozzi M (2007). An experimental analysis of the effects of compaction on asphalt pavement macrotexture. In: Proceeding of International Conference on Advanced Characterisation of Pavement and Soil Engineering Materials, Athens, Greece.

Dahir S (1979). A Review of aggregate selection criteria for improved wear resistance and skid resistance of bituminous surfaces. J Test Eval 7(5): 245–253.

Daniels D (2004). Ground Penetrating Radar, second ed. The Institution of Electrical Engineers, London.

Delgadillo R, Bahia H (2008). Effects of temperature and pressure on hot mixed asphalt compaction: field and laboratory study. J Mater Civ Eng 20(6): 440–448.

Dessouky S, Diaz M (2015). Evaluation of asphalt mixes workability and compactability using laboratory and accelerated field testing. In: Proceedings of TMS Middle East - Mediterranean Materials Congress on Energy and Infrastructure Systems, MEMA 2015, Doha, Qatar.

Diamanti N, Redman D, Giannopoulos A (2010). A study of GPR vertical crack responses in pavement using field data and numerical modelling. In: Proceedings of 13th International Conference on Ground Penetrating Radar, Lecce, Italy.

Do M-T, Tang Z, Kane M, de Larrard F (2007). Pavement polishing—Development of a dedicated laboratory test and its correlation with road results. Wear 263: 36–42.

Elsafey M, Herry C, Abd El Halim O, Goubran R, Goodman S (2009). Utilization of infrared imaging as a tool of hot and warm asphalt mixes. In: Proceedings of Sixth International Conference on Maintenance and Rehabilitation of Pavements and Technological Control MAIREPAV6. Turin, Italy.

Ergun M, Iyinam S, Iyinam A (2005). Prediction of road surface friction coefficient using only macro- and microtexture measurements. J Transp Eng 131(4): 311–319.

Flir Systems (2007). ThermaCAM Researcher: Users Manual. Flir Systems.

Fontes L, Pereira P, Trichês G, Pais J, Ferreira A (2008). Skid resistance and texture of compacted asphalt mixes evaluated by the IFI in laboratory. In: Proceedings of EPAM 3- 3rd European Pavement and Asset Management Conference, Coimbra, Portugal, 7-9 July 2008.

Friel S, Kane M, Woodward D (2013). Use of Wehner Schulze to predict skid resistance of Irish surfacing materials. In: Proceedings of Airfield and Highway Pavements Conference: Sustainable and Efficient Pavements, Los Angeles.

Fuentes L, Gunaratne M, Izeppi E, Flintsch G, Martinez G (2012). Determination of pavement macrotexture limit for use in International Friction Index model. Transp Res Rec 2306:138-143.

Furuya H, Tsukimoto Y, Koseki H, Mansell T, Gallivan V, and Uchiyama K 2010. Innovative QC/QA compaction method for HMA pavement using Intelligent Compaction (IC) technology. In: Proceedings of 11th International Conference on Asphalt Pavements, Nagoya, Japan.

Gaussorgues G (1994). Infrared Thermography. Chapman & Hall, London.

Georgiou P, Loizos A (2014). A laboratory compaction approach to characterize asphalt pavement surface friction performance. Wear 311: 114–122.

Georgiou P, Sideris L, Loizos A (2015). Evaluation of the effects of gyratory and field compaction on asphalt mix internal structure. Mater Struct 49(1): 665–676.

Georgiou P, Loizos A, Leventis A (2015). Influence of compaction method on stiffness performance of asphalt specimens. In: Proceedings of 6th International Conference Bituminous Mixtures and Pavements (ICONFBMP), Thessaloniki, Greece.

Goodman SN, Hassan Y, Abd El Halim AO (2006). Preliminary estimation of asphalt pavement frictional properties from Superpave gyratory specimen and mix parameters. Transp Res Rec 1949: 173–180.

Harman T, Bukowski J, Moutier F, Huber G, McGennis R (2002). History and Future Challenges of Gyratory Compaction: 1939 to 2001. Transp Res Rec 1789:200–207.

Hartman AM, Gilchrist MD, Walsh G (2001). Effect of mixture compaction on indirect tensile stiffness and fatigue. J Transp Eng 127(5): 370–378.

Harvey J, Monismith CL, Sousa JB (1994). An investigation of field-and laboratory–compacted asphalt-rubber, SMA, recycled and conventional asphalt-concrete mixes using SHRP project A-003A equipment. J Assoc Asphalt Paving Technol 63: 511-560.

Hassan NA, Airey GD, Khan R, Collop AC (2012). Nondestructive characterisation of the effect of asphalt mixture compaction on aggregate orientation and segregation using X-ray computed tomography. Int J Pavement Res Technol 5(2): 84-92.

Henault J, Larsen D (2006). Thermal imaging of hot-mix asphalt paving projects in connecticut. Transp Res Rec 1946: 130–138.

Herold M, Roberts D, Noronha V, Smadi O (2008). Imaging spectrometry and asphalt road surveys. Transp Res Part C Emerg Technol 16: 153–166.

Huang YH (2004). Pavement analysis and design. 2nd edition, Upper Saddle River, NJ: Prentice Hall.

Huh JD, Nam YK (2000). Study of compaction density in closed form. Transp Res Rec 1712: 66–73.

Hunter AE, Airey GD, Collop AC (2004). Aggregate orientation and segregation in laboratory-compacted asphalt samples. Transp Res Rec 1891: 8–15.

Hunter A, McGreavy L, Airey GD (2009). Effect of compaction mode on the mechanical performance and variability of asphalt mixtures. J Transp Eng 135(11): 839-851.

Ibos L, Marchetti M, Boudenne A, Datcu S, Candau Y, Livet J (2006). Infrared emissivity measurement device: principle and applications. Meas Sci Technol 17: 2950-2956.

Iwama M, Airey GD, Hunter AE (2007). Influence of asphalt mixture compaction method and specimen size on internal structure and mechanical properties. In: Proceedings of Advanced Characterisation of Pavement and Soil Engineering Materials, Athens, Greece, 1063-1073.

Kassem E, Scullion T, Masad E, Claros G (2008). Influence of field compaction pattern on asphalt pavement uniformity. J Assoc Asphalt Paving Technol 77: 257-298.

Kassem E, Scullion T, Masad E, Chowdhury A (2012). Comprehensive evaluation of compaction of asphalt pavements and a practical approach for density predictions. Transp Res Rec 2268: 98-107.

Katicha S, Al-Qadi IL, Flintsch G, Loulizi A. (2011). Effect of compaction method on the resilient modulus of Hot-Mix Asphalt. In: Proceedings of Transportation Research Board 90th Annual Meeting, Washington, DC.

Khan ZA, Al-Abdul Wahab HI, Asi I, Ramandhan R (1998). Comparative study of asphalt concrete laboratory compaction methods to simulate field compaction. Constr Build Mater 12: 373–384.

Kowalski KJ, McDaniel RS, Olek J (2008). Development of a laboratory procedure to evaluate the influence of aggregate type and mixture proportions on the frictional characteristics of flexible pavements. J Assoc Asphalt Paving Technol 77: 35–70.

Leiva F, West R (2008). Relationships between laboratory measured characteristics of HMA and field compactability. J Assoc Asphalt Paving Technol 77: 183–220.

Leiva F, West R (2008). Analysis of HMA field compactability using the Accumulated Compaction Pressure (ACP) concept. In: Proceedings of Transportation Research Board 87th Annual Meeting, Washington, DC.

Leng Z, Al-Qadi IL, Lahouar S (2011). Development and validation for in situ asphalt mixture density prediction models. NDT & E Int 44(4): 369–375.

Leng Z, Al-Qadi IL, Shangguan P, Son S (2012). Field application of Ground Penetrating Radar for asphalt mixture density measurement: A Case Study of Illinois Route 72 Overlay. Transp Res Rec 2304: 133–141.

Linden R, Mahoney J, Jackson N (1989). Effect of compaction on asphalt concrete performance. Transportation Research Record 1217: 20-28.

Loizos A, Plati C (2007). Accuracy of pavement thicknesses estimation using different ground penetrating radar analysis approache. NDT & E Int 40(2): 147-157.

Loulizi A, Al-Qadi IL, Lahouar S (2003). Optimization of ground-penetrating radar data to predict layer thicknesses in flexible pavements. J Transp Eng 129: 93–99.

Mahoney J, Muench S, Pierce L, Read S, Jakob H, Moore R (2000). Construction-related temperature differentials in asphalt concrete pavement: identification and assessment. Transp Res Rec 1712: 93–100.

Maldague X (2001). Theory and practice of infrared technology for nondestructive testing. J. Wiley & Sons, Canada.

Masad E, Muhunthan B, Shashidhar N, Harman T (1999). Internal structure characterization of asphalt concrete using image analysis. J Comput Civ Eng 13(2): 88–95.

Masad E, Muhunthan B, Shashidhar N, Harman T (1999). Quantifying laboratory compaction effects on the internal structure of asphalt concrete. Transp Res Rec 681: 179–185.

Masad E, Scarpas A, Rajagopal KR, Kassem E, Koneru S, Kasbergen C (2016). Finite element modelling of field compaction of hot mix asphalt. Part II: Applications. Int J Pavement Eng 17(1): 24-38.

Maser K, Scullion T (1991). Automated detection of pavement layer thicknesses and subsurface moisture using Ground Penetrating Radar. Transportation Research Board Paper.

Megali G, Cacciola M, Ammendola R, Moro A, Pratico FG, Morabito FC (2010). Assessing reliability and potentiality of nonnuclear portable devices for asphalt mixture density measurement. J Mater Civ Eng 22(9): 874-886.

Mollenhauer K, Wistuba M (2016). Influence of asphalt compaction procedure on 3D deformation properties. Int J Pavement Eng 17(1): 5-12.

Muraya PM (2007). Homogeneous test specimens from gyratory compaction. Int J Pavement Eng 8(3): 225-235.

Papagiannakis T, Zelelew H, Agaian S (2014). Comparing image processing techniques for asphalt concrete X-ray CT images. In: Proceedings of the International Conference on Asphalt Pavements, Raleigh, North Carolina, USA.

Partl M, Flisch A, Jönsson M (2003). Gyratory compaction analysis with computer tomography. Road Mater Pavement Des 4(4): 401-422.

Partl M, Bahia H, Canestrari F, de la Roche C, Di Benedetto H, Piber H, et al. (2013). Advances in interlaboratory testing and evaluation of bituminous materials. State-of-the-Art Report of the RILEM Technical Committee 206-ATB Series: RILEM State-of-the-Art Reports, Springer, London.

Peterson RL, Mahboub KC, Anderson RM, Masad E, Tashman L (2004). Comparing superpave gyratory compactor data to field cores. J Mater Civ Eng 16(1): 78–83.

Plati C, Loizos A (2013). Estimation of in-situ density and moisture content in HMA pavements based on GPR trace reflection amplitude using different frequencies. Journal of Applied Geophysics 97: 3-10.

Plati C, Georgiou P, Loizos A (2014). Use of infrared thermography for assessing HMA paving and compaction. Transp Res Part C Emerg Technol 46: 192–208.

Plati C, Georgiou P, Loizos A (2016). Influence of different roller compaction modes on asphalt mix performance. Int J Pavement Eng 17(1): 64–70.

Plati C, Georgiou P, Loizos A (2016). A comprehensive approach for the assessment of HMA compactability using GPR technique. Near Surface Geophysics 14(2): 117–126.

Rahman M, Grenfell J, Arulanandam S, Ianakiev A (2013). Influence of thermal segregation on asphalt pavement compaction. Transp Res Rec 2347: 71–78.

Ramírez A, Gallego J, Marcobal JR, Blázquez C (2015). Development of new laboratory equipment for measuring the accelerated polishing of asphalt mixes. Wear 322-323: 164–170.

Renken P (2000). Influence of specimen preparation onto the mechanical behaviour of asphalt mixtures. In: Proceedings of the 2nd Eurasphalt & Eurobitume Congress, Barcelona, Spain, 729–735.

Rezaei A, Masad E, Chowdhury A, Harris P (2009). Predicting asphalt mixture skid resistance by aggregate characteristics and gradation. Transp Res Rec 2104: 24–33.

Roimela P (1998). Ground Penetrating Radar surveys in pavement quality control 1996-1997. Tielaitoksen selvityksiä 4/1998. Rovaniemi, Finland (English abstract), 55 p.

Russ JC (2011). The image processing handbook. 6th ed, CRC Press, Boca Raton.

Saadeh S, Tashman L, Masad E, Mogawer W (2002). Spatial and directional distribution of aggregates in asphalt mixes. J Test Eval 30(6): 483–491.

Saarenketo T (1997). Using Ground-Penetrating Radar and dielectric probe measurements in pavement quality control. Transp Res Rec 1575: 34-41.

Saarenketo T, Scullion T (2000). Road evaluation with ground penetrating radar. Journal of Applied Geophysics 43: 119-138.

Saarenketo T (2012). Recommendations for guidelines for the use of GPR in asphalt air voids content measurement, INTERREG: Mara Nord.

Scherocman J (2006). Compaction of stiff and tender asphalt concrete mixes. In: Transp Res Circ E-C105. Transp Res Board, 69-83.

Schmitt R, Johnson C, Bahia H, Hanz A (2009). Effects of temperature and compaction effort on field and lab densification of HMA. J Assoc Asphalt Paving Technol 78: 171-208.

Sefidmazgi RN, Tashman L, Bahia HU (2012). Internal structure characterization of asphalt mixtures for rutting performance using imaging analysis. J Assoc Asphalt Paving Technol 81: 109-134.

Sefidmazgi RN, Bahia HU (2014). Effect of compaction conditions on aggregate packing using 2-dimensional image analysis and the relation to performance of HMA. Mater Struct 47(8): 1313–1324.

Shangguan P, Al-Qadi IL, Leng Z, Schmitt R, Faheen A (2013). Innovative approach for asphalt pavement compaction monitoring using Ground Penetrating Radar. Transp Res Rec 2347: 79–87.

Shangguan P, Al-Qadi IL, Lahouar S (2014). Pattern recognition algorithms for density estimation of asphalt pavement during compaction: a simulation study. Journal of Applied Geophysics 107: 8–15.

SHRP (1993). SHRP's Layer Moduli Backcalculation Procedure. SHRP-P-655, National Research Council Washington, DC.

Smith B, Diefenderfer B (2004). Evaluating nonnuclear measurement devices to determine in-place pavement density. Transp Res Rec 1900: 56-64.

Smith B, Diefenderfer B (2008). Comparison of nuclear and nonnuclear pavement density testing devices. Transp Res Rec 2081: 121-129.

Sousa JB, Harvey J, Painter L, Deacon JA, Monismith CL (1991). Evaluation of laboratory procedures for compacting asphalt –aggregate mixtures, Report No. SHRP-A-UWP-91-523, Strategic Highway Research Program, National Research Council, Washington DC.

Steven B (2009). Friction testing of pavement preservation treatments: Temperature Corrections and Operator/Machine Variability, Technical Memorandum: UCPRC-TM-2008-05.

Stroup-Gardiner M, Law M, Nesmith C (2000). Using infrared thermography to detect and measure segregation in hot mix asphalt pavements. Int J Pavement Eng 1(4): 265–284.

Stroup-Gardiner M, Nixon J, Das P (2004). Automated temperature profiling during hot-mix asphalt construction. Transp Res Rec 1900: 41–49.

Tashman L, Masad E, Peterson B, Saleh H (2001). Internal structure analysis of asphalt mixes to improve the simulation of superpave gyratory to field conditions. J Assoc Asphalt Paving Technologists 70: 605–655.

Tashman L, Masad E, D'Angelo J, Bukowski J, Harman T (2002). X-ray tomography to characterize air void distribution in superpave gyratory compacted specimens. Int J Pavement Eng 3(1): 19-28.

Ter Huerne HL, Doree AG, Miller SR (2009). Monitoring hot mix asphalt temperature to improve homogeneity and pavement quality. In: Proceedings of Sixth International Conference on Maintenance and Rehabilitation of Pavements and Technological Control MAIREPAV6. Turin, Italy.

Thenoux G, Sandoval G (2011). Stiffness modulus behavior in Hot Mix Asphalt. In: Proceedings of Transportation Research Board 90th Annual Meeting, Washington, DC.

Thyagarajan S, Tashman L, Masad E, Bayomy F. (2010). The heterogeneity and mechanical response of hot mix asphalt laboratory specimens. Int J Pavement Eng 11(2): 107-12.

Von Quintus H, Scherocman J, Hughes C, Kennedy T (1991). Asphalt-Aggregate Mixture Analysis System, AAMAS. National Cooperative Highway Research Program (NCHRP) Report 338, Transp Res Board, Washington, DC.

Wambold JC, Antle CE, Henry JJ, Rado Z (1995). International PIARC experiment to compare and harmonize texture and skid resistance measurement, PIARC, Technical Committee on Surface Characteristics, France.

Williams K, Cox B, Howard I, Cooley LA (2015). Asphalt concrete field compactibility models focusing on lift thickness. In: Proceedings of Transportation Research Board 94th Annual Meeting, Washington, DC.

Willoughby K, Mahoney J, Pierce L, Uhlmeyer J, Anderson K (2002). Construction-related asphalt concrete pavement temperature and density differentials. Transp Res Rec 1813: 68–76.

Xu Q, Chang G, Gallivan V (2012). Development of a systematic method for intelligent compaction data analysis and management. Constr Build Mater 37: 470-480.

Yeaman J (2005). Are we afraid on the IFI?, International Surface Friction Conference: roads and runways: improving safety through assessment and design, 1-4 May, Christchurch, New Zealand.

Yue ZQ, Bekking W, Morin I (1995). Application of digital image processing to quantitative study of asphalt concrete microstructure. Transp Res Rec 1492: 53–60.

Zelelew HM, Papagiannakis AT (2011). A volumetrics thresholding algorithm for processing asphalt concrete X-ray CT images. Int J Pavement Eng 12(6): 543-551.

Zelelew HM, Papagiannakis AT (2011). Wavelet-based characterization of aggregate segregation in asphalt concrete X-ray computed tomography images. Int J Pavement Eng 12(6): 553–559.